

**The Role of Protistan Plankton
in Eastern Boundary Upwelling Systems and
Cyclonic Eddies in the Oceanic Carbon Pump**

vom Fachbereich Biologie
der Rheinland-Pfälzischen Technischen Universität Kaiserslautern-Landau
zur Verleihung des akademischen Grades Dr. rer. nat. genehmigte

Dissertation

von

Sven Nicolai Katzenmeier, M.Sc., geb. in Ludwigshafen am Rhein

Mündliche Prüfung: 01.03.2024

Dekan:

Prof. Dr. Stefan Kins

Promotionskommissionsvorsitzender:

Prof. Dr. Stefan Kins

Berichterstattende:

Prof. Dr. Thorsten Stoeck

Prof. Dr. Matthias Hahn

DARLEGUNG DES EIGENANTEIL

Sven Nicolai Katzenmeier

The Role of Protistan Plankton in Eastern Boundary Upwelling Systems and Cyclonic Eddies in the Oceanic Carbon Pump

Planung und Umsetzung der BMBF Projekte REEBUS und CUSCO wurde von GEOMAR Helmholtz-Zentrum für Ozeanforschung Kiel größtenteils durchgeführt. Verantwortlich für die Planung der Untersuchung von Protistenplankton im koordinierten Projekt REEBUS war Thorsten Stoeck. Die Dimensionierung der Eddies wurde von Tim Fischer durchgeführt. Hans-Werner Breiner, Megan Gross und Maren Nothof standen mir unterstützend bei den Feldkampagnen zur Seite.

Die Abbildungen 9, 29 und 30, sowie Tabelle 12, Ergänzungsdatei 1, 2, 16 und 19 beruhen auf Daten, welche von GEOMAR Helmholtz-Zentrum für Ozeanforschung Kiel bereitgestellt wurden. Die in Kapitel 3.3 und Kapitel 7.2 erstellten Abbildungen und Tabellen beruhen auf den mikroskopischen Zählungen, welche in Zusammenarbeit mit Sören Salvatore, Megan Gross, Sophie Wallitt, Felix Heidt und Lukas Damm der Rheinland-Pfälzischen Technischen Universität Kaiserslautern-Landau ausgezählt wurden.

Die vorliegende Einschätzung über die erbrachte Leistung von Dritten wurde mit den genannten Personen einvernehmlich abgestimmt.

15.12.2023 _____

Datum, Unterschrift Doktorand/in

15.12.2023 _____

Datum, Unterschrift Betreuer/in

DARLEGUNG ALLER BENUTZTEN HILFSMITTEL UND HILFESTELLUNGEN

Sven Nicolai Katzenmeier

The Role of Protistan Plankton in Eastern Boundary Upwelling Systems and Cyclonic Eddies in the Oceanic Carbon Pump

Die Analyse der Daten erfolgte mit dem Programm RStudio v4.0.5. Die Arbeit wurde von Megan Gross, Maren Nothof, Mahshid Oladi, Verena Rubel und Julia Zimmer der Rheinland-Pfälzischen Technischen Universität Kaiserslautern-Landau Korrektur gelesen.

15.12.2023 _____

Datum, Unterschrift Doktorand/in

Erklärungen und Anlagen entsprechend § 6 der Promotionsordnung des FB Biologie:

Ich erkläre wahrheitsgemäß, dass

- mir die Promotionsordnung des Fachbereichs Biologie der Technischen Universität Kaiserslautern vom 27.November 2018 bekannt ist,
- ich die eingereichte Dissertation selbst angefertigt und, alle für die Arbeit benutzten Hilfsmittel und Hilfestellungen in der Arbeit angegeben habe,
- ich die Dissertation oder Teile hiervon bisher nicht als Prüfungsarbeit für eine staatliche oder andere wissenschaftliche Prüfung eingereicht habe,
- ich
 - die gleiche oder eine andere Abhandlung nicht bei einem anderen Fachbereich oder einer anderen Universität als Dissertation eingereicht habe,
 - die gleiche oder eine andere Abhandlung bei einem anderen Fachbereich oder einer anderen Universität als Dissertation eingereicht habe, mit folgendem Erfolg:

- mir im Falle einer **kumulativen Dissertation** die in § 8, Abs. (5) und (6) genannten Voraussetzungen und Besonderheiten bekannt sind und in meiner Dissertation werden erfüllt.
- Bei erfolgreich abgeschlossenem Promotionsverfahren wünsche ich zu meiner in Deutsch ausgestellten Promotionsurkunde zusätzlich eine englische Version: ja
 Nein

Kaiserslautern 04.03.2024

Ort

Datum

Unterschrift

CONTENTS

I.	Introduction	5
1	Eastern Boundary Upwelling Systems & Eddy Dynamics	2
1.1	Eastern Boundary Upwelling Systems	2
1.2	Eddy Dynamics	4
1.3	Importance of EBUS & Eddies for Planktonic Food Webs & the Biological Carbon Pump	5
1.4	Influence of Climate Change on the Global Ocean.....	8
1.5	State of the Art in Protistan Plankton Assessment in Eastern Boundary Upwelling Systems & Eddies.....	12
1.6	Goal of this Study.....	17
II.	Mesoscale Cyclonic Eddy Dynamics Shape Structure & Function of Protistan Plankton Communities in the Canary Current System	20
2	Material & Methods	21
2.1	Eddy Characterization & Description	21
2.2	Sampling Stations & Water Column Layers	23
2.2.1	Nutrients & Physical Parameters	25
2.3	Protistan Plankton Assessment in the Canary Current System.....	25
2.3.1	DNA-Filter Preparation	25
2.3.2	DNA Extraction & Amplification	26
2.3.3	Sequencing, Quality Control, Clustering & Taxonomic Assignment.....	27
2.3.4	Statistical Analyses.....	28
2.4	Functional Traits Derived from Taxonomical Assignment.....	29
2.4.1	Ecological Strategies & Functional Richness.....	29
2.5	Microbial Abundances & Carbon Flow Assessment in the Canary Current System	30
2.5.1	Incubation Setup	30
2.5.2	Epifluorescence Microscopy	31
2.5.3	Phagotrophy Estimators.....	32
2.5.4	Statistical Analyses.....	33

3	Results	34
3.1	Protistan Plankton Assessment in the Canary Current System	34
3.1.1	Physicochemical Structures of the Eddies and References Samples	34
3.1.2	Sequence Data Overview	35
3.1.3	Alpha Diversity of Protistan Plankton Communities in the Canary Current System.....	36
3.1.4	Dissimilarities between Eddy Specific Protistan Plankton Communities.....	39
3.1.5	Taxonomic Composition of Protistan Plankton Communities	42
3.2	Functional Annotation of Protistan Plankton Communities	46
3.2.1	Validation of Functional Trait Approach	46
3.2.2	Functional Richness of Protistan Plankton Communities	49
3.2.3	Functional Strategies of Protistan Plankton Communities	51
3.3	Microbial Abundances & Carbon Flow in the Canary Current System.....	55
3.3.1	Prokaryotic & Protistan Abundances	55
3.3.2	Grazing Effect & Carbon Flow	57
3.3.3	Correlation Analysis	59
3.3.4	Multiple Linear Regression	61
3.3.5	Model Validation.....	64
4	Discussion	67
4.1	Effect of Eddies on the Protistan Plankton Community	67
4.1.1	Eddy Dispersal Enhances Regional Protistan Plankton Diversity	67
4.1.2	Specific Protistan Plankton Communities in Different Aged Eddies	69
4.2	Functional Annotation of Protistan Plankton Communities	73
4.2.1	Eddy Dispersal Enhances Regional Protistan Plankton Functional Diversity	73
4.2.2	Resilience & Robustness of Eastern Boundary Upwelling Systems	75
4.3	Impact of Mesoscale Eddies on Microbial Abundances & Carbon Flow	77
4.3.1	Mesoscale Eddies Harbor Elevated Microbial Abundances	77
4.3.2	Eddies Enhance Microzooplankton Grazing of Prokaryotes.....	79
5	Summary & Conclusion	81

III. Effect of Light & Upwelling Intensity on the Protistan Plankton Structure & Function in the Humboldt Current System.....	83
6 Material & Methods	84
6.1 Study Site, Mesocosm Assembly & Manipulation	84
6.1.1 Light & Upwelling Manipulation.....	85
6.2 Water Sampling at the Peruvian Coast.....	87
6.2.1 Nutrients & Physical Parameters.....	88
6.3 Protistan Plankton Assessment in the Humboldt Current System	89
6.3.1 DNA-Filter Preparation	89
6.3.2 DNA Extraction & Amplification	89
6.3.3 Sequencing, Quality Control, Clustering & Taxonomic Assignment.....	89
6.3.4 Statistical Analysis	90
6.4 Microbial Abundances & Carbon Flow in the Humboldt Current System...	91
6.4.1 Incubation Setup.....	91
6.4.2 Statistical Analysis	92
7 Results	93
7.1 Protistan Plankton Assessment in the Humboldt Current System	93
7.1.1 Physicochemical Properties of the Mesocosms.....	93
7.1.2 Sequence Data Overview	96
7.1.3 Alpha Diversity of Protistan Plankton Communities in the Humboldt Current System.....	96
7.1.4 Dissimilarities between Mesocosm Specific Protistan Plankton Communities.....	100
7.1.5 Taxonomic Composition of Protistan Plankton Communities.....	103
7.2 Microbial Abundances & Carbon Flow in the Humboldt Current System.	113
7.2.1 Prokaryotic & Protistan Abundances	113
7.2.2 Grazing Effect & Prokaryotic Turnover Rate	115
7.2.3 Correlation Analysis.....	118

8	Discussion	121
8.1	Protistan Plankton Dynamics in the Humboldt Current System	121
8.1.1	Effect of Light & Upwelling Scenarios on Regional Protistan Plankton Diversity	121
8.2	Microzooplankton Bacterivory in the Humboldt Current System	127
8.2.1	Impact of Light & Upwelling Scenarios on Microbial Abundances & Carbon Flow	127
9	Subject II: Summary & Conclusion	132
IV.	Synthesis.....	134
V.	Abstract / Zusammenfassung.....	139
	Abstract	140
	Zusammenfassung.....	143
VI.	References	146
VII.	Appendix	185
	List of Figures	186
	List of Tables	191
	List of Equations	193
	Supplementary Files / Contents of enclosed USB stick.....	194
	Acronyms	201
	Chemicals.....	204
VIII.	Acknowledgments	205
IX.	Curriculum Vitae	207

I. Introduction

1 Eastern Boundary Upwelling Systems & Eddy Dynamics

1.1 Eastern Boundary Upwelling Systems

The most productive ecosystems in the global oceans are coastal upwelling regions, especially the four Eastern Boundary Upwelling Systems (EBUS) associated with their respective cold currents. In the Atlantic Ocean, the Canary Current runs along North Africa and the Benguela Current along the South African coast. In the Pacific Ocean, the California Current streams along the coast of North America and the Humboldt Current passes South America (Figure 1). Although they cover less than 1% of the global ocean area, they support up to 7% of global primary production and more than 20% of the global marine fish harvest (Chavez and Messié, 2009; Cushing, 1971; Pauly and Christensen, 1995; Ryther, 1969). Despite the small area EBUS occupies, a tremendous yield is caused by the upwelled nutrient-rich water transported by the equatorward cold currents. Not only does the astonishingly high productivity provide the basis of life for 80 million people, but it also has resulted in numerous scientific endeavors for understanding these regimes over the last decades (Abrahams et al., 2021; Bakun and Nelson, 1991; Bonino et al., 2019; Brady et al., 2019; Chavez and Messié, 2009; García-Reyes et al., 2015; Gruber et al., 2011; Messié and Chavez, 2015; Pegliasco et al., 2015; Varela et al., 2021).

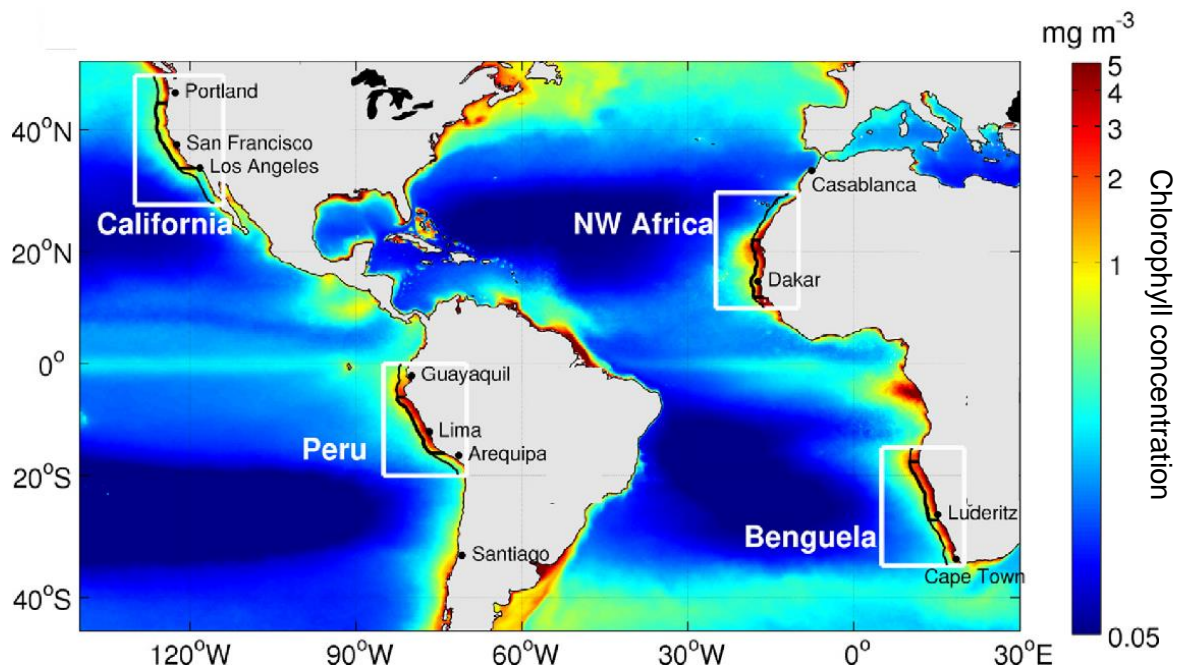


Figure 1. Location of the four EBUS (white boxes). Mean chlorophyll concentrations in mg/m^3 by Sea-Wide Field-of-view Sensor (SeaWiFS) data are colored. Modified from Messié and Chavez 2015.

The coastal upwelling process of waters from deeper layers is regulated by Ekman dynamics (Ekman, 1905). This ocean circulation is mainly driven by the interaction of winds and the Coriolis force (Price et al., 1987). Due to equatorward alongshore winds (northerly winds in the northern hemisphere and southerly winds in the southern hemisphere), surface waters are exposed to wind friction and are thus shifted. The forced movement of the upper layer leads to the friction of water in the deeper layers. Thus, the cold nutrient-rich deep water is drawn to the photic zone following the principle of mass conservation. However, the movement is deflected to the right in the northern hemisphere and to the left in the southern hemisphere resulting in a westward water motion due to the Coriolis force. With increasing water depth, the layers are slowed down due to the water drag. The direction of movement is deviating progressively from the wind direction, a phenomenon known as the Ekman Spiral (Figure 2a; Cushman-Roisin and Beckers, 2011). This condition results in a net water movement at an angle of 90° to the equatorward alongshore winds, inducing an offshore Ekman transport of upwelled water masses and their associated carbon and nutrient contents.

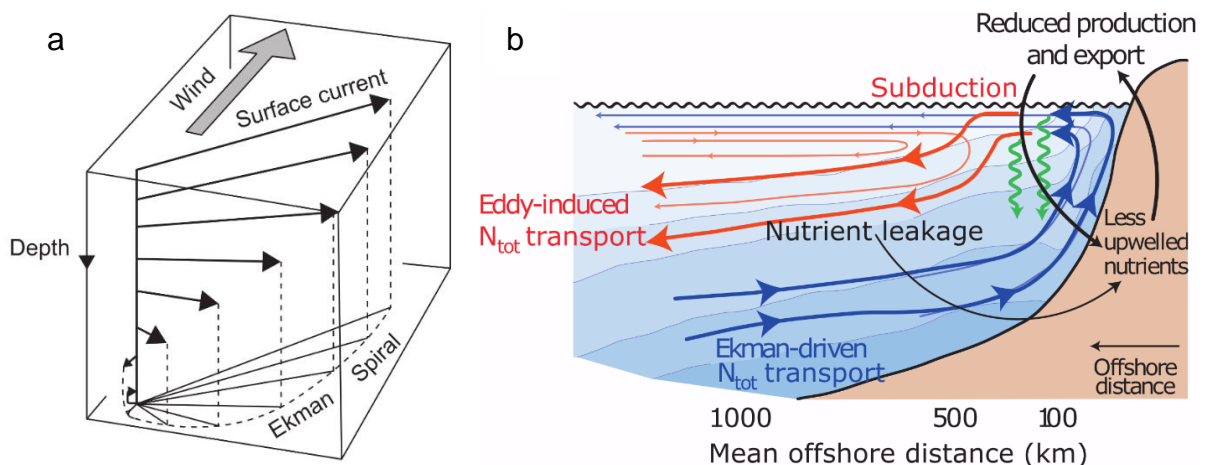


Figure 2. Upwelling dynamics. a) Ekman spiral. Schematic movements of water layers due to wind stress and the water drag, resulting in a drifting net water movement at an angle of 90° to the upwelling-favorable winds. Adapted from Cushman-Roisin et al. (2011). b) Schematic view of the nutrient upwelled waters and the mesoscale eddy-induced reduction of nutrients at the nearshore. Adapted from Gruber et al. (2011).

This export of water masses and resources for primary production is further reinforced by meso- and submesoscale physical processes such as eddies (Figure 2b; Gruber et al., 2011). The eddy-induced reduction of primary production by depriving resources at the nearshore (100 km) leads to an increased nutrient regime in the oligotrophic open oceans (Gruber et al., 2011; Mahadevan, 2014; Pinardi et al., 2015; Stramma et al., 2013). Thereby, eddies regulate the structure and diversity of ambient plankton communities (Bibby et al., 2008; Brown et al., 2008;

Jagadeesan et al., 2019; Landry et al., 2008; Lévy et al., 2014; Liu et al., 2018; Tilman et al., 1982).

1.2 Eddy Dynamics

Mesoscale eddies are omnipresent circular currents of water masses in the global ocean, which can span from 10 – 200 km in diameter (Chelton et al., 2007; Condie and Condie, 2016; Shih et al., 2020). They can reach a life span of several weeks to more than one year before dissipating (Chen and Han, 2019). Eddies are mainly generated from baroclinic instabilities (Kurian et al., 2011). Their formation is influenced by shear forces from opposing currents, seabed topology, upwelling filaments, wind forcing, shoreline irregularities or a combination thereof (Batten et al., 2004; Dilmahamod et al., 2021; McGillicuddy, 2016). In the Canary Current System (CanCS) the cause of eddy formation is likely induced by the current shear and by the effect of the slope topography (Mittelstaedt, 1991). In EBUS, eddies can enclose the freshly upwelled water masses and export them into the oligotrophic ocean (Gruber et al., 2011; Mahadevan, 2014; Stramma et al., 2013). The high rotational velocity of the eddy field, which is often multiple orders of magnitude higher than the mean flow field, results in entrapped water bodies, where the exchange with the surrounding waters is reduced significantly or ceased entirely (McGillicuddy, 2016).

Three mesoscale eddy types with varying properties have been described so far (Figure 3): cyclonic (CE), anticyclonic (ACE) and anticyclonic mode water eddies (ACME; also intra-thermocline eddy; Angel and Fasham, 1983; D'Asaro, 1988; Kostianoy and Belkin, 1989; McGillicuddy and Robinson, 1997; McWilliams, 1985; Thomas, 2008). Identification of eddy types was primarily carried out using satellite data to validate the following properties (Cesar-Ribeiro et al., 2020; Sun et al., 2017; Wu and Chiang, 2007). CEs are mainly characterized by a depression of the sea level and a reduced sea surface temperature within the core. ACEs, in contrast, are associated with an increased temperature and an elevation in the eddy core. However, a considerable number of ACEs have reduced temperatures and only a weak elevation of isopycnals, the so-called ACMEs. Additionally, regarding the vertical stratification, depressed isopycnals are located beneath the eddy core of ACMEs (McGillicuddy, 2016; Schütte et al., 2016).

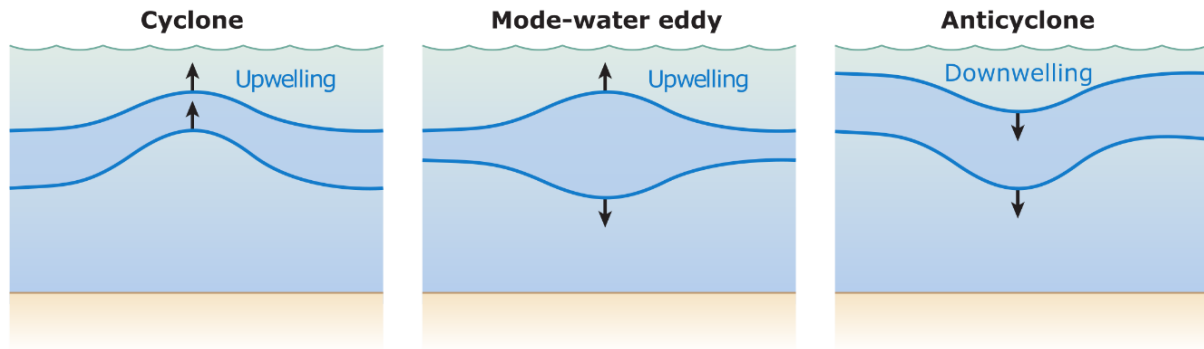


Figure 3. Depression and elevation of the three eddy types associated with the isopycnal displacements. In cyclones and mode-water eddies, isopycnal elevation causes upwelling and in anticyclones downwelling due to isopycnal depression. Adapted from McGillicuddy et al. (2016).

As the names imply, eddies differ in the direction of rotation leading to contrasting processes that drive nutrient dispersal dynamics. CEs rotate counterclockwise while ACEs rotate clockwise in the northern hemisphere resulting in a slow upwelling or a downwelling inside the eddy core, respectively. ACMEs are a special case where a combination of elevated and depressed isopycnals stack. In this ‘chimera eddy’ upwelling also occurs due to eddy–wind interactions (Karstensen et al., 2017). These upwelling regimes can frequently provide new nutrients to further modulate their biotic communities until they dissipate and merge with the surrounding waters. Protistan plankton can undergo successional changes in their structure after being entrapped in eddies at the nearshore while propagating westward (Brown et al., 2008; Cesar-Ribeiro et al., 2020; Owen, 1980). However, knowledge on succession patterns and how the diversity of protistan plankton communities is shaped due to mesoscale features is scarce. Even more, the functional aspects of these changes, and their impacts on aquatic food webs and the entire ecosystem have been rarely investigated (Ramond et al., 2021).

1.3 Importance of EBUS & Eddies for Planktonic Food Webs & the Biological Carbon Pump

Planktonic organisms, including eukaryotes (i.e., phytoplankton and zooplankton) and prokaryotes (i.e., Bacteria and Archaea), are essential within aquatic trophic networks (Cotner and Biddanda, 2002). They fulfill numerous roles to sustain life in its contemporary form like the primary production of oxygen and biomass (Field et al., 1998), maintaining biogeochemical cycles and nutrient recycling (Caron, 1994; Caron et al., 1988) as well as the degradation of dead cell material (Hollibaugh and Azam, 1983). Food web dynamics are of particular interest (Figure 4) to the scientific community as they play a crucial role in regulating ecosystem structure, stability and function (Thompson et al., 2012). Food webs have complex trophic

interactions, including predation and herbivory, competition, mutualism, commensalism and parasitism, which are regulated by bottom-up, top-down or wasp-waist controls (Brett and Goldman, 1997; Cury et al., 2000; Dolan et al., 2002; Lynam et al., 2017; Šimek et al., 1999; Strom, 2000). These can even alter the microbial community composition (Calbet and Landry, 1999; Chow et al., 2014; Genitsaris et al., 2015; Paterson et al., 2007; Walters and Moriarty, 1993). In the mid-1970s, microorganisms received special recognition with the discovery of the microbial loop, which is composed of phytoplankton, phagotrophic protists, bacteria and organic carbon (Azam et al., 1983; Beers and Stewart, 1971; Berk et al., 1977; Landry and Hassett, 1982; Pomeroy, 1974). It should be noted that the ‘loop’ concept is a highly simplified version of the actual microbial food web. Trophic interactions between protistan plankton together with different modes of energy acquisition (e.g., predation, mixotrophy, symbiosis) elaborate these networks, thereby demonstrating the necessity to systematically unravel the complexity of the pivotal functions microorganisms exert in marine ecosystems (Andersson et al., 2017; Fenchel, 2008; Pomeroy et al., 2007).

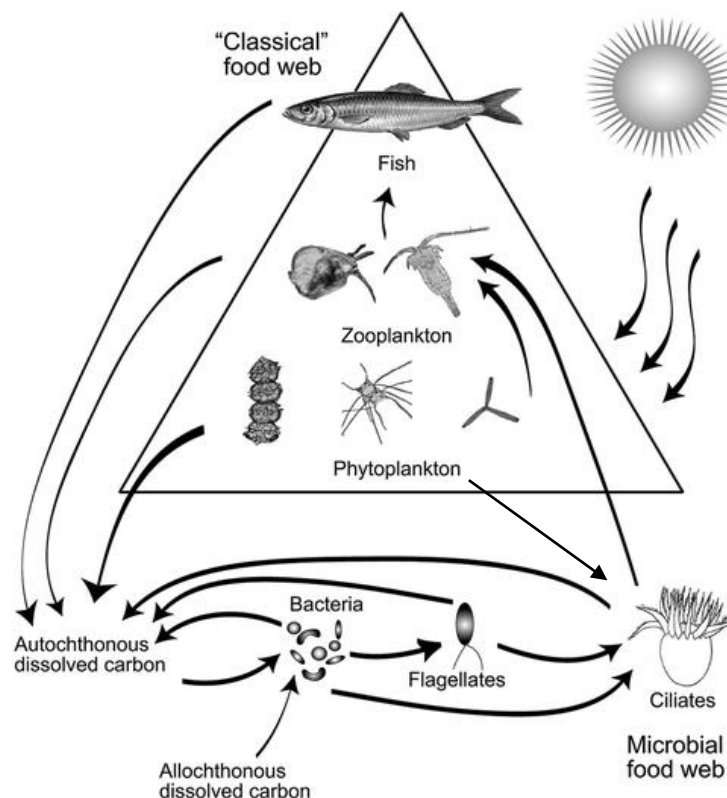


Figure 4. The simplified pelagic food web. Trophic interactions (energy flux) are separated into two parts: The microbial loop components (base) and the classical food web (black triangle). Energy fluxes are marked by arrows. Figure modified after Andersson et al. (2017).

The standing stock of marine phytoplankton accounts for <1% of the global plant biomass (Bar-On et al., 2018; Sigman and Hain, 2012), while they are responsible for approximately half of the global net primary production and contribute to ~40% the total fixed carbon on Earth (Falkowski, 1994). Especially diatoms occupy a crucial role in contributing up to ~40% of the primary production in the ocean (Falkowski et al., 1998) and the particulate organic carbon export (Jin et al., 2006). Already theorized by Margalef's mandala, diatoms can best develop in nutrient-rich, turbulent photic zones. In EBUS, these conditions can be met and diatoms have been reported to dominate the protistan plankton community and can cause harmful blooms (Margalef, 1978; Pitcher et al., 2017; Wyatt, 2014). Carbon is efficiently transmitted in the food chain by herbivorous protists (i.e., heterotrophic or mixotrophic dinoflagellates and ciliates) which can consume the entire daily phytoplankton production (Sherr and Sherr, 1994). Furthermore, bacterivorous protists like heterotrophic and mixotrophic nanoflagellates and small ciliates graze the bacterial biomass, which may account for 30 times the bacterial standing stock (Kisand and Zingel, 2000; Sherr and Sherr, 1994). Energy and carbon sources of heterotrophic bacteria consist of dissolved organic matter (DOM) and particulate organic matter (POM; Barber, 2007). DOM and POM deposition is mainly replenished autochthonously via primary production by phytoplankton and through excretion by protists (Barber, 2007; Kritzberg et al., 2004). Additionally, allochthonous sources like atmospheric aerosols, e.g., Saharan dust, are gaining an increasingly prominent role (Ventura et al., 2021). These interactions enable the transfer of organic carbon to higher trophic levels via the linkage between the microbial loop and the classical metazoan food web (Barber, 2007). Multicellular zooplankton (e.g., copepods, crustaceans, invertebrates, larval fish) consume larger phytoplankton, followed by predators (e.g., large fish, octopus, sharks), which actively hunt or ambush the primary and secondary consumers. This dependency of multicellular organisms on all single-celled components of the food web demonstrates that hotspots of high protistan plankton abundances are targets for species of higher trophic levels. Hence, the diversity of primary consumers and predators is influenced by protistan plankton diversity (García-Comas et al., 2016; Singer et al., 2021).

The impacts of phytoplankton hotspots on the fishing industry cannot be neglected. In the CanCS and the Humboldt Current System (HCS), forage fish, like Pacific/European sardines (*Sardina pilchardus*/*Sardinops sagax*) and the Peruvian/European anchovy (*Engraulis ringens*/*E. encrasicolus*), are highly dependent on protistan plankton and provide the prevailing fishery revenue (Arístegui et al., 2004; Peck et al., 2021; Salvattecchi et al., 2018).

Besides the high carbon transfer efficiency of protistan plankton communities, their contribution to the carbon export in meso- or bathypelagic layers through sinking organisms, particles, aggregates or fecal pellets is essential for the biological carbon pump (Buesseler et al., 2020; Tréguer et al., 2018). However, energy flux and export carbon efficiency are determined by certain species (Degerman et al., 2018; Martin and Tortell, 2008; San Martin et al., 2006) and are therefore strongly affected by protistan plankton community composition (Brown et al., 2008; Legendre and Michaud, 1998; Michaels and Silver, 1988). Changes in physical and biogeochemical factors, e.g. temperature, light, oxygen concentration and nutrient availability, can severely impact protistan plankton (Atkinson et al., 2021, 2003; Madoni and Bassanini, 1999; Rose and Caron, 2007), altering the microbial and multicellular community composition, trophic interactions and thus the biological carbon pump (Arndt and Nomdedeu, 2016; Beardall and Raven, 2004; Doney et al., 2012; Irwin and Finkel, 2008; Petchey et al., 1999; Sarmiento et al., 2004). Therefore, understanding the consequences of mesoscale features and upwelling effects in EBUS for predicting the influences of global warming and climate change on structures and function of protistan plankton communities is of compelling necessity.

1.4 Influence of Climate Change on the Global Ocean

The certainty that the immediate climate change and global warming are triggered by the increasing concentration of greenhouse gases has a major consensus with at least 99% of peer-reviewed literature (Lynas et al., 2021). Fossil fuel combustion, as the root determinant, has surged the atmospheric carbon dioxide (CO₂) concentration to 410 ppm. Compared to preindustrial concentration, this represents an increase by nearly 50%, a rapid growth rate that has never been experienced by humankind before (Doney et al., 2020; Gingerich, 2019; Heinze et al., 2021). Fortunately, the ocean acts as a major carbon sink with a CO₂ uptake of 22 million metric tons per day, thus decelerating the temperature increase (Feely et al., 2008). However, reducing the anthropogenic CO₂ emissions into the atmosphere by roughly one-quarter creates additional impediments like ocean acidification (Heinze et al., 2015). Multiple impacts on the global ocean via cascading effects due to human greenhouse emissions have already been verified as follows: an increase of up to 1.1°C of global air and sea surface temperatures in the last century (Lee et al., 2023); sea level rising by ~0.2 m since 1900 (Lee et al., 2023; Rahmstorf et al., 2007); ocean acidification with a decrease of the pH in surface waters by 0.1 (~30% hydrogen ion concentration increase) since preindustrial times (Doney et al., 2020); and intensification of atmospheric pressure gradients magnifying alongshore winds (Harley et al.,

2006; Sydeman et al., 2013; Figure 5). Pessimistic assessments (Representative Concentration Pathways, RCP 8.5), assuming a constant increase of human greenhouse gas emission, predict a rise in sea level of 52-98 cm (Horton et al., 2014), ocean acidification of surface waters by an increase of 0.4 pH and an increase in water temperature by 4°C by the end of this century (Lee et al., 2023; Sampaio et al., 2021). The expected consequences on EBUS, mesoscale features and their associated biocenosis are highly diverse and, to a limited extent hard to predict and may be subject to uncertainties (García-Reyes et al., 2015). Thus, numerous scientists have been engaged in modeling the fate of EBUS in recent decades (Bakun, 2017, 1990; Bakun et al., 2015, 2010; García-Reyes et al., 2015; Rykaczewski et al., 2015; Xiu et al., 2018).

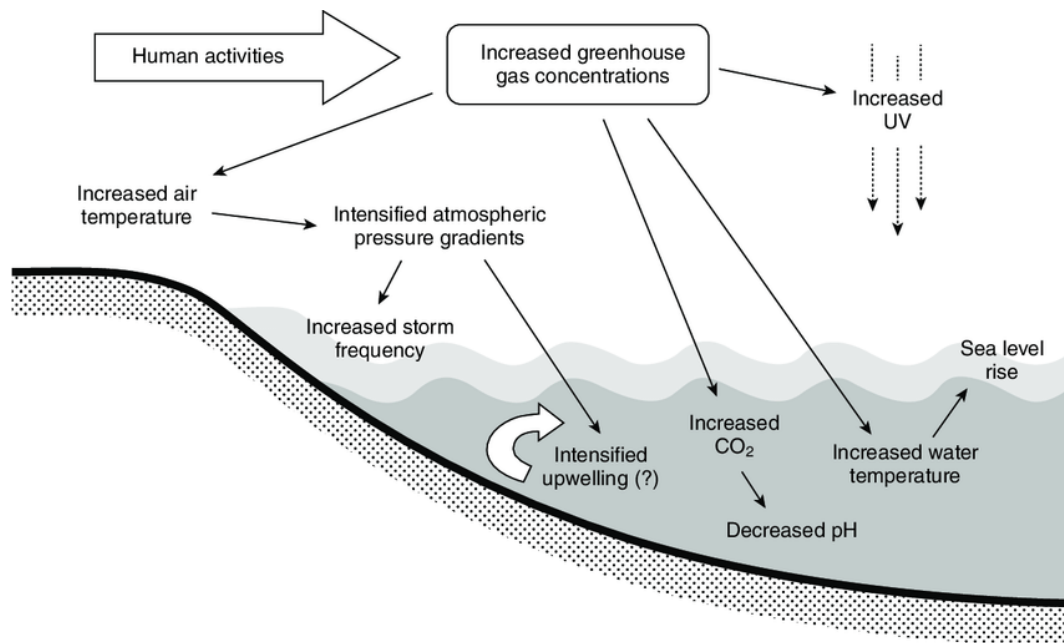


Figure 5. Anthropogenic climate change impacts on the global ocean. Fossil fuel combustion, as the main driver of enhanced greenhouse gas concentrations, is responsible for several abiotic changes in the global ocean. Figure adapted from Allison et al. (2011; original version from Harley et al., 2006).

A major consensus among the results of numerical simulations is the increased vertical stratification of the water column due to increased temperature (Bakun et al., 2015; Winton et al., 2013). This may lead to an accumulation of nutrients and marginal oxygen concentrations as a consequence of reduced ventilation and higher respiration rates (Keeling et al., 2010; Rykaczewski and Dunne, 2010). The decrease in oxygen may cause an increase in hypoxia events, such as dead zones or noxious gas emissions (Sampaio et al., 2021). On the other hand, the previously mentioned magnification of alongshore winds will probably enhance the upwelling intensity and the offshore Ekman transport (i.e., the ‘Bakun hypothesis’; Figure 6;

Bakun, 1990). Thus, a buffer effect could partially counteract the rise in temperature due to an enhanced pumping of cold nutrient-rich water (Bakun et al., 2015). Moreover, a hypothesis proposed by Rykaczewski et al. (2015) states the poleward (equatorward) intensification (reduction) of upwelling-favorable winds due to the poleward shift of the Hadley cell (Grise and Davis, 2020; Studholme and Gulev, 2018). Thus, a decrease (increase) of upwelling intensity in the equatorward (poleward) boundary and the relocation of the complete EBUS in poleward regions can be assumed (Rykaczewski et al., 2015). Another influence of the intensified winds is related to the mesoscale features. Predictions estimate an enhancement of eddy activity in EBUS, which is mostly neglected in modeling approaches, accelerating the offshore transport of upwelled waters (Xiu et al., 2018).

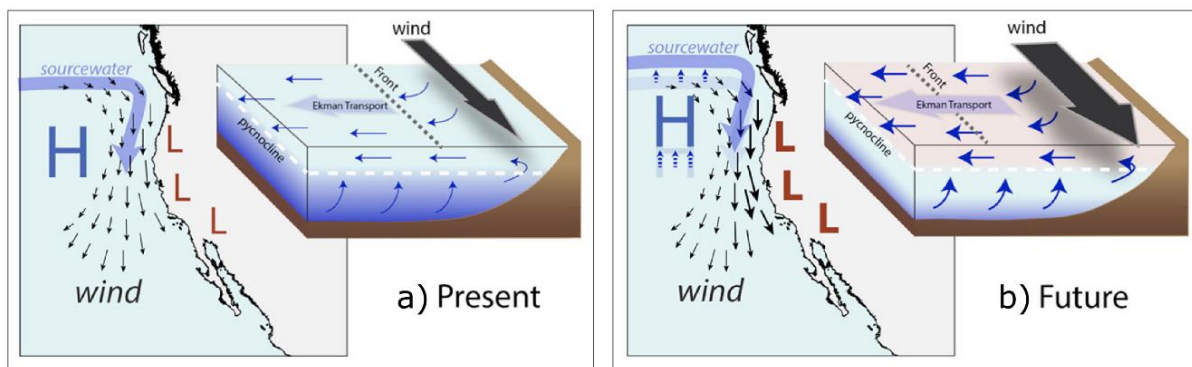


Figure 6. Predicted changes of EBUS due to climate change. a) Contemporary schema of coastal upwelling. b) Future schema of coastal upwelling. H is oceanic high; L is continental thermal low. Intensification of wind and currents are represented by the arrow's thickness. Figure adapted from Bakun et al. (2015).

The above-introduced physical and biogeochemical changes could have severe consequences on the biocenosis of EBUS. The increased nutrient concentrations caused by upwelled water within the poleward boundaries of EBUS may lead to an intensification of primary production (Doney et al., 2012; Xiu et al., 2018), even generating harmful algal blooms in extreme cases (Hallegraeff, 2010; Smayda, 2000), potentially followed by oxygen deprivation due to accompanying respiratory microorganisms (Chan et al., 2008; Deutsch et al., 2005; Keeling et al., 2010). These oxyclines can act as a major barrier for migration of organisms and possibly compress favorable habitats (Bakun et al., 2015; Grantham et al., 2004; Orsi et al., 2012; Stramma et al., 2012, 2010). Contradictorily, the enhanced wind stress may decrease phytoplankton production as a consequence of deepening the oceanic mixed layer, which results in light limitation (Bakun et al., 2015; Oyarzún and Brierley, 2019). The decrease

in upwelling on the equatorward region of EBUS may lead to reduced primary production and trophic transfer efficiency as a result of nutrient limitation, which may have dramatic consequences for higher trophic levels (Behrenfeld et al., 2006; Roemmich and McGowan, 1995).

Influences caused by global warming and ocean acidification reach from altering species interactions to shifting local communities and food web structures (Gibert et al., 2019; Petchey et al., 1999; Sanford, 1999; Spisla et al., 2021). Food webs with highly efficient energy transfer rates achieved by few trophic interactions can experience dramatic changes if only one component is temperature sensitive (Arndt and Nomdedeu, 2016; Hofer, 2018; Ullah et al., 2018). Furthermore, relocation of species to preferential habitats in higher latitudes due to the temperature rise is a contemporary reality and no longer just in the realm of possibility (Barton et al., 2016; Brussard, 1992; Poloczanska et al., 2013; Richardson and Schoeman, 2004; Thomas et al., 2012; Thomas and Gillingham, 2015).

All induced abiotic changes can affect zoo- and, phytoplankton, as well as fish physiology (e.g., generation times, swimming abilities, ontogeny, etc.), resulting in a phenological mismatch (Bakun and Weeks, 2004; Ji et al., 2010; Little et al., 2020) and a spatial or temporal disruption between prey and predator ('match-mismatch hypothesis'; Cushing, 1990). This leads to the facilitation of primary production, thereby causing its offshore transport, reduced fish population and ultimately fishing incursions (Bakun et al., 2015; Mills et al., 2013). The biological impacts of climate change entail multiple threats, which may also influence the whole fishing industry and numerous self-employed fishermen, who are dependent on their daily catches at the coastline. For instance, the sardine population in Moroccan fishery zones diminished, leading to the collapse of the fishery in the 1990s, presumably due to reduced upwelling (Belveze and Erzini, 1983). A contemporary case is the delayed upwelling in the California current with a cascading effect from primary producers to zooplankton and finally to fish (Barth et al., 2007; Mackas et al., 2006; Thomas and Brickley, 2006). The ensuing occurrence of hypoxic events, the temperature increase and the ocean acidification, may result in a restructuring of the predominant organisms, thus altering ecosystem structure, stability, and function.

Intensification of upwelling-friendly winds, followed by an increased mesoscale eddy activity have been identified as important factors in future variations of EBUS. Consequently, nutrient availability increases in coastal and offshore local areas (Xiu et al., 2018). The repercussion of the spatial distortion of EBUS and the intensified eddy dynamics, both of which

amplify the upwelling intensity locally, are dependent on the enhancement of nutrient concentration. The ‘optimal environmental window hypothesis’ states a maximum primary production in case of moderate upwelling. Weak upwelling constrains primary production by nutrient limitation and strong upwelling affects primary production by turbulence and offshore transport (Cury and Roy, 1989). The actual consequences of mesoscale features and changes in upwelling intensity on protistan plankton communities are, however, unresolved. Obstacles entail the linkage between physical and ecological models, the knowledge gap in nonlinear response of food web structures to biogeochemical changes, and the data shortage regarding biogeochemical and biological inventories (Bach et al., 2020; García-Reyes et al., 2015; Hewitt et al., 2020, 2017).

On the other hand, EBUS is known as resilient and robust in their response to natural variability, whereas a fast recovery and maintenance of ecosystem function was documented during short-term climate extremes (Bakun et al., 2015; García-Reyes et al., 2015). This resilience and robustness could be allocated to the concept of the ‘functional redundancy hypothesis’ where the loss of an individual species is replaced by other species with similar function (Biggs et al., 2020; Naeem, 1998; Walker, 1992). This was observed in the decadal shifts between sardine and anchovy populations in the Pacific Ocean attributed to atmospheric or oceanic variation (Chavez et al., 2003). However, the impending climate change may cross the scope of the recorded variabilities in EBUS (Bakun et al., 2015; Sydeman et al., 2013).

1.5 State of the Art in Protistan Plankton Assessment in Eastern Boundary Upwelling Systems & Eddies

Light and nutrient limitations are well-known as severe factors impeding or altering phytoplankton growth, community structure, biochemical composition and biomass (Domingues et al., 2017; Falkowski, 1984; Harrison et al., 1990; Moal et al., 1987; Thorat et al., 2023). Furthermore, distinct light intensities can affect the photoacclimation of phytoplankton leading to the generation of additional or larger light-harvesting pigments under poor light conditions (Falkowski and Owens, 1980; Halsey and Jones, 2015) or the accumulation of more carbohydrates with increasing light intensity (Chapman and Craigie, 1978; Vitova et al., 2015). Nutrient limitation is ubiquitous in the oligotrophic open ocean and gets attenuated by autochthonous or allochthonous nutrient input to a certain extent (Eppley and Peterson, 1979; Hecky and Kilham, 1988; Moore et al., 2013). In the open ocean, mesoscale features like eddy dynamics or Saharan dust input by atmospheric deposition are major

mechanisms for nutrient supply (Baker et al., 2003; McGillicuddy and Robinson, 1997; Shih et al., 2020; van der Jagt et al., 2018). Phytoplankton in coastal waters are less afflicted by the availability of macronutrients and micronutrients due to the supply via upwelling or by human activities (Chavez and Messié, 2009; Duce et al., 2008; Gruber and Galloway, 2008; Seitzinger et al., 2010). The latter can even lead to an oversupply of nutrients causing harmful algae blooms in individual cases (Nwankwegu et al., 2019; Paerl et al., 2016). However, nutrients are still restricting plankton dynamics in coastal ecosystems and EBUS. Analyzing the Redfield ratio of macronutrients (106 Carbon:16 Nitrogen: 1 Phosphorus) is an applicable indication to identify the limiting factors obstructing phytoplankton dynamics (Redfield, 1958). Nitrogen was assumed to be the most important factor limiting phytoplankton growth (Hopkinson, 1985), but phosphorus was also found to be a limiting factor in some parts of the ocean (Wu et al., 2000). However, as research has progressed, more and more limiting substances have come to light. Besides the elements of the Redfield ratio, silicic acid concentrations, which are crucial resources for diatoms to construct their shells, can have a limiting effect (Krause et al., 2019). The accessibility of metals as micronutrients is assumed to be influencing marine protistan plankton (Brand et al., 1983). In particular, iron deficiency may play a crucial role in the peculiar displacement between nitrogen supply and phytoplankton generation in the HCS (Messié and Chavez, 2015). In the two North Atlantic eddies, analyses revealed that iron, which catalyzes electron transfer reactions in photosynthetic and respiratory pathways, exhibited a pivotal contribution to the bottom-up control of phytoplankton productivity (Browning et al., 2021; Morel et al., 1991).

Our understanding on how the diversity and energy fluxes (e.g., carbon transfer from prokaryotes to protists) of protistan plankton are coupled to eddy dynamics remains insufficient due to the difficulty of locating and sampling these highly dynamic hydrographic features (Ramond et al., 2021). Furthermore, previous studies investigating eddy biocenosis while committed to protistan plankton community composition relied on microscopic (Hernández-Hernández et al., 2020) or chemotaxonomic methods like CHEMTAX for identification (Barlow et al., 2017; Carvalho et al., 2019). Although these studies have provided valuable insights, chemotaxonomic methods have a low taxonomic resolution and may be inaccurate due to several abiotic and biotic factors (e.g., irradiance, spectral distribution of light, growth phase) (Higgins et al., 2011). In microscopic identification only a minor proportion of plankton taxa can be resolved (Abad et al., 2016; Eiler et al., 2013; García-Gómez et al., 2020; Visco et al., 2015). With the advent of advanced molecular methods (polymerase chain reaction (PCR), Sanger sequencing) the hidden black box of uncultivable or unnoticed taxa began to unravel

(Díez et al., 2001; López-García et al., 2001; Moon-van der Staay et al., 2001). Next-generation high-throughput sequencing (HTS; e.g., Illumina, Pyrosequencing) of specific barcodes using environmental DNA (eDNA metabarcoding) elevated the molecular approaches in assessing microbial communities even further (de Vargas et al., 2015; Dunthorn et al., 2014; Pernice et al., 2016; Stoeck et al., 2010). Metabarcodes are specific marker genes with a variable region beyond species level (optimal case) confined by conserved taxon-specific sections in the DNA. The conserved DNA regions are ubiquitous throughout all target organisms and are used for taxon-specific primer annealing. The variable region is the amplification target by PCR and HTS (Taberlet et al., 2018). Through high-resolution algorithms, like Divisive Amplicon Denoising Algorithm (DADA2), the sequencing bias can be reduced to obtain high-quality sequences which can then be clustered into amplicon sequence variants (ASVs; Amir et al., 2017; Callahan et al., 2016; Edgar, 2016). The precision and accuracy with respect to ecological surveys for the approach of ASVs have displayed at least as good results as previous DNA-based methods (Callahan et al., 2017; Eren et al., 2015, 2013; Needham et al., 2017). After the ASVs have been created, the underlying sequence can be taxonomically assigned using sequence-databases (e.g., PR² reference data-base for SSU rRNA gene sequences), which allows detailed insight into the targeted microbial community (Guillou et al., 2013). Also, compared to traditional methods, the analysis of eDNA using taxonomic molecular barcodes, in conjunction with HTS and computational tools for bulk sequence data processing, provides a more in-depth comprehension of protistan plankton communities (Burki et al., 2021; de Vargas et al., 2015; García-Gómez et al., 2020; Stoeck et al., 2010).

Quantifying the grazing pressure protists inflict on prokaryotes is of major concern in better understanding the role of protistan plankton with respect to the biological carbon pump. Therefore, multiple methods estimating protistan bacterivory have been developed, which can be classified into three principal categories (direct inference, tracer technique and manipulation technique), each with distinct benefits and shortcomings (Gasol and Kirchman, 2018). The direct inference technique quantifies the active enzymes involved in the digestion of bacterial cell walls or determines the ingested prey organisms in protistan food vacuoles (González et al., 1993; Jezbera et al., 2005; Vrba et al., 1993). Although the accuracy may be highest when using the direct inference technique, it is the least commonly used. The primary reason for this is the need for reliable conversion factors for digestion rate and enzyme activities, which have low accuracy (Dolan and Šimek, 1998; Sherr and Sherr, 1999). Calculating phagotrophy by measuring the growth rate of prey and predators in incubations where grazing is suppressed via dilution, size-fractionation or metabolic inhibitors belongs to the category of manipulation

techniques (Landry and Hassett, 1982; Taylor and Pace, 1987; Wright and Coffin, 1984). The separation between prey and predator has methodological drawbacks where a complete isolation can practically not be achieved (Gasol and Kirchman, 2018). Problems in the selection of inhibitor concentration arise from overdosing and affecting nontarget organisms, or from inadequate dispensing, which does not sufficiently suppress bacterivory (Tremaine and Mills, 1987). In dilution experiments, with time scales of at least 12-24 h, changes in microbial community composition and thus food web interactions can influence the output of growth rates and the calculated phagotrophy estimations (Agis et al., 2007). The category of tracer techniques aims at monitoring the disappearance or incorporation into food vacuoles of fluorescently labeled bacteria (FLB) or fluorescent polycarbonate microspheres (MS) as bacterial analogues (Hammer et al., 2001; Marrasé et al., 1992; Sherr et al., 1987; Smalley et al., 1999). The approach of measuring the disappearance of tracers is also conducted in long-term incubations (12 – 24 h), leading to the identical issue as dilution experiments. In addition, rejection of FLB or MS through chemosensory prey recognition by protists can prevent determining the natural rate of bacterivory (Sakaguchi et al., 2001; Wootton et al., 2007). Although the tracer technique may underestimate the actual grazing pressure, the lowest boundaries can be determined to compare carbon transfer efficiencies.

One study associated with carbon transfer analyzes connected with mesoscale eddies in the CanCS was conducted by Boras et al. (2010). Boras and colleagues investigated “the effect of oceanic eddies on microbial processes, with emphasis on bacterial losses due to protists and phages [...]”. They observed higher grazing pressure on bacteria by protists in ACE and the lowest bacterial mortality due to protists in CE, which was overshadowed by viral losses (Boras et al., 2010). Even though this study established fundamental knowledge on the control mechanisms for bacterial production in this region, no information on the generation time or place of origin of the mesoscale features was emphasized. Thus, indications or inferences related to the ‘life stage’ of the eddies are omitted entirely, which, however, can be a decisive factor regarding the function and community structure of marine plankton.

In general, scientific knowledge and data regarding protistan plankton community composition and carbon fluxes are poorly represented for the CanCS and even the tropical Atlantic (Schmoker et al., 2013; Wickham et al., 2022). Or in the words of Wickham et al. (2022): “[...] there is still much to unravel in both the functional diversity of microzooplankton communities and the trophic interactions within the microbial food web.” This confirms the enormous gap in understanding the present variations of eddy dynamics, let alone predicting the consequences of climate change.

For the first time, in this study, eDNA metabarcoding was applied to investigate marine plankton community structures in three cyclonic eddies of varying ages in the CanCS. Additionally, short-term incubation experiments were conducted, estimating bacterivory by phagotrophic protists to gain an insight into the carbon transfer between two trophic levels. Specifically, the influence of cyclonic eddies on the regional diversity and function (carbon flux) of protistan plankton communities was investigated. For this purpose, samples were analyzed from the deep-chlorophyll maximum (DCM), directly below the DCM (sub-DCM) and the oxygen minimum zone (OMZ). The DCM plays a pivotal role in nutrient cycling, biological carbon pumping and energy flux (Cullen, 2015) and the OMZ is associated to operate as a trap or sieve for the carbon export from eddies to meso- and bathypelagic waters (Chavez and Messié, 2009). This part of my PhD study was conducted in the framework of the coordinated project REEBUS (Role of Eddies in the Carbon Pump of Eastern Boundary Upwelling Systems – Demonstration Case Canary Current System).

The comprehension of the mechanistic processes in controlling the protistan plankton communities, as well as the associated energy fluxes and organic matter export is still in the early stages. In spite of the fact that multiple scientists have investigated the variations in coastal upwelling, no major endeavors were conducted to mimic the implications on biocenosis of shifts in upwelling intensities coupled with and without light limitations as proposed as viable consequences for EBUS (Bakun et al., 2015; García-Reyes et al., 2015). First comprehensive research was conducted during the ‘KOSMOS mesocosm study 2017’ in the coastal upwelling system off Peru with emphasis on the influence of upwelling events (Bach et al., 2020; Min et al., 2023; Sswat et al., 2019). Peer-reviewed research articles referring to the obtained insights are partially published but currently (June 2023) still under development and unavailable. An associated recent publication by Min et al. (2023) addressed monitoring community changes (bacteria, phytoplankton, invertebrates, and vertebrates) in one upwelling-treated mesocosm in relation to the unenclosed ocean using multi-marker eDNA metabarcoding. They detected mesocosm-specific communities dominated by dinoflagellates, presumably a consequence of “[...] salinity-driven stratified conditions in the mesocosm and the warm conditions brought about by the coastal El Niño [...]”. However, the influence induced by distinct light intensities as an independent factor and in combination with the effects of varying upwelling scenarios was disregarded. Therefore, a follow-up project was initiated using an in-situ mesocosm experimental set-up to improve our understanding of the biological and biogeochemical processes triggered by varying light and nutrient conditions in the HCS at the Peruvian coast. Employing mesocosm setups as imitations of natural systems has been proven as a valuable

technique in assessing potential changes induced by abiotic variables in protistan plankton communities (Alvarez-Fernandez et al., 2018; Bach et al., 2020; Escaravage et al., 1999; Hernández-Hernández et al., 2018; Spisla et al., 2021; Stibor et al., 2019). Analogous to the eddy investigation, eDNA metabarcoding was applied to obtain a detailed insight on the structural changes of protistan plankton communities and grazing experiments were performed to determine the bacterivory by protistan plankton. This component of my doctoral thesis was conducted within the collaborative project CUSCO (Coastal Upwelling System in a Changing Ocean).

Both REEBUS and CUSCO campaigns belong to the multidisciplinary consortium under the subject ‘Importance of climate change in coastal upwelling areas’ funded by the Federal Ministry of Education and Research. These field studies provide an unprecedented comprehension of vital processes in plankton dynamics and valuable information for linking physical and ecological models to predict future consequences for EBUS.

1.6 Goal of this Study

In this thesis, the influences of mesoscale eddy dynamics and the effects of light and nutrient availability on the structure and function of protistan plankton community composition in EBUS were analyzed. Advancing our perception of these relationships is essential in light of climate change and the postulated alteration of these ecosystems. This work is therefore subdivided into the following topics:

Subject I: Mesoscale cyclonic eddy dynamics shape structure and function of protistan plankton communities in the Canary Current System

Subject I is part of the multidisciplinary project REEBUS associated to the work package WP5. Here, three cyclonic eddies of varying ages and distances in offshore migration from the place of origin in the CanCS were investigated. The following objectives with the corresponding hypothesis (H) were addressed:

- 1) The goal is to reveal the structural response of protistan plankton communities to differently aged eddy features in DCM, sub-DCM and OMZ using eDNA metabarcoding and determining the environmental factors shaping these communities.

This part of my thesis is based on the submitted manuscript to Deep-Sea Research Part II:

Katzenmeier, S. N., Nothof, M., Breiner, H.-W., Fischer, T., and Stoeck, T.: Mesoscale cyclonic eddies born in an Eastern Boundary Upwelling System enhance microbial eukaryote diversity in oligotrophic offshore waters.

- H_E1.1: Alpha diversity is higher in non-eddy influenced waters and is enhanced by merging of the eddies and surrounding waters as no nutrient input can favor the dominance of specific taxa to the detriment of others.
 - H_E1.2: Protistan plankton communities in a specific eddy are more congruent compared to other eddies and the surrounding waters due to the succession pattern following the entrapment of water and westward propagation after eddy generation. The vertical layers between different eddies and non-eddy impacted sites share similarities due to the stratification of the water column.
- 2) This section aims to assess the functional diversity and ecological strategies (ES) implementing an innovative approach adapted from Ramond et al. (2021) in assigning functional traits to taxonomically assigned eDNA sequences.
- H_E2.1: Functional diversity in young eddies is lower in contrast to aged eddies as well as the surrounding waters due to the fact that freshly trapped nearshore water masses support the dominance of rapidly adaptable phytoplankton species.
 - H_E2.2: Protistan plankton in eddy-entrapped waters exercise specific ES compared to the background waters due to the selective hydrographic dynamics in these mesoscale features.
- 3) Ship-board grazing experiments were conducted to assess the abundance and the carbon transfer from prokaryotes to protists as a major component of the microbial food web and to determine the abiotic factors that alter these.
- H_E3.1: Abundances of bacteria and protists, as well as the quantity of carbon transmitted between these trophic levels are highest in recently generated eddies due to the weak but continuous upwelling and freshly entrapped upwelled nutrient-rich waters.

Subject II: Effect of light and upwelling intensity on the protistan plankton community structure and function in the Humboldt Current System

Analysis corresponding to subject II were done in the framework of the ‘AQUACOSM’ grant ‘The trophic role of bacterivorous protistan plankton in a changing coastal upwelling system (BacPro)’ integrated within the project CUSCO. In this experimental design, effects of nutrient availability on the protistan plankton community were investigated by mimicking varying upwelling intensities in the HCS. Additionally, the influence of light intensity on protistan plankton was assessed via shading the mesocosm bags. The subsequent research topics with their respective hypothesis were pursued:

- 1) The objective is to reveal the functional and structural response of protistan plankton communities to light as well as upwelling intensity using eDNA metabarcoding.
 - H_C1.1: Protistan plankton communities develop uniquely according to varying light exposures due to light limitation for photosynthetic pathways in experimental set-ups with shaded irradiance.
 - H_C1.2: Protistan plankton communities progress distinctively in compliance to ‘low’ or ‘high’ upwelling owing to nutrient limitation for primary production.

- 2) The purpose of this segment is to analyze the abundances and quantify the carbon transfer from prokaryotes to protists using short-term grazing in different light and upwelling conditions.
 - H_C2.1: The highest upwelling intensity promotes higher bacterial abundances as well as higher abundances of phototrophic protists due to the reduced top-down and bottom-up control, respectively.
 - H_C2.2: Bacterial and protistan abundances and the carbon transfer efficiency between these trophic levels are highest in bright light, as mixotrophic protists benefit in high light and drastically contribute to the grazing pressure on prokaryotes.

Conclusively, a synthesis is presented that identifies the similarities and disparities between the two systems under study. The main findings are further more highlighted in a conceptual overview. In addition, the fundamental question of how the emerging impacts of climate change might affect the protistan plankton structure and function in EBUS is shortly recapitulated.

II. Mesoscale Cyclonic Eddy Dynamics Shape Structure & Function of Protistan Plankton Communities in the Canary Current System

2 Material & Methods

2.1 Eddy Characterization & Description

Field campaigns to investigate the eddy perturbation were performed on the RV Meteor (RV research vessel) during two separate cruises, the M156 (July 3rd to August 1st 2019) and M160 (23rd November to 20th December 2019) in the eastern tropical North Atlantic (Figure 7). Eddies were identified prior to the expeditions via sea surface height satellite imaging using Archiving, Validation and Interpretation of Satellite Oceanographic (AVISO) or Copernicus Marine Environment Monitoring Service (CMEMS) data and targeted during the cruises. While traversing the eddy field, the actual dimensions of the features and the direction of rotation were classified precisely using velocity data by the Acoustic Doppler Current Profiler (ADCP; Huang et al., 2023). The eddy boundaries, i.e., the assumed ‘trapping-radius’ of water masses, were classified due to zero vorticity measured by ADCP. The generation time of the eddies was determined utilizing the Angular Momentum Eddy Detection and Tracking Algorithm (AMEDA; Le Vu et al., 2018). Additionally, far-field stations outside the eddy influence were analyzed as references (i.e., Cap Blanc, CB; Cape Verde Ocean Observatory, CVOO). Eddies were named according to their rotational character, the year of the expedition, as well as the latitude and longitude of the rotational center at the time of sampling.

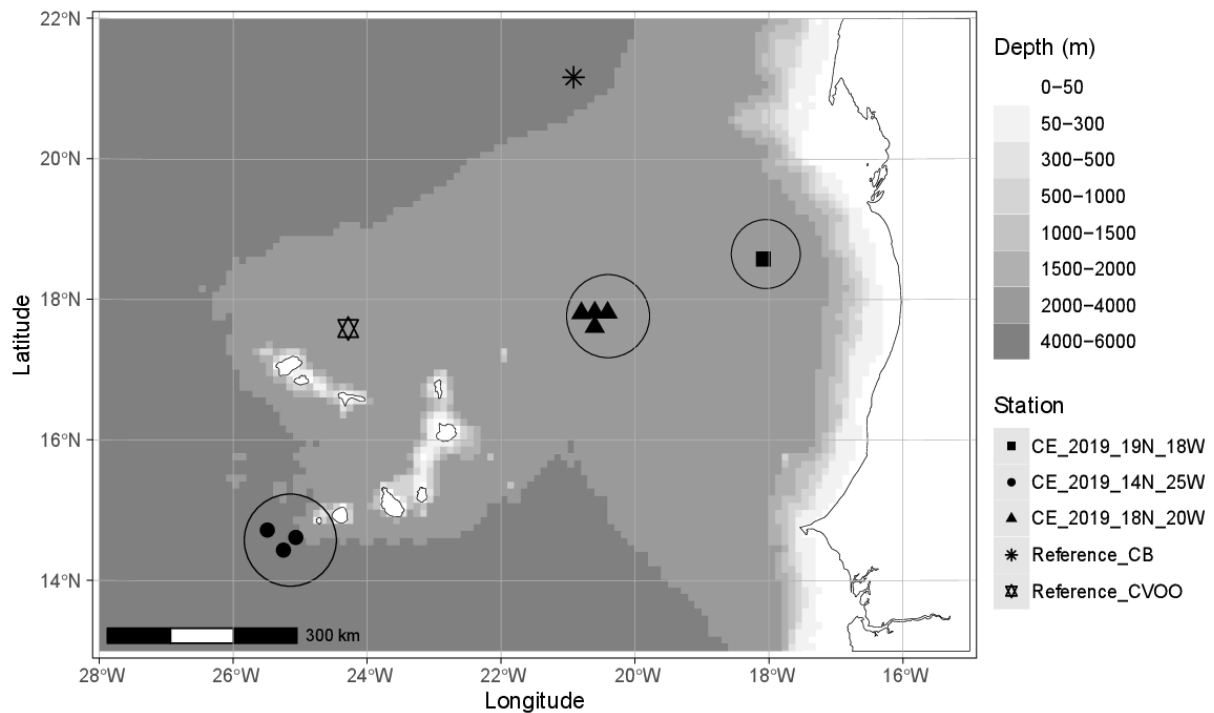


Figure 7. Map of the study area in the Canary Current System. Bathymetry data from the R package ggOceanMaps v1.2.6 (Vitakari, 2022) are grayscale colored. The sampling locations are marked by symbols and the blank circles represent the eddy circumference.

Eddy 1: CE_2019_19N_18W

The first eddy (CE_2019_19N_18W) was explored during the M156 cruise on July 22nd 2019. ADCP data identified a cyclonic eddy with a center of rotation situated at the coordinates 18.73 °N, 18.03 °W and a zero-vorticity diameter of about 70 km. The life-span of this cyclone was approximately six weeks and the place of origin was approximately 18°N, 17°W.

Eddy 2: CE_2019_18N_20W

The second eddy (CE_2019_18N_20W) was analyzed between November 30th and December 3rd 2019 on the M160 research voyage. The rotation was determined as counterclockwise, which characterized this eddy as cyclonic. The coordinates of the center of rotation were at 17.73 °N, 20.43 °W with a diameter of about 75 km. The generation time of the eddy was approximately 12 weeks prior to sampling and originated from 18°N, 18°W.

Eddy 3: CE_2019_14N_25W

The dimensions of the third eddy (CE_2019_14N_25W) were assessed between November 23rd and November 25th 2019 on the M160 expedition. This cyclonic eddy had the center of rotation at the coordinates 14.50 °N, 25.03 °W with 65 km in diameter. The precise sampling procedure and data acquisition were conducted between December 13th and 15th 2019.

However, the CE_2019_14N_25W was presumably already in decay at this time. The eddy converted from the typical vortex-shape to an ellipsoid, which impaired its accurate localization and dimensioning due to the lack of accurate ADCP velocity data. This eddy was several months old and developed from the coast of Senegal at 13°N, 17°W.

All three eddies were categorized as cyclones due to the counterclockwise rotation of water masses. Eddy 1 was the youngest and Eddy 3 was the oldest or an already disintegrated vortex. The distance to the coastline (Eddy 1, ~230 km; Eddy 2, ~470 km; Eddy 3, ~1040 km with 18 °N, 16 °W defined as shore) as a proxy for the life-span of the three mesoscale features likewise advocates the differentiated ages determined by AMEDA. ADCP analysis and AMEDA tracking were performed by the institute 'GEOMAR Helmholtz-Zentrum für Ozeanforschung Kiel'.

2.2 Sampling Stations & Water Column Layers

The selection of sampling stations inside the eddies was based on the presumed dimensions estimated via pre-screening of AVISO and CMEMS satellite images (Cesar-Ribeiro et al., 2020; Moutzouris-Sidiris and Topouzelis, 2021; Wu and Chiang, 2007). Referring to these satellite data, samplings were arranged along east-west and north-south transects through the preliminary eddy centers CE_2019_18N_20W and CE_2019_14N_25W. For the CE_2019_19N_18W vortex only an east-west transect was analyzed. Three sampling locations were selected for each transect: one in the central core, one approximately midway to the boundary, and one in the outer edge of the eddy (i.e., five sites for CE_2019_18N_20W and CE_2019_14N_25W; three sites for CE_2019_19N_18W). Based on the evaluated ADCP data, the exact vortex dimensions were refined (unpublished data by Tim Fischer), and the sampling points were aligned correspondingly (Table 1). This entailed the post hoc exclusion of two sampling sites from both CE_2019_18N_20W and CE_2019_19N_18W and one sampling site from CE_2019_14N_25W. These initial stations were located outside the zero-vorticity boundary and were potentially exposed to water mass exchange with surrounding oligotrophic background waters. Furthermore, one reference site with no evidence of direct eddy perturbation in the vicinity was sampled during both M156 (Reference_CB) and M160 (Reference_CVOO).

Table 1. Sampling overview. Location and sampling date of stations in the zero-velocity boundary of the eddies and the reference stations sampled during the M156 and M160 cruise.

Sampling station	Latitude	Longitude	Location	Date	Cruise
CE_2019_19N_18W	18.58	-18.08	Eddy 1	07/22/2019	M156
CE_2019_18N_20W(1)	17.61	-20.60	Eddy 2	11/30/2019	M160
CE_2019_18N_20W(2)	17.81	-20.80		12/02/2019	M160
CE_2019_18N_20W(3)	17.82	-20.60		12/03/2019	M160
CE_2019_18N_20W(4)	17.81	-20.41		12/03/2019	M160
CE_2019_14N_25W(1)	14.44	-25.25	Eddy 3	12/13/2019	M160
CE_2019_14N_25W(2)	14.62	-25.07		12/13/2019	M160
CE_2019_14N_25W(3)	14.72	-25.49		12/15/2019	M160
Reference_CB	21.17	-20.92	Reference	07/12/2019	M156
Reference_CVOO	17.59	-24.28		12/09/2019	M160

For each station, three samples in the water column (DCM, sub-DCM, OMZ) were determined according to the fluorescence and oxygen concentration during CTD (conductivity, temperature, density) casts. The DCM was characterized by the highest concentration of chlorophyll, the sub-DCM by the chlorophyll minimum right beneath the DCM and the OMZ by the minimal oxygen concentrations. For measuring these parameters, a Seabird 911 plus CTD system installed with temperature-conductivity-oxygen sensors, as well as turbidity and chlorophyll photometers, was used to identify the layers during the veering procedure of the CTD cast (Figure 8; Supplementary File 1). The heaving process was utilized to collect water samples at the appropriate layers with 10 L Niskin bottles assembled to a CTD-Rosette. Approximately 20 L of water was collected for each layer, with 3 L used for grazing experiments and 15 L used for eDNA-metabarcoding. The corresponding water depths for DCM and sub-DCM were in the epipelagic (0 - 200 m) and for the OMZ in the mesopelagic (200 – 1000 m) zone (Supplementary File 2).

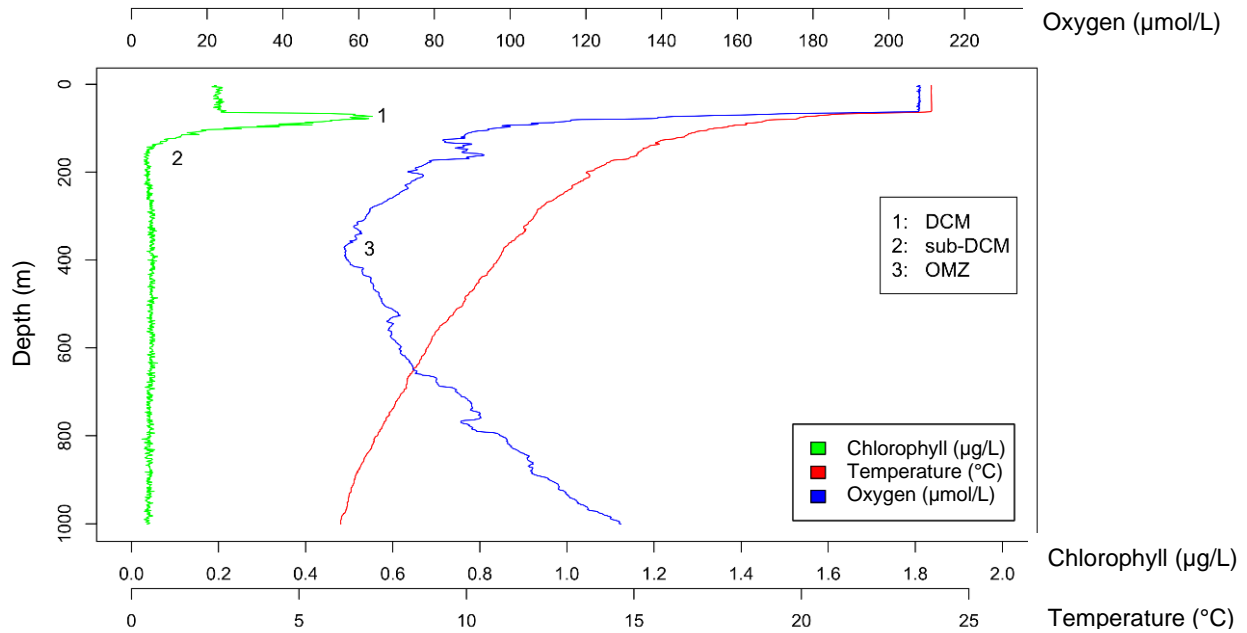


Figure 8. Exemplary CTD-profile. Exemplary CTD-profile during the M160 cruise for the station Reference_CVOO. Chlorophyll concentration in $\mu\text{g/L}$ (green) and oxygen concentration in $\mu\text{mol/L}$ (blue) were decisive parameters for determining the sample layers (DCM, sub-DCM, OMZ). Additionally, temperature in $^{\circ}\text{C}$ (red) is shown and the complete graphics of all CTD-profiles are presented in Supplementary File 1. DCM: deep-chlorophyll-maximum; OMZ: oxygen minimum zone.

2.2.1 Nutrients & Physical Parameters

Measurements of physicochemical data (i.e., temperature, oxygen, salinity, fluorescence, turbidity, and density) were obtained from the CTD system. A volumetric titration using the Winkler method was used to determine the precise dissolved oxygen concentration (Strickland and Parsons, 1968). The nutrient concentrations (i.e., phosphate, PO_4 ; nitrate, NO_3 ; orthosilicic acid, $\text{Si}(\text{OH})_4$) of each layer were measured photometrically with an AutoAnalyzer (QuAatro; Seal Analytical) using continuous flow analysis onboard from duplicate samples of unfiltered seawater (Grasshoff et al., 1999). Nutrient and oxygen measurements were performed by the ‘GEOMAR Helmholtz-Zentrum für Ozeanforschung Kiel’.

2.3 Protistan Plankton Assessment in the Canary Current System

2.3.1 DNA-Filter Preparation

Protistan plankton community composition was analyzed using eDNA. Therefore, water samples were filtered onto $0.65 \mu\text{m}$ pore-sized Durapore® membrane filters (diameter 47mm, Merck KGaA, Darmstadt, Germany) using a rotarus® peristaltic pump (Hirschmann

Laborgeräte GmbH & Co. KG, Eberstadt, Germany). Three replicates were taken with roughly 5 L of water per eddy and reference sample. The filters were placed into cryogenic vials (Cryogenic vials True North™, Carl Roth GmbH + Co. KG, Karlsruhe, Germany) and preserved using LifeGuard Soil Preservation Solution (MoBio, Laboratories Inc., QIAGEN Company, Düsseldorf, Germany). Until further processing in the laboratory of the Rheinland-Pfälzischen Technischen Universität Kaiserslautern-Landau (RPTU) samples were stored on site at -20 °C in a freezer and subsequently shipped off to Germany by a reefer container.

2.3.2 DNA Extraction & Amplification

DNA was extracted from each individual replicate using the DNeasy PowerWater Kit (QIAGEN GmbH, Hilden, Germany) according to the manufacturer's protocol. The hypervariable V9 region of the small subunit ribosomal ribonucleic acid (SSU rRNA) gene was amplified from the extracted DNA following a standard protocol (Stoeck et al., 2010). Briefly, the 1391F as forward primer and the EukB as reverse primer were utilized to target the V9 18S rDNA as a molecular taxonomic barcode during PCR (Table 2). Primers had specific barcode identifiers attached for the construction of libraries containing up to 10 samples in the subsequent preparations.

Table 2. Primer sequences. Nucleotide sequences of the forward and reverse primers used to amplify the V9 18S rDNA.

Name	Sequence	Reference
V9 Forward 1391F (Position 1629–1644)	5'-GTACACACCGCCCGTC-3'	Stoeck et al., 2010
V9 Reverse EukB (Position 1774–1797)	5'-TGATCCTTCTGCAGGTTACCTAC-3'	Stoeck et al., 2010

The PCR protocol consisted of an initial denaturation step at 98°C for 30 s, followed by 30 cycles of denaturation (10 s at 98°C), annealing (20 s at 61°C), elongation (25 s at 72°C) and a final five-minute extension at 72°C. The reaction mix contained the eDNA, GC-buffer, bovine serum albumin (BSA), deoxynucleoside triphosphates (dNTP's), Phusion high fidelity DNA polymerase and the primer-pairs adjusted to a final volume of 50 µL with double-distilled water (ddH₂O; Table 3). PCR products were validated regarding fragment length using gel-electrophoresis and were subsequently frozen at -20 °C until preparation for HTS.

Table 3. Components for polymerase chain reaction. Reaction mixture for polymerase chain reaction to amplify the V9 18S rDNA.

Components	Volume in μL	Concentration
DNA-Template	0.5 – 1	-
GC-Buffer ¹	10	5 x
BSA ¹	2	20 mg/ml
dNTP's ¹	1	10mM/ nucleotide
Phusion High Fidelity DNA Polymerase ¹	0.5	1 unit/ μl
Primer 1391F (Position 1629–1644) ²	0.5	100 mM
Primer Euk B (Position 1774–1797) ²	0.5	100 mM
ddH ₂ O	34.5-35	-

¹ NEB; ² Biomers

2.3.3 Sequencing, Quality Control, Clustering & Taxonomic Assignment

PCR products were thawed and pooled into libraries consisting of up to 10 samples with individual barcodes. Paired-end Illumina MiSeq sequencing was conducted by SeqIT GmbH & Co. KG (Kaiserslautern, Germany). The resulting sequence data files are deposited at the Sequence Read Archive of the National Center for Biotechnology Information under project number PRJNA795916. Illumina libraries were demultiplexed based on the specific barcodes of each sample and primers were removed from sequences using CUTADAPT v1.18 (Martin, 2011). The FASTX toolkit (RRID: SCR_05534) was then used to sort the sequences in the same read direction. Afterwards, the sequences were processed with the DADA2 algorithm (Callahan et al., 2016) using the DADA2 package v1.8 in RStudio v4.0.5 as described for hypervariable taxonomic marker genes from metabarcoding studies (Forster et al., 2019). Here, the V9 sequences were filtered using *filterAndTrim* with `truncLen=80` and `maxEE=1`, where the truncation length was determined based on quality scores following Ewing and Green (1998). The most stringent maxEE was chosen to ensure maximum quality of the datasets. Read1 and Read2 sequences were merged using DADA2's *mergePairs* function utilizing a minimum overlap of 20 nucleotides and an allowed mismatch of two. The *uchime-denovo* algorithm in VSEARCH was used to eliminate potential chimeras from the sequences (Edgar et al., 2011). Taxonomic assignment was conducted using the PR² reference database for eukaryotic SSU rDNA sequences (Guillou et al., 2013), with the last common ancestor (LCA) as a decision criterion and a syntax cut-off of 0.8 (Edgar, 2016). Replicates were then pooled to reduce PCR and HTS bias. Finally, unassigned eukaryotes, streptophytes and metazoan

sequences together with singletons were removed to reduce ecologically uninformative noise and to focus on the single-celled protistan plankton sequences. The resulting ASV-to-sample matrix was then used for all statistical analyses.

2.3.4 Statistical Analyses

The data analysis was performed using the program RStudio v4.0.5 (R Core Team, 2021) and the packages *vegan* v2.6-2 (Oksanen et al., 2022) and *stats* v4.3.0 (R Core Team, 2021). Graphical visualizations were conducted with *ggplot2* (Wickham, 2016) and base R. In the first step, the similarity of sampling sites based on their physicochemical properties was quantified and illustrated by a principal component analysis (PCA) using the *rda* function. Therefore, physicochemical parameters were scaled to a 0-1 value range using the *rescale* function of the *scale* v1.1.1 package (Wickham and Seidel, 2020) to ensure equal weighting in the PCA calculations. Correlations of the abiotic parameters with ordination axes were derived from the PCA output. Rarefaction analysis was performed to visually verify the degree of sample saturation and sufficient sequencing depth. The number of sequences per sample was standardized to the smallest sequence size with the *rrarefy* function to 131,108 sequences for the complete dataset. The Shannon-Wiener Index H' and the ASV richness were then calculated as a measure of alpha diversity. Furthermore, the significant disparities between sampling stations were calculated using a Kruskal-Wallis test with the *kruskal.test* function from base R and a post-hoc pairwise Wilcoxon test (*pairwise.wilcox.test* function) with Bonferroni corrected p-values.

Beta diversity measures were calculated using the Bray-Curtis Index (BC) and the *metaMDS* function, which transformed the computed BC similarity values to a distance matrix for non-metric multidimensional scaling (NMDS). Physicochemical parameters were then fitted into the ordination analysis using the *envfit* function of the *vegan* package. The squared correlation coefficient (R^2) and the significance of fitted vectors was assessed with a Monte Carlo analysis of 1000 permutations. Permutational multivariate analysis of variance (PERMANOVA, with 9999 permutations) determined the significant differences between groups for the generated distance matrix using the *adonis2* function. Supplementary to the complete beta-diversity analysis, the dissimilarities within each individual sampling depth (DCM, sub-DCM and OMZ) were investigated. Therefore, the normalization using *rrarefy* was performed for each individual depth layer (214,045 for the DCM dataset, 131,108 for the sub-DCM dataset and 237,637 for the OMZ dataset), thus, enabling the extraction of the utmost

information of each individual dataset. The calculated BC-dissimilarities were then visualized in distance dendrograms.

Taxonomic composition was analyzed on the phylum level to identify the most dominant phyla in the proportional distribution of assigned sequence reads. These dominant phyla were then investigated on the family level for a higher taxonomic resolution. The proportion of assignable ASVs on species or genus level was deemed insufficient, hence a higher taxonomic resolution was not applied.

2.4 Functional Traits Derived from Taxonomical Assignment

2.4.1 Ecological Strategies & Functional Richness

Functional groups or ES were deduced from the ASV-to-sample matrix applying a novel concept which was just recently used by Ramond et al. (2019, 2021) for phytoplankton communities in tidal fronts. The assignment of functional groups using functional traits for the taxonomically assigned ASVs followed the authors' protocol based on the systematic approach by Maire et al. (2015). In the first step, the publicly available functional trait database (<https://www.seanoe.org/data/00405/51662/>, accessed on 22nd Sept. 2022; Ramond et al., 2018) for taxonomic references was used to annotate the following categories with certain traits to the ASV table: cell size, cover, shape, ingestion mode, motility, presence and acquisition of chloroplast, colony style, body symmetry, polarity, presence/absence of spicules and symbiotic life style. As a result, a sub-dataset was generated where all traits could be assigned. This sub-dataset included 4,542 taxonomic references out of 28,180 total taxonomically assigned ASVs.

ES were then generated from the sub-dataset which was transformed into a Gower distance matrix using K-means partition comparisons with the simple structure index (SSI) criterion to reveal clusters of ASVs with analogous trait associations (Ramond et al., 2019) via the *cascadeKM* function. Subsequently, the relative distribution of these functional groups across all samples was analyzed. The authenticity of the sub-dataset with respect to the distribution of the trait-annotated ASVs of the sampling stations was validated. Therefore, the proportion of shared ASVs was calculated and illustrated using Venn diagrams for the complete ASV table and the reduced dataset with annotated functions utilizing the *ggvenn* function from the *ggvenn* v0.1.9 package (Yan, 2021). Additionally, BC similarities were calculated and an NMDS was computed from the trait-based ASV table for each sampling station. PERMANOVA (with 9999 permutations) assessed the significant variations between groups for the created distance matrix using the *adonis2* function.

Furthermore, functional richness, which is defined as “the amount of niche space occupied by the species within a community” (Mason et al., 2005), was calculated. Therefore, the reduced ASV table was transformed into a presence-absence table with the annotated trait data, and therefrom the functional richness was computed across all stations using the FD package in R. The resulting functional richness was then correlated to the ASV richness and the Shannon index from the complete dataset to verify the reliability of the presence-absence transformed sub-dataset using the Spearman method and evaluation was done following Chan (2003).

Significant differences were analyzed using Kruskal-Wallis test with the R base function *kruskal.test*, followed by a pairwise comparison applying the Wilcoxon test with Bonferroni adjusted p-values from the stats package utilizing the *pairwise.wilcox.test* function.

2.5 Microbial Abundances & Carbon Flow Assessment in the Canary Current System

2.5.1 Incubation Setup

To investigate the trophic transfer efficiency from prokaryotes to phagotrophic protists, short-term grazing experiments were conducted using the class I tracer technique (Gasol and Kirchman, 2018; Strom, 2000). Therefore, triplicate incubations of one liter sampling water were performed in ethylene-vinyl acetate-bags (EVA-bags) following the time-series of 0, 20 and 45 minutes (Oikonomou et al., 2015). Fluorescently labeled polymer microspheres with 0.5 μm in diameter (MS, Fluoresbrite® Plain YG Microspheres, Polyscience, Hirschberg an der Bergstraße, Germany) were used as bacterial analogs. They ought to reflect a concentration between 10-20% of the bacterial standing stock in the incubations (Gast et al., 2018; Sherr et al., 1987). The size of MS and the added concentration to the incubations were determined prior to the experimental procedures via DAPI-staining (4',6-diamidino-2-phenylindole) and epifluorescence microscopy (Porter and Feig, 1980). The injection of the MS followed by gently rotating the EVA-bags for homogenization, signified the start of the grazing experiment. Directly after addition of the MS, subsamples (50 mL) were taken (timepoint 0 minutes) and preserved with formaldehyde to a final concentration of 3.0% to enumerate bacterial analogs, as well as protistan and bacterial abundances. At timepoints 20 and 45 minutes further samples (100 mL each) were taken from the incubations for an estimation of the actual grazing rates of phagotrophic protists. These subsamples were preserved using the Lugol's formalin technique (final concentration of 0.5% alkaline Lugol solution; 3.0% borate buffered formalin),

preventing further grazing and egestion of MS by flagellates (Kemp et al., 1993). Fixed subsamples were stored at ambient temperature for at least 1 hour until further processing.

The preserved subsamples were then drawn onto Isopore membrane filters with a specific pore size depending on the objective of the subsequent enumeration (filter diameter 25 mm, Merck KGaA, Darmstadt, Germany). Subsamples of timepoint 0 minutes were split into 2-3 mL water filtered on 0.2 μm pore-sized membranes for investigating the bacterial and MS abundance. Protistan abundance was calculated from 0.6 μm pore-sized filters with 25 mL sample water. Timepoints 20 and 45 minutes were utilized to investigate the grazing rate from 2.0 and 5.0 μm pore-sized filters with 25 and 30 mL water volume, whereas the 5.0 μm filter represents a retention sample. Prepared membrane filters were stored at $-20\text{ }^{\circ}\text{C}$ and transported to the home laboratory by refrigerated shipping containers for further processing.

2.5.2 *Epifluorescence Microscopy*

Prior to epifluorescence microscopy, three small sections ($\sim 1/6$ filter piece each) were excised from the complete membranes and individually stained with the dye 4',6-diamidino-2-phenylindole (DAPI). DAPI is a prevalent DNA-specific fluorescent stain with a high affinity of binding in the minor groove of adenine-thymine rich DNA sequences (Kapusinski, 1995). This dye is excited by a wavelength of about 365 nm and emits light at > 397 nm and is widely applied to determine microbial cell abundances (Karner et al., 2001; Martinez-Varela et al., 2021; Porter and Feig, 1980; Schmitz et al., 2011). The complete staining process was conducted in the dark. Therefore, 50 μL DAPI ($1\ \mu\text{g mL}^{-1}$) were pipetted on each filter piece and allowed to react for ~ 4.5 minutes. The fragments were then cleansed in distilled water for ~ 30 seconds to remove extant DAPI and rinsed in 80% ethanol to accelerate the drying process. Subsequently, dyed filter pieces were put on glass slides and mounted with one drop of Vectashield Antifade Mounting Media (Biozol, Eching, Germany), impeding the bleaching of the dye. Stained filters were stored at $4\text{ }^{\circ}\text{C}$ for a maximum of 5 days before enumeration via microscopy.

Abundances of microbial cells and ingested particles were enumerated using the Zeiss Axiostar plus (Carl Zeiss Microimaging, Göttingen, Germany) equipped with a monochromatic camera (QICam B, Intas Science Imaging Instruments, Göttingen, Germany) and a W-PL 10x/23 eye piece with an integrated measurement grid (Equation 1). Cell abundances were counted with the filter set Zeiss 02 (excitation: G 365 nm, beam splitter: FT 395, emission: LP 420) due to the emission spectra of DAPI. MS with an excitation maximum of 441 nm and an emission maximum of 485 nm were analyzed using a Zeiss 09 filter set (excitation: BP 450-

490 nm, beam splitter: FT 510, emission: LP 515). MS and prokaryotic concentrations were determined using a 100-x magnification oil immersion plan achromatic objective with a numerical aperture of 1.25. Protistan abundances were investigated with a 63-x magnification oil immersion plan apochromatic objective with a numerical aperture of 1.4. For representative purposes, ten grids were counted for each filter fragment to record cell abundances, and 100 protists were randomly screened to enumerate ingested MS.

$$\text{cell abundance [mL}^{-1}] = n * A * A_c^{-1} * V^{-1}$$

Equation 1. Calculation of cell and microsphere abundance. Particle and organism abundances were calculated per milliliter. n is the mean value of counted cells in 10 grids. A represents the filter area and A_c the grid area in μm^2 . V is the volume of subsamples drawn on each filter in mL.

2.5.3 Phagotrophy Estimators

The average number of incorporated MS in 100 protists was plotted against the incubation time (timepoint 20 and 45 minutes) in order to determine the ingestion rate of tracer particles. Regression analyses were used to determine the trend line of the uptake curve (Supplementary File 3). The slope of the linear portion of the regression line indicates the MS ingestion rate (Unrein et al., 2007). By multiplying the ingestion rate of MS with the ratio of natural prokaryotic abundance and microsphere abundance, the average grazing rate of one individual protist was determined (Equation 2.I). The ecologically relevant grazing effect is the concentration of prokaryotes which are consumed by all phagotrophic protists in a specific time. It is determined by multiplying the grazer abundance by the grazing rate (Equation 2.II). Furthermore, the carbon transfer efficiency can be estimated by the grazing effect utilizing the average carbon content of a single bacterium with 20 fg as proposed by Lee and Fuhrman (1987).

$$\text{I. grazing rate (prokaryotes grazer}^{-1} \text{ h}^{-1}) = \text{ir} * C_{\text{prokaryotes}} * C_{\text{MS}}^{-1}$$

$$\text{II. grazing effect (prokaryotes mL}^{-1} \text{ h}^{-1}) = \text{gr} * C_{\text{grazer}}$$

Equation 2. Calculation of grazing rate (I) and grazing effect (II). The ingestion rate (ir) of food particles in MS grazer⁻¹ h⁻¹ is multiplied by the concentrations of bacteria ($C_{\text{prokaryotes}}$) and divided by the MS concentration (C_{MS}) in cells/mL. The grazing rate (gr) is the number of prokaryotes grazer⁻¹ h⁻¹ and C_{grazer} is the concentration of phagotrophic protists in cells/mL. MS: microspheres.

2.5.4 Statistical Analyses

The statistical analyses were performed using the program RStudio v4.0.5 and the packages ggpubr v0.4.0 (Kassambara, 2020), olsrr v0.5.3 (Hebbali, 2020), stats v4.3.0 (R Core Team, 2021), relaimpo v2.2-6 (Grömping, 2006) and ggplot2 v3.3.6 (Wickham, 2016) for graphical visualization. To assess the variability of the abundances and grazing effect in each eddy/reference station and depth layer, boxplots were generated and examined for significant differences. Analyses were performed using Kruskal-Wallis test with the R base function *kruskal.test*. The post-hoc pairwise comparison was conducted with the Wilcoxon test and Bonferroni adjusted p-values from the stats package utilizing the *pairwise.wilcox.test* function.

Correlation analyses were used to investigate the extent to which environmental factors influence the microbial parameters studied. Spearman rank test was applied to identify significant correlations between the physicochemical parameters and the prokaryotic and protistan abundances as well as the grazing effect. Additionally, the impact of the microbial variables amongst each other was calculated.

Predictions of microbial cell abundance and grazing effect with abiotic parameters using multiple linear regression were executed using the *lm* function of base R for each depth layer (DCM, sub-DCM, OMZ), separately. Therefore, the triplicate samples were used to increase sample size. The first model was built using the environmental factors i.e. salinity, turbidity, temperature, nitrate, silicate, phosphate, oxygen concentration, and microbial cell abundance. In the second step, a forward and backward stepwise selection of the physicochemical parameters was applied to identify the most parsimonious model according to the Akaike's information criterion (AIC; Arnold, 2010). The variance inflation factors (VIFs) were then inspected to reduce multicollinearity. Those environmental parameters were removed in descending order of VIF values until $VIF < 10$ was acquired (Groß, 2003). The next model-step was an introduction of interaction terms for the remaining environmental factors, followed by a repetition of the stepwise selection in regards to parsimony. This final model was then examined for normal distribution of residuals with the *ols_test_normality* command of the olsrr package. Subsequently, using the *boot.relimp* and *booteval.relimp* function from the relaimpo package the relative importance accounted for by each explanatory variable of the model's coefficient of determination was investigated. Supplementary, regression analysis and Lin's concordance correlation coefficient (CCC) were used to determine the consistency between the measured and predicted values (Lin, 1989) and evaluated following the stringent assessment system of McBride (2005).

3 Results

3.1 Protistan Plankton Assessment in the Canary Current System

3.1.1 *Physicochemical Structures of the Eddies and Reference Samples*

Physicochemical data for the eddy and reference stations were analyzed in a principal component analysis (PCA; Figure 9). The three depth layers (DCM, sub-DCM and OMZ) followed a gradient along the PCA axis 1 that explained 93.2% of the observed variation in the abiotic parameters. The three eddies and the reference sites were distinctly stronger associated with the PCA axis 2, which accounted for a variation of 3.5%. In general, orthosilicic acid and macronutrient concentrations increased from DCM to sub-DCM and OMZ. Salinity, fluorescence, temperature, and dissolved oxygen decreased in the water column for each station. The distinction of sampling stations was notably more pronounced in the DCM layer along both axes. In the sub-DCM and even more so in the OMZ, the environmental parameters were quite similar, resulting in clusters of samples, where even the reference sites and the eddy stations were located in close proximity to each other. The environmental parameters which separated the stations along the PCA axis 2 could not be identified. Noteworthy, the characteristics of the youngest eddy comprised the lowest temperature and the highest nitrate concentration of the DCM layer, as well as the most pronounced oxygen minimum zone. The middle-aged eddy, on the other hand, had the lowest orthosilicic acid concentrations. Furthermore, the fluorescence was notably higher in this eddy compared to the other DCM stations.

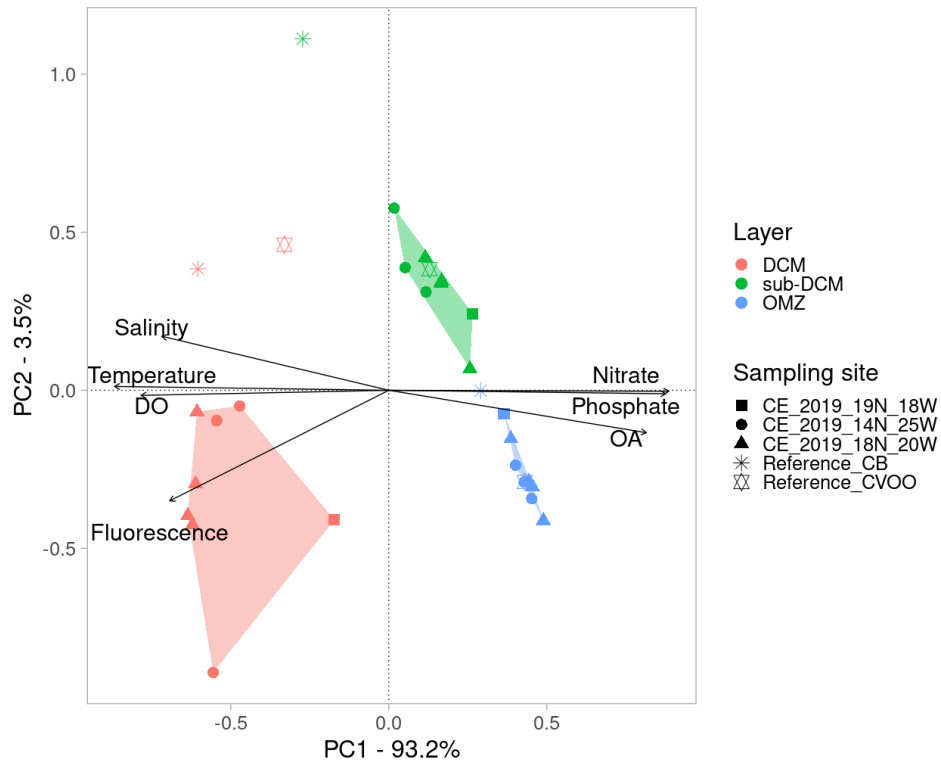


Figure 9. Principle component analysis based on the physicochemical parameters. Eddy samples are connected forming segments for the specific depth layers (colored) and sampling sites are indicated by symbols. DCM: deep-chlorophyll-maximum; OMZ: oxygen minimum zone; OA: orthosilicic acid; DO: dissolved oxygen.

3.1.2 Sequence Data Overview

After removing uninformative sequences from the taxonomically assigned ASV table, between 131,108 (min) and 1,261,983 (max) high quality (HQ) sequences were retained (Supplementary File 4). The subsequent normalization of read counts to the minimum sequence number of the smallest sample size resulted in 131,108 reads per sample. Furthermore, the standardization to the smallest sequence size was applied to each depth layer, yielding 214,045 (DCM), 131,108 (sub-DCM) and 237,637 (OMZ) reads per sample. Rarefaction curves indicated that all samples with rarefied read counts were sequenced to the point of near saturation (Supplementary File 5).

3.1.3 Alpha Diversity of Protistan Plankton Communities in the Canary Current System

The alpha diversity measures, ASV richness as well as the Shannon Index (H'), were mostly congruent for all samples of the individual eddy or reference sites in the respective depth layer (Supplementary File 6). The overall highest ASV richness was obtained from the sample of the oldest eddy CE_2019_14N_25W (sample 1) with 4454 ASVs in the sub-DCM and the highest H' (sample 3) with a value of 6.53 in the OMZ. The lowest alpha diversity measures were found in the OMZ layer of the middle-aged eddy CE_2019_18N_20W (sample 4) with an ASV richness of 1037 and an H' of 3.27. In the DCM, the ASV richness and H' of protistan plankton community at the reference sites notably exceeded those in the eddies (Figure 10). However, the plankton communities in the decaying eddy stood out as the most diverse (H') and ASV-rich samples in the OMZ (except H' for CE_2019_14N_25W sample 1 compared to Reference_CVOO). In the sub-DCM, it was apparent that the youngest and the middle-aged vortex had the lowest H' and richness of ASVs. The middle-aged eddy also stood out with the smallest alpha diversity measures in the OMZ. The concatenated sites, where the average diversity measure for each eddy and both reference sites was calculated, showed significant differences between the stations (Kruskal-Wallis $p < 0.01$) for both ASV richness and H' (Supplementary File 7). Especially, the middle-aged eddy CE_2019_18N_20W had the overall lowest H' (4.62) and ASV richness (1660), thus featured the protistan plankton community with the lowest alpha diversity across all layers (Figure 10). This eddy was also the only vortex with significant differences between the reference stations for both alpha diversity measures (Wilcoxon test with Bonferroni corrected $p < 0.01$). Furthermore, the same eddy had significantly lower H' compared to the oldest eddy (Wilcoxon with Bonferroni corrected $p < 0.01$; Supplementary File 7).

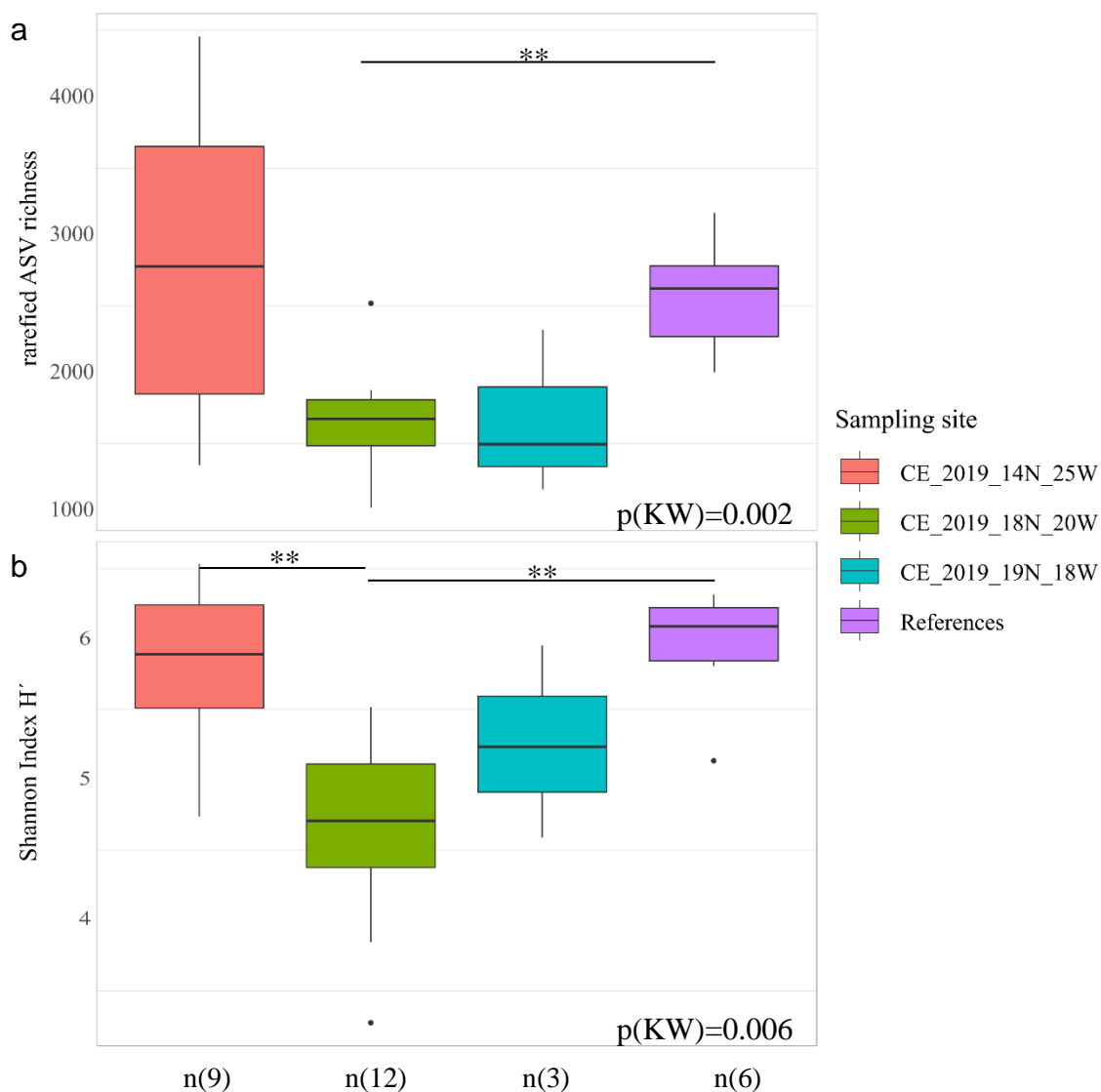


Figure 10. Boxplots visualizing alpha diversity measures. a) Rarefied ASV richness for concatenated eddy and reference samples over the depth layers. Pairwise Wilcoxon test revealed significant differences with $p < 0.01$ for two group comparisons highlighted by asterisks. b) Shannon Index H' for concatenated eddy and reference samples over the depth layers. Pairwise Wilcoxon test revealed significant differences with $p < 0.01$ for one group comparison highlighted by asterisks. The boxplot horizontal line represents the median value, whiskers represent the minimum and maximum values. Outliers are indicated as filled circles. KW: Kruskal Wallis; n: number of samples.

In a second step, it was investigated to which degree the three different eddies elevated the regional diversity of protistan plankton within the background waters (reference samples; Figure 11), due to the eddy-induced transport of entrapped protistan communities into offshore regions. All eddies increased the regional diversity considerably in terms of ASV richness. The decaying eddy had the highest increase in diversity (220% for Reference_CB and 171% for Reference_CVOO) and the youngest eddy showed the least effect (178% for Reference_CB and 146% for Reference_CVOO) on protistan ASV richness for the samples integrated over all depth layers. In general, the regional ASV richness increased more in deeper waters (sub-DCM,

OMZ) compared to the shallow DCM. The Shannon Index H' did not reflect the pattern and trend of the ASV richness. H' slightly increased or decreased with the introduction of an eddy entrapped community into the background waters (references). Especially the middle-aged eddy showed a decrease in diversity (H') in the sub-DCM and the OMZ when merged with the reference sites.

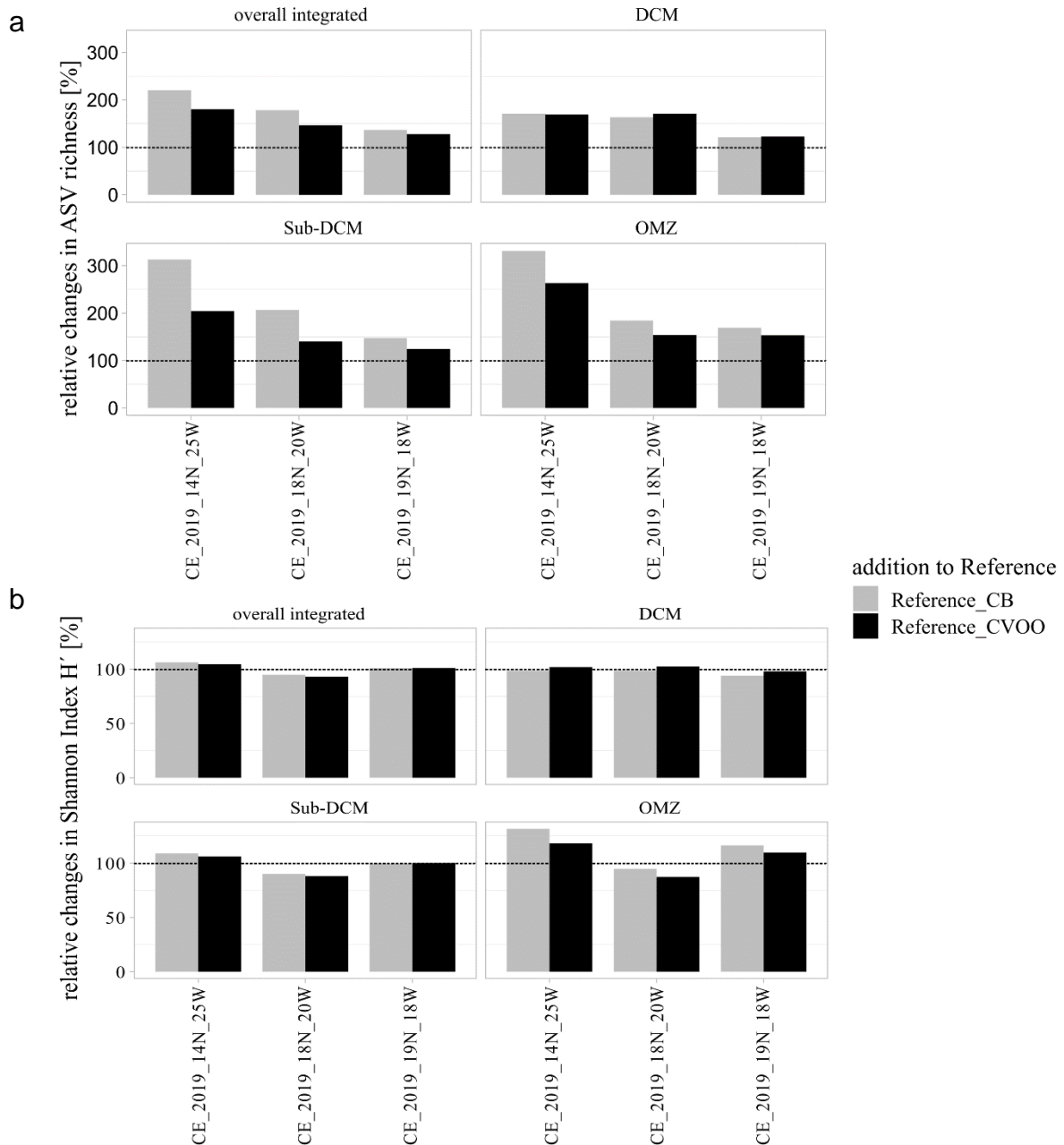


Figure 11. Bar plot showing changes in alpha diversity measures. a) Relative changes in Rarefied ASV richness after merging eddy and reference samples for the concatenated depth strata and for DCM, sub-DCM, and OMZ. b) Relative changes in Shannon Index H' after merging eddy and reference samples separately for the concatenated depth strata and for DCM, sub-DCM, and OMZ. 100% corresponds to no change and is indicated by the dotted line. DCM: deep-chlorophyll-maximum; OMZ: oxygen minimum zone.

3.1.4 Dissimilarities between Eddy Specific Protistan Plankton Communities

The BC dissimilarities of all samples were visualized in an NMDS (stress: 0.121; Figure 12) and tested for significant differences using PERMANOVA for the depth layers (DCM, sub-DCM, OMZ) and the individual sampling stations (References, Eddy 1, Eddy 2, and Eddy 3), as well as a combination thereof (Supplementary File 8). The protistan plankton communities displayed a distinct pattern along the NMDS axis 1, where the different depth strata (for eddies and references) were distributed. A significant gradient in the water column from the DCM towards the OMZ reaching from low to high axis 1 values was revealed (PERMANOVA, $p < 0.001$, $F=7.02$). The individual eddies and reference sites were mostly divided along the NMDS axis 2, with protistan communities from the stable 3-month-old eddy in the upper axis 2 value range (PERMANOVA, $p < 0.001$, $F=3.00$). The interaction term, which depicts the group differences within the depth strata between the distinct eddies and references revealed significant associations (PERMANOVA, $p < 0.001$, $F=2.00$). The young CE_2019_19N_18W eddy was associated with low axis 2 values and the decaying vortex was arranged as an intermediate. The samples of the two reference stations were as distinct as the samples of two different eddies. It should be noted that the plankton community structure of one sample from the oldest eddy (sample 1) differed severely from the two other samples of this eddy in the OMZ. Multiple physicochemical parameters were significantly correlated with the protistan plankton community structures ($p < 0.001$; Table 4). The depth gradient along the NMDS axis 1 from the sunlit DCM to the mesopelagic OMZ was positively correlated and fitted with a high correlation coefficient (> 0.87) to macronutrients (nitrate, phosphate, silicate). Fluorescence, temperature, salinity, and dissolved oxygen had significant negative correlations ($p < 0.001$; $R^2 > 0.68$) with the distribution from the DCM towards the OMZ strata. Neither of the environmental parameters surveyed had a pronounced association with the NMDS axis 2. Therefore, the abiotic factors responsible for the variation of the protistan plankton community structure within the individual eddy depth layers remained substantially concealed.

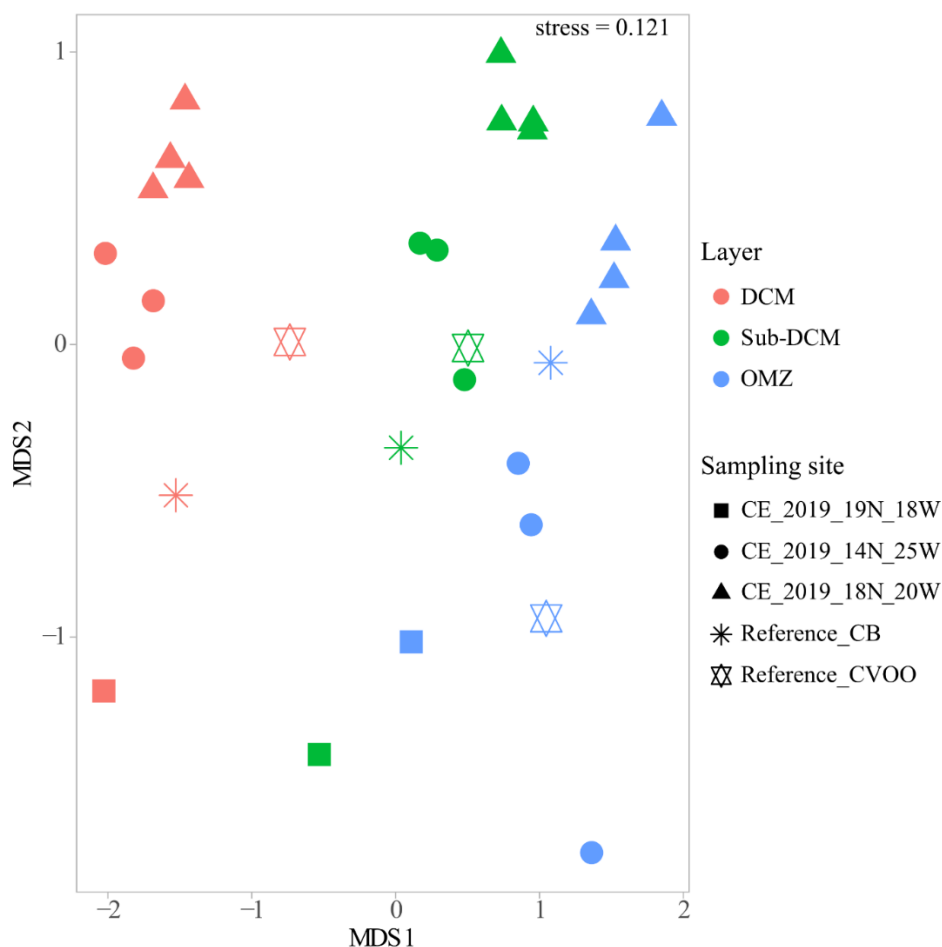


Figure 12. NMDS of protistan plankton community structures based on Bray-Curtis distances. The specific depth layers are colored and sampling sites are differentiated by symbols. DCM: deep-chlorophyll-maximum; OMZ: oxygen minimum zone.

Table 4. Correlation of the environmental parameters to the NMDS ordination. *Envfit* results of the physicochemical parameters. R^2 : coefficient of determination.

Parameter	NMDS1	NMDS2	R^2	p-value
Nitrate	0.85	-0.41	0.90	0.0001
Phosphate	0.84	-0.43	0.88	0.0001
Orthosilicic acid	0.85	-0.40	0.87	0.0001
Temperature	-0.84	0.48	0.93	0.0001
Salinity	-0.76	0.45	0.77	0.0001
Dissolved oxygen	-0.66	0.49	0.68	0.0001
Density	0.81	-0.47	0.88	0.0001
Fluorescence	-0.86	0.33	0.84	0.0001
Turbidity	-0.78	-0.12	0.62	0.0002

The construction of BC-based dendrograms provided a detailed insight of the protistan plankton community structure for the sampling stations in the three individual depth layers (Figure 13). The reference stations and all three eddies were divided into separate clusters in the DCM. Here, the community structure of the youngest eddy was most similar to the reference sites, followed by the decaying one. In the sub-DCM, the trapped protistan community of the oldest eddy samples formed a cluster with the references, suggesting a relatively high similarity between the decaying eddy and the non-eddy-influenced open ocean. The other two eddies (CE_2019_19N_18W and CE_2019_18N_20W) remained as distinct clusters. In the mesopelagic OMZ, all samples, except for the middle-aged eddy, converged into the same cluster.

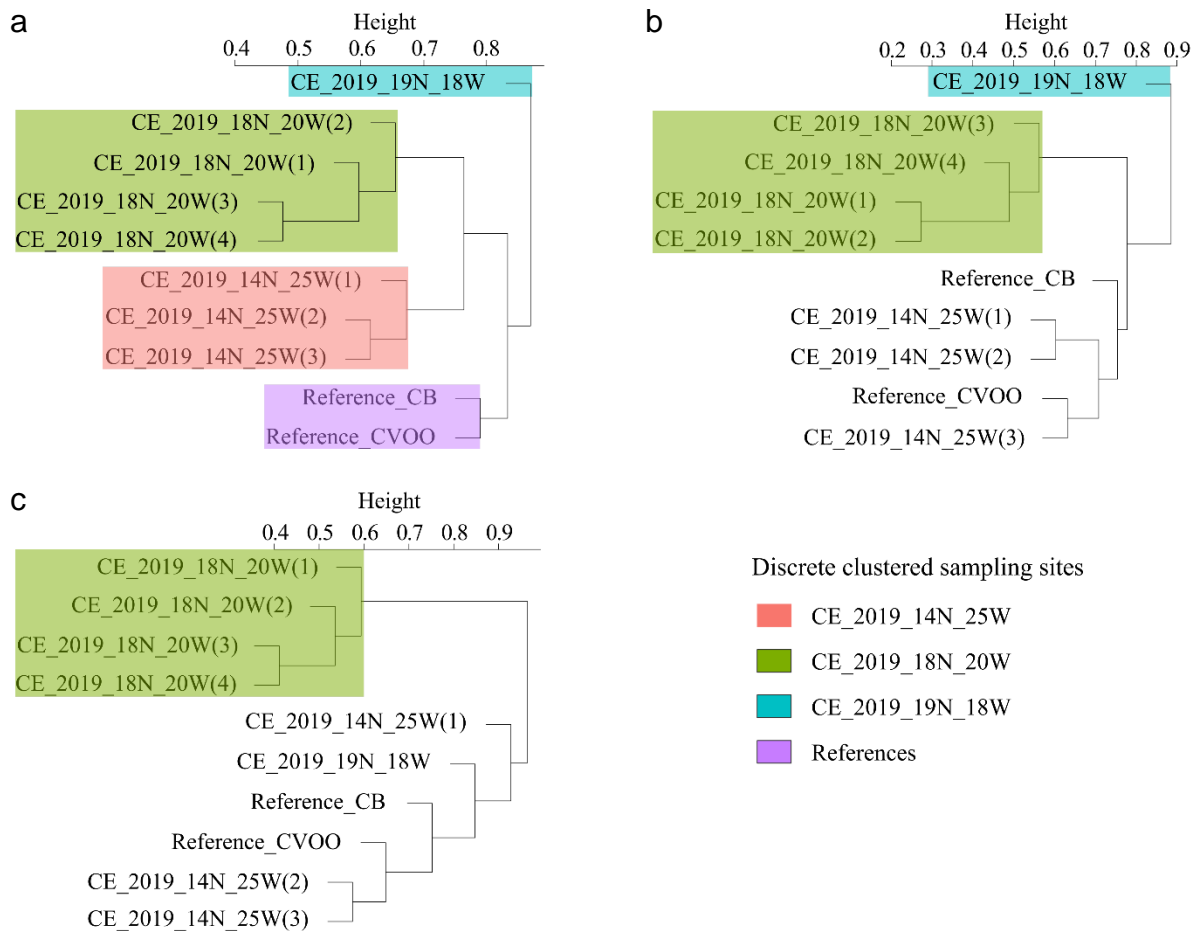


Figure 13. Beta-diversity dendrogram of protistan plankton community structures based on Bray-Curtis dissimilarities. a) DCM; b) sub-DCM; c) OMZ depth layers for all samples. Only the individual clusters of specific eddy samples or references are colored. DCM: deep-chlorophyll-maximum; OMZ: oxygen minimum zone.

3.1.5 Taxonomic Composition of Protistan Plankton Communities

The most abundant sequences, in terms of relative abundance of reads on the phylum level, were assigned to dinoflagellates in the DCM (Figure 14). They were in general followed by Radiolaria, Discoba and Haptophyta. Discrepancies of this rule were the higher proportion of sequences attributed to chlorophytes and a lower proportion of Discoba assigned sequences in the youngest eddy compared to all other samples. Similar patterns were observed in the sub-DCM and OMZ, which were dominated by dinoflagellates, radiolarians, Discoba and haptophytes. Below follows the description of the taxonomic inventory of these four most frequently encountered taxon groups at a higher taxonomic resolution (family level). Therefore, the taxonomic assignment of sequence reads for the eddy sampling station and depth layers were averaged, which enabled a streamlined description of the variation among the eddies, reference stations and the respective depth strata. As a rule, the differences between the taxonomic inventories were notably smaller among individual eddies and depth layers compared to the inter-sample comparison (Supplementary File 9).

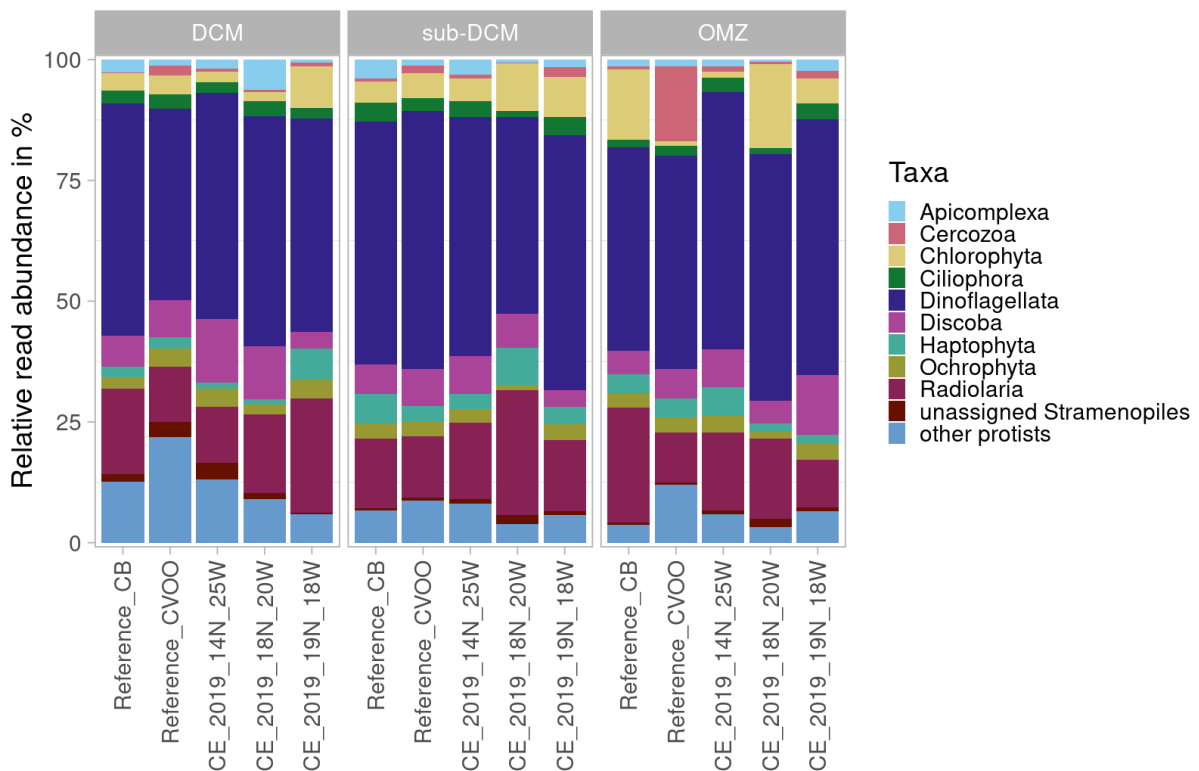


Figure 14. Taxonomic inventories of protistan plankton ASVs. The bars represent the relative abundance of ASVs assigned to each of the different taxon groups at the phylum-level. Only the top ten most abundant taxa are shown individually and the remaining taxa are grouped under other protists. DCM: deep-chlorophyll-maximum; OMZ: oxygen minimum zone.

Haptophyta (Figure 15): In the DCM, *Chrysochromulinaceae* and *Phaeocystaceae* were the most dominant families of haptophytes in all samples. The youngest eddy was characterized by a relative read abundance of nearly 90% of *Chrysochromulinaceae*. *Vice versa*, *Phaeocystaceae* were accordingly less abundant in the DCM compared to all other mesoscale features and the reference background waters in the DCM. This also applied to unassigned *Prymnesiophyceae*, accounting for roughly 25% of the non-disturbed-eddy samples and for 10% and 20% in eddies CE_2019_18N_20W and CE_2019_14N_25W, respectively. Interestingly, the HAP-clade-2 assigned sequences were marginal in all eddy DCM samples but represented 5% and 14% in Reference_CB and Reference_CVOO. The fraction of the HAP-clade-4 increased strikingly for the deeper sub-DCM waters. Especially in the background waters and the decaying eddy, but also, to a lesser extent, in the remaining eddies this taxon showed an increase in relative abundance. *Chrysochromulinaceae* declined substantially from DCM to sub-DCM in the young eddy CE_2019_19N_18W and was superseded by the HAP-clade-5 which dominated the sequence reads with a relative abundance of 43%. In the three months aged eddy CE_2019_18N_20W, *Phaeocystaceae* accounted for the majority of haptophyte assigned sequences with 81% in the sub-DCM.

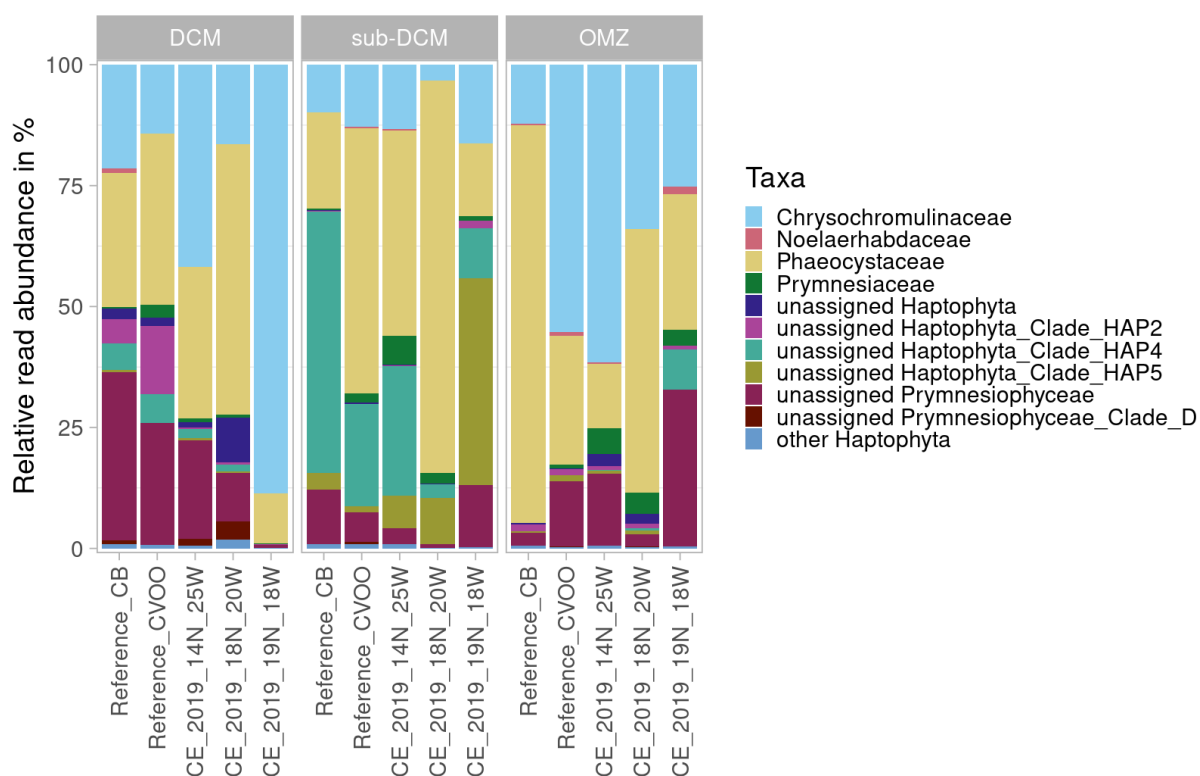


Figure 15. Taxonomic inventories of haptophyte-assigned ASVs. The bars represent the relative abundance of ASVs assigned to *Haptophyta* at the family-level. Only the top ten most abundant taxa are shown individually and the remaining taxa are grouped under other *Haptophyta*. DCM: deep-chlorophyll-maximum; OMZ: oxygen minimum zone.

Radiolaria (Figure 16): The most abundant radiolarians, regarding the relative sequence reads, were Spumellarida (unassigned and Spumellarida Group I) in all samples. A remarkable increase in Spumellarida Group I from the DCM to the sub-DCM and the OMZ was observed in all samples. Arthracanthida-Symphycanthida-unassigned and Collospheridae-assigned sequences had the highest proportion and together accounted for 63% of all radiolarian sequences in the DCM of the youngest eddy. The stable eddy CE_2019_18N_20W was characterized by its relatively high proportions of acantharean and RAD-B group in the DCM. Polycystinea (including Collodaria and Nassellaria) assigned sequences were negligible in most DCM samples but accounted for 21% and 16% in the collapsing eddy CE_2019_14N_25W as well as the CVOO background waters, respectively.

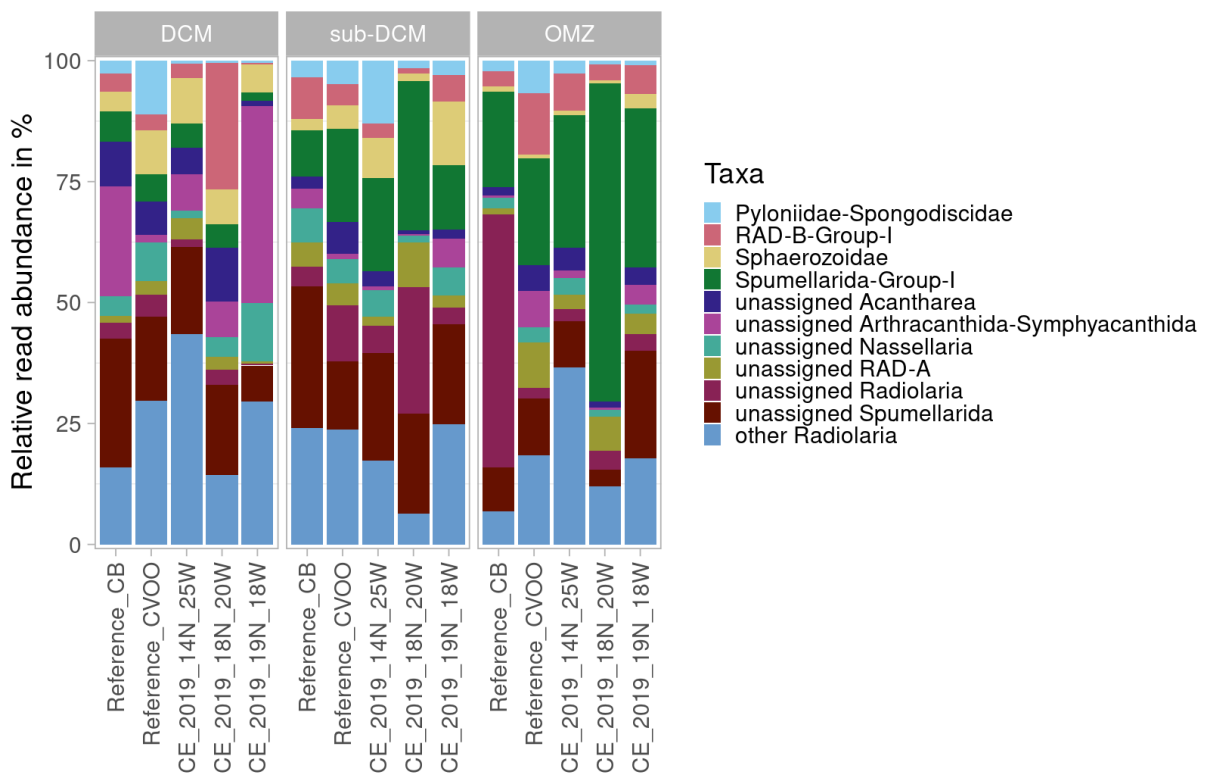


Figure 16. Taxonomic inventories of radiolarian-assigned ASVs. The bars represent the relative abundance of ASVs assigned to Radiolaria at the family-level. Only the top ten most abundant taxa are shown individually and the remaining taxa are grouped under other Radiolaria. DCM: deep-chlorophyll-maximum; OMZ: oxygen minimum zone.

Discoba (Figure 17): The predominant proportion of Discoba-assigned sequences, with up to 98% in the Reference_CB, were accounted to unassigned Diplonema, which could not be further classified. Noticeable deviations were found in the DCM and sub-DCM samples of the recently generated vortex CE_2019_19N_18W as well as the OMZ samples of the collapsing

eddy CE_2019_14N_25W, which distinguished themselves from the other samples by containing proportionately high abundances of deep-sea pelagic diplomonids (DSPD) group 1.

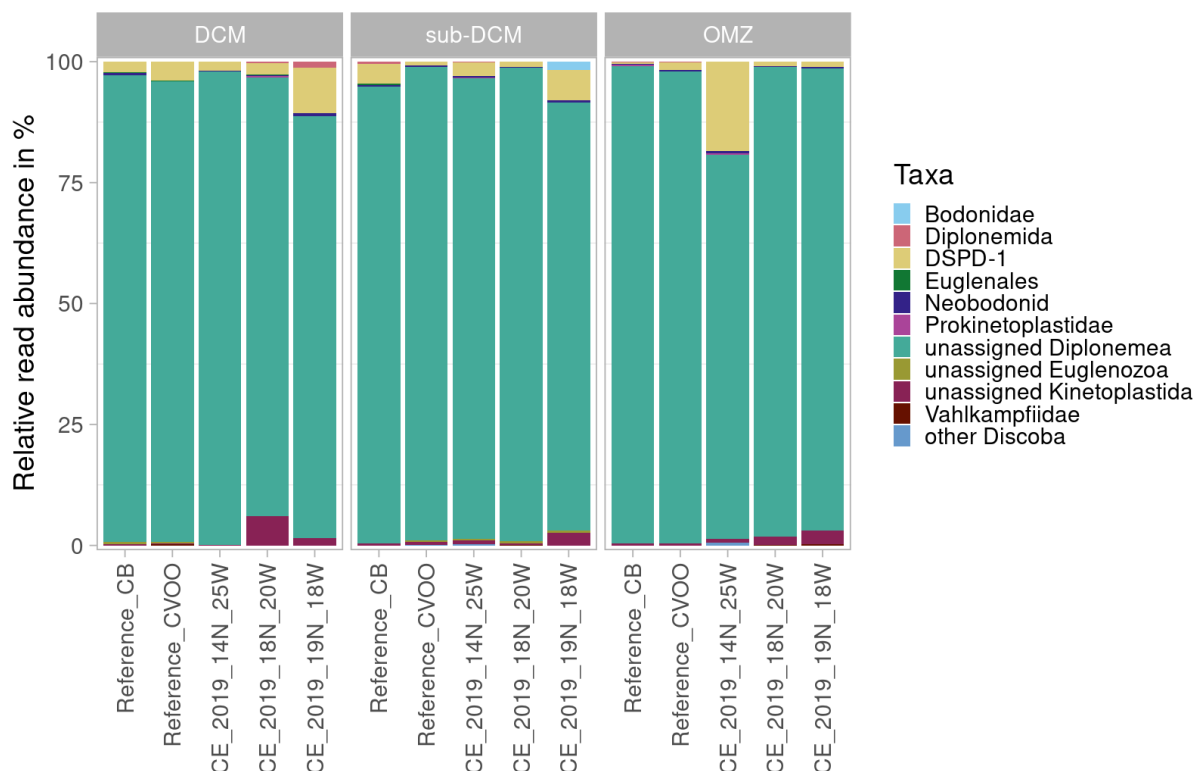


Figure 17. Taxonomic inventories of Discoba-assigned ASVs. The bars represent the relative abundance of ASVs assigned to Discoba at the family-level. Only the top ten most abundant taxa are shown individually and the remaining taxa are grouped under other Discoba. DCM: deep-chlorophyll-maximum; OMZ: oxygen minimum zone.

Dinoflagellata (Figure 18): The dinoflagellate community composition was relatively consistent in all eddies, reference waters and across all vertical water layers. They were generally dominated by the two taxonomic clades Dino-Group I and Dino-Group II (also termed Marine Alveolates Group I and II or Syndiniales Group I and II). In distinction to the other samples, the youngest eddy had prevalent sequence reads of the Dino-Group-III, particularly in the sub-DCM. The relatively high fraction of unassigned Dinophyceae, which includes numerous ecologically distinct orders, decreased from DCM to sub-DCM and OMZ. The increase of unassigned dinoflagellates, that also escaped further taxonomic classification, from DCM to sub-DCM and OMZ in all samples is also notable. However, both taxa, unidentified Dinophyceae and dinoflagellates, accounted for up to 43% (DCM of Reference_CB) of all dinoflagellate sequences in the region under study.

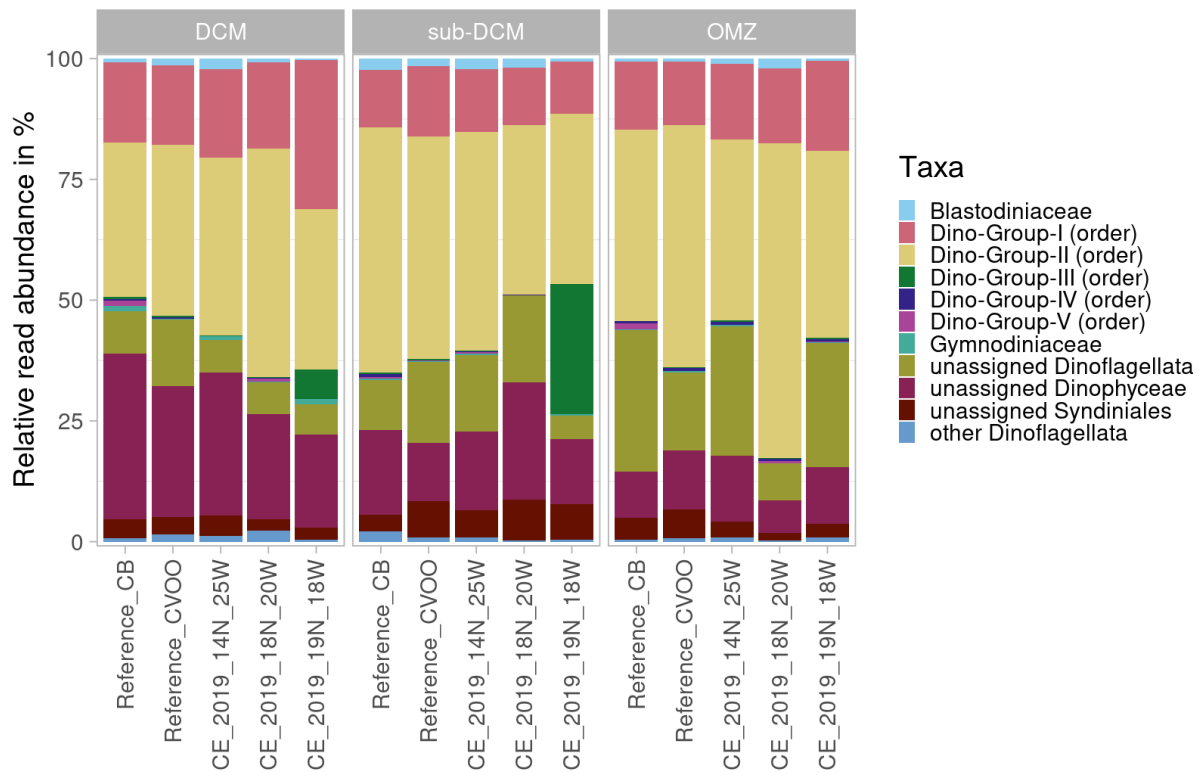


Figure 18. Taxonomic inventories of dinoflagellate-assigned ASVs. The bars represent the relative abundance of ASVs assigned to Dinoflagellata at the family-level. Only the top ten most abundant taxa are shown individually and the remaining taxa are grouped under other Dinoflagellata. DCM: deep-chlorophyll-maximum; OMZ: oxygen minimum zone.

3.2 Functional Annotation of Protistan Plankton Communities

3.2.1 Validation of Functional Trait Approach

The public trait database was aligned to the taxonomically assigned ASV table resulting in a reduced dataset that covered approximately 15% of the sequences and about 16% of the targeted ASVs. In the first step, the authenticity of the condensed ASV dataset was inspected by comparing the distribution of shared ASVs of the complete and the downscaled ASV-to-sample matrix for individual eddies and the non-eddy-disturbed reference sites (Figure 19). The proportion of shared ASVs (between the investigated groups) never exceeded 1% and the average variation remained below 0.3%.

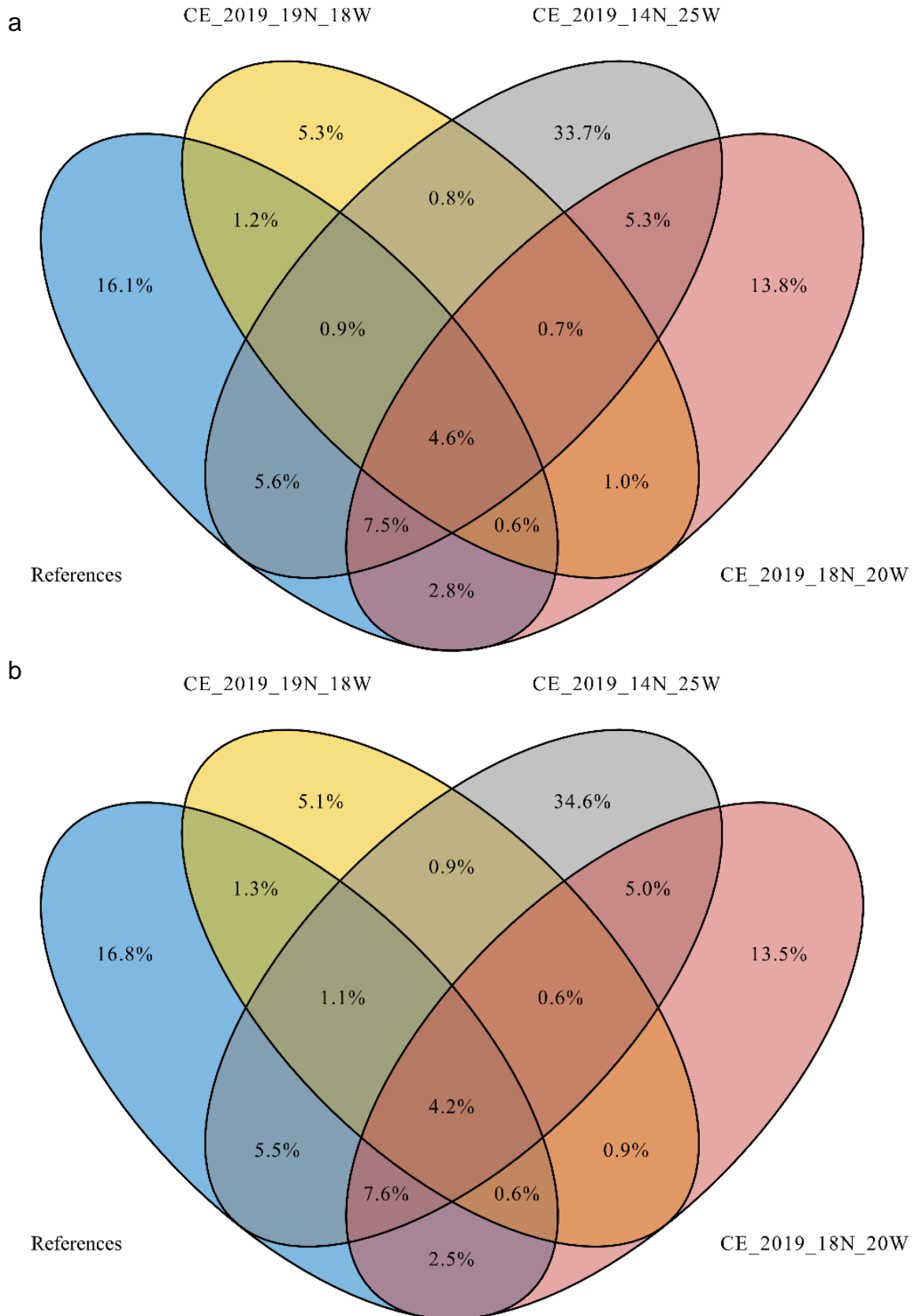


Figure 19. Venn diagrams for the distribution of the shared and unique ASVs. a) Unique and common ASV distribution in the three eddies and reference sites calculated for the original ASV-to-sample matrix. b) Unique and common ASV distribution in the three eddies and reference sites calculated for the reduced ASV-to-sample matrix after alignment to the trait-database.

A second verification step was performed using the BC dissimilarities of the downscaled protistan plankton community (Figure 20) to determine whether analogous patterns to those in the initial dataset could be observed (see Figure 12). Samples from the three depth layers DCM, sub-DCM and OMZ (including the reference samples) were still distributed predominantly along NMDS axis 1. The protistan community structures for the individual stations still followed a gradient along axis 2. The stable eddy CE_2019_18N_20W remained in the upper axis 2 co-domain and the decaying eddy CE_2019_14N_25W continued its occupation as the intermediate position between the other two eddies. Sample 2 in the DCM of the collapsing vortex lied outside the intermediate position, as well as sample 1 in the OMZ of the same eddy was invariably different compared to the other two OMZ samples. However, a notable alteration was the convergence of the youngest eddy CE_2019_19N_18W from the lower axis 2 value range to a more medial localization. The plankton structure of the two reference sites within each individual depth layer was still as dissimilar to each other as the samples of two discrete eddies. Albeit the exact pattern shifted to some extent, the PERMANOVA analysis still confirmed significant effects of the depth layers ($p < 0.001$, $F=5.39$) and the sampling sites ($p < 0.001$, $F=2.33$), as well as a combination thereof ($p < 0.001$, $F=1.65$), on the protistan plankton community structure (Supplementary File 10).

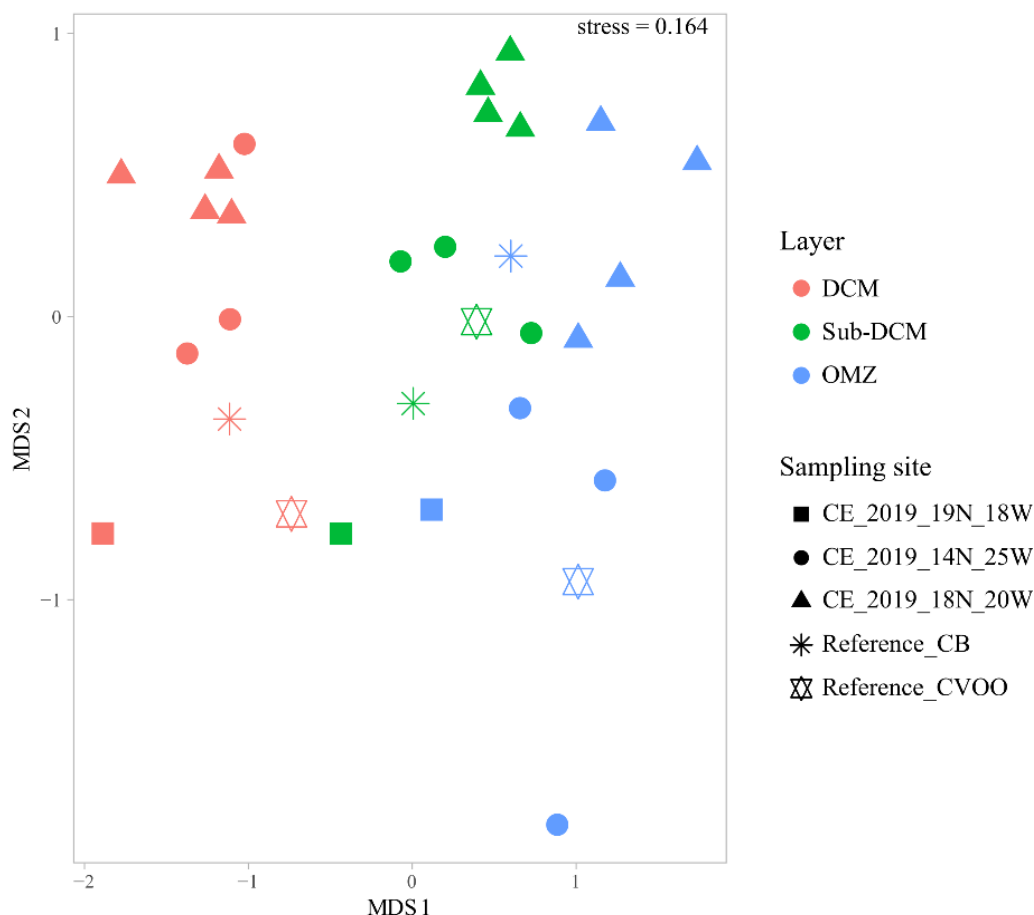


Figure 20. NMDS of downscaled protistan plankton community structures based on Bray-Curtis distances. The specific depth layers are colored and sampling sites are differentiated by symbols. DCM: deep-chlorophyll-maximum; OMZ: oxygen minimum zone.

3.2.2 Functional Richness of Protistan Plankton Communities

Functional diversity was determined by the proxy functional richness, an index ranging between 0 and 1. The values were generally high reaching up to 0.81 (maximum in the sub-DCM Sample 1 of eddy CE_2019_14N_25W) and with the lowest functional richness of 0.64 (minimum in the sub-DCM Sample 2 of the eddy CE_2019_18N_20W). After integrating the samples of the distinct eddy and reference sites, the peak functional richness was observed for the non-eddy-disturbed background waters (0.74 ± 0.04), followed by the disintegrating eddy (0.73 ± 0.04) and the youngest vortex (0.70 ± 0.02 ; Figure 21). The species of the protistan plankton community in the three-month-old eddy CE_2019_18N_20W (0.69 ± 0.06) occupied the least niche space. Subsequent statistics using Kruskal-Wallis ($p < 0.05$) and the post hoc Wilcoxon test revealed significant differences between the background waters and the robust eddy CE_2019_18N_20W ($p < 0.05$; Supplementary File 11 a).

There were no considerable differences in functional richness between the DCM, sub-DCM and OMZ of the individual sampling sites (Supplementary File 11 b). The average values for functional richness were 0.71 ± 0.03 for the DCM, 0.7 ± 0.05 for the sub-DCM and 0.73 ± 0.04 for the OMZ.

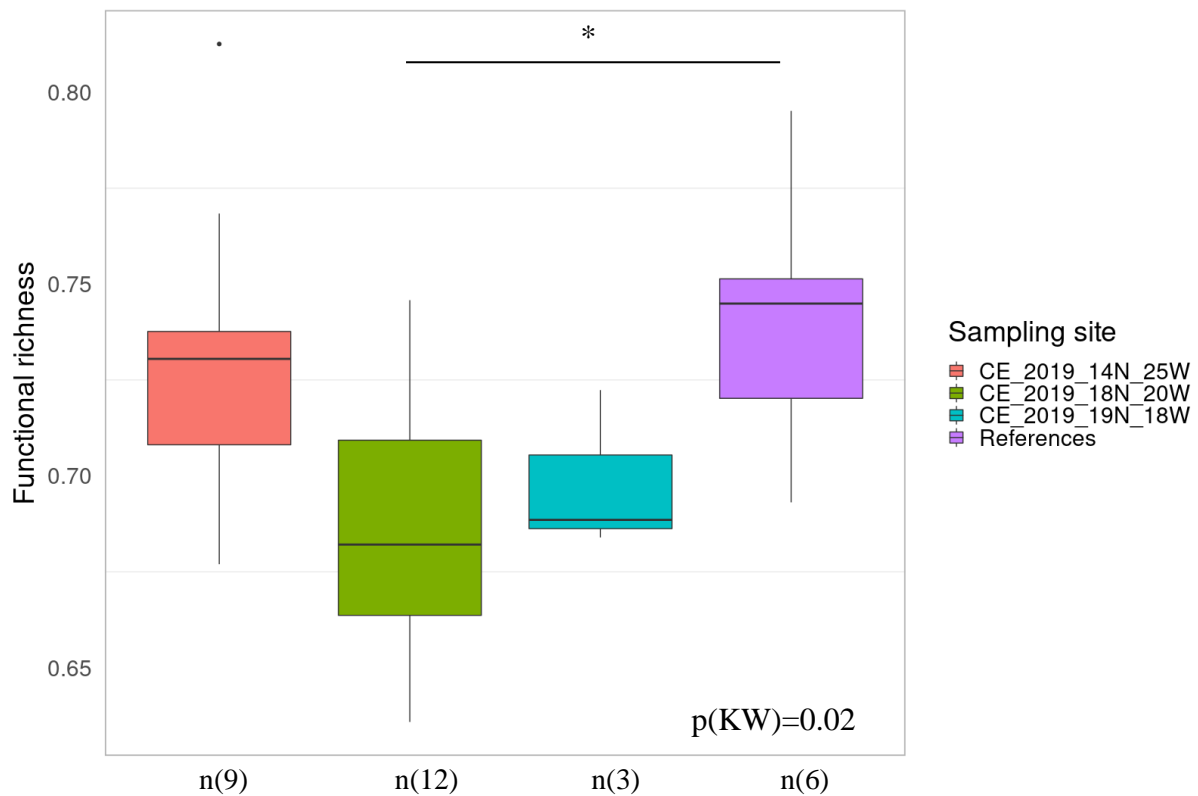


Figure 21. Boxplot visualizing functional richness derived from the functional traits. Functional richness calculated for eddy and reference samples merged over the depth layers. Pairwise Wilcoxon test revealed significant differences with $p < 0.05$ for one group comparison highlighted by an asterisk. The boxplot horizontal line represents the median value, whiskers represent the minimum and maximum values. Outliers are indicated as filled circles. KW: Kruskal Wallis; n: number of samples.

Correlations between the functional richness and the alpha diversity determinants (ASV richness and Shannon Index H') substantiated the results computed for the functional diversity index (Table 5). The Spearman correlation coefficient was applied to qualitatively diagnose the consensus between the used functional diversity index and the alpha diversity measurements. The coherence was investigated for all sampling stations and the individual depth layers. All analyses were significant ($p < 0.05$) and revealed a 'moderate' or 'very strong' correlation degree ($\rho > 0.63$) except for the OMZ samples. Despite not being significant ($p > 0.05$), the coherency of these mesopelagic waters was 'fair' between functional richness and the alpha diversity measurements ($\rho = 0.48$ for Shannon Index H' ; $\rho = 0.5$ for ASV richness).

Table 5. Statistics for Spearman correlation between functional richness and the alpha diversity measurements. Grading of ρ was done following Chan et al. (2003). FR: functional richness; H' : Shannon Index; ρ : Spearman correlation coefficient.

Samples	FR vs. H'			FR vs. ASV richness		
	ρ	p-value	Grading	ρ	p-value	Grading
All samples	0.63	<0.001	Moderate	0.74	<0.001	Moderate
DCM	0.77	0.014	Very strong	0.84	0.004	Very strong
Sub-DCM	0.77	0.014	Very strong	0.79	0.010	Very strong
OMZ	0.48	0.204	Fair	0.50	0.143	Fair

3.2.3 Functional Strategies of Protistan Plankton Communities

Ecological strategies or functional groups were generated using partition clustering with the K-means algorithm and the SSI-criterion on the trait-assigned ASV matrix. The grouping results identified ten distinct clusters (Supplementary File 12) with a unique combination of annotated traits (Supplementary File 13). In some ES, categories were represented by multiple characteristics, yet some were dominated by certain traits (Table 6).

Table 6. Dominant features of ecological strategies (ES). Main traits of the ten ES and examples derived from taxonomic composition at the family and phylum levels.

ES	Dominant traits	Examples; Family (Phyla)
1	Ingestion: extern; Motility: attached; Polarity: heteropolar; Symbiosis: parasitic Symmetry: bilateral	Porosporidae (Apicomplexa); Blastodiniaceae (Dinoflagellata); Cephaloidophoridae (Apicomplexa)
2	Chloroplast: endosymbiotic; Cover: siliceous; Ingestion: intern; Motility: floater; Polarity: heteropolar; Shape: amoeboid; Symmetry: radial	Acanthodesmoidea (Radiolaria); Plagiacanthoidea (Radiolaria); Eureyrtidioidea (Radiolaria)

Table 6 (continued).

3	Motility: swimmer; Shape: round; Polarity: heteropolar	Pelagomonadaceae (Ochrophyta); Kareniaceae (Dinoflagellata); Suessiaceae (Dinoflagellata)
4	Cover: naked; Ingestion: intern; Motility: gliding; Shape: amoeboid; Symmetry: asymmetrical	Paramoebidae (Lobosa); Monosigidae (Choanoflagellida); Filoreta (Cercozoa);
5	Chloroplast: constitutive; Cover: organic; Motility: swimmer; Polarity: heteropolar; Shape: round; Symmetry: bilateral	Phaeocystaceae (Haptophyta); Mamiellaceae (Chlorophyta); Prymnesiaceae (Haptophyta)
6	Chloroplast: endosymbiotic; Cover: strontium sulfate; Ingestion: intern; Motility: floater; Polarity: isopolar; Shape: amoeboid	Gigartaconidae (Radiolaria); Sticholonchidae (Radiolaria); Class Acantharea (Radiolaria)
7	Ingestion: intern; Motility: swimmer; Polarity: heteropolar	Massiteriidae (Cercozoa); Colepidae (Ciliophora); Gonyaulacaceae (Dinoflagellata);
8	Chloroplast: endosymbiotic; Colony: elongated; Cover: siliceous; Ingestion: intern; Motility: floater; Shape: round; Symmetry: spherical	Sphaerzoidae (Radiolaria); Collophidiidae (Radiolaria); Polar-centric-Mediophyceae (Ochrophyta)
9	Ingestion: intern; Polarity: heteropolar; Shape: elongated	Stephanocidae (Choanoflagellida); Tintinnidae (Ciliophora); Radial-centric-basal- Coscinodiscophyceae (Ochrophyta)
10	Cover: organic Ingestion: osmotrophic; Shape: round	Labyrinthulaceae (Sagenista); Pseudoperkinsidae (Mesomycetozoa); Chytriodiniaceae (Dinoflagellata)

The proportional contribution of these functional groups was calculated for the eddies and reference sites in all three depth layers (Figure 22). All ten ecological strategies (ES 1-10) were represented in each of the samples. The high abundance of ES 6 was prominent, especially in the DCM layer of Reference_CB (38%) and the youngest eddy (32%). The functional properties of ES 6 were best described by the following traits: endosymbiotic chloroplast, mostly strontium-sulfate cell cover, internal ingestion, floater, isopolar, amoeboid body shape, macro size class, with spicules. All ASVs assigned to this group were radiolarians with the top five most abundant ASVs assigned to Arthracanthida-Symphycanthida, Acantharea-Group-I, *Gigartacon muelleri*, Acantharea-Group-II, *Sticholonche*. Another prevalent group was ES 5 in reaching more than half of the relative abundance of the stable eddy in the sub-DCM. ES 5 was characterized by having constitutive chloroplasts, a round body shape with typically organic cell cover and predominantly by a free-swimming motion type. The top five ASVs contributing most to the relative abundance of ES 5 belonged to *Phaeocystis* (haptophyte), *Pterosperma cristatum* (chlorophyte), Prymnesiophyceae (haptophyte), Mamiellaceae (chlorophyte) and *Chrysochromulina scutellum* (haptophyte). A noticeable abundance peak was observed for the ES 9 of Reference_CVOO, which accounted for the majority of relative abundance with a value of 42%. The unique combination of attributes of ES 9 predominantly included: chloroplast-free, with a siliceous or organic cell cover, an internal ingestion, mostly attached or occasionally swimmers, heteropolar, with an elongated body shape, macro-sized and with spicules. The top five most abundant ASVs in ES 9 were taxonomically assigned to Tintinnidae and *Dictyocysta* (both ciliates), Stephanoecidae Group H and Group I (both choanoflagellates) and the diatom *Actinocyclus* (ochrophyte). The only functional group characterized by a parasitic lifestyle was ES 1, which had the highest contribution in the three-month-old stable eddy with up to 35% in relative abundance (DCM). The most frequent ASVs were Porosporidae (Apicomplexa), *Blastodinium mangini* and *Hematodinium* (both dinoflagellates) and *Cephaloidophora* (Apicomplexa). The relatively high proportions of ES 7 in the deeper water layers (sub-DCM with 17% and OMZ with 18%) of the youngest eddy and the OMZ of the Reference_CVOO were noteworthy. Distinguishing features of ES 7 were best described by the following trait combinations: mostly chloroplast-free, mostly naked with occasional organic cell cover, internal ingestion, swimmer, heteropolar, round to elongated body shape, nano to macro size class, and no spicules. The top five most abundant ASVs that were typical for ES 7 were taxonomically assigned to *Cryothecomonas* (cercozoan), *Pelagostrobilidium* (ciliate), *Ciliophrys* (ochrophyte), *Gonyaulax* (dinoflagellate) and Planomonadidae Group-1 (Hilomonadea).

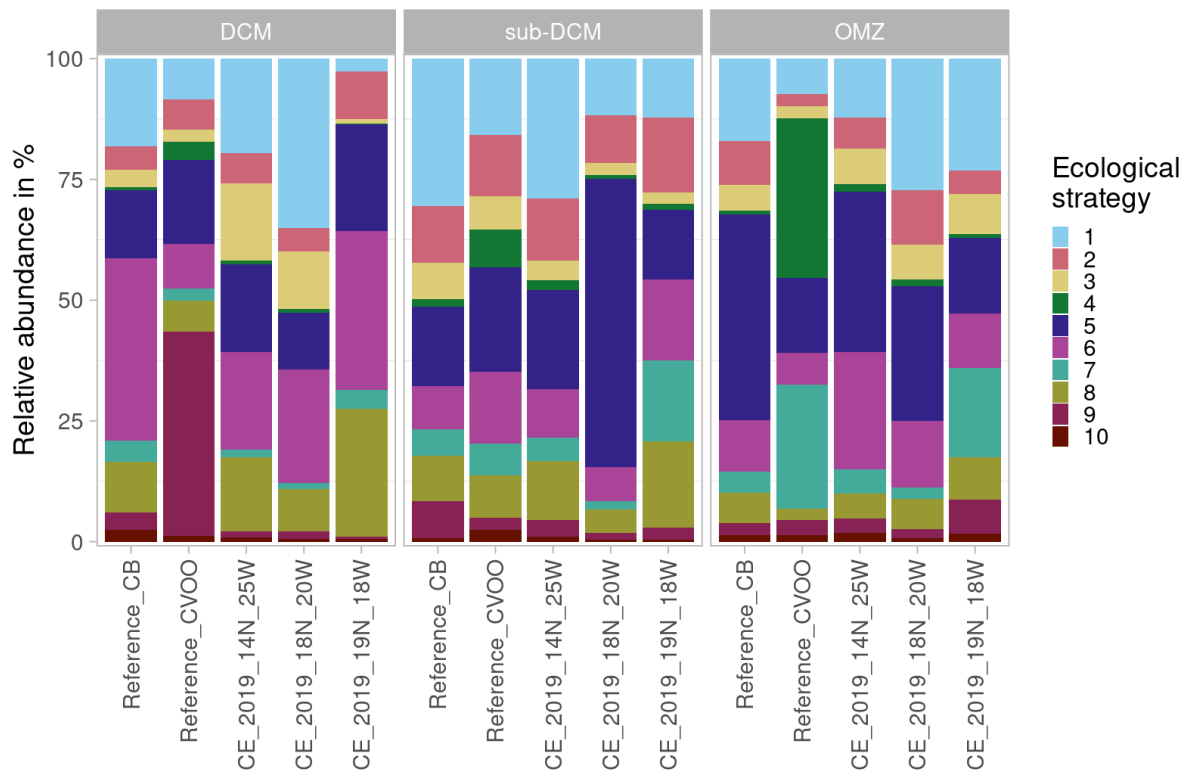


Figure 22. Ecological strategies distribution for sampling sites and depth layers. The bars represent the relative abundance of ASVs assigned to individual ecological strategies. DCM: deep-chlorophyll-maximum; OMZ: oxygen minimum zone.

Subsequent statistical analysis (Kruskal-Wallis and post hoc Wilcoxon test) revealed significant variations between the combined depth strata for the stable eddy with each sampling site (Table 7). The aged eddy had significantly lower relative abundances in three ES groups (ES 7, ES 9 and ES 10) compared to the non-eddy-impacted references. Likewise, the three-month-aged eddy had significantly lower relative abundances of ASVs assigned to the ES 10 compared to the other two eddies and reference sites and in ES 7 compared to the youngest vortex. No significant differences in ES groups were found between the disintegrating and the freshly generated eddy. Furthermore, no significant deviations were detected between those two eddies compared to the non-eddy-impacted references.

Table 7. Significant differences between ecological strategies (ES) of the sampling stations. Kruskal Wallis test (KW), followed by pairwise Wilcoxon test was used to calculate significant differences.

ES	Group 1	Group 2	p (KW)	Adjusted p-value
10	CE_2019_18N_20W	CE_2019_14N_25W	0.0006	0.004
10	Reference	CE_2019_18N_20W		0.001
7	CE_2019_18N_20W	CE_2019_19N_18W	0.0003	0.026
7	CE_2019_18N_20W	CE_2019_14N_25W		0.034
7	Reference	CE_2019_18N_20W		0.001
9	Reference	CE_2019_18N_20W	0.0079	0.019

Only two ES showed significant differences across depth strata (Table 8). These disparities were only observed between the DCM and the other two depth strata and no significant differences between OMZ and sub-DCM were detected. The ES 6 was more frequently represented in the DCM compared to both the OMZ and the sub-DCM. In the OMZ, ES8 was also found to be significantly less abundant compared to the DCM.

Table 8. Significant differences between Ecological strategies (ES) of the depth layers Kruskal Wallis test (KW), followed by pairwise Wilcoxon test was used to calculate significant differences. DCM: deep-chlorophyll-maximum; OMZ: oxygen minimum zone.

ES	Group 1	Group 2	p (KW)	Adjusted p-value
6	DCM	sub-DCM	0.0024	0.0006
6	DCM	OMZ		0.0345
8	DCM	OMZ	0.0011	0.0002

3.3 Microbial Abundances & Carbon Flow in the Canary Current System

3.3.1 Prokaryotic & Protistan Abundances

Abundances of both prokaryotic and protistan cells, declined severely with depth from the photic DCM layer (maximum in the youngest eddy with $18.85 \pm 1.86 \times 10^5$ prokaryotes mL⁻¹ and 1734 ± 562 protists mL⁻¹) to the mesopelagic OMZ layer (minimum in the Reference_CVOO with $3.86 \pm 0.86 \times 10^4$ prokaryotes mL⁻¹ and 497 ± 40 protists mL⁻¹;

Supplementary File 14). This decline occurred within all individual sampling sites in varying degrees, nevertheless, considerable fluctuations existed between the stations and depth strata (Figure 23). In the DCM bacterial concentrations decreased from the youngest eddy ($18.85 \pm 1.86 \times 10^5$ cells mL⁻¹) to the stable eddy ($14.98 \pm 1.26 \times 10^5$ cells mL⁻¹), to the reference sites ($3.05 \pm 1.11 \times 10^5$ cells mL⁻¹) and finally to the collapsing eddy ($2.34 \pm 0.55 \times 10^5$ cells mL⁻¹). Identical patterns were observed in the sub-DCM and the OMZ, albeit with an average reduction in concentrations of approximately $71 \pm 16\%$ and $78 \pm 12\%$ compared to the photic DCM, respectively. Protistan abundance patterns varied between the shallow depth layer and the deeper waters. In the DCM, the mean number of cells decreased in the following order of precedence: youngest eddy ($1734 \pm 562 \times 10^5$ cells mL⁻¹), stable eddy ($1460 \pm 341 \times 10^5$ cells mL⁻¹), collapsing eddy (1392 ± 267 cells mL⁻¹) and reference sites (775 ± 234 cells mL⁻¹). The succession for the deeper waters was, in descending order of cell concentration, collapsing eddy, to stable eddy, to youngest eddy and finally the non-eddy-disturbed background waters. The decline in concentrations of protists with increasing depth was less drastic compared to the prokaryotic reduction and reached about $35 \pm 17\%$ and $44 \pm 12\%$ on average for the sub-DCM and the OMZ compared to the shallow DCM, accordingly. Statistical analyses are presented in Supplementary File 15 and significant differences ($p < 0.05$) are emphasized in Figure 23.

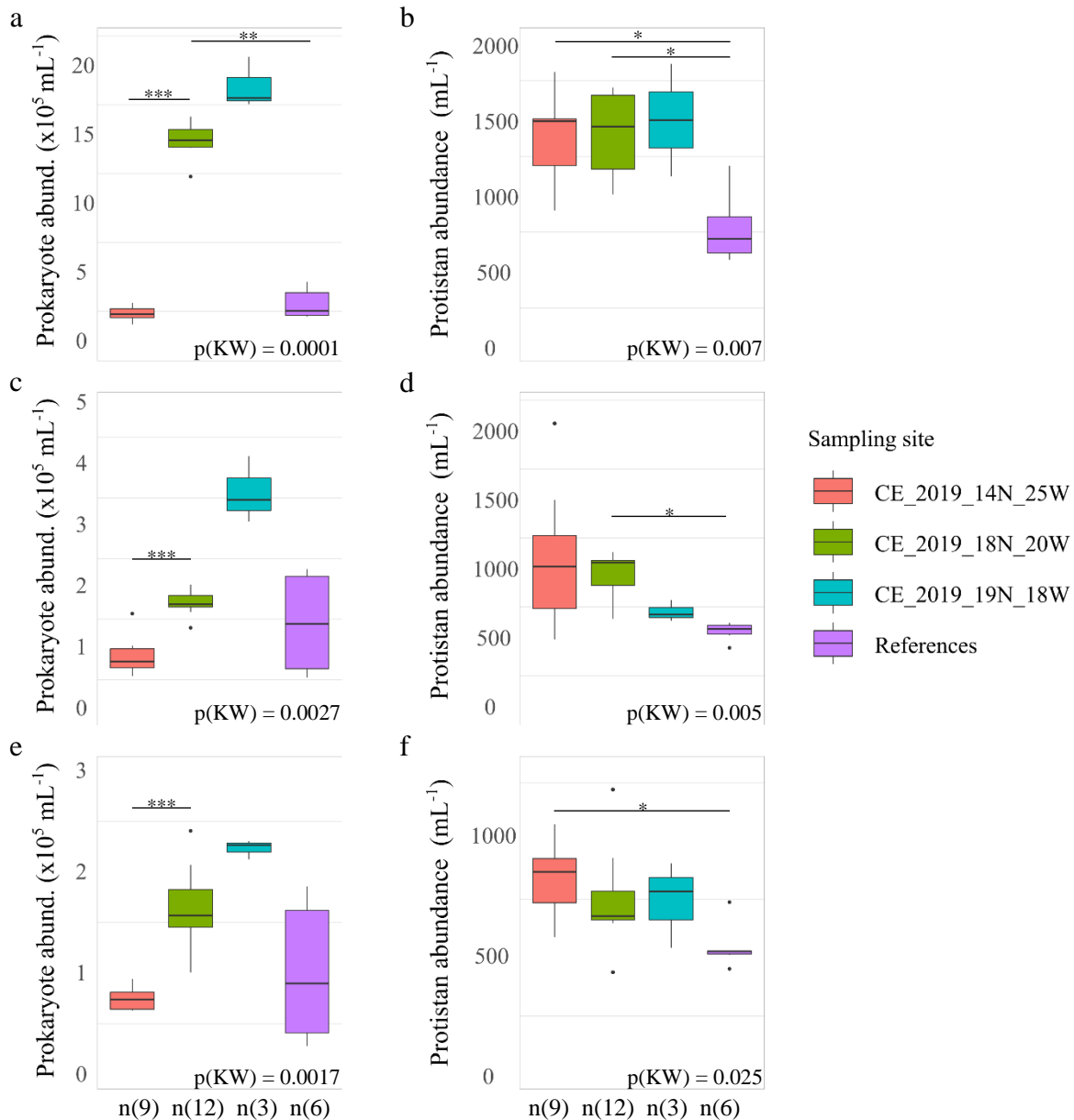


Figure 23. Boxplots visualizing abundances of prokaryotes (a, c, e) and protists (b, d, f). The concentrations for the individual depth layers are represented in a, b for DCM; c, d for sub-DCM; e, f for OMZ. The boxplot horizontal line represents the median value, whiskers represent the minimum and maximum values. Outliers are indicated as filled circles. Significant variations were first identified using Kruskal-Wallis (KW) test with ad hoc pairwise Wilcoxon test and are highlighted by asterisks (*: $p < 0.05$; **: $p < 0.01$; ***: $p < 0.001$). abund.: abundance; DCM: deep-chlorophyll-maximum; OMZ: oxygen minimum zone; n: number of samples.

3.3.2 Grazing Effect & Carbon Flow

A decline in phagocytosed prokaryotes and carbon transfer efficiency with depth was determined for all discrete eddies (Figure 24). The carbon flow is omitted from the description because it displayed precisely the same behavior as the grazing effect but can be viewed in detail in Supplementary File 14 or in Figure 24. The general pattern of decreasing grazing effect was ranked from the youngest to oldest eddy. The magnitude of ingested bacteria varied greatly

within each depth layer. In the shallow DCM, 7784 ± 2194 cells mL⁻¹ h⁻¹ were devoured by all protists in the 3-week-old eddy, 2543 ± 746 cells mL⁻¹ h⁻¹ in the stable 3-month-old eddy and only 453 ± 194 cells mL⁻¹ h⁻¹ in the disintegrating eddy. This accounted for prokaryotic turnover rates of 10%, 4%, and 5% d⁻¹, respectively. A remarkable decrease in the grazing effect was observed in the second oldest vortex with about 90% (269 ± 85 cells mL⁻¹ h⁻¹) in the sub-DCM, albeit with minor changes in the turnover rate with $\sim 3\%$ d⁻¹. The ingested bacteria diminished moderately to 6192 ± 1784 cells mL⁻¹ h⁻¹ and to 148 ± 62 cells mL⁻¹ h⁻¹ for the youngest and collapsing eddy, correspondingly. A minuscule grazing effect compared to the freshly generated eddy (3126 ± 868 cells mL⁻¹ h⁻¹) was observed for the two aged eddies with approximately 90 ± 38 cells mL⁻¹ h⁻¹. Deviations from the generic reduction with depth occurred in the integrated reference sites and demonstrated a peculiar trend. The sub-DCM (1162 ± 1225 cells mL⁻¹ h⁻¹) had the highest grazing effect followed by a slight decrease in the deeper OMZ (1103 ± 1249 cells mL⁻¹ h⁻¹) and with the lowest value in the DCM (959 ± 864 cells mL⁻¹ h⁻¹). The tremendously large standard deviations occurred on account of the fact that both reference sites exhibited quite differing results (Supplementary File 14). Reference_CVOO followed the general decline of grazing effect within deeper waters and had marginal amounts of phagocytosed prokaryotes (DCM: 190 ± 39 cells mL⁻¹ h⁻¹; sub-DCM 48 ± 4 cells mL⁻¹ h⁻¹; OMZ: 18 ± 4 cells mL⁻¹ h⁻¹). On the other hand, Reference_CB, with the atypical pattern, had more than 100-fold of magnitude higher grazing effects. In the epipelagic DCM and sub-DCM, the increase in the number of bacteria ingested was less severe compared to the mesopelagic OMZ, but still reached an approximately 10- and 50-fold higher value, respectively. Statistical analyses are provided in Supplementary File 15 and significant differences ($p < 0.05$) are indicated in Figure 24.

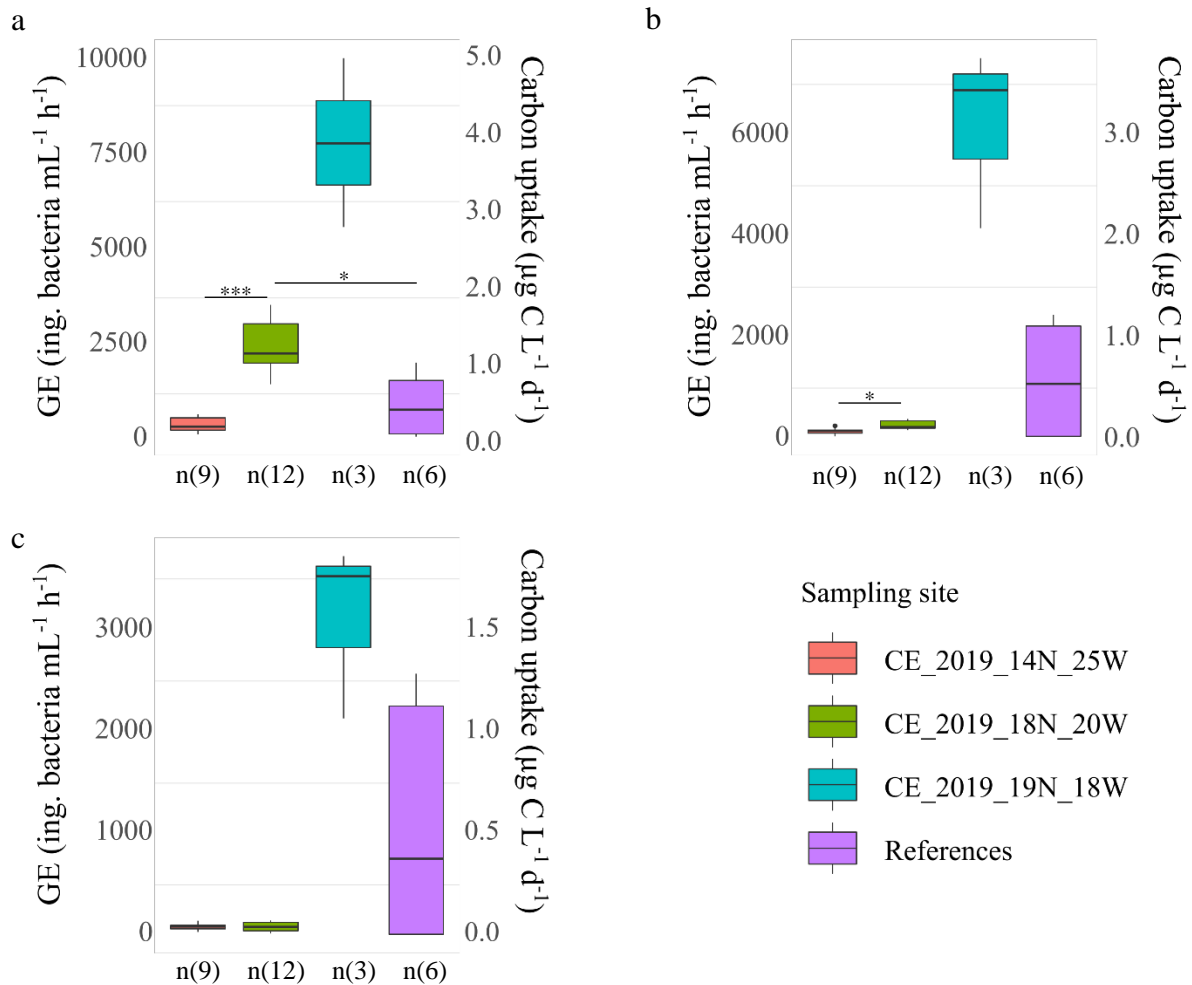


Figure 24. Boxplot visualizing grazing effect and carbon flow. The results for the individual depth layers are represented in a for DCM; b for sub-DCM; c for OMZ. The boxplot horizontal line represents the median value, whiskers represent the minimum and maximum values. Outliers are indicated as filled circles. Significant variations were first identified using Kruskal-Wallis test (DCM: $p = 0.0003$; sub-DCM: $p = 0.0091$; OMZ: $p = 0.0741$) with ad hoc pairwise Wilcoxon test and are highlighted by asterisks (*: $p < 0.05$; **: $p < 0.01$; ***: $p < 0.001$). GE: grazing effect; ing.: ingested; C: carbon; DCM: deep-chlorophyll-maximum; OMZ: oxygen minimum zone; n: number of samples.

3.3.3 Correlation Analysis

Correlation analysis was applied using the Spearman rank test to identify significant correlations between the physicochemical parameters and the prokaryotic and protistan abundances as well as the grazing effect (Figure 25). Nutrients (phosphate, nitrate, orthosilicic acid) correlated negatively with the microbial abundances and the determined grazing effect (Spearman $\rho < -0.57$; $p \leq 0.01$). Temperature, salinity, and turbidity were positively correlated with the microbial parameters (Spearman $\rho > 0.6$, $\rho > 0.48$, $\rho > 0.52$ respectively; $p < 0.05$). Likewise, fluorescence had a strong significant association to the protistan abundance (Spearman $\rho = 0.81$; $p < 0.001$) and a moderate linkage to the bacterial abundance and the

grazing effect (Spearman $\rho = 0.61$, $p = 0.45$, respectively, $p < 0.05$). Dissolved oxygen had no significant correlation with the respective microbial parameters ($p > 0.05$). The microbial measurements were interconnected and the correlation analysis revealed a strong association between the grazing effect and the prokaryotic abundance (Spearman $\rho = 0.86$; $p < 0.001$). Less pronounced coefficients were calculated for the correlation between the protistan abundance and the grazing effect (Spearman $\rho = 0.48$; $p < 0.05$), and similarly for the protistan and bacterial abundances (Spearman $\rho = 0.52$; $p < 0.01$).

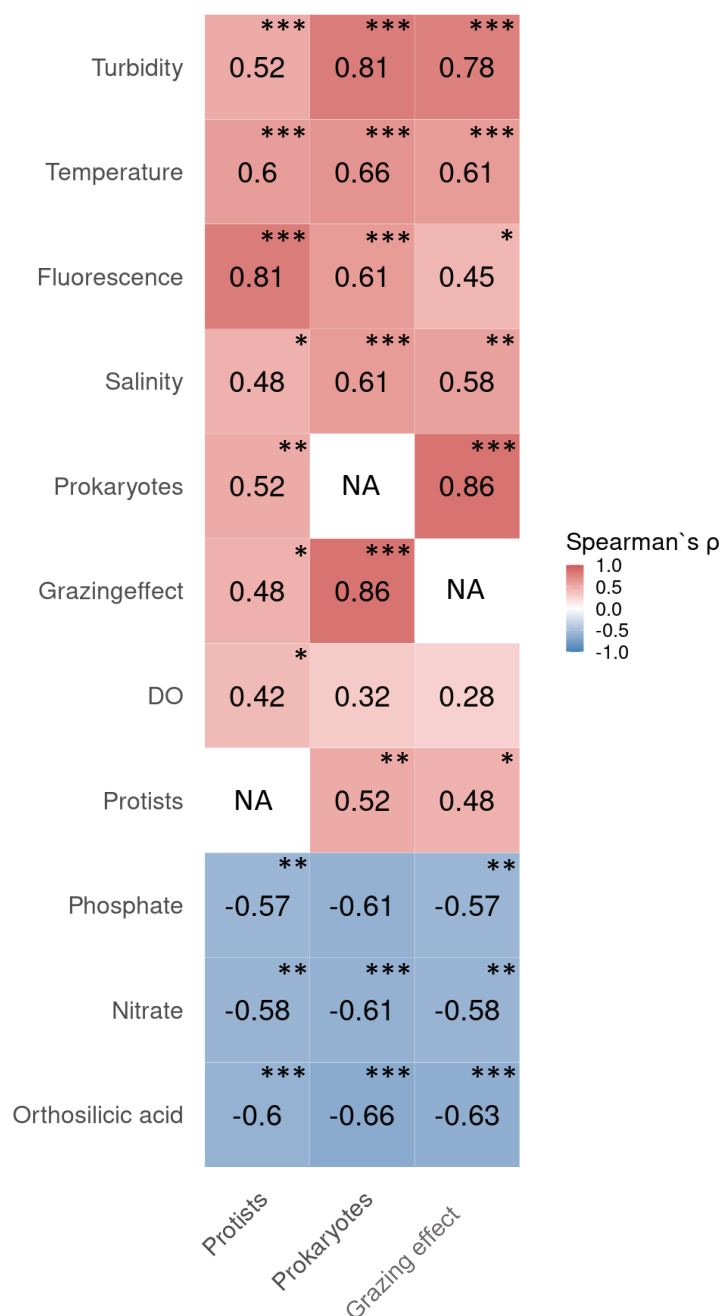


Figure 25. Correlation of physicochemical parameters, grazing effect, prokaryotic and protistan abundances. Color scale represents Spearman's ρ ; and not applicable (NA). Significant correlations are highlighted by asterisks (*: $p < 0.05$; **: $p < 0.01$; ***: $p < 0.001$). DO: dissolved oxygen; NA: not applicable.

3.3.4 Multiple Linear Regression

Multiple linear regression was used for comprehending the influence and the interaction of physicochemical parameters as well as the possibility of predicting the microbial measurements. To reduce collinearity, models were built for each depth layer, separately. The most parsimonious models to explain microbial cell abundance (prokaryotes and protists) and grazing effect with the prerequisite of residual normal distribution and marginal multicollinearity were selected (Table 9). For most investigated dependent variables in combination with the individual depth layers, models could be generated. The only exceptions were the models of the sub-DCM layer, where protistan cell abundance and grazing effect as dependent variable did not satisfy the requirements (parsimony and residual normal distribution). The coefficient of determination (R^2) varied greatly for the individual regressions and reached from 0.27 to 0.94 for the OMZ with protistan abundance as dependent variable and the DCM with prokaryotic cell counts as dependent variable, respectively. Overall, the model for prokaryotic concentrations had the highest coefficient of determination (R^2 : DCM, 0.94; sub-DCM 0.64; OMZ, 0.85), followed by the grazing effect (R^2 : DCM, 0.90; OMZ, 0.74). The least explanations were found in the DCM and the OMZ for the protistan cell abundances with a coefficient of determination of 0.60 and 0.27, accordingly.

Table 9. Multiple linear regression model statistics. The respective models were investigated for normal distribution of residuals with the Kolmogorov-Smirnov test (KS). R^2 , coefficient of determination. NA: not applicable; DCM: deep-chlorophyll-maximum; OMZ: oxygen minimum zone.

Model	p(KS)	F-statistics	Adjusted R^2	p-value
DCM bacteria	0.81	74.15	0.94	***
Sub-DCM bacteria	0.18	16.18	0.64	***
OMZ bacteria	0.97	31.62	0.85	***
DCM protist	0.51	20.54	0.60	***
Sub-DCM protist			NA	
OMZ protist	0.99	5.80	0.27	**
DCM grazing	0.11	48.41	0.90	***
Sub-DCM grazing			NA	
OMZ grazing	0.75	38.51	0.74	***

(*: $p < 0.05$; **: $p < 0.01$; ***: $p < 0.001$)

The environmental parameters were highly collinear, and many (up to 6) explanatory variables had to be removed to acquire acceptable VIFs. The remaining physicochemical drivers in their most parsimonious combination were unique for each depth strata and explanatory variable (Table 10). Prokaryotic abundance in the DCM were best explained by salinity (~42% of R²), silicate (~42% of R²), nitrate concentration (~11%) and three interaction terms (salinity x nitrate; silicate x nitrate; salinity x silicate), together accounting for only ~5% of R². In the sub-DCM, only two factors (turbidity and fluorescence) and a combination thereof remained in explaining the bacterial concentration. For the same dependent variable in the OMZ, nitrate (~30% of R²), oxygen concentration (~28% of R²), turbidity (~20% of R²) and an interaction between turbidity and oxygen (~16% of R²) were the most influential parameters. For the protistan cell abundance and the grazing effect regression analysis in the mesopelagic OMZ, only two factors (salinity and bacterial abundance; turbidity and salinity, accordingly) remained in each case and no interaction terms improved the AIC value. Likewise, for the model in the photic DCM describing protistan cell concentrations two independent variables remained (turbidity and temperature). For the same shallow depth layer, turbidity, salinity, temperature, silicate, and nitrate concentrations explained the grazing effect in the best modality following the parsimony principle.

Table 10. Physicochemical parameters and the interaction terms of the respective models based on parsimony generation. Variance inflation factors (VIF) were only inspected before adding interactions to the model. SE: standard error; R²: coefficient of determination; NA: not applicable; DCM: deep-chlorophyll-maximum; OMZ: oxygen minimum zone.

Model	Drivers	Estimate (\pm SE)	p-value	VIF	Relative importance of R ² in %
DCM bacteria	Intercept	1824.5 (\pm 260.8)	***	/	/
	Salinity (Sal)	-49.5 (\pm 7.1)	***	1.69	42.2
	Orthosilicic acid (OA)	-1481.3 (\pm 600.7)	*	2.56	41.6
	Nitrate (Nit)	245.7 (\pm 116.8)	*	2.99	11.4
	Sal:Nit	-6.8 (\pm 3.2)	*	/	1.9
	OA:Nit	1.3 (\pm 0.4)	**	/	1.8
	Sal:OA	40.4 (\pm 16.5)	*	/	1.2

Table 10 (continued).

Sub-DCM bacteria	Intercept	-36.8 (± 12.7)	**	/	/
	Turbidity (T)	-36.8 (± 12.7)	**	1.12	67.4
	Fluorescence (F)	516.4 (± 168.5)	**	1.12	22.7
	T:F	-6481.7 (± 2951.4)	*	/	9.9
OMZ bacteria	Intercept	63.9 (± 8.7)	***	/	/
	Nitrate	-0.4 (± 0.05)	***	5.41	30.1
	Oxygen (Oxy)	-0.9 (± 0.2)	***	3.69	28.2
	Turbidity (T)	-551.0 (± 100.1)	***	3.85	19.8
	Protistan conc.	0.8 (± 0.3)	**	1.14	5.8
	T:Oxy	10.0 (± 2.2)	***	/	16.2
DCM protist	Intercept	-3093.8 (± 945.0)	**	/	/
	Turbidity	11088.4 (± 1747.6)	***	1.26	82.5
	Temperature	143.77 (± 39.0)	**	1.26	17.5
Sub-DCM protist	NA				
OMZ protist	Intercept	68910.4 (± 21258.6)	**	/	/
	Salinity	-1935.1 (± 602.7)	**	1.63	58.5
	Bacteria conc.	187.7 (± 65.0)	**	1.63	41.5
DCM grazing	Intercept	2.2×10^5 ($\pm 5.9 \times 10^4$)	**	/	/
	Turbidity	1.7×10^4 ($\pm 1.0 \times 10^4$)	0.090	5.58	38.0
	Salinity	-5632.5 (± 1566.1)	**	6.22	24.0
	Temperature	-664.9 (± 166.1)	***	3.06	15.0
	Orthosilicic acid	-2099.6 (± 367.5)	***	4.75	15.0
	Nitrate	118.6 (± 89.8)	0.200	5.84	8.8
Sub-DCM grazing	NA				
OMZ grazing	Intercept	-1.7×10^5 ($\pm 7.6 \times 10^4$)	*	/	/
	Turbidity	1.4×10^5 ($\pm 2.7 \times 10^4$)	***	1.78	64.1
	Salinity	4377 (± 2182)	0.056	1.78	35.9

(*: $p < 0.05$; **: $p < 0.01$; ***: $p < 0.001$)

3.3.5 Model Validation

The accuracies of the models for predicting the measured microbial parameters fluctuated considerably depending on the variable and the depth layers. The regression analysis for the bacterial abundance yielded a high coefficient of determination ($R^2 > 0.72$; $p \leq 0.006$) and were evaluated with a substantial accordance ($CCC = 0.97$) between measured and predicted values (Table 11, Figure 26.a). The precisions of the models to predict protistan concentrations (Figure 26.b) had a moderate strength of agreement with a CCC of 0.92. The computed regression coefficients were likewise moderate for both depth layers (DCM, $R^2 > 0.51$, $p = 0.037$; OMZ, $R^2 > 0.59$, $p = 0.021$).

Table 11. Regression analysis of measured and predicted values. Coefficient of determination (R^2) and significance of regression analysis for the predicted parameters in each depth layer if applicable. DCM: deep-chlorophyll-maximum; OMZ: oxygen minimum zone.

Regression	R^2	p-value
DCM bacteria	0.87	< 0.001
Sub-DCM bacteria	0.87	< 0.001
OMZ bacteria	0.72	0.006
DCM protist	0.51	0.037
OMZ protist	0.59	0.021
DCM grazing	0.84	0.001
OMZ grazing	0.59	0.021

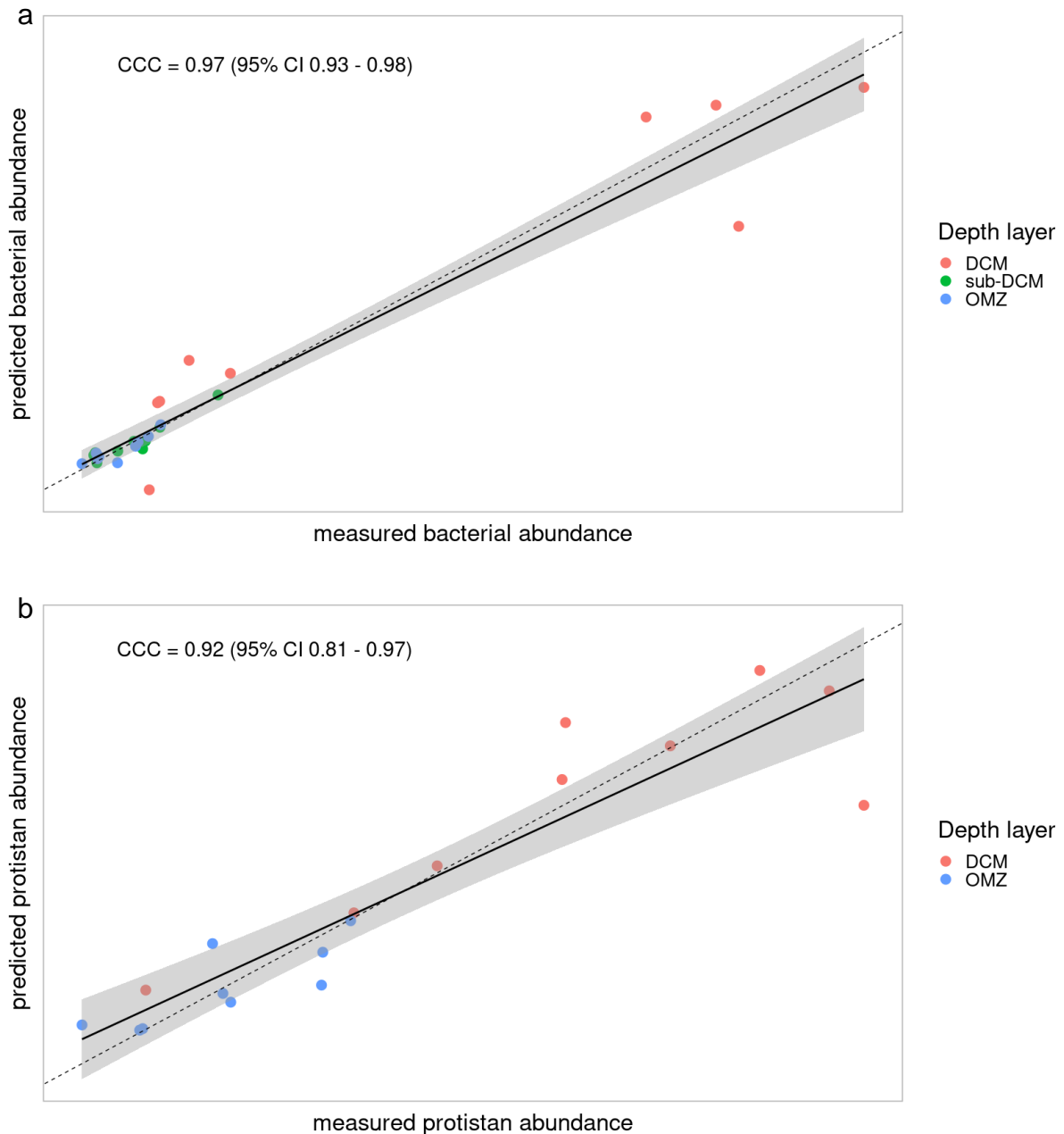


Figure 26. Predicted versus measured prokaryote abundance (a) and protistan abundance (b) using the multiple linear regression models for the respective depth layers. CCC with 95% CI are added. The dotted line indicates a perfect prediction, the black line and the grey area the depth integrated regression line and 95% confidence intervals, respectively. CCC: concordance correlation coefficient; CI: confidence interval; DCM: deep-chlorophyll-maximum; OMZ: oxygen minimum zone.

The validation of the grazing effect models produced the most unprecise predictions (CCC=0.58; Figure 27). Especially in the OMZ, the correlations between prediction and measured values were poor ($R^2 > 0.59$; $p = 0.021$). On the other hand, the DCM model had a high correlation between measured and predicted grazing effects ($R^2 > 0.84$; $p = 0.001$). After the removal of two outliers (>3 times standard deviation for the respective depth layer) the

evaluation of McBride's strength-of agreement criteria changed from poor (CCC = 0.58) to a substantial accordance (CCC = 0.97).

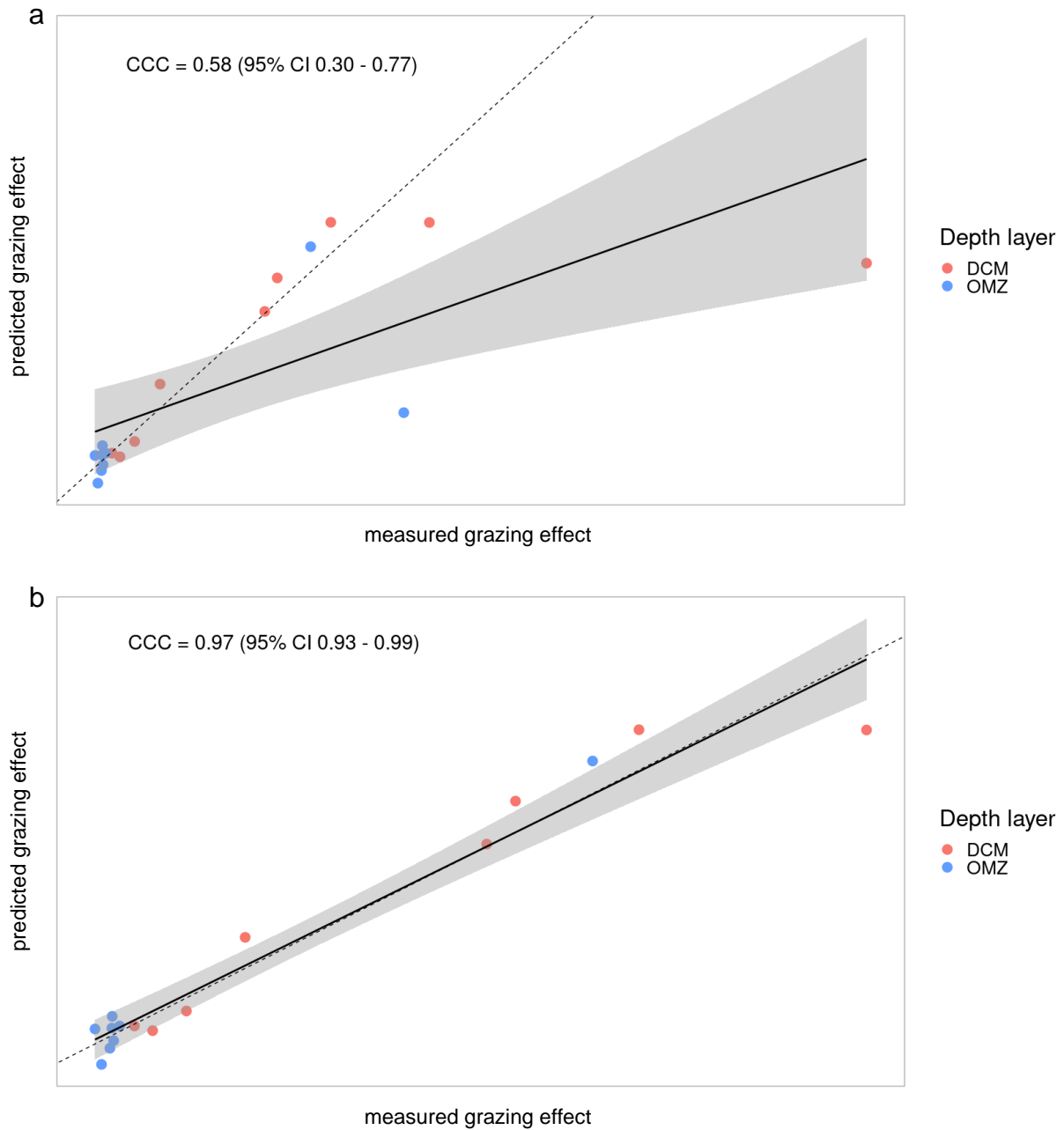


Figure 27. Predicted versus measured grazing effect with (a) and without outliers (b) using the multiple linear regression models for the respective depth layers. CCC with 95% CI are added. The dotted line indicates a perfect prediction, the black line and the grey area the depth integrated regression line and 95% confidence intervals, respectively. CCC: concordance correlation coefficient; CI: confidence interval; DCM: deep-chlorophyll-maximum; OMZ: oxygen minimum zone.

4 Discussion

4.1 Effect of Eddies on the Protistan Plankton Community

4.1.1 *Eddy Dispersal Enhances Regional Protistan Plankton Diversity*

Theories elucidating the irregularities in the overall trend of increasing diversity from poleward to equatorward regions are numerous (Ibarbalz et al., 2019). Most of them have their eligibility, but cannot fully account for all variability (Pianka, 1966). First theories like the ‘productivity hypothesis’ and the ‘climatic stability hypothesis’ were predominantly declined due to ‘the paradox of enrichment’ (Connell and Orias, 1964; Klopfer, 1959; Riebesell, 1974; Tubay et al., 2013). EBUS provides clear examples for this paradox with their negative correlation between productivity and diversity in coastal compared to offshore regions. However, this enigma can be explained seemingly plausible. EBUS with variable nutrient input via upwelling promotes the growth of rapidly growing species, which can lead to the dominance of individual species or even phytoplankton blooms and thereby exhibit a low diversity (Barton et al., 2010; James et al., 2022; Pitcher et al., 2018, 2017; Vallina et al., 2014). This corresponds well with this thesis’ findings of an analogous relationship between diversity (ASV richness) and generation time of the eddies as well as the higher diversity determined in the background waters as hypothesized in H_{E1.1}. Furthermore, this study coincides with the ‘intermediate disturbance/dispersal hypothesis’ which states that the highest diversity occurs in an ecosystem with a certain level of disruption/dispersal (Connell, 1978; Mouquet and Loreau, 2003). The results showed that through dispersal of the entrapped water masses in an eddy (disruption), the regional diversity of the subtropical oceanic offshore region was enhanced.

Dispersal mechanisms, responsible for structuring community composition and altering diversity patterns, are postulated in ecological theory and emphasized as crucial factors (Cadotte, 2006; Grainger and Gilbert, 2016; Yamaguchi, 2022). Mouquet and Loreau (2003) theorized that until a certain tipping-point, an increasing rate of dispersal corresponds to an increase in alpha-diversity, while regional beta-diversity declines. Model-based estimations associate highly diverse ocean regions with ocean circulations due to the divergence from steady-state conditions to subtle variability by providing niche space and refuges (‘environmental heterogeneity hypothesis’; Barton et al., 2010; Huisman, 2010; Stein et al., 2014). Extending approaches in numerical simulations, with respect to mesoscale eddy activity, predicted western boundary currents as locally driven plankton diversity hotspot in contrast to EBUS as dispersal-driven diversity hotspots (Clayton et al., 2013). However, the authors

assumed that eddy dynamics contribute not only to the dispersal of immigrant plankton types but also harbor the role of niche segregation for both the immigrant and local plankton communities (Chust et al., 2013; Clayton et al., 2013). Using the ecosystem model framework DARWIN to determine the effect of eddy advection on local and regional phytoplankton diversity likewise confirmed Mouquet's and Loreau's hypothesis (Lévy et al., 2014). This thesis provides the first circumstantial evidence for the dispersal-driven mechanism on the protistan plankton diversity structure in the CanCS.

The detection of an increase in protistan plankton diversity was simulated by combining protistan communities from reference samples with the protistan communities introduced to the oligotrophic offshore regions by eddy dynamics. Through this mirrored eddy dispersal, an increase in the ASV richness could be determined for all water layers. However, the Shannon Index H' demonstrated minor changes in comparison to the ASV richness and even decreased for the combination of the aged eddy CE_2019_18N_20W and the reference samples. This peculiar finding is possibly explained by the parameters contributing to the calculation of the Shannon Index H' , which lays emphasis not only on the richness but also on the evenness of the community (Spellerberg and Fedor, 2003; Shannon and Weaver, 1949). Thus, a protistan plankton community with high species (ASV) richness and low evenness was prevalent after merging of the stations, which might be related to the progressive changes in aging eddies. Another viable scenario is that the eddy was in the process of disintegrating, a possibility indicated by the ellipsoidal shape and the lack of accurate ADCP data of the oldest eddy. Therefore, the oldest eddy may have already mingled with background water, exhibiting similar dominant species (ASVs) as the reference sites leading to the decrease in H' . CE_2019_18N_20W was also the only eddy which originated from the coast of Senegal potentially harboring a variety of rare immigrant plankton species resulting in the raised ASV richness.

The DCM exhibited the most pronounced variations in the protistan plankton communities between the eddies. With increasing depth (sub-DCM and OMZ), the community structure gradually converged, which is congruent with the abiotic parameters of the sampled sites as hypothesized in H_E1.2. The physicochemical parameters also corroborated well with the general characteristics of young cold core eddies with generally lower temperatures, salinity and pronounced fluorescence (Belkin et al., 2022; Dilmahamod et al., 2021). The sub-mesoscale and fine-scale structure of especially young eddy cores can include multiple water masses with distinct abiotic properties which, of course, could impact biotic aspects like protistan community structure and trophic interactions. The distinctive characteristics of eddies

are mostly retained while propagating westward to the open ocean due to the stratification and velocities of the water masses (Dilmahamod et al., 2021; Leach and Strass, 2019). Albeit leakage or intrusion between eddy and background water, seasonal and hydrographic effects, as well as split, merge and linking events from or into two eddies may occur (Hall and Lutjeharms, 2011; Lamont and Barlow, 2017; Liu et al., 2019). These supplementary perturbations could further alter protistan plankton community structures emphasizing the need to monitor sub-mesoscale eddies on a high temporal and spatial scale from its generation until the inevitable disintegration of the eddy.

4.1.2 Specific Protistan Plankton Communities in Different Aged Eddies

All three eddies harbored distinctive protistan plankton communities and thus played diverse roles for the biological carbon pump in the open ocean. The young eddy CE_2019_19N_18W was characterized by a relatively high abundance of Chlorophyceae, which favors colder and low salinity habitats. This photosynthetic class of green algae is thus preferentially encountered in coastal areas and it has been shown that they assimilate large amounts of CO₂ (Kaladharan et al., 2009; Tragin and Vaultot, 2018). Further taxa associated with the shallow layer of the young eddy were the Arthracanthida-Symphycanthida clades, which are generally assumed to decrease in their abundance in accordance with deeper water layers, as found in this study (Mars Brisbin et al., 2020). They were detected in a variety of ecosystems (Gutierrez-Rodriguez et al., 2019; Hu et al., 2018) and play a pivotal role for the primary production and in the biological carbon pump (Decelle et al., 2013). They are able to host the haptophyte *Phaeocystis* as photosymbionts which exhibit enhanced photosynthetic efficiency after integration compared to their free living form (Decelle et al., 2019). Furthermore, it has been shown that these radiolarians can contribute up to one-quarter of the particulate organic matter (POC) flux to the deep sea due to their dense skeletons (Belcher et al., 2018; Decelle et al., 2013). The reduced relative abundance in the DCM of all other samples may result from depleted strontium that acantharians require to produce one of the most dense skeletons (Decelle et al., 2013). Iron deficiency in aged eddies could likewise serve as a crucial limitation in the ability of the host-symbiont relationship to maintain elevated photosynthetic activity resulting in a decreased competitiveness (Decelle et al., 2019; Geider and La Roche, 1994; Moore et al., 2013). The family Chrysochromulinaceae is another taxon that had the highest relative abundance in the DCM of the youngest eddy. The genus *Chrysochromulina* (family Chrysochromulinaceae) thrives under low salinity and nutrient-rich conditions, which

is characteristic for freshly upwelled waters entrapped by mesoscale eddies (Dahl et al., 2005; Dilmahamod et al., 2021). The main mode of energy acquisition for these haptophytes is a mixotrophic life style (especially the genera *Prymnesium*, *Haptolina* and *Chrysochromulina*; John et al., 2022). Massive contributions of haptophytes to the total bacterivory in marine systems were reported, but also the phagotrophic consumption of organic matter and other protists was described (Estep and MacIntyre, 1989; Frias-Lopez et al., 2009; Unrein et al., 2014). Furthermore, species belonging to the family Chrysochromulinaceae caused harmful algae blooms that resulted in massive slumps of fish stocks, albeit this has not been reported for the CanCS (Aalto et al., 2023; Hallegraeff et al., 2021; John et al., 2022).

The haptophyte assigned sequence reads in the shallow layer of the four-months aged eddy CE_2019_18N_20W were dominated by Phaeocystaceae where *Phaeocystis* is one of the only described genera (Adl et al., 2019). *Phaeocystis* is an ubiquitously distributed algae capable of bloom formation, and responsible for affecting food-web structure by evading grazing due to their colony forming ability (Nejstgaard et al., 2007; Schoemann et al., 2005; Smith Jr et al., 1991). Researchers are especially interested in these haptophytes for their capability in producing dimethyl sulfide as cloud forming nuclei. Thus, *Phaeocystis* harbors the potential for climate regulation (Charlson et al., 1987; Stefels et al., 1995). The low nitrogen concentration in the DCM of eddy CE_2019_18N_20W may be attributed to this genus as studies reported the efficient removal of nitrate by *Phaeocystis* (Arrigo et al., 2000; Smith Jr et al., 1998). As previously described, *Phaeocystis* is one of the major endosymbionts of Arthracanthida-Symphycanthida. The four-month-old eddy had less sequence reads assigned to Arthracanthida-Symphycanthida compared to the young eddy. However, the paramount taxon of acantharians was most dominant compared to all other samples which also conceals the possibility of symbiotic relationships with increased photosynthetic efficiencies (Decelle et al., 2019). The radiolarian clade RAD-B, also called Taxopodida, was predominant in the DCM of CE_2019_18N_20W and could be encountered in all depth layers of all samples. Even though a cosmopolitan and vertical distribution through the complete water column was reported, the lack of knowledge in regards to trophic strategy and possible symbionts does not allow interpretation from an ecological perspective (Biard, 2022).

The oldest eddy CE_2019_14N_25W, in addition to its peculiar shape, gave the impression of being in a disintegrating state, as the taxonomic signatures resembled the protistan plankton communities of the reference and eddy sites. The loss of velocity of the water circulation accompanied by the irregular shape of this eddy indicated the possibility of intensified intrusion and leakage events (Cesar-Ribeiro et al., 2020; Liu et al., 2019). These

have presumably been responsible for the formation of a hybrid protistan plankton community between the entrapped eddy waters and the surrounding background waters.

The Discoba assigned sequence reads were prevalently characterized by the class Diplonemea in all sampling sites throughout all water layers. This highly diverse group of planktonic eukaryotes, especially in the deep ocean, demonstrates the lack of current knowledge in regards to their ecology and function in the oceanic ecosystem (Flegontova et al., 2016). Even though studies recommended the exclusion from phototrophic and mixotrophic life styles and suggested symbiotic, parasitic or phagotrophic modes of energy acquisition, few studies narrowed down the possibilities (Flegontova et al., 2016; Lukeš et al., 2015; Valach et al., 2023). The role of diplomids in the oceanic food web is mostly unknown but they could play a crucial role in the trophic carbon transfer between multiple trophic levels as suggested by Vallach and colleagues (2023). However, this remains to be validated in further studies for several taxa within Diplonemea, as subspecific groups could occupy diverse ecological functions.

Dinoflagellates were the most dominant phylum in regards to relative sequence reads but had no noticeable changes in their relative read abundance throughout the samples. The only evident taxonomic signature within the phylum was the Dino-group III in the DCM and especially in the sub-DCM of the youngest eddy, potentially due to parasite-host dynamics, as this group belongs to the parasitic taxon of Syndiniales. However, scarce knowledge in respect to possible host exists for group III. A contemporary study revealed *Bathycoccus*, Dictophyceae and Katablepharidophyta as potential hosts by applying network analysis (Nagarkar and Palenik, 2023). However, they emphasize the potential of metazoans as targets, which remains to be investigated in future research. Young eddies or coastal areas of the CanCS could be considered to further elucidate the ecology of Syndiniales group III. Dino group I and II were the other prevalent dinoflagellates assigned to the parasitoid order of Syndiniales. They dominated all sampling sites throughout each depth layer. The Syndiniales groups parasitize predominantly other dinoflagellates, acanthareans, bacillariophyta as well as other radiolarians and Cercozoa, but also metazoans (Guillou et al., 2008; Käse et al., 2021; Nagarkar and Palenik, 2023; Siano et al., 2011). Syndiniales species inevitably kill their host and have even been referred to as 'serial parasitic killers' (Chambouvet et al., 2008; Guillou et al., 2008). Thus, they may have an essential role in the top-down control of protistan plankton communities and the particulate carbon flux to abyssal depths (Anderson et al., 2023).

The deeper water layers were characterized by substantially dissimilar protistan plankton communities compared to the DCM. The plankton structure of the youngest and oldest eddy became increasingly more similar to the taxonomic signatures of the reference sites with increasing depth. An exception was the apparently robust four-month-old eddy, which still contained distinctive taxonomic inventories in the sub-DCM and OMZ. Especially the Haptophyta and Radiolaria assigned sequence reads revealed noticeable changes. The relative abundance of the Haptophyta-Clade-HAP-4 increased in the sub-DCM of the reference sites, the old eddy and, to a lesser extent, in the youngest eddy. Additionally, a remarkable rise in the proportion of Haptophyta-Clade-HAP-5 was detected in the youngest, to a lower degree in the stable eddy and even less pronounced in the reference and old eddy samples. Ecological functions and the contribution to the oceanic carbon pump of HAP-4 and HAP-5 clades are unknown due to the fact that they were described exclusively based on environmental RNA/cDNA sequences (Egge et al., 2015). Studies suggested a vertical distribution in the water column for these taxa, advising for further efforts in elucidating the biogeographical distribution and environmental preferences for these haptophytes (Bittner et al., 2013; Gran-Stadniczeňko et al., 2017). The observation that both haptophyte clades were numerically marginal throughout the OMZ in all samples suggests sensitivity to oxygen deficiency. A steady increase in the radiolarian community was detected in the relative abundance of Spumellarida in accordance with deeper strata. This study corroborates well with previous findings where Spumellarida were associated with deeper and oxygen-depleted waters (More et al., 2018). Furthermore, it was suggested that they are potential hosts for Syndiniales species (Suter et al., 2022) and contribute substantially to the carbon sequestration via particulate carbon flux to the deep ocean (Preston et al., 2020). The exceptionally high proportion of Spumellarida in the robust eddy system indicates that this taxon group outcompetes other radiolarians and thrives in eddy-entrained deep-water masses, especially under oxygen-deprived conditions.

4.2 Functional Annotation of Protistan Plankton Communities

4.2.1 *Eddy Dispersal Enhances Regional Protistan Plankton Functional Diversity*

Solutions to the ‘paradox of the plankton’ try to unravel the coexistence of multiple different plankton species despite their competitive behavior for limited resources (Hutchinson, 1961). The combination of various mechanisms like external forcing dynamics (spatial heterogeneity, environmental fluctuations, etc.), temporal and spatiotemporal effects as well as biotic behavior and trophic interactions appear as convincing theories (Roy and Chattopadhyay, 2007). In numerical approaches, scientists tried to simulate this paradox by applying varying niche space and neutrality as stabilizing and equalizing factors, respectively, or incorporating intraspecific variations into their models (Cesar-Ribeiro et al., 2020; Chesson, 2000; Haegeman and Loreau, 2011; Menden-Deuer and Rowlett, 2014; Segura et al., 2011; Vergnon et al., 2012). These stabilizing and equalizing factors are leading to the exertion of distinct ecological functions across different taxon groups and size classes. However, model simulations and experimental procedures tend to not grasp the full complexity of nature, generating a wide range of niche space in a confined area with a variety of protistan plankton species (Klépanski et al., 2022). To dwell deeper into the eddy-induced perturbations (external forcing dynamics) on the protistan plankton functions a trait-approach was applied to determine the functional richness and ES associated with these mesoscale features.

The assignment of the biological traits to the ASV matrix resulted only in a limited yield of ~15% of the original dataset. Therefore, a quantitative and qualitative procedure was applied to validate the reduced output. The percentage of overlap between the two datasets was compared for all sampling sites and revealed only negligible variation. Hence, no eddy or reference station was disproportionately represented. The qualitative approach was to determine changes in the dissimilarities between the samples which yielded noticeable variations compared to the complete dataset. Due to the slight convergence of the youngest eddy to the reference sites and the stable to the old eddy, elements of the uniqueness have been deprived and the results should be interpreted with caution. However, the variations induced by mesoscale eddies would probably be more severe with an extended dataset.

Functional richness represents the amount of functional trait space occupied by the species (ASVs) in the protistan plankton community (Mason et al., 2005). The calculated functional richness of the samples was in general relatively high, indicating a diverse community with pronounced niche complementarity (Cesar-Ribeiro et al., 2020; Mason and de Bello, 2013). An identical pattern to the alpha diversity measures (ASV richness and Shannon

Index H') was observed for functional richness, which verified the robustness of the applied method by showing a positive correlation. The reference sites and the oldest eddy demonstrated the highest functional richness and the stable and youngest eddies had the lowest values on average as hypothesized in H_E2.1. This is exactly the opposite finding compared to a previous study that examined anticyclonic eddies from the Agulha current (Cesar-Ribeiro et al., 2020). However, even though southern hemisphere anticyclones could be comparable to northern hemisphere cyclones in regards to upwelling dynamics, the ages of the eddies were far older (7-24 months) compared to this current study. Furthermore, the Agulha current is a western boundary system which, as previously mentioned, is considered a locally-driven plankton hotspots, leading to lower alpha and functional diversity in maturing eddies as opposed to eddies emanating from EBUS.

The results in this thesis suggest a more severe competitive exclusion in younger eddies, and a more profound co-existence of protistan plankton species in aged eddies and the surrounding background waters in eastern boundary systems. Competitive exclusion could be derived from the enhanced fitness of the dominant species under the prevailing conditions (Behrenfeld et al., 2022). In the youngest eddy, exhibiting the highest nutrient concentrations, fast-growing species could outcompete other species at the expense of functional richness (James et al., 2022; Vallina et al., 2014). This confirms model approaches in which species with slower division rate are extinguished until species with similar fitness remain. This logical predicament is however only applicable to random mortality rates across the whole community (Behrenfeld et al., 2021). In the stable eddy, which exhibited ultra-oligotrophic conditions, resilient and species adapted to nutrient deficiencies could thrive selectively constraining protistan plankton favoring nutrient-rich waters (Sharoni and Halevy, 2020). This is in contrast to the oldest eddy where more frequent mixing events, by leakage and intrusion of background water, lead to an elevated functional richness by amalgamating both plankton communities (Liu et al., 2019; Moisan et al., 2017). Thus, the coupling of neutrality in regards to physiological processes and stabilization concerning the occupation of niche space seem as fundamental components structuring the coexisting and exclusion patterns in protistan plankton communities. However, the relatively high functional richness coupled with its low range is an indication that the competitive exclusion is not quite as extensive, possibly due to major mechanisms like selective predation pressure and resource partitioning (Sooria et al., 2022).

4.2.2 Resilience & Robustness of Eastern Boundary Upwelling Systems

No ES was unique throughout a distinct eddy or reference site, even though competitive exclusion likely occurred and the relative proportion of the taxonomic structure revealed noticeable differences. This indicates pervasive functional redundancy over distinct plankton groups and the hypothesis $H_{E2.2}$ has to be rejected. The fact that all strategies consisted of paraphyletic taxa affiliated to multiple phyla, except for ES 2 and ES 6 consisting exclusively of radiolarians, further supports the assumption of functional redundancy. However, functional redundancy is not necessarily a demerit, as it is recognized to correlate with resilience and robustness of an ecosystem by providing a degree of buffering capacity in the face of biodiversity loss (Bell et al., 2005; Biggs et al., 2020). Concentrated efforts in examining functional redundancy in the open ocean are not frequently attenuated due to the complexity and the lack of knowledge in regards to biodiversity, function and trophic interactions of protistan plankton (Daam et al., 2019; Wickham et al., 2022). However, recent field studies investigating the roles of marine plankton communities likewise revealed a redundancy in the exerted ES in and between the North Atlantic Ocean and a tidal front (Ramond et al., 2023, 2021, 2019). In a numerical model approach, this concept of functional redundancy in marine protistan plankton was also confirmed (Dutkiewicz et al., 2021). Dutkiewicz and colleagues (2021) demonstrated in their computational simulation a certain degree of redundancy across divergent species and emphasized ‘the multifunctionality context of biodiversity’ (Gamfeldt et al., 2008). They describe this concept as a negative connection between the functional redundancy and the ecosystem functions: as the range of performed ecosystem functions expand, a decline in redundancy should be observed if it is not maintained by an increase in biodiversity. This hypothesis could also explain the lack of a unique ES in the dataset of this thesis due to the relatively high and congruent functional diversity. However, an eddy specific ES could still be concealed in the trait-unassigned ASV inventories which emphasizes the knowledge gap about protistan diversity and their ecology in marine systems (Daam et al., 2019; Wickham et al., 2022).

Although no unique strategy was determined, the relative proportions of ES associated to the mesoscale eddies and the reference sites differed. The ES consisted of ecological key functions related to top-down control through parasites, carbon fixation through free-living microalgae, phototrophic endosymbionts, or phagotrophic lifestyles. However, by examining the relative abundance and the associated taxa for the ES limitations in the trait approach became obvious. The minuscule contribution of ES 1, consisting of single-celled eukaryotes with a parasitic lifestyle, in the youngest eddy illustrated the insufficiency in assigning traits to

individual ASVs. Through comparison with the relative contribution of Syndiniales assigned sequence reads in the taxonomic composition, a far larger proportion of ES 1 was to be expected. Likewise, the dominant presence of ES 9 (in DCM) and ES 4 (in OMZ) in the CVOO reference station did not reflect the taxonomic composition as they were composed exclusively of rare taxa. Of course, rare taxon groups may also be subject to ecological drift due to environmental shaping, but they play a minor role in the contemporary function of an ecosystem (Caron and Countway, 2009; Dlugosch et al., 2022). The rare protistan microbiome can have a reinforcing effect on the ecosystem function, but is mainly recognized as a seed community that could substitute the prevalent taxa after severe environmental stress (Caron and Countway, 2009; Ramond et al., 2023). Furthermore, the scarce protistan assemblage could play a pivotal role during succession patterns of the community structure in eddies as they mature and drift westward.

The deficiencies of the trait approach could be mitigated by further efforts to extend the trait database to include a larger pool of protistan plankton species. In combination with an elevated sequencing depth, an increased resolution in the compilation of the ecosystem functions would be possible. Integrating additional factors (e.g., nutrient dynamics, acclimatization, prey/predator interactions) could elaborate the biogeographic distribution of protistan plankton and explain the determined patterns in the context of the functional role they exhibit. Nevertheless, the results in this thesis could demonstrate functional richness patterns induced by eddy perturbations and provide circumstantial evidence for the robustness and resilience of EBUS.

4.3 Impact of Mesoscale Eddies on Microbial Abundances & Carbon Flow

4.3.1 *Mesoscale Eddies Harbor Elevated Microbial Abundances*

Research on food web dynamics in the Atlantic open ocean is largely unattenuated, especially with respect to mesoscale eddy perturbations and the deeper ocean (Long et al., 2021; Wickham et al., 2022). The bacterial mortality by protistan-mediated top-down control has several implications. On the one hand, protistan bacterivory ensures carbon transfer from prokaryotes to higher trophic levels and makes the dissolved and particulate organic matter indirectly available to the classical food web (Andersson et al., 2017; Gasol et al., 2009). On the other hand, grazing of prokaryotes influences biogeochemical cycles and impedes carbon export to the deep ocean (Iversen, 2023; Le Quéré et al., 2016). Therefore, the determination and the understanding of microbial abundances and the trophic linkage between prokaryotes and microbial eukaryotes is of great importance. The results in this thesis are consistent with most previous studies investigating prokaryotic and protistan abundances in marine systems and partially support the assessments by Boras and colleagues (2010) exploring grazing pressure on bacteria with emphasis on eddy activity. The determined findings obtained in this dissertation suggest elevated abundances and grazing effect in younger cyclonic eddies despite potential seasonal fluctuations.

The infamous azoic hypothesis by Forbes, postulated in the mid-19th century, assumed no life in the deepest part of the ocean (>550 m) due to observations of decreasing number of species coupled with the immense pressure, darkness, and the severe coldness with increasing depth (Anderson and Rice, 2006). Even though his theory has since been invalidated, Forbes was to be proven right about the general decline in the species abundance as we descend in the water column. However, there are of course exceptions in the case of special environmental features (e.g., black and white smokers, cold springs, eddies) due to deviating physicochemical conditions (Belkin et al., 2022; Boras et al., 2010; Georgieva et al., 2021). A large-scale campaign across the Atlantic, Indian, and Pacific oceans revealed a decline in the abundance of prokaryotes and heterotrophic microbial eukaryotes with increasing depth (Pernice et al., 2015). This agrees well with the findings of this study. Peaks of abundances measured in the DCM are likewise consistent to previous reports of the tropical Atlantic Ocean (Boras et al., 2010; Wickham et al., 2022; Winter et al., 2008).

The high values of bacteria in the DCM of the young and the stable eddy ($\sim 1.5 - 2.5 \times 10^6$ cells mL⁻¹) resemble the data by Winter et al. (2008; $\sim 2.1 \times 10^6$ cells mL⁻¹) and could result from eddy driven upwelling of nutrients. This conclusion is reinforced by two of the main

factors shaping the prokaryotic abundance in the DCM revealed by the multiple linear regression model. Here, low salinity and high nutrient (nitrate) concentration best described the bacterial density and were mainly associated with young and robust eddies (Dilmahamod et al., 2021). The oldest eddy and reference sites harbored approximately an order of magnitude fewer bacteria in the DCM, which is comparable to the findings of Boras et al. (2010) and some stations investigated by Winter and colleagues (2008). The sub-DCM and OMZ bacterial abundances did not deviate severely from literature values with a relatively wide range of $\sim 0.3 - 7.7 \times 10^5$ cells mL⁻¹ in similar depths (Boras et al., 2010; Pernice et al., 2015; Winter et al., 2008). Primary drivers relating to the number of prokaryotes in the sub-DCM and the OMZ were fluorescence and oxygen, respectively. Elevated fluorescence signals due to higher pigment concentrations and intensification of the OMZ (oxygen reduction) are cyclonic eddy characteristics, indicating the pivotal role of these features in influencing microbial abundances (Abdala et al., 2022; Sarma et al., 2018). Furthermore, the remarkable finding that the stable eddy exhibited a comparable bacterial cell count in the sub-DCM to that in the DCM of the reference sites suggests an eddy-induced influence on the vertical distribution of prokaryotes. This assumption is further supported by the elevated (similar) abundance of the sub-DCM (OMZ) in the youngest eddy in comparison to the reference DCMs.

The reported abundances of unicellular eukaryotes in the eastern tropical Atlantic Ocean focused mostly on specific groups (dinoflagellates, ciliates, and heterotrophic nanoflagellates; Boras et al., 2010; Pernice et al., 2015; Wickham et al., 2022). Therefore, it is problematic to compare the data directly. However, by combining the literature values to approach whole community abundances, up to 1700 cells mL⁻¹ in the shallow layers and by an order of magnitude lower in deeper waters (Boras et al., 2010; Pernice et al., 2015), with similar counts in the western Atlantic Ocean (Rocke et al., 2015) were reported. In comparison, the results obtained during this study had higher values ($\sim 30-50\%$) and resembled whole community datasets as obtained in the Indian Ocean (Not et al., 2008). Pernice and colleagues (2015) acquired these group-specific low counts likewise for the Indian Ocean during their expedition (Atlantic, Indian, and Pacific oceans), which corroborates the accuracy of the result in this thesis. The highest microbial eukaryote counts in the DCM were measured in the youngest eddy, followed by the stable and oldest eddy and the reference sites. Furthermore, the reference stations had the lowest abundance in all water layers. Belkin et al. (2022) and Boras et al. (2010) revealed analogous results by comparing cyclonic eddies with anticyclone and background stations in the southeastern Mediterranean Sea and the eastern tropical Atlantic Ocean, respectively. The identification of key physicochemical parameters in predicting protistan

abundances associated with eddy dynamics in multiple linear regression models yielded no satisfactory results for the DCM (sub-DCM: parsimonious model conditions could not be realized). A higher temperature as a primary driver for the DCM is counterintuitive to eddy characteristics as eddies should entrap cold and nutrient-rich coastal waters (Belkin et al., 2022; Dilmahamod et al., 2021). Indeed, the eddy sample obtained during the M156 cruise exhibited the lowest temperature with the highest protistan abundance but only accounted for a minor fraction of the model input. The stable and oldest eddy, however, had up to 2°C higher temperatures compared to the reference sites. Possible explanations are seasonal or diurnal variations as well as intrusion of warm water in the eddy core due to split, merge or linking events while westward propagation (Hall and Lutjeharms, 2011; Kettle et al., 2009; Lamont and Barlow, 2017; Liu et al., 2017, 2019). The second main factor in the DCM describing protistan abundances was turbidity which had been previously associated to cyclonic eddy activity (Stramma et al., 2013). In the OMZ, lower salinity values and high bacterial concentration corresponded to an elevated count of microbial eukaryotes, which was previously reported (Belkin et al., 2022; Boras et al., 2010; Dilmahamod et al., 2021). This furthermore supports the idea that mesoscale cyclonic eddies are “productive oases in the marine desert” (Belkin et al., 2022) of the open Atlantic Ocean.

4.3.2 Eddies Enhance Microzooplankton Grazing of Prokaryotes

The protist mediated top-down control of prokaryotes was comparable to bacterial mortality rates described by Boras et al. (2020) in cyclonic eddies ($\sim 0.8\text{-}40\% \text{ d}^{-1}$) and background waters ($\sim 0.0\text{-}43\% \text{ d}^{-1}$) in the open Atlantic Ocean. However, the actual grazing effects were up to seven times higher in the youngest eddy due to the pronounced bacterial abundances and thus, an elevated encounter rate. In comparison to nearshore prokaryotic turnover rates ($\sim 65\text{-}101\% \text{ d}^{-1}$) of the CanCS the acquired data are at best at the lower end of the spectrum (Wickham et al., 2022). The wide range of prokaryotic turnover rates could hint to further control mechanisms like viral lysis as reported for the Atlantic Ocean (Boras et al., 2010; Mojica and Brussaard, 2020). In addition, higher trophic levels may be another factor that exerts further top-down control which can lead to changes in the protistan plankton community structure and thus, alter carbon transfer efficiency (Vanni and Findlay, 1990; Vargas and González, 2004). The highest grazing effects were determined in the DCM for the youngest and the stable eddy which emphasizes the role of cyclones for trophic interactions. Furthermore, the model approach could clearly identify main factors associated to eddy characteristics as higher

turbidity and nitrate concentrations, while lower salinity and temperature values corresponded to elevated bacterial top-down control (Belkin et al., 2022; Boras et al., 2010; Dilmahamod et al., 2021; Stramma et al., 2010). This result hints to the theory that cyclonic eddies with their hydrographic features support carbon transfer to higher trophic levels and thus, support ecosystem services. However, the overall pattern rather suggests a subordinate eddy influence in deeper waters as the highest grazing effects were associated to the M156 cruise with the Reference_CB and the youngest eddy. The other two eddies and the Reference_CVOO exhibited far less bacterial ingestion rates in the sub-DCM and the OMZ, albeit always with higher rates in eddy-sites during their respective expedition. These variations between cruises as well as individual stations in determining grazing effects could result from methodological, physiological, and temporal reasons.

Methodological drawbacks could result from the application of bacterial analogs. Skewed grazing rates due to chemosensory prey recognition paired with non-preferential ingestion of microspheres by protistan plankton could be consequences of this approach (Pace and Bailiff, 1987; Sherr et al., 1987; Wootton et al., 2007). Seasonal variations in the eastern tropical Atlantic Ocean are well known (Yu et al., 2006). One example is the seasonal nutrient input by Saharan dust deposition associated with increased bacterial mortality by phagotrophic protists (Tsiola et al., 2017). It was reported that allochthonous Saharan dust precipitation into the tropical Atlantic Ocean peaks around July, which corroborates well with the M156 cruise (Engelstaedter et al., 2006; van der Does et al., 2020). Indeed, enhanced aerosol concentrations were recorded during the M156 cruise compared to the M160 expedition, which reinforces this assumption (Devresse et al., 2023). Another potential influence was related to the fact that time constraints on the research vessel led to variable sampling times. As a result, diurnal variations in bacterial feeding capacity could not be excluded (Marrasé et al., 1992). Furthermore, intra- and interspecific variability of unicellular eukaryotes has been shown to influence the top-down control of bacteria. These include individual fitness, stage in cell cycle, nutritional mode, and size classes of the grazers (Boenigk, 2002; Cleven and Weisse, 2001; Unrein et al., 2007). The biotic differences are ubiquitous in all samples, hence, the contemporary grazing effect with all its natural variations could be surveyed. The preferential exclusion of diurnal and seasonal effects, however, could only be achieved by multiple continuous sampling procedures focused on microbial carbon transfer experiments. Despite these limitations, the results provided evidence for elevated microbial abundances in cyclonic eddies as well as a higher efficiency in carbon transfer between trophic levels which corroborates well with hypothesis H_{E3.1}.

5 Summary & Conclusion

Mesoscale cyclonic eddies, which emerge in the CanCS, are predominantly confined ecosystems that contain unique protistan plankton structures. While these mesoscale features propagate westward into the oligotrophic open ocean, the enclosed plankton communities evolve and influence the biological carbon pump and food web dynamics disparately. The results could identify eddies as mechanisms responsible for dispersal-driven diversity hotspots, which may alter the ecosystem function in the offshore region of the Atlantic Ocean. Furthermore, eddies function as a residence harboring elevated abundances of microbial organisms in the oligotrophic open ocean.

The distinctive plankton communities associated to each individual eddy are presumably a consequence of the different development stages, and the place and time of origin of these mesoscale features. Younger eddies revealed a more pronounced competitive exclusion and co-existence of protistan plankton communities as aged eddies as well as the background waters. These differences are assumably due to the coupling of neutrality in regard to physiological processes and stabilization mechanisms concerning the occupation of niche space. An overlap of ES in the rare taxa community of all sampling sites, hence a functional redundancy of protistan plankton species, provided circumstantial evidence for the robustness and resilience of EBUS.

Seasonal effects and the location of the eddy generation could affect the initial seed community in the entrapped waters and may contribute to the dissimilarities and the subsequent evolution of the community. Hence, further research should focus on analyzing these mesoscale features with high temporal and spatial scale from the creation to the decay across all seasons and differing places of origin. The lifespan of eddies could furthermore influence the ecosystem in vastly different ways as the results indicate a divergent pace of development in the water layers. The shallow layers appear to evolve more rapidly in contrast to the deeper water layers as the youngest eddy revealed a distinct plankton community in the DCM but resembled the background waters in the OMZ. The taxonomic inventories demonstrate that eddies promote ecological key taxa such as phototrophs, parasites, endosymbionts, phagotrophic and climate regulating protistan plankton.

Ecologically valuable mechanisms such as the top-down control of different organisms and associated particulate carbon fluxes to the deep sea are thereby facilitated. Combined with enhanced photosynthetic activity and thus carbon fixation, and with the potential to produce

increased concentrations of cloud condensation nuclei in cyclonic eddies, these mesoscale features could mitigate the impending climate change. Especially considering recent estimates predicting that eddy activity will intensify in future climate change scenarios on a global scale. Younger cyclonic eddies, however, could counteract the carbon sequestration to abyssal depths by an elevated microbial abundance and trophic transfer of carbon. Thus, eddies promote food web efficiency which simultaneously impede sinking of dissolved and particulate organic matter.

Future research should focus on the quantification between mechanisms promoting carbon sequestration and the carbon flow within the food web to determine the prevalent effect of cyclonic eddies on the oceanic carbon pump. The findings in this dissertation could show an eddy-induced influence on the vertical distribution of unicellular organisms which, however, did not invalidate the general decline of prokaryotes and microbial eukaryotes with deeper water layers within the boundaries of an eddy. The trophic linkage with organisms of higher trophic levels poses another future research question in eddies as the interactions of multicellular organisms with protistan plankton could further alter the biological carbon pump as well as food web dynamics. Furthermore, the impact of ACEs and ACMEs on protistan plankton dynamics and the carbon pump should be analyzed, as their frequency of generation is likewise expected to intensify in response to climate change. Nevertheless, the data obtained in this study increased the current knowledge on the effect of mesoscale cyclonic eddies in offshore waters off Northwest Africa and could play a pivotal role in future model approaches assessing the fate of EBUS.

III. Effect of Light & Upwelling Intensity on the Protistan Plankton Structure & Function in the Humboldt Current System

6 Material & Methods

6.1 Study Site, Mesocosm Assembly & Manipulation

An examination of the influence of upwelling intensity and light limitation on protistan plankton communities was conducted in the southeast Pacific. The experimental setup was assembled 6 km from the coastline of La Punta (Callao, Peru) at the northeastern part of the Isle of San Lorenzo (12.06 °S, 77.24 °W; Figure 28) during the austral summer 2020 (28th February to 3rd April 2020). Eight Kiel Off-Shore Mesocosms for future Ocean Simulations (KOSMOS M1-M8, (Riebesell et al., 2013) were deployed and moored on February 19th 2020 by the research vessels BIC Humboldt and IMARPE VI. The mesocosm consisted of underwater bags (12 m in length and 2 m in diameter) made of polyurethane foil secured to flotation frames. The frames were additionally equipped with a cover and attached spikes to obstruct birds from perching and defecating into the experiment. The bags were kept underwater with nets of 3 mm mesh size mounted on the top and bottom openings to exclude larger organisms from entering but still enable water exchange with the open Pacific.

The start of the experiment was marked by the enclosure of the bags on February 28th 2020 (day 0). Therefore, the bottom nets were replaced by sediment traps and the bags were lifted ~1.5 m above sea surface preventing mixing with the surrounding waters. Finally, all remaining larger organisms (i.e., jellyfish, larvae, fish) were removed by a 1 mm mesh sized net.

Biofouling of the mesocosms was impeded by regularly cleaning the outer walls of the bags by divers and by cleaning the inside walls with a specifically designed ring-shaped double-bladed wiper (Bach et al., 2016; Riebesell et al., 2013).

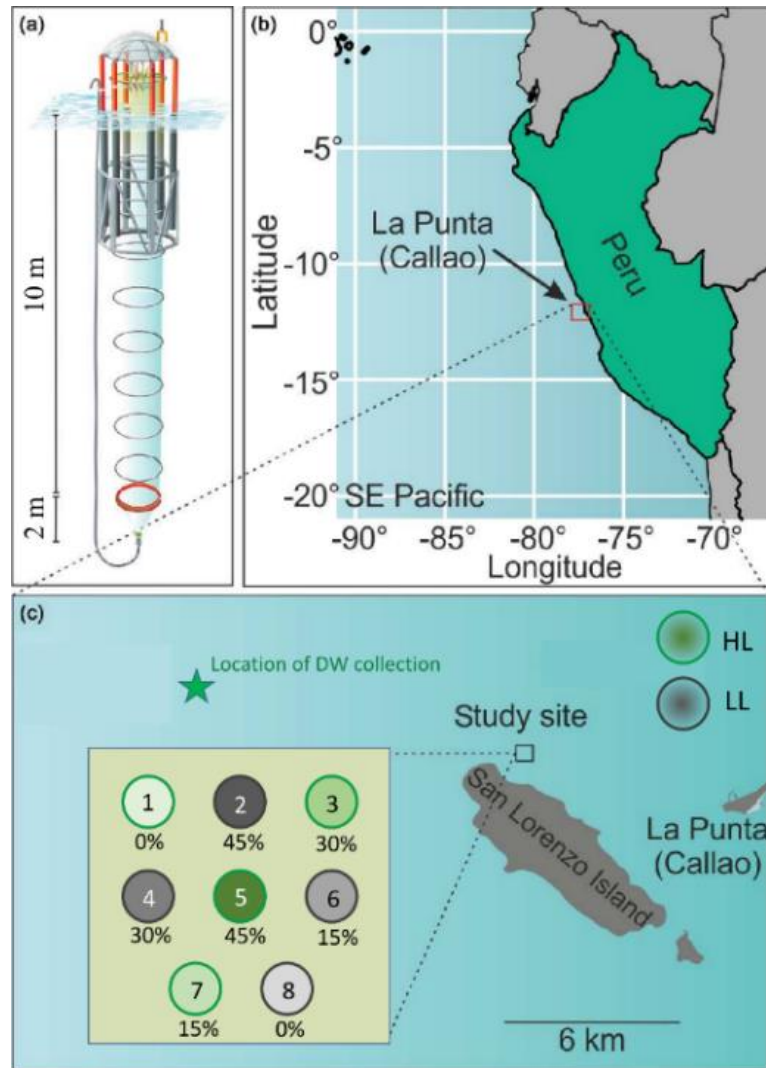


Figure 28. Experimental design and study location. a) Dimensions of one mesocosm with an underwater bag. Please note the size ratio for the underwater bag is not to scale. b) Large-scale map of the study site in the Humboldt Current System. c) Detailed map of the study area and the mesocosm arrangement for the light and upwelling manipulation. The star marks the location where the collection of the deep-water (DW) occurred. The percentages indicate the volume of water exchanged with DW for each mesocosm. This corresponds to the darkening of the color. The high light (HL), as no manipulation, and low light (LL) to simulate austral winter are colored green and gray, respectively. Modified from Bach et al. (2020).

6.1.1 Light & Upwelling Manipulation

Light limitation was achieved by shading the enclosure bags of four KOSMOS (M2, M4, M6, M8) with opaque polyurethane foil, which are called low light (LL) mesocosms hereafter. The high light (HL) KOSMOS (M1, M3, M5, M7) had transparent bags and represent the unmanipulated or natural light intensities during austral summer. In the HL mesocosm, the averaged photosynthetically active radiation (PAR), measured by CTD (CTD167M, Sea and Sun Technologies), in the water column was $173 \mu\text{mol photons m}^{-2} \text{s}^{-1}$. The shaded bags reduced the intensity of light by $\sim 50\%$ resulting in a mean PAR of $86 \mu\text{mol photons m}^{-2} \text{s}^{-1}$.

Upwelling simulations were achieved by replacing enclosed mesocosm water with nutrient rich deep-water (DW). Therefore, three upwelling intensities (15%, 30%, 45%), where the particular percentages can be comprehended as the volume of water exchanged, and one reference (0%) with no DW addition were selected. However, to mimic varying upwelling intensities in the KOSMOS, multiple necessary procedures had to be addressed beforehand. The first step was determining the volumes of the contained water masses for each mesocosm to enumerate the amount of water exchanged with DW. For this purpose, a calibrated NaCl (sodium chloride) solution was evenly dispersed in the water column to increase the salinity by a small margin. Through CTD measurements before and after the brine addition, the changes in salinity were documented. This enabled the calculation of the enclosed water volumes through the changes in salinity and the sea water densities for each mesocosm via the volumes of NaCl solution added (Supplementary File 16; Czerny et al., 2013). The DW was collected according to Bach et al. (2020) and Taucher et al. (2017). Briefly, on March 6th 2020, nutrient rich DW was gathered using a 100 m³ deep-water collector at 40 m depth based on the IMARPE time-series transect (Graco et al., 2017). The water exchange took place on March 11th (day 13) for the LL and on March 12th (day 14) for the HL mesocosms using a submersible pump (Grundfos SP 17-5R, pump rate ~18m³ h⁻¹). The thereby obtained nutrient concentrations in the treated mesocosms mirrored concentrations in natural upwelling areas (Table 12; Hauschildt et al., 2021; Igarza et al., 2019; Messié et al., 2009). An additional manipulation was the introduction of fish larvae (120 *Engraulis ringens* and 70 *Anisotremus scapularis*) on March 17th in each KOSMOS. The implementation of a new trophic level in the enclosures may have further effects on the protistan plankton communities.

Table 12. Nutrient concentrations of the mesocosms. Nutrient concentrations of each KOSMOS after deep-water (DW) addition on day 15 and the 100% DW. It should be noted that the nutrient concentrations do not reflect the concentration directly after DW injection due to the time delay in the process and water sampling. HL: high light; LL: low light; M: mesocosm.

KOSMOS	Light	Upwelling [%]	NO₃⁻ [μmol/L]	PO₄³⁻ [μmol/L]	Si(OH)₄ [μmol/L]
M1	HL	0	0.00	0.87	7.90
M2	LL	45	11.3	1.83	15.40
M3	HL	30	11.1	1.48	12.60
M4	LL	30	8.10	1.48	14.10
M5	HL	45	13.30	1.69	12.90
M6	LL	15	3.60	1.22	14.50
M7	HL	15	4.60	1.17	11.10
M8	LL	0	11.30	1.83	15.40
DW	-	100	30.60	2.45	15.90

6.2 Water Sampling at the Peruvian Coast

Small rigid-hulled inflatable boats stationed at the harbor of La Punta were used to conduct sampling at the mesocosm site. They were moored to the flotation frames to maintain a stable base while sampling. A hose (10 m length, 0.05 m diameter) was used to collect mesocosm water from the complete water column. Approximately 12 L of water was taken from each mesocosm and filled into plastic containers. The samples were transported to the laboratory facilities in tubs filled with seawater to reduce heating and covered with opaque polyurethane foil to prevent sun exposure. Due to logistic reasons and the experimental efforts, only four mesocosms could be processed per sampling day. The exact sequence of sampling proceeded according to the subsequent Table 13. It should be mentioned that briefly before day 21, COVID-19 regulations were so severe as to raise anxiety about abandoning the experiment. Whereupon the schedule was changed on short notice for day 21 and day 23, accordingly. In preparation for the abortion of the experiment, the mesocosms were selected to still allow a light and upwelling comparison even if day 21 would have been the final sampling. However, official authorization from the Peruvian government allowed the continuation of the project, and as of day 27, the previous scheme could be reinstated.

Table 13. Sampling scheme of mesocosms. The sampling sequence has changed (day 21/23) during the field campaign due to the possibility of experiment termination due to COVID-19 regulations. HL: high light; LL: low light; M: mesocosm.

Date	Experimental day	Mesocosm
02/28/2020	1	HL0; HL15; HL30; HL45
03/01/2020	3	LL0; LL15; LL30; LL45
03/05/2020	7	HL0; HL15; HL30; HL45
03/07/2020	9	LL0; LL15; LL30; LL45
03/13/2020	15	LL0; LL15; LL30; LL45
03/15/2020	17	HL0; HL15; HL30; HL45
03/19/2020	21	HL0; HL45; LL0; LL45
03/21/2020	23	HL15; HL30; LL15; LL30
03/25/2020	27	HL0; HL15; HL30; HL45
03/27/2020	29	LL0; LL15; LL30; LL45
03/31/2020	33	HL0; HL15; HL30; HL45
04/02/2020	36	LL0; LL15; LL30; LL45

6.2.1 Nutrients & Physical Parameters

Temperature, oxygen, pH, salinity, chlorophyll a (Chl-a) and PAR were measured by the CTD sensor system. The data were subsequently averaged for the complete water column. Samples for nutrient measurement were taken by 5 L ‘integrating water samplers’ (Hydro-Bios, Kiel) over a depth of 0 - 10 m. Triplicate samples were filtered (0.45 µm pore size, Sterivex, Merck, Darmstadt, DE) and analyzed by a QuAAtro AutoAnalyzer (SEAL Analytical with an XY-2 Sampler, Mequon, US) to colorimetrically measure PO_4^{3-} , $\text{Si}(\text{OH})_4$, NO_3^- , NO_2^- (Morris and Riley, 1963; Mullin and Riley, 1955; Murphy and Riley, 1962). All physicochemical parameters were determined by the CUSCO 2020 consortium.

6.3 Protistan Plankton Assessment in the Humboldt Current System

6.3.1 DNA-Filter Preparation

To investigate the changes in protistan plankton community composition eDNA-metabarcoding was utilized. In order to collect the DNA, the procedure followed Chapter 2.3.1 using the same equipment and materials. Briefly, water samples were filtered onto 0.65 μm pore-sized Durapore[®] membrane filters using the rotarus[®] peristaltic pump. Three replicates were taken per mesocosm, each with roughly 3 L of water. The filters were placed into cryogenic vials and preserved using LifeGuard Soil Preservation Solution. Samples were stored at -20°C until further processing in the laboratory of the RPTU.

6.3.2 DNA Extraction & Amplification

The DNA extraction and amplification via PCR were performed exactly as described in Chapter 2.3.2. In short, the DNeasy PowerWater Kit was used to extract the DNA according to the manufacturer's protocol. Following Stoeck et al. (2010) the hypervariable V9 region of the 18S rDNA gene was amplified using the 1391F as forward primer and the EukB as reverse primer (see Table 2 for details). The PCR reaction mix contained the eDNA, GC-buffer, BSA dNTP's, Phusion high fidelity DNA polymerase and the primer-pairs with a final volume of 50 μL filled with ddH₂O (see Table 3 for details). The sequential order of the PCR comprised an initial denaturation step (98°C for 30 s), followed by 30 cycles of denaturation (10 s at 98°C), annealing (20 s at 61°C), elongation (25 s at 72°C) and a final five-minute extension at 72°C . The expected fragment length of approximately 150 base pairs was verified using gel-electrophoresis and PCR products were subsequently frozen at -20°C until preparation for HTS.

6.3.3 Sequencing, Quality Control, Clustering & Taxonomic Assignment

The procedures for sequencing, quality control, clustering and the taxonomic assignment was likewise conducted as described in Chapter 2.3.3. To briefly recapitulate, the company SeqIT GmbH & Co. KG performed the paired-end Illumina MiSeq sequencing. The raw data files are attached as Supplementary File 17. With CUTADAPT v1.18 (Martin, 2011) primers were removed and the FASTX toolkit (RRID: SCR_05534) sorted the sequences in the same read direction. The DADA2 algorithm was applied (Callahan et al., 2016) using the exact

same settings of the functions as described before (`truncLen=80`; `maxEE=1`, `minOverlap= 20`). Afterwards, chimeras were removed with the *uchime-denovo* algorithm in VSEARCH (Edgar et al., 2011). The remaining sequences were then taxonomically assigned using the PR² database (Guillou et al., 2013) with the LCA (syntax cut-off of 0.8; Edgar, 2016). HTS and PCR bias were reduced by pooling the replicates. Finally, the ASV table was cleared from singletons, unassigned eukaryotes, streptophyta and metazoan sequences to reduce uninformative reads. The resulting ASV-to-sample matrix was then used for all statistical analyses (supplementary File 18).

6.3.4 Statistical Analysis

The data analysis was performed using the program RStudio v4.0.5 and the packages *vegan* v2.6-2 (Oksanen et al., 2022), *stats* v4.3.0 (R Core Team, 2021), *car* v3.0-11 (Fox and Weisberg, 2019), *relaimpo* v2.2-6 (Grömping, 2006) and *rstatix* v0.7.0 (Kassambara, 2021). Graphics were performed using *ggplot2* (Wickham, 2016) and base R. In the first step, the development of nutrient dynamics and physicochemical parameters during the course of the experiment were visualized. These were examined for variations induced by the light or upwelling treatments. Rarefaction curves were generated using the *rarecurve* function in *vegan* to evaluate the degree of sample saturation. Subsequently, alpha diversity parameters (Shannon-Wiener Index H' , Simpson Index D, ASV richness and evenness) were analyzed using the rarefied dataset as a standardization to the smallest sequence size of all samples. Alpha diversity measures were studied for the HL and the LL mesocosms concatenated over time and in their development during the experiment for each upwelling treatment. Analysis of covariance (ANCOVA) was used to determine significant effect of light and upwelling treatment. Therefore, model building was performed with the *lm* function of the *stats* package. The residuals were tested for normality and the homogeneity of variance with the *shapiro_test* function and the *levene_test* function of the *rstatix* package, respectively. After confirmation of normality and variance homogeneity of residuals, the ANCOVA was conducted with the *aov* function and the *Anova* function of the *stats* and *car* packages, respectively.

Beta diversity analysis was investigated using the BC dissimilarity on the Hellinger transformed data set and visualized in an NMDS (Legendre and Gallagher, 2001; Rao, 1995). With the *adonis2* function, PERMANOVA (9999 permutations) calculated significant differences induced by the mesocosm manipulations between the protistan plankton. A consecutive correlation between the physicochemical parameters and biological parameters to

the ordination analysis was performed using the *envfit* function in *vegan*. The biotic parameters were depicted from the functional trait data base (<https://www.seanoe.org/data/00405/51662/>, accessed on September 22nd 2022; Ramond et al., 2018). To focus only on direct functional aspects, only ingestion modes (osmotrophic, saprotrophic, intern, extern) and the symbiotic lifestyles (parasite, commensalistic, mutualistic photosynthesis) were the target of interest, while shape, cover, spicules, etc. were disregarded.

In order to obtain an insight into the taxonomic variations induced by the treatments, the protistan plankton community composition was analyzed on phylum level. Significant effects of light and upwelling treatment for the top abundant phyla (cumulative read abundance >10%) were investigated using ANCOVA as described above. The most abundant family for each phylum affected by light or upwelling was likewise tested for treatment effects by ANCOVA.

6.4 Microbial Abundances & Carbon Flow in the Humboldt Current System

6.4.1 Incubation Setup

The fundamental approach to perform the incubations was identical to the detailed description in Chapter 2.5.1. Specifications in the realization of the CUSCO grazing experiments in contrast to the shipboard grazing experiment during REEBUS were made due to logistical constraints on board. Since sufficient time and equipment were available prior to the experiment, the following arrangements could be implemented to perform the experiments more accurately. Self-mounted LED lights were dimmed for the LL mesocosm incubations (LL ~80%) and were illuminated at full intensity for the HL mesocosms (HL 100%). The EVA-bags were stored between sampling procedures in water-filled intermediate bulk containers with constant water circulation to ensure exposure to uniform light conditions. Furthermore, the experiments were carried out in a temperature-controlled container at ~18 °C, which reflected the average in-situ temperature of the sea.

The epifluorescence microscopy and the determination of protistan and bacterial abundances as well as the phagotrophy estimators were performed according to the previously mentioned descriptions (for details see Chapter 2.5.2 & Chapter 2.5.3).

6.4.2 *Statistical Analysis*

The statistical analysis was performed using the program RStudio v. 4.0.5 and the packages car v3.0-11 (Fox and Weisberg, 2019), stats v4.3.0 (R Core Team, 2021), and rstatix v0.7.2 (Kassambara, 2021) for statistical analysis and ggplot2 v3.3.6 (Wickham, 2016) for graphical visualization. ANCOVA was used to determine significant effect of light and upwelling treatment as described in Chapter 6.3.4. Additionally, the temporal development of abundances and phagotrophy estimators was investigated.

Spearman rank test was applied to identify significant correlations between the physicochemical parameters and the prokaryotic and protistan abundances as well as the grazing effect and prokaryotic turnover rate.

7 Results

7.1 Protistan Plankton Assessment in the Humboldt Current System

7.1.1 *Physicochemical Properties of the Mesocosms*

Chemical and physical parameters of the mesocosms exhibited changes during the course of the experiment and between treatments (Supplementary File 19). The pH (Figure 29.a) was influenced by the light treatment and was always higher in the HL mesocosms ($\text{pH} = 8.2 \pm 0.1$) compared to the LL mesocosms ($\text{pH} = 8.0 \pm 0.1$). The effect of the DW treatment on the pH was observed on the sampling day (LL: day 15; HL: day 17) directly after addition. The pH declined depending on the simulated upwelling intensity and increased steadily thereafter until the end of the experiment. Oxygen concentrations (Figure 29.b) followed a similar trend being affected primarily by the light treatment (HL: $\text{O}_2 = 6.3 \pm 0.6$ mg/L; LL: $\text{O}_2 = 5.5 \pm 0.4$ mg/L), especially in the first 20 days of the experiment. The pattern on day 15 (LL) and day 17 (HL) after DW addition was reversed for dissolved oxygen as opposed to pH. High upwelling intensities exhibited in general higher oxygen concentrations (except HL30 and HL45). The concentration declined continuously for the HL treatment but slightly increased or remained constant for the LL mesocosms. Temperature (Figure 29.c) did not follow a specific rule and remained fairly constant (17.9 ± 0.3 °C) with no substantial differences between the light treatments (HL: 17.9 ± 0.4 °C; LL: 17.9 ± 0.3 °C).

Nutrient dynamics were clearly shaped by light and the artificial upwelling intensities. In general, concentrations of nitrate, silicate and phosphate were higher in LL treated mesocosms, but all were subject to severe changes over the duration of the campaign. Nitrate (Figure 30.a) was depleted before DW addition to the mesocosms and increased proportionally to the administered upwelling intensities. After the peak in nitrate content, its concentration decreased steadily. Remarkably, in the HL0 and LL0 setups nitrate levels increased slightly to day 20, whereupon the concentrations dropped to marginal levels. Phosphate (Figure 30.b) and silicate (Figure 30.c) concentrations were never depleted before DW dosing. While phosphate dropped substantially to day 7/9, silicate remained constant in the pre-DW phase. Silicate concentration constantly decreased in the post-DW phase, especially for the HL45 and LL45 with a steep decline between day 13/15 and day 21. Phosphate content peaked right after simulating the upwelling intensities of 30 and 45% and declined thereafter. Peculiarly, the phosphate concentration increased for the 0 and 15% mesocosms up to day 29 (LL0).

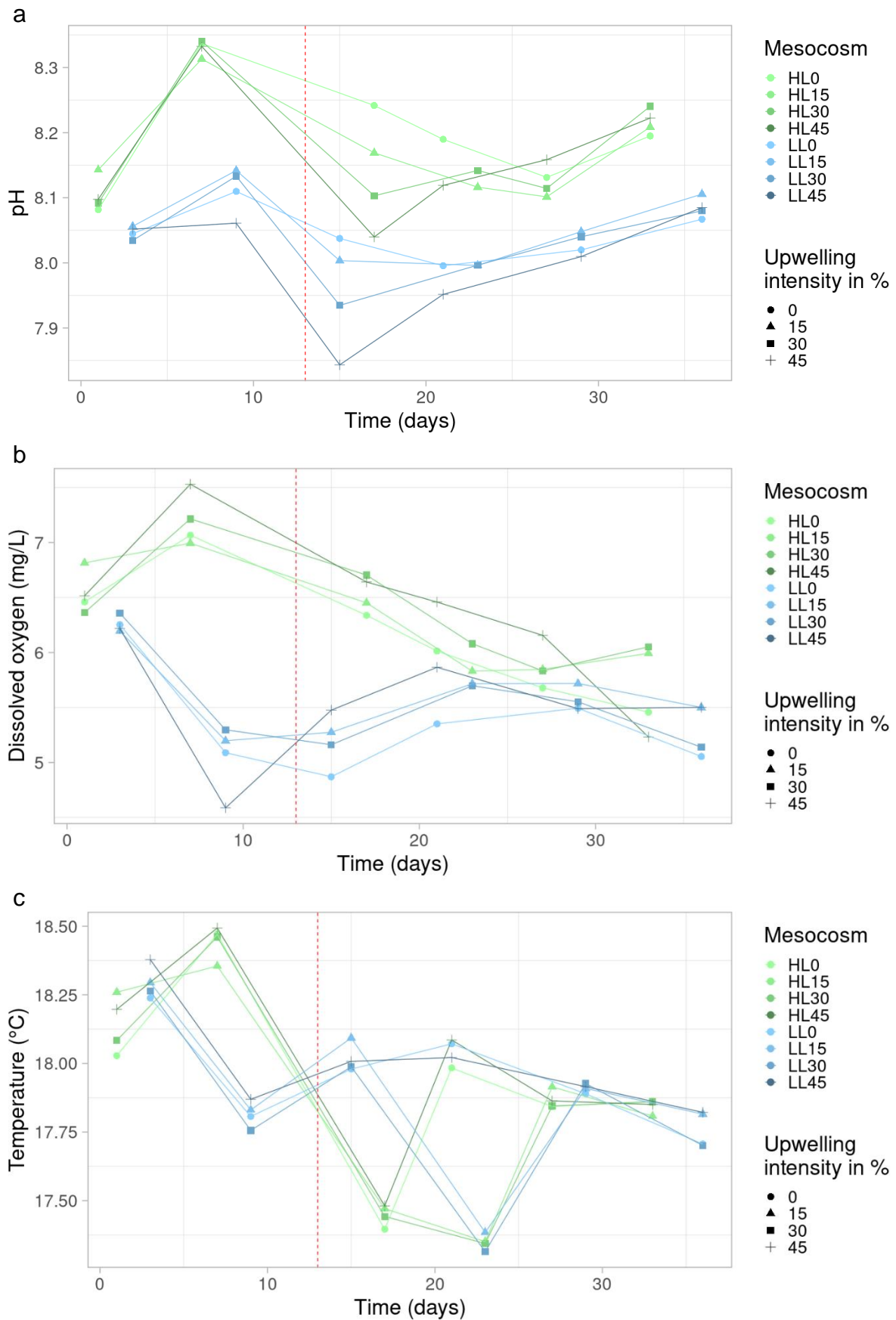


Figure 29. pH (a), dissolved oxygen (b) and temperature (c) development in the mesocosms. Deep-water addition is highlighted by the red dashed line. Light treatment is colored in green for high light (HL) and blue for low light (LL).

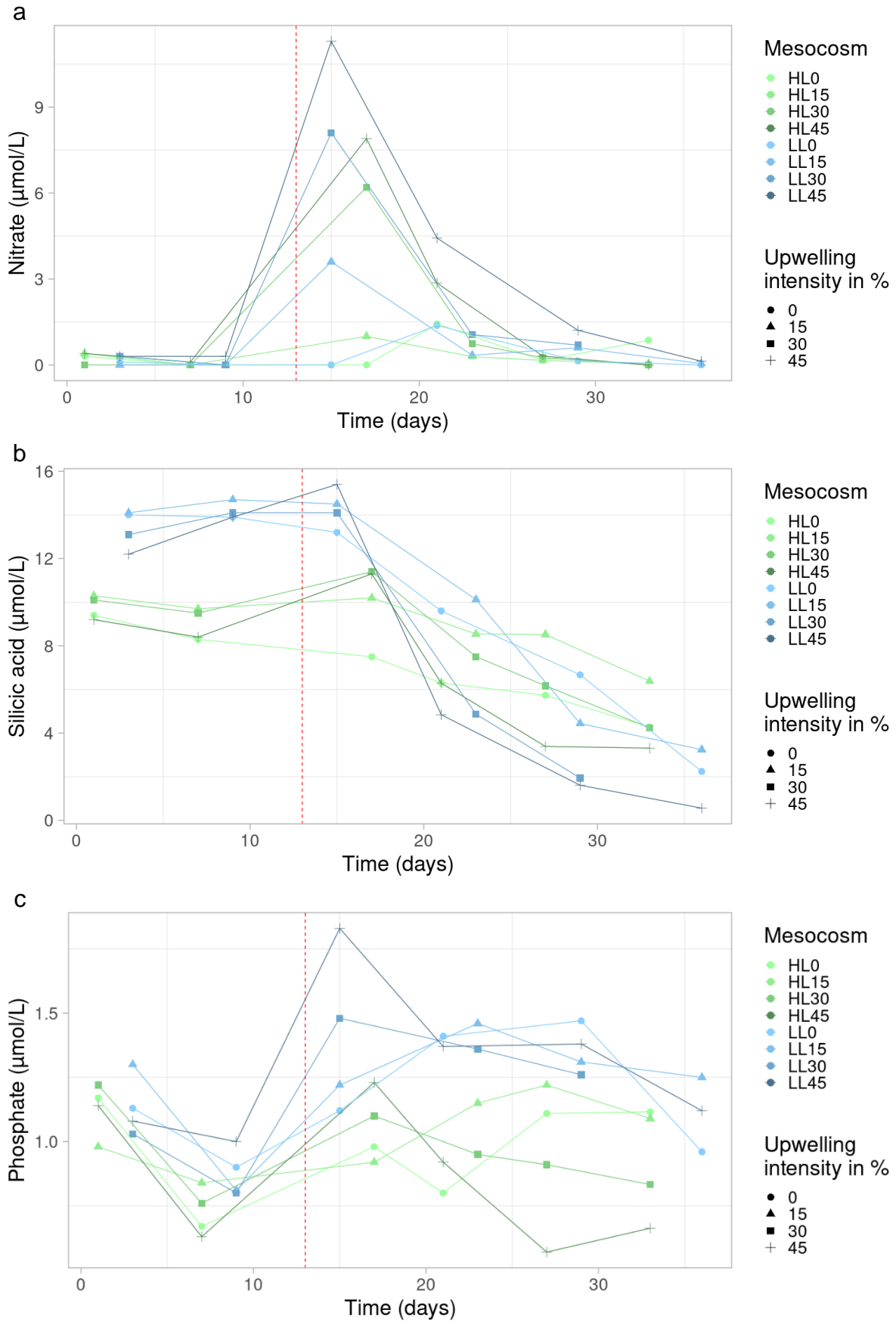


Figure 30. Nitrate (a), silicate (b) and phosphate (c) development in the mesocosms. Deep-water addition is highlighted by the red dashed line. Light treatment is colored in green for high light (HL) and blue for low light (LL).

7.1.2 Sequence Data Overview

After removing singletons, unassigned sequences, and non-target ASVs (Metazoa, Streptophyta) from the taxonomical assignment, between 111,796 (min) and 1,168,080 (max) high-quality sequences were obtained (Supplementary File 20). The subsequent normalization of read counts for alpha diversity comparison to the minimum sequence number of the smallest sample size resulted in 111,796 reads per sample. The point of saturation was reached for most of the samples, as indicated by the rarefaction curves (Supplementary File 21 a-d).

7.1.3 Alpha Diversity of Protistan Plankton Communities in the Humboldt Current System

The alpha diversity measures (evenness and ASV richness) as well as Shannon (H') and Simpson (D) indices were the most diverse in HL (0.59 ± 0.07 , 1581 ± 376 , 4.33 ± 0.54 and 0.94 ± 0.05 , respectively) compared to the LL (0.56 ± 0.06 , 1433 ± 435 , 4.04 ± 0.46 and 0.94 ± 0.03 respectively) mesocosms (raw data in Supplementary File 22). The treatments of the artificially induced upwelling had corresponding effects in both HL and LL (Figure 31 and Figure 32). The values increased in accordance with the upwelling intensity for the evenness ($R^2 = 0.91$ for HL; $R^2 = 0.99$ for LL) from 0.57 ± 0.06 (HL0) to 0.62 ± 0.10 (HL45) and 0.52 ± 0.07 (LL0) to 0.59 ± 0.07 (LL45). Analogous behavior was determined in the H' following the pattern of lower diversities in 0% upwelling (HL: 4.18 ± 0.47 ; LL: 3.67 ± 0.53) and higher diversities in 45% upwelling (HL: 4.62 ± 0.84 ; LL: 4.31 ± 0.47). Albeit minor changes in the D index can represent a considerable deviation, no substantial variation in the HL treatments ($R^2 = 0.07$; HL0: 0.94 ± 0.03 ; HL45: 0.94 ± 0.09) were determined. However, D responded in an identical way as H' and evenness for the LL mesocosms to the DW addition (LL0: 0.90 ± 0.05 ; LL45: 0.95 ± 0.03). The ASV richness exhibited a noteworthy pattern for both HL and LL mesocosms, where the 30% and not the 45% upwelling intensity exhibited the highest ASV richness (HL30: 1768 ± 279 ; LL30: 1607 ± 416) within their light treatment.

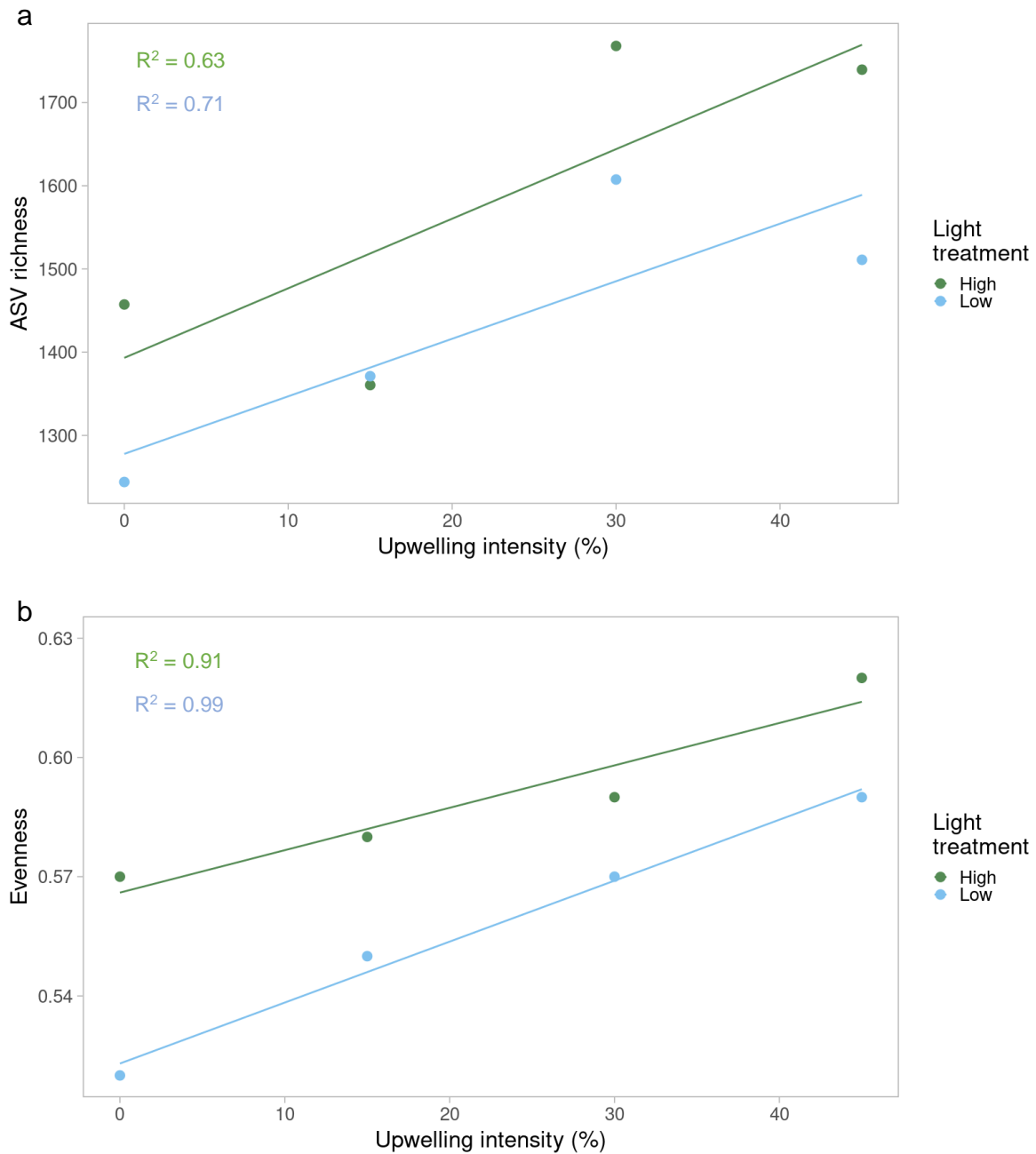


Figure 31. ASV richness (a) and evenness (b) dependent on upwelling intensity and light manipulation derived from integrating all time points. The evenness and ASV richness were calculated for the rarefied data set. The light treatments are colored. Linear trendlines and coefficient of determination (R^2) for each light treatment were calculated using linear regression analysis.

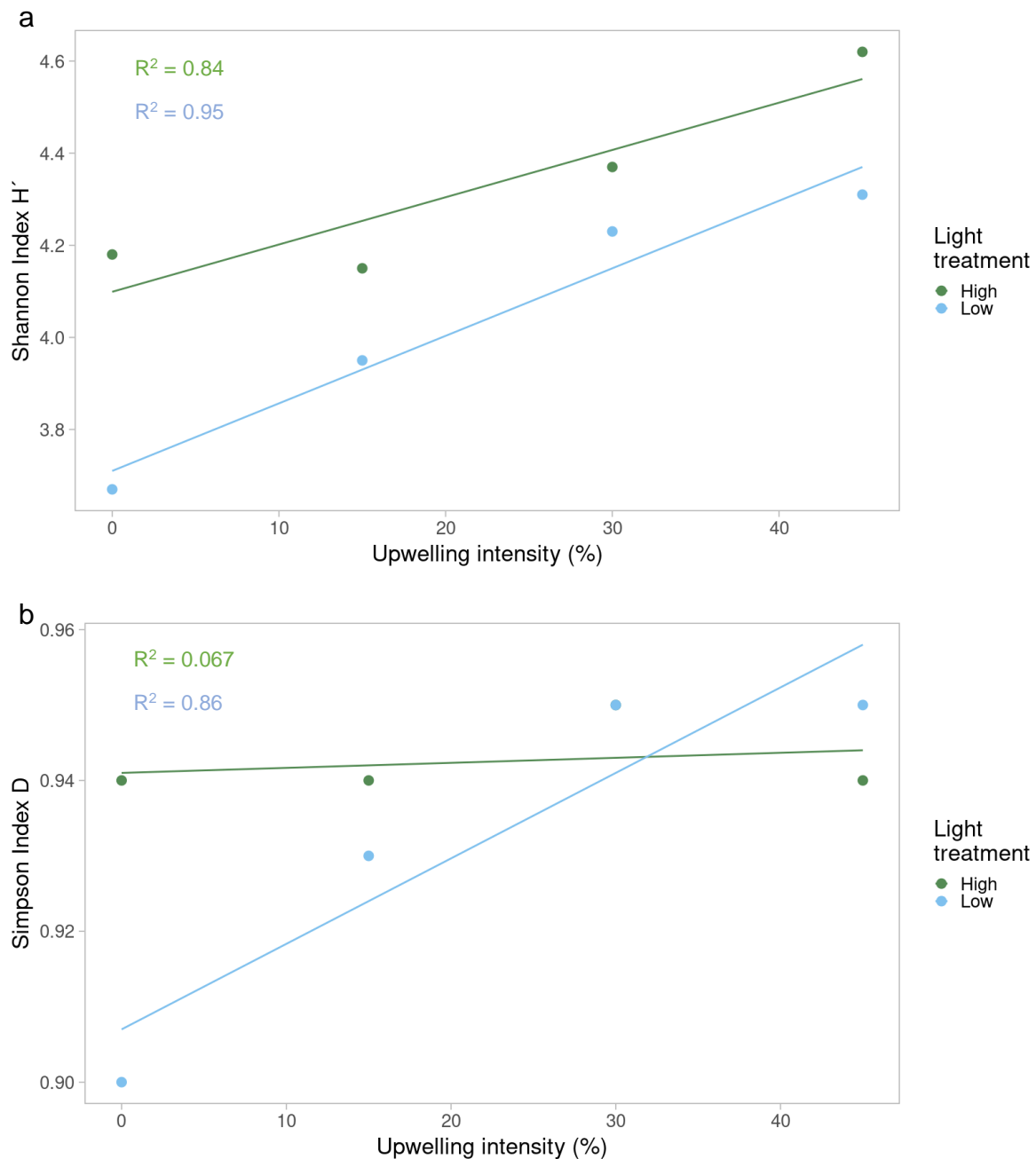


Figure 32. Shannon Index (a) and Simpson Index (b) dependent on upwelling intensity and light manipulation derived from integrating all time points. The Shannon and Simpson index were calculated for the rarefied data set. The light treatments are colored. Linear trendlines and coefficient of determination (R^2) for each light treatment were calculated using linear regression analysis.

The requirements for ANCOVA analysis, normal distribution, and homogeneity of variances for the residuals, were fulfilled (Table 14). Significant effect of upwelling intensity for all alpha diversity measurements were calculated (ANCOVA, $p < 0.05$; Table 15). The calculated percentage of variance explained using the sum of squares (SS) revealed the highest explanation reaching up to 61.3% (evenness). The Simpson Index D had the least variation

explained by upwelling intensity with 42.1%, since the HL treatment showed no severe changes. The light treatment was responsible for around one-third of the explained variation for the evenness and the Shannon Index H' (ANCOVA, $p < 0.05$) but had no significant effect on the ASV richness and the Simpson Index D.

Table 14. Shapiro Wilk and Levene's test results for each alpha diversity measurement. Verification of the normal distribution and variance homogeneity for ASV richness, evenness, Shannon and Simpson Index.

Model	Test	Statistics	p-value
ASV richness	Shapiro Wilk	0.952	0.730
	Levene	0.483	0.513
Evenness	Shapiro Wilk	0.910	0.351
	Levene	0.297	0.606
Shannon Index H'	Shapiro Wilk	0.916	0.398
	Levene	0.278	0.617
Simpson Index D	Shapiro Wilk	0.853	0.101
	Levene	0.052	0.827

Table 15. Analysis of covariance (ANCOVA) for each alpha diversity measurement. ANCOVA test results for the mesocosm manipulations, their interactions, and the residuals for each alpha diversity measurement. DF: degrees of freedom; SS: sum of squares.

Alpha diversity	ANCOVA	DF	SS	F	p-value
ASV richness	Light treatment	1	43758	2.59	0.1830
	Upwelling intensity	1	131256	7.76	0.0495
	Interaction	1	1174	0.07	0.8052
	Residual	4	67653		
Evenness	Light treatment	1	0.0021	56.33	0.0017
	Upwelling intensity	1	0.0038	101.4	0.0005
	Interaction	1	0.0001	3.27	0.1450
	Residual	4	0.0002		

Table 15 (continued).

Shannon Index H'	Light treatment	1	0.17	19.78	0.0112
	Upwelling intensity	1	0.35	41.12	0.0030
	Interaction	1	0.01	1.28	0.3210
	Residual	4	0.03		
Simpson Index D	Light treatment	1	0.0002	2.67	0.1778
	Upwelling intensity	1	0.0008	10.80	0.0303
	Interaction	1	0.0006	8.53	0.0432
	Residual	4	0.0003		

7.1.4 Dissimilarities between Mesocosm Specific Protistan Plankton Communities

In an NMDS (stress: 0.089) the beta diversity which was calculated using the BC dissimilarities for all samples was illustrated (Figure 33). Significant variations between the samples induced by the diverse treatments (light and upwelling) were tested using PERMANOVA (Supplementary File 23). Light treatments revealed significant differences on the protistan plankton communities (PERMANOVA, $F = 3.66$, $p < 0.001$). In the pre upwelling phase, the mesocosm communities distinguished themselves along the NMDS axis 1, where HL protistan communities were encircled by the LL samples. After the upwelling simulation, the HL samples were partitioned along the NMDS axis 2 from the LL samples, with HL communities in the upper and LL communities in the lower axis range. Pre upwelling samples were clustered in the lower NMDS axis 1 values whereas post upwelling samples were further separated in the higher axis values. It should be emphasized that the HL0 and LL0 mesocosms followed this pattern even though they were never exposed to nutrient rich DW and therefore, have not been subjected to any upwelling treatment. Furthermore, the individual upwelling intensities had no obvious pattern albeit having a significant effect on the protistan plankton communities in the post-upwelling phase (PERMANOVA, HL: $F = 1.87$, $p < 0.01$; LL: $F = 1.33$, $p < 0.01$).

The envfit function was used to determine significant correlations between the protistan plankton community structures and the physicochemical parameters (Figure 33 and Supplementary File 24). Temperature and silicate concentration had a significant correlation along the NMDS axis 1 and were linked to the pre upwelling samples (R^2 : 0.26, 0.52 respectively; $p < 0.01$). In contrast, high salinity and density values corresponded to the post

upwelling communities (R^2 : 0.42; $p=0.0001$). The high light and low light separation along NMDS axis 2 were associated with phosphate and dissolved oxygen concentration as well as pH. Maximum phosphate concentrations were linked to the LL samples (R^2 : 0.53; $p=0.0001$), while high pH and oxygen values were significantly correlated to the HL protistan communities (R^2 : 0.4, 0.42, respectively; $p<0.001$).

In a subsequent step, the relative abundance of annotated functions for the different forms of symbiosis and the phagotrophic modes of ingestion from the trait database were analyzed for significant correlations to the NMDS structure (Figure 34 and Supplementary File 25). The ASVs without assigned symbiosis traits and the internal and external phagotrophic modes showed significant associations to the NMDS axis 1 (R^2 : 0.25, 0.72, 0.48, respectively; $p<0.01$). They were most prominent in the initial protistan communities prior to DW addition. Likewise, saprotrophic and commensalistic relationships significantly correlated with the pre to post upwelling gradient but were eminent in the post DW addition communities (R^2 : 0.16, 0.2, respectively; $p<0.05$). Furthermore, the saprotrophs were more associated to the HL samples and the relative abundance of commensalistic ASVs were higher in the LL mesocosms. Mutualistic photosynthetic relationships were correlated with NMDS axis 2 (R^2 : 0.25 respectively; $p=0.0013$) and leading in relative ASV abundance for the HL protistan plankton communities. Parasitic and osmotrophic protistan plankton were associated to the LL samples after DW addition and correlated significantly with the NMDS axis 2 (R^2 : 0.15, 0.6, respectively; $p<0.05$).

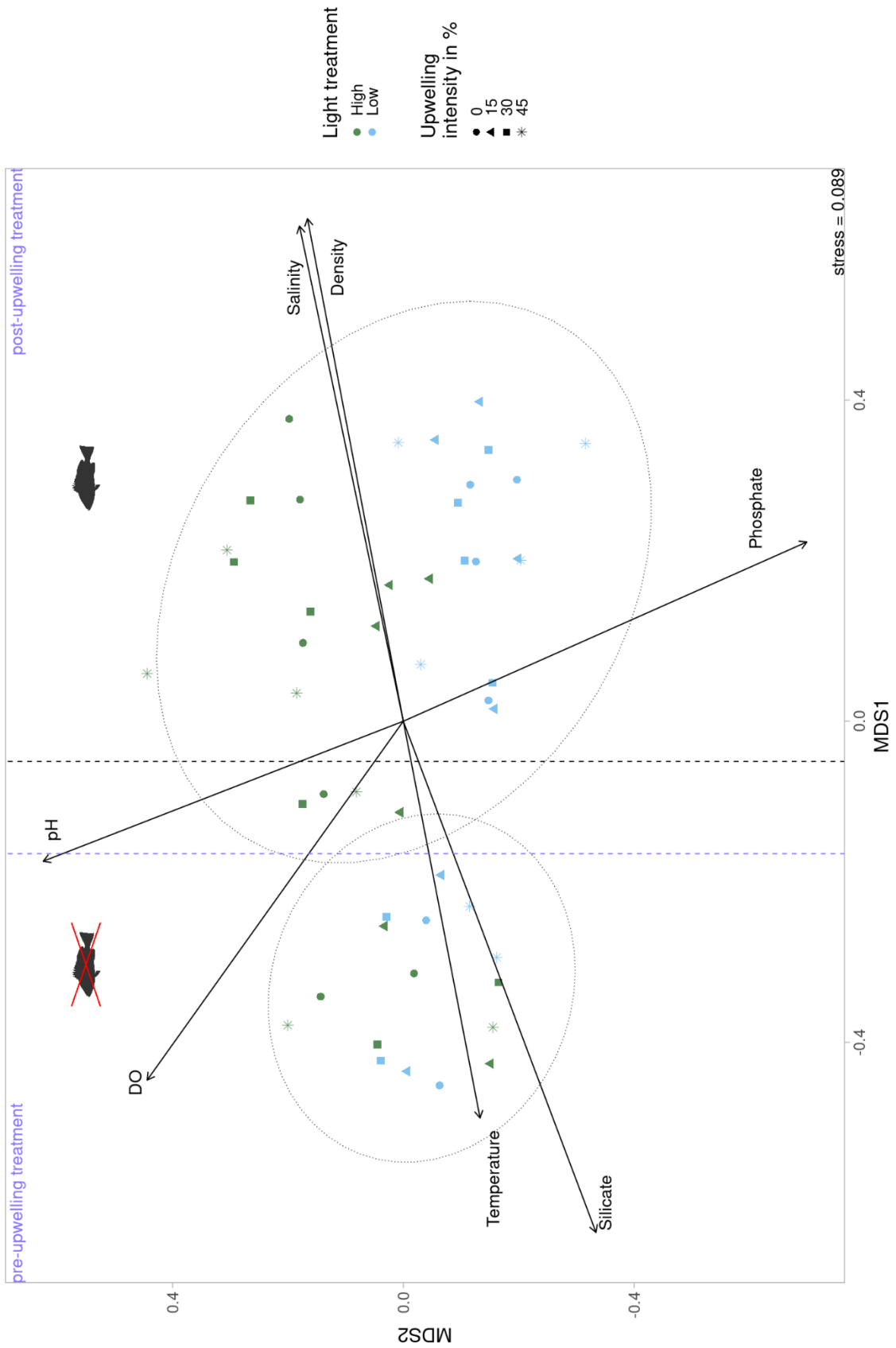


Figure 33. NMDS of protistan plankton community structures based on Bray Curtis distances. The light treatments are colored and the upwelling intensities are highlighted by symbols. Black circles are the 95% confidence intervals of samples pre and post upwelling. The black dashed line separates the samples without and with fish larvae addition. The blue dashed line separates the samples before and after deep-water treatment. DO: dissolved oxygen.

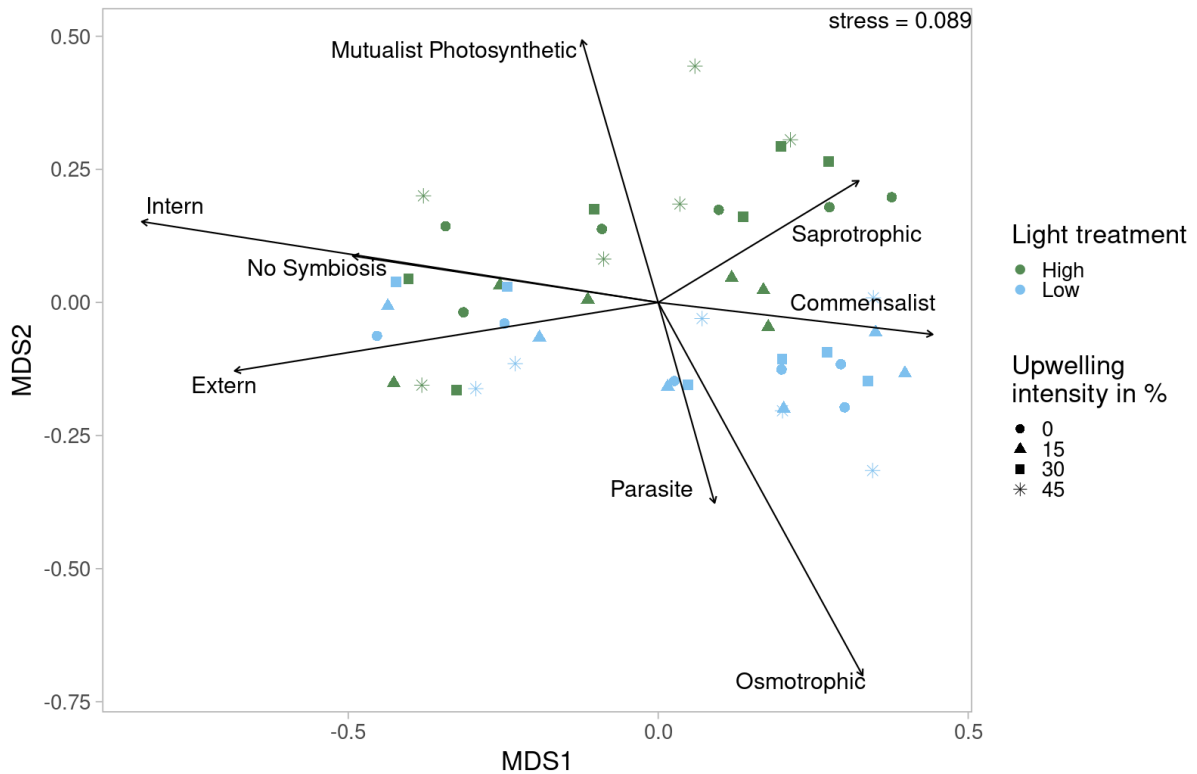


Figure 34. NMDS of protistan plankton community structures based on Bray-Curtis distances with significantly correlated biotic functions. The light treatments are colored and the upwelling intensities are highlighted by symbols. Intern: internal ingestion; Extern: external ingestion; Mutualist.: mutualistic.

7.1.5 Taxonomic Composition of Protistan Plankton Communities

The dominant phylum over all samples was Dinoflagellata with $24.6 \pm 8.5\%$ in relative abundance of reads. The second most abundant sequences were assigned to ochrophytes ($16.6 \pm 5.5\%$) followed by haptophytes ($15.0 \pm 5.9\%$) and chlorophytes ($11.6 \pm 5.2\%$). Less frequent reads in descending order belonged to the phyla Cercozoa, Mesomycetozoa, Radiolaria and Ciliophora, each with proportions below 10% but still above 1%. However, the succession and proportions in read abundances varied depending on the light treatment (Figure 35 and Table 16). In the HL mesocosms, dinoflagellate sequences accounted for $29.1 \pm 7.3\%$, while they represented $20.1 \pm 7.3\%$ in the LL mesocosms. The samples of the LL treatments followed the pattern where Ochrophyta ($18.8 \pm 5.9\%$), Haptophyta ($15.2 \pm 6.1\%$) and Chlorophyta ($14.4 \pm 5.7\%$) succeeded in this sequential order in terms of read abundance. On the other hand, in the HL mesocosms, the haptophytes ($14.8 \pm 6.0\%$) superseded as the second most abundant, followed by ochrophytes ($14.3 \pm 4.2\%$) and chlorophytes ($8.8 \pm 2.6\%$). One should mention that the relative abundances of haptophytes were not particularly different between the light treatments. The relative abundance of chlorophyte assigned sequence reads, however, had been

reduced by almost half in HL compared to LL samples. Regarding the less prevalent sequence reads, Cercozoa ($6.3 \pm 4.3\%$) succeeded ciliates ($3.1 \pm 1.3\%$) and radiolarians ($3.0 \pm 1.4\%$), followed by Mesomycetozoa ($2.6 \pm 4.2\%$) in the HL mesocosms. The Mesomycetozoa ($5.3 \pm 6.0\%$) assigned sequences accounted for more than double the proportion in LL samples compared to the HL protistan communities. Cercozoans ($4.9 \pm 1.9\%$), radiolarians ($2.7 \pm 2.0\%$) and ciliates ($2.6 \pm 2.0\%$) represented the rear of noteworthy taxa mentioned for the LL treatment. The residual frequency of around 18% and 16% was composed of the remaining 24 taxon groups for the HL and LL samples, respectively (Supplementary File 18). The protistan plankton community composition was relatively consistent across the upwelling intensity treatments for both light treatments. Discrepancies of this rule were the relative decline of ciliates in the HL0 compared to the other treatments where Ciliophora had fairly steady abundances. Another noticeable deviation was the Mesomycetozoa in the HL15 sample on day 33. They were up to a magnitude higher in relative read abundances compared to all other HL samples on day 33. Likewise, the striking disparity between the LL45 sample on day 29 and the other LL samples revealed up to 3 times higher sequence reads for ochrophytes and less than half the proportion of haptophytes.

Table 16. Dominant protistan plankton groups associated to the specific treatments. Chlorophyta, Dinoflagellata, Haptophyta and diatoms arranged in decreasing order of relative abundance for the specific treatment.

	Low Light	Low Nutrients	Low Light	High Nutrients	High Light	Low Nutrients	High Light	High Nutrients
Decreasing relative abundance ↓	Chlorophyta		Diatoms		Dinoflagellata		Dinoflagellata	
	Dinoflagellata		Haptophyta		Haptophyta		Haptophyta	
	Haptophyta		Chlorophyta		Diatoms		Diatoms	
	Diatoms		Dinoflagellata		Chlorophyta		Chlorophyta	

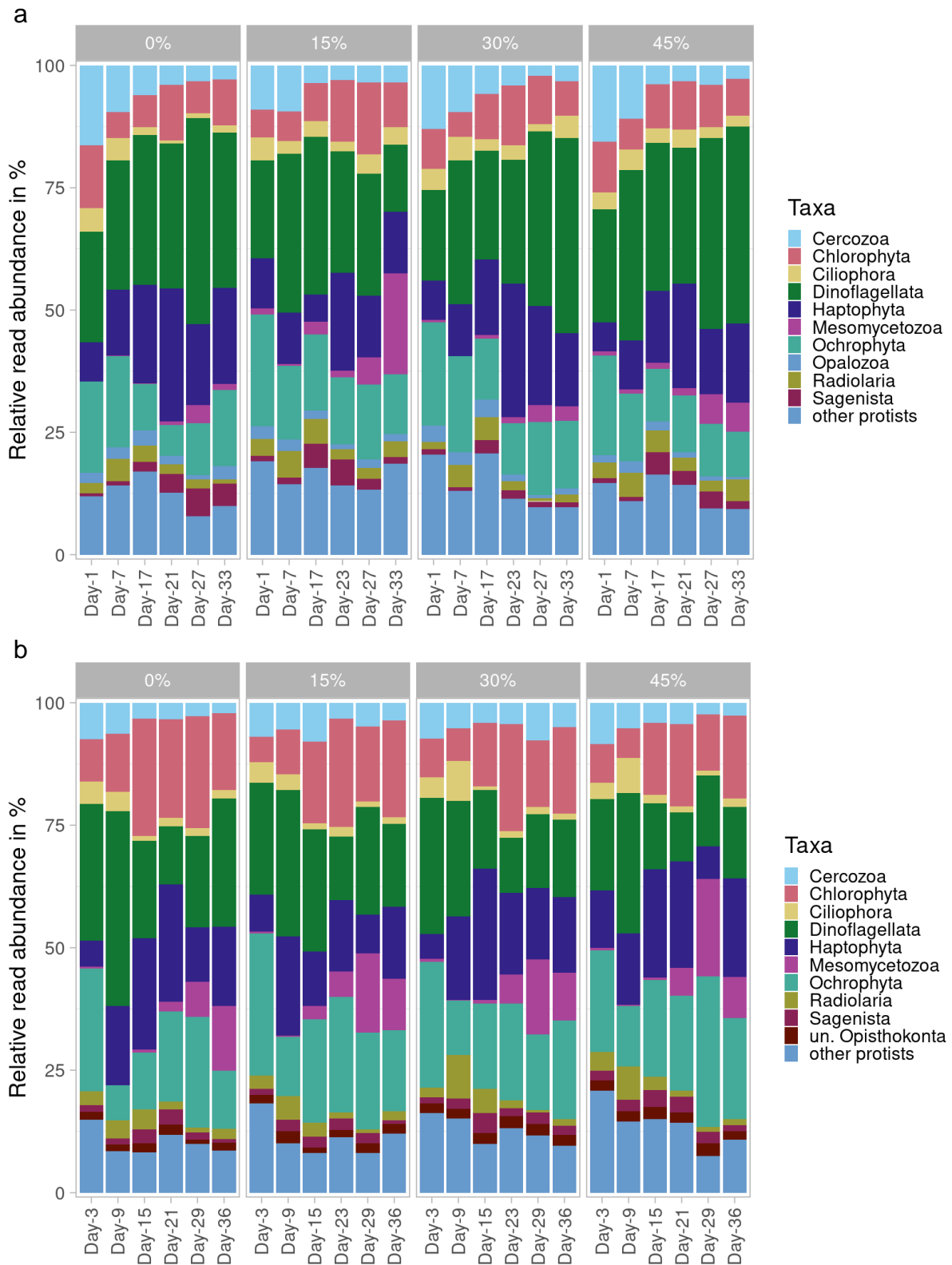


Figure 35. Taxonomic inventories of protistan plankton ASVs reads for (a) HL mesocosm and (b) LL mesocosms. The bars represent the relative abundance of ASVs assigned to each of the different taxon groups at the phylum level.

Treatment effects were analyzed in more detail by ANCOVA for the most abundant phyla: chlorophytes, dinoflagellates, haptophytes, Mesomycetozoa and ochrophytes. Normal distribution of residuals and homogeneity of variance were verified (Table 17), thus ANCOVA analysis could be conducted without data transformation.

Table 17. Shapiro Wilk and Levene's test results for the relative abundance of the most dominant plankton groups. Verification of the normal distribution and variance homogeneity for Chlorophyta, Dinoflagellata, Haptophyta, Mesomycetozoa and Ochrophyta.

Model	Test	statistics	p-value
Chlorophyta	Shapiro-Wilk	0.929	0.503
	Levene	0.00032	0.986
Dinoflagellata	Shapiro-Wilk	0.937	0.578
	Levene	0.496	0.508
Haptophyta	Shapiro-Wilk	0.831	0.061
	Levene	0.367	0.567
Mesomycetozoa	Shapiro-Wilk	0.862	0.125
	Levene	0.736	0.424
Ochrophyta	Shapiro-Wilk	0.948	0.694
	Levene	0.093	0.771

Noteworthy patterns could be identified by visualizing the changes in relative abundance for the light manipulation integrated over the upwelling intensities (Figure 36) and statistically tested by ANCOA (Table 18). Chlorophyta were significantly influenced by the light and upwelling manipulation, as well as their interaction ($p < 0.05$). Especially, the light treatment explained 84% of the variance (sum of squares). Although significant, the upwelling intensity and the interaction term only explained 6.3% and 5.4% of the total variation. Remarkable was the steady decrease of chlorophyte assigned sequence reads with increasing upwelling intensity. The light manipulation was likewise the main effect for the changes in relative abundance of dinoflagellates with 80.6% and ochrophytes with 75.3% of the total sum of squares ($p < 0.01$). The upwelling intensity, however, was not significant, even though ochrophytes increased in their relative abundance and decreased for dinoflagellates with rising

upwelling intensity in LL samples could be observed. Mesomycetozoa were not significantly influenced by either tested parameter albeit an obvious difference in light treatment with up to four times higher relative abundance for LL samples. The light manipulation also had the highest explanatory power of the variation with 54.8%, albeit it was not significant ($p = 0.0795$). Haptophyta had no significant main effect at all and the majority of the variation remained unexplained with 94.0% of the sum of squares allocated to the residuals.

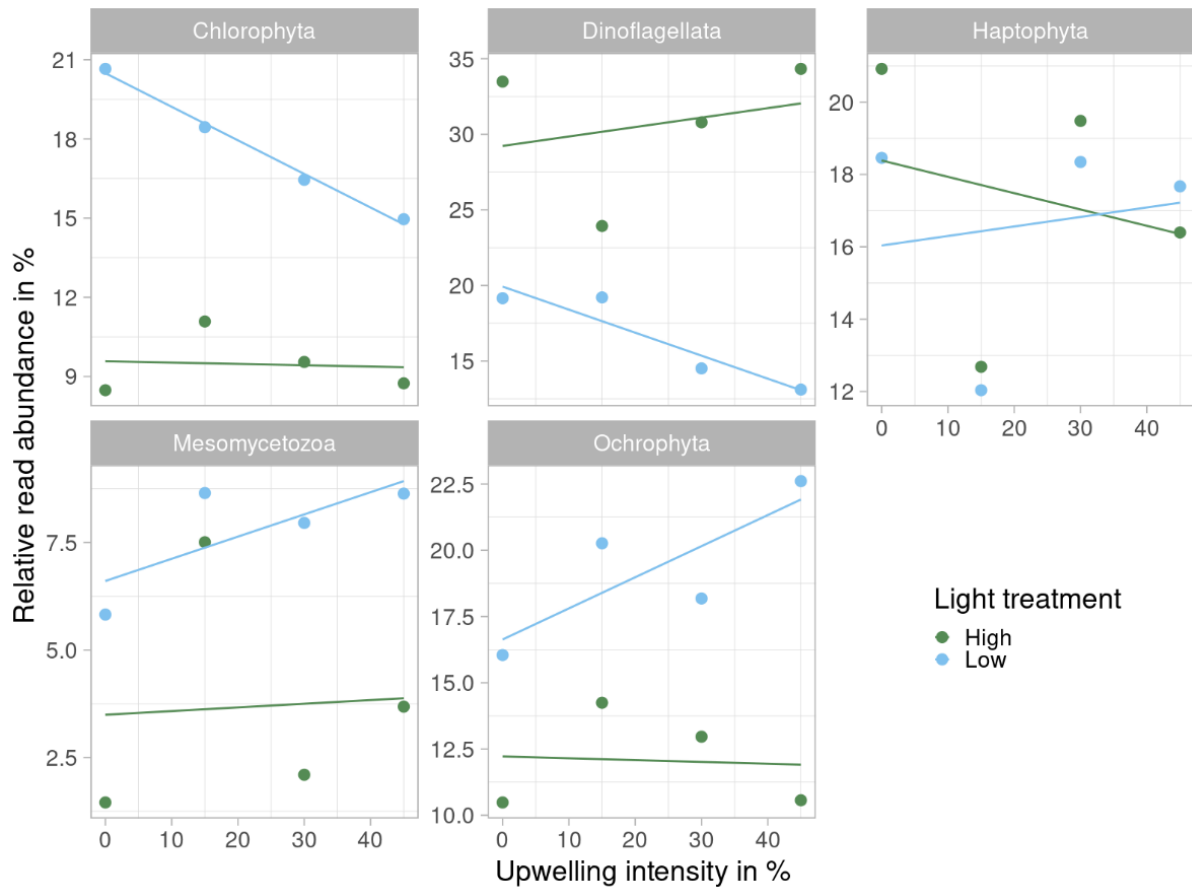


Figure 36. Changes in relative read abundance of the five most abundant phyla in relation to upwelling intensities derived from integrating all time points. The light treatments are colored and a respective trend line is added.

Table 18. Analysis of covariance (ANCOVA) for the most dominant plankton groups. ANCOVA test results for the mesocosm manipulations, their interactions, and the residuals for Chlorophyta, Dinoflagellata, Haptophyta, Mesomycetozoa and Ochrophyta. DF: degrees of freedom; SS: sum of squares.

Model	ANCOVA	DF	SS	F	p-value
Chlorophyta	Upwelling intensity	1	9.84	9.31	0.0379
	Light treatment	1	133.32	126.11	0.0004
	Interaction	1	8.40	7.94	0.0479
	Residual	4	4.23		
Dinoflagellata	Upwelling intensity	1	4.53	0.27	0.6283
	Light treatment	1	399.82	24.20	0.0079
	Interaction	1	25.95	1.57	0.2783
	Residual	4	66.08		
Haptophyta	Upwelling intensity	1	0.20	0.01	0.9173
	Light treatment	1	1.10	0.07	0.8079
	Interaction	1	2.87	0.18	0.6966
	Residual	4	65.35		
Mesomycetozoa	Upwelling intensity	1	2.03	0.33	0.5943
	Light treatment	1	33.25	5.47	0.0795
	Interaction	1	1.04	0.17	0.7001
	Residual	4	24.33		
Ochrophyta	Upwelling intensity	1	6.87	1.49	0.2896
	Light treatment	1	103.95	22.50	0.0090
	Interaction	1	8.69	1.88	0.2422
	Residual	4	18.48		

The dominant families of the top five phyla were investigated to determine if the same main effects still prevailed and the same patterns occurred in regards to their relative read abundance (Figure 37). The first step was validating the variance homogeneity and the normal distribution of residuals by Levene's test and the Shapiro-Wilk test, respectively (Table 19). Since the testing hypothesis could be rejected ($p > 0.05$), a variance homogeneity and a normal

distribution of residuals were accepted and ANCOVA could be applied for each taxon group (Table 20).

Table 19. Shapiro Wilk and Levene's test results for the relative abundance of the dominant families within the most abundant phyla. Verification of the normal distribution and variance homogeneity for Abeoformidae Group MAIP 2, Dino-Group-I-Clade-4, Polar-centric-Mediophyceae, Suessiaceae, unassigned Chlorellales and unassigned Dinophyceae.

Model	Test	Statistics	p-value
Abeoformidae Group MAIP 2	Shapiro-Wilk	0.934	0.55
	Levene	0.133	0.728
Dino-Group-I-Clade-4	Shapiro-Wilk	0.976	0.941
	Levene	0.026	0.878
Polar-centric-Mediophyceae	Shapiro-Wilk	0.968	0.879
	Levene	0.153	0.709
Suessiaceae	Shapiro-Wilk	0.859	0.119
	Levene	3.3	0.119
unassigned Chlorellales	Shapiro-Wilk	0.879	0.184
	Levene	0.255	0.632
unassigned Dinophyceae	Shapiro-Wilk	0.932	0.539
	Levene	0.650	0.451

Abeoformidae Group MAIP 2 (MAIP: Marine Ichthyosporea) dominated the Mesomycetozoa and exhibited the same trend with up to four times higher read abundances in LL samples compared to HL samples. ANCOVA calculated a significant light influence with an explanatory power of 57.9% of total sum of squares ($p < 0.05$). The most prevailing family in the phylum Ochrophyta was Polar-centric-Mediophyceae. The HL samples did not fluctuate heavily along the distinct upwelling intensities opposed to the LL samples which correlated positively with the upwelling intensity. The responsible main effect for the changes in the relative abundance was also the light manipulation (ANCOVA, $p < 0.05$; 69.3% of total sum of squares). The dominant member in Chlorophyta was the order Chlorellales, which could not be further classified. Similar patterns to the Polar-centric-Mediophyceae were observed for Chlorellales in HL samples. In LL mesocosms exactly the opposite trend was perceived: with higher upwelling intensities lower relative read abundances were measured. The main effect

was once again light, with a calculated explanatory value of 80% (ANCOVA, $p < 0.001$). Multiple groups contributed to the overall dominance of dinoflagellates wherefore three highly dominant dinoflagellate taxa were examined: Suessiaceae, Dino-Group-I-Clade-4 and unassigned Dinophyceae. Suessiaceae had no significant effects tested by ANCOVA ($p > 0.05$), nevertheless, this family showed a negative trend in relative read abundance with higher upwelling intensities for both light treatments. Similar patterns were observed for the Dino-Group-I-Clade-4, which was confirmed via ANCOVA ($p < 0.05$). In this case, the upwelling intensity even explained 55.4% of the variance. The interaction term and the light manipulation yielded further explanatory power with 20.6% (ANCOVA, $p < 0.05$) and 13.5% (ANCOVA, $p = 0.086$), respectively. The unassigned Dinophyceae had a steady relative abundance of approximately 2% in the HL samples and doubled for the LL samples between 0% and 45% upwelling intensity. However, the major effect responsible for changes in relative abundance was again contributed to the light treatment (ANCOVA, $p < 0.05$; 55.7% of total sum of squares). Haptophyta were disregarded in this examination due to the unexplained variance of the previous statistical analysis (see Table 18).

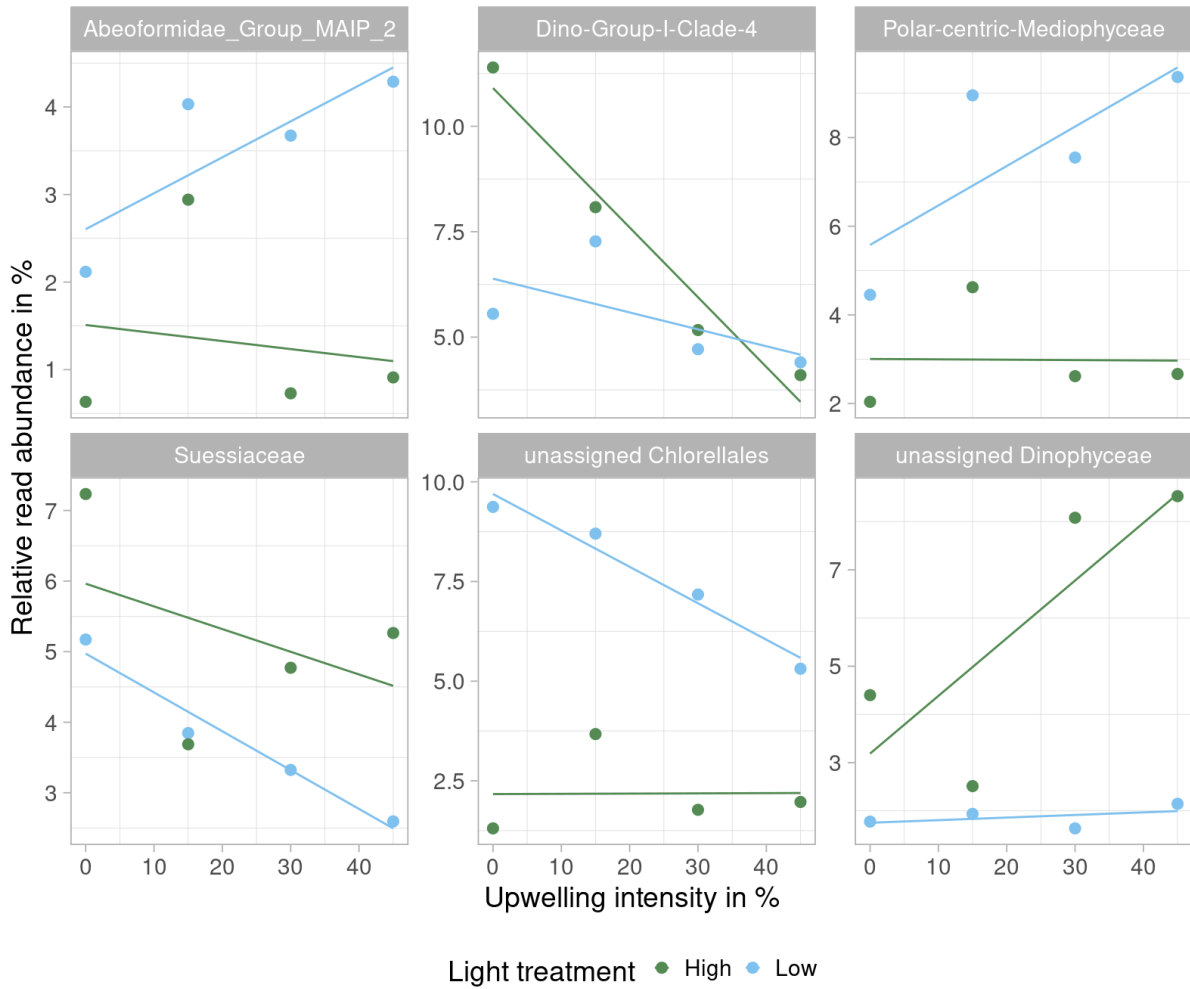


Figure 37. Changes in relative read abundance of the dominant families within the most abundant phyla in relation to upwelling intensities derived from integrating all time points. The light treatments are colored and a respective trend line is added.

Table 20. Analysis of covariance (ANCOVA) for the relative abundance of the dominant families within the most abundant phyla. ANCOVA test results for the mesocosm manipulations, their interactions, and the residuals Abeoformidae Group MAIP 2, Dino-Group-I-Clade-4, Polar-centric-Mediophyceae, Suessiaceae, unassigned Chlorellales and unassigned Dinophyceae. DF: degrees of freedom; SS: sum of squares.

Model	ANCOVA	DF	SS	F	p-value
Abeoformidae Group MAIP 2	Upwelling intensity	1	0.57	0.51	0.5141
	Light treatment	1	8.89	8.85	0.0409
	Interaction	1	1.42	1.27	0.3230
	Residual	4	4.47		
Dino-Group-I-Clade-4	Upwelling intensity	1	23.72	20.99	0.0101
	Light treatment	1	5.78	5.12	0.0864
	Interaction	1	8.82	7.81	0.0490
	Residual	4	4.52		
Polar-centric- Mediophyceae	Upwelling intensity	1	4.37	1.79	0.2524
	Light treatment	1	42.20	17.26	0.0142
	Interaction	1	4.53	1.85	0.2451
	Residual	4	9.78		
Suessiaceae	Upwelling intensity	1	4.28	3.06	0.1549
	Light treatment	1	4.53	3.25	0.1459
	Interaction	1	0.29	0.21	0.6700
	Residual	4	5.58		
unassigned Chlorellales	Upwelling intensity	1	4.64	5.20	0.0848
	Light treatment	1	59.61	66.80	0.0012
	Interaction	1	4.76	5.33	0.0821
	Residual	4	3.57		
unassigned Dinophyceae	Upwelling intensity	1	8.80	3.75	0.1248
	Light treatment	1	32.10	13.69	0.0208
	Interaction	1	7.35	3.13	0.1514
	Residual	4	9.38		

7.2 Microbial Abundances & Carbon Flow in the Humboldt Current System

7.2.1 Prokaryotic & Protistan Abundances

Bacterial abundances for HL mesocosms were in general lower ($4.6 \times 10^6 \pm 1.7 \times 10^6 \text{ mL}^{-1}$) compared to LL mesocosms ($5.3 \times 10^6 \pm 2.0 \times 10^6 \text{ mL}^{-1}$, raw data in Supplementary File 26). In contrast, more protistan cells were present in the HL samples ($3.5 \times 10^4 \pm 2.6 \times 10^4 \text{ mL}^{-1}$) than in the LL samples ($2.7 \times 10^4 \pm 1.8 \times 10^4 \text{ mL}^{-1}$). However, after verifying the normality of residuals and homogeneity of residual variances, no significant effect could be determined by means of ANCOVA ($p > 0.05$). The same applied to the upwelling simulation, which did not yield a significant explanatory value ($p > 0.05$), but patterns could still be observed. Prokaryotic abundance decreased in relation to the upwelling intensity for LL samples ($R^2 = 0.43$) but did not exhibit any correlation to the DW addition for HL samples ($R^2 = 0.032$; Figure 38). Peculiar were the relatively low bacterial counts at the 30% upwelling intensity.

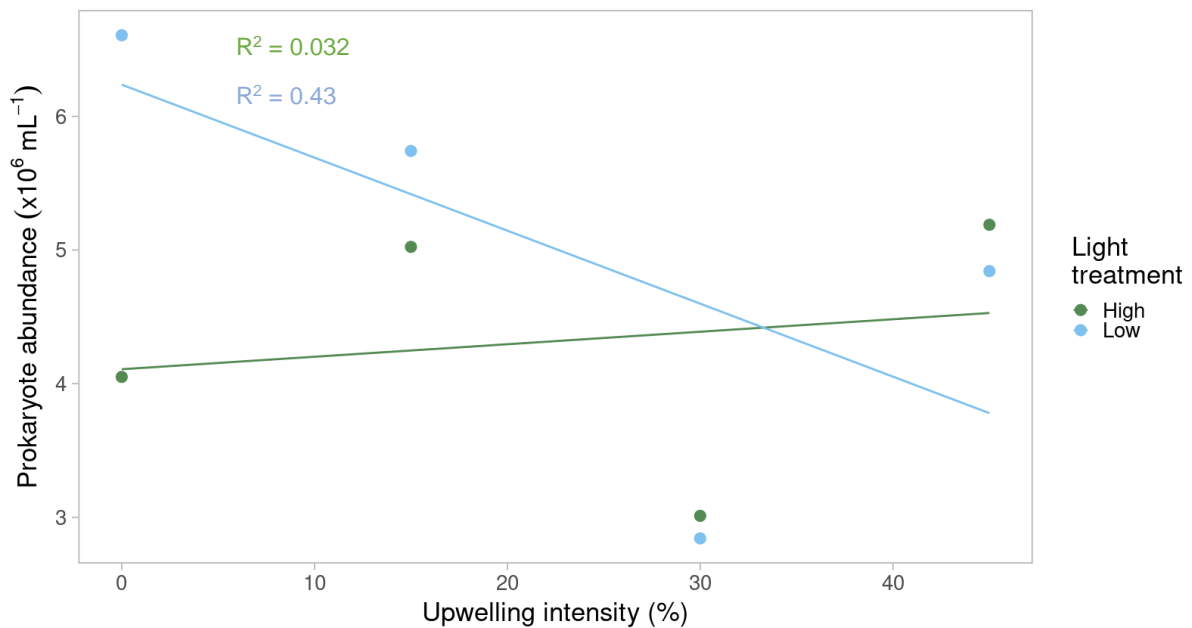


Figure 38. Prokaryotic abundance for upwelling intensities derived from integrating all time points. The light treatments are colored. Linear trendlines and coefficient of determination (R^2) for each light treatment were calculated using linear regression analysis.

Protistan abundance tendencies showed a reversed pattern. The number of protistan cells in LL mesocosms revealed no correlation with the upwelling intensities ($R^2 = 0.081$). The HL samples, on the other hand, displayed an increased protistan abundance with higher upwelling intensity ($R^2 = 0.59$; Figure 39).

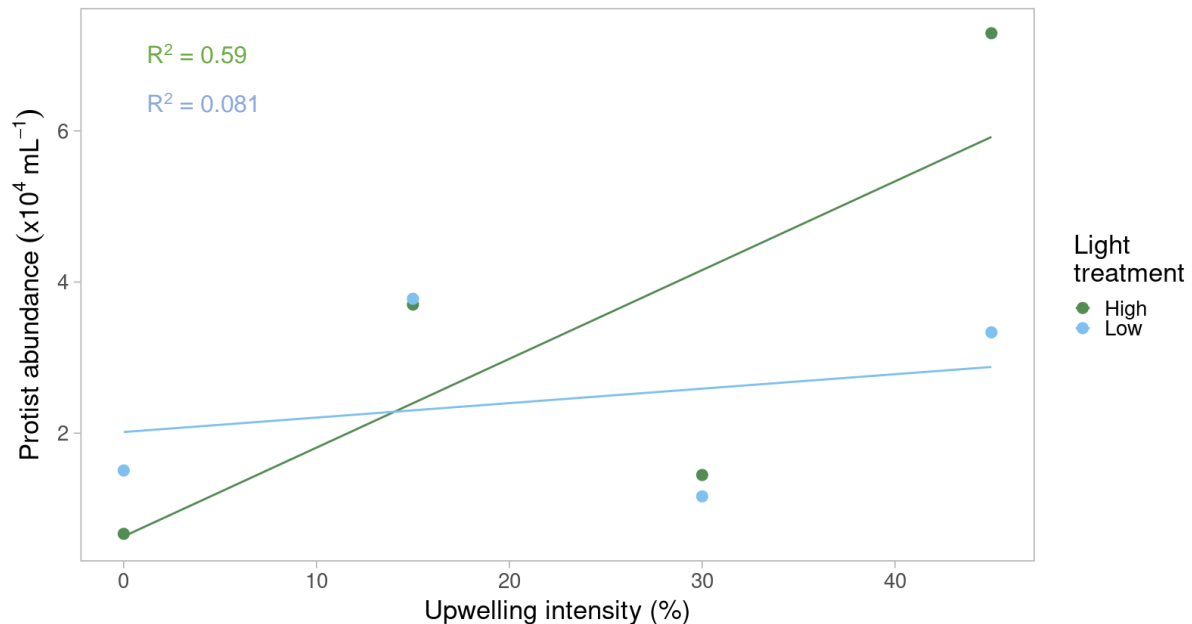


Figure 39. Protistan abundance for upwelling intensities derived from integrating all time points. The light treatments are colored. Linear trendlines and coefficient of determination (R^2) for each light treatment were calculated using linear regression analysis.

Temporal changes in abundance showed strong fluctuations. The bacteria increased in abundance for the first phase of the experimental setup and started declining right after the DW addition into the mesocosms (Figure 40.a). It has to be noted, that the same phenomenon occurred in the 0% mesocosms even though no nutrient-rich DW was exchanged. Only one sample was available for the 30% mesocosms in the pre-upwelling phase, however the decline in prokaryotic abundance could also be observed in the later days of the post-upwelling stage.

A decline of protistan cell abundance in the early days of the experiment could be detected in the mesocosms (Figure 40.b). After DW addition, a sharp increase of single-celled eukaryotes was observed for the 15% and 45% mesocosms. This peak declined steadily thereafter, except for the HL45 mesocosm where the upward trend remained. However, no sample >30 days was accessible for HL45. The 0% upwelling samples had fairly constant protistan abundances but they declined overall between the first and last sampling procedure. The same behavior was observed in the 30% mesocosms with no peak in protistan cell abundance after DW addition.

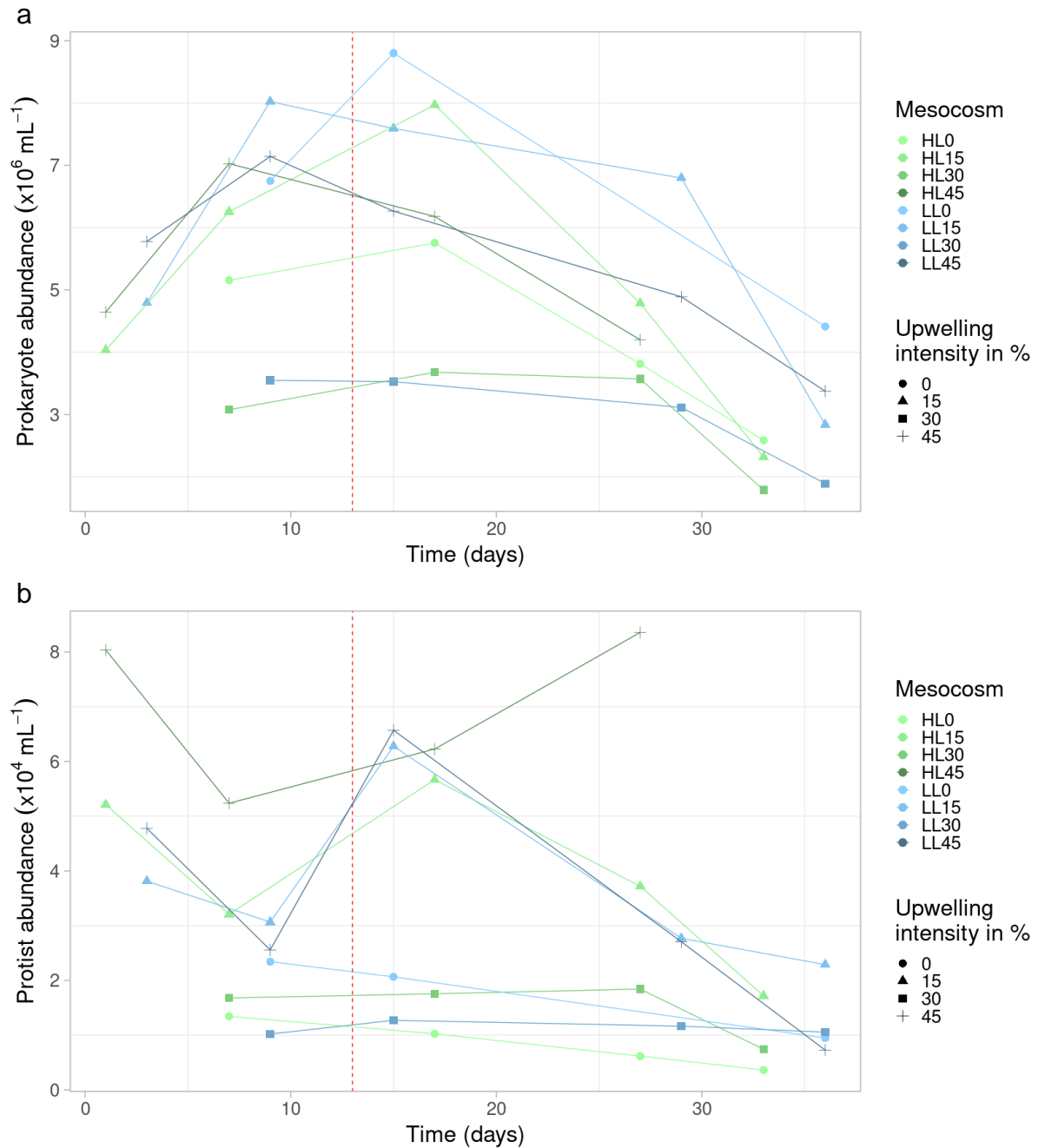


Figure 40. Development of prokaryote (a) and protistan (b) abundance in the mesocosms. Deep-water addition is highlighted by the red dashed line. Light treatment is colored in green for high light (HL) and blue for low light (LL).

7.2.2 Grazing Effect & Prokaryotic Turnover Rate

The Shapiro-Wilk test and Levene's test were not significant for the linear models of the phagotrophy estimators, therefore, normal distribution of residuals and homogeneity of residual variances could be assumed. This allowed the further approach of analyzing the impact of light and upwelling manipulation by ANCOVA. No significant effect of the treatments could

be determined for either the grazing effect nor the prokaryotic turnover rate. Nevertheless, tendencies could be observed (Figure 41 and Figure 42). In the LL treatment, no correlation of grazing effect with the upwelling intensity was measured ($R^2 = 0.046$). By contrast, the grazing effect in the HL mesocosms had a moderate positive correlation ($R^2 = 0.49$). Like the bacterial abundances, a low grazing effect was determined in the 30% samples. The grazing effect was higher in HL mesocosms ($4.0 \times 10^5 \pm 8.1 \times 10^5 \text{ cells mL}^{-1} \text{ h}^{-1}$) compared to LL mesocosms ($2.9 \times 10^5 \pm 4.7 \times 10^5 \text{ cells mL}^{-1} \text{ h}^{-1}$), albeit having an immense standard deviation (raw data in Supplementary File 26). The same applied to the bacterial turnover rate with $206 \pm 505\%$ of the bacterial standing stock per day in HL samples and $117 \pm 169\%$ of the prokaryotic standing stock per day in LL mesocosms. Apparently, the exceedingly large standard deviations resulted from the substantial temporal and mesocosm specific variations (Figure 43).

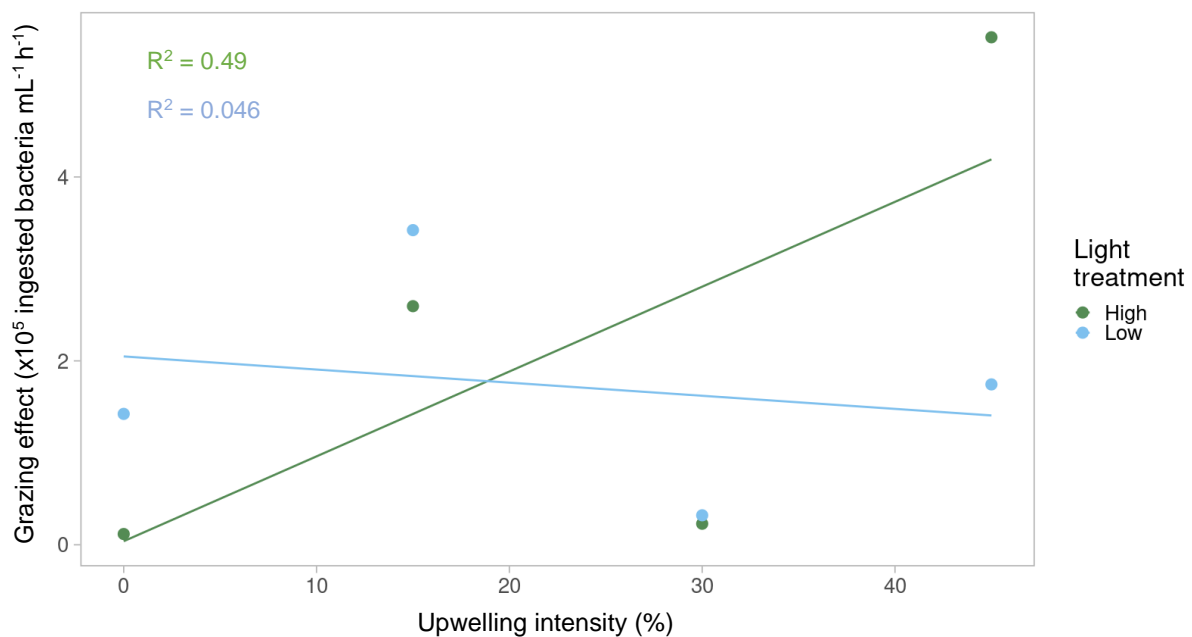


Figure 41. Grazing effect for upwelling intensities derived from integrating all time points. The light treatments are colored. Linear trendlines and coefficient of determination (R^2) for each light treatment were calculated using linear regression analysis.

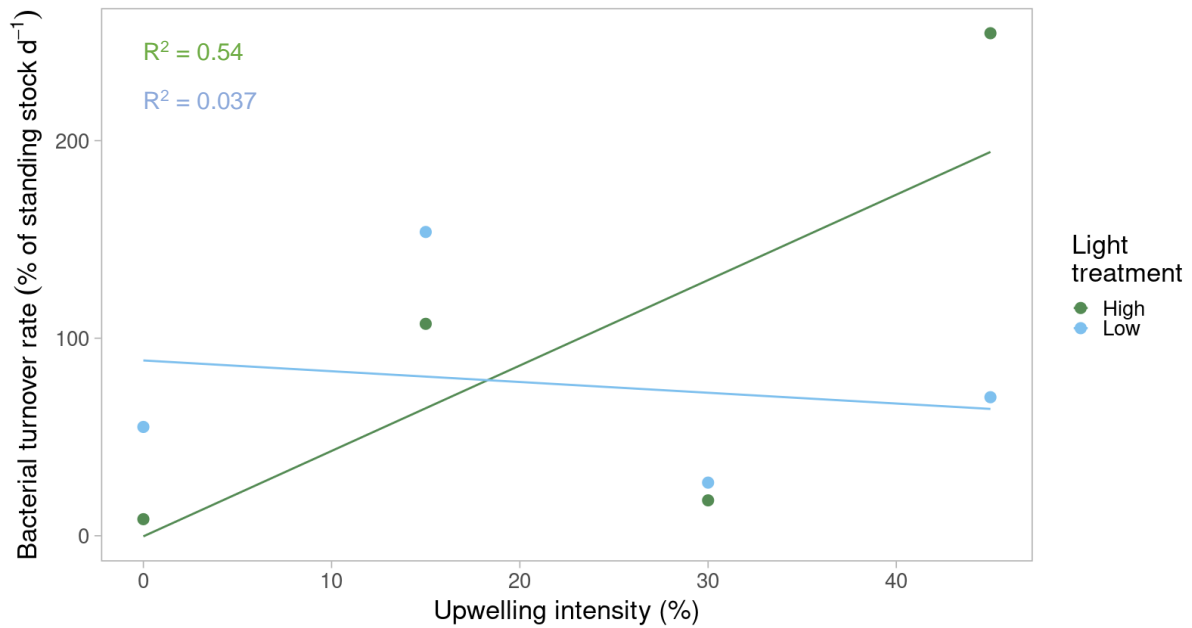


Figure 42. Prokaryotic turnover rate for upwelling intensities derived from integrating all time points. The light treatments are colored. Linear trendlines and coefficient of determination (R^2) for each light treatment were calculated using linear regression analysis.

In the pre-upwelling phase, tremendous grazing effects could be calculated with up to 2.4×10^6 cells $\text{mL}^{-1} \text{h}^{-1}$ (HL15) and 1.7×10^6 cells $\text{mL}^{-1} \text{h}^{-1}$ (LL0). This corresponded to a ~15 times and ~6 times bacterial turnover rate of the standing stock per day in HL15 and LL0, respectively. The remaining samples had lower values and did not exceed a grazing effect of 1.0×10^6 cells $\text{mL}^{-1} \text{h}^{-1}$ or a 5 times prokaryotic turnover rate per day. Especially the 30% samples had the lowest values again. In all mesocosms that had been subjected to an addition of DW (except the HL15) an enhancement of grazing effect and prokaryotic turnover rate was registered after treatment. No increase in the grazing effect and turnover rate in the mesocosms HL0 and LL0 could be recorded. During the post-upwelling phase, a general decrease in grazing effect was calculated between day 15 and 17 ($3.3 \times 10^5 \pm 3.4 \times 10^5$ cells $\text{mL}^{-1} \text{h}^{-1}$) and the last days (27 – 36; $1.0 \times 10^5 \pm 1.5 \times 10^5$ cells $\text{mL}^{-1} \text{h}^{-1}$) of the experiment. The prokaryotic turnover rate mirrored the grazing effect exactly and declined from 118 ± 120 to $63 \pm 92\%$ of the bacterial standing stock per day in this time frame. However, individual deviations from this pattern could be detected, as for example the increase between day 29 and day 36 of LL15.

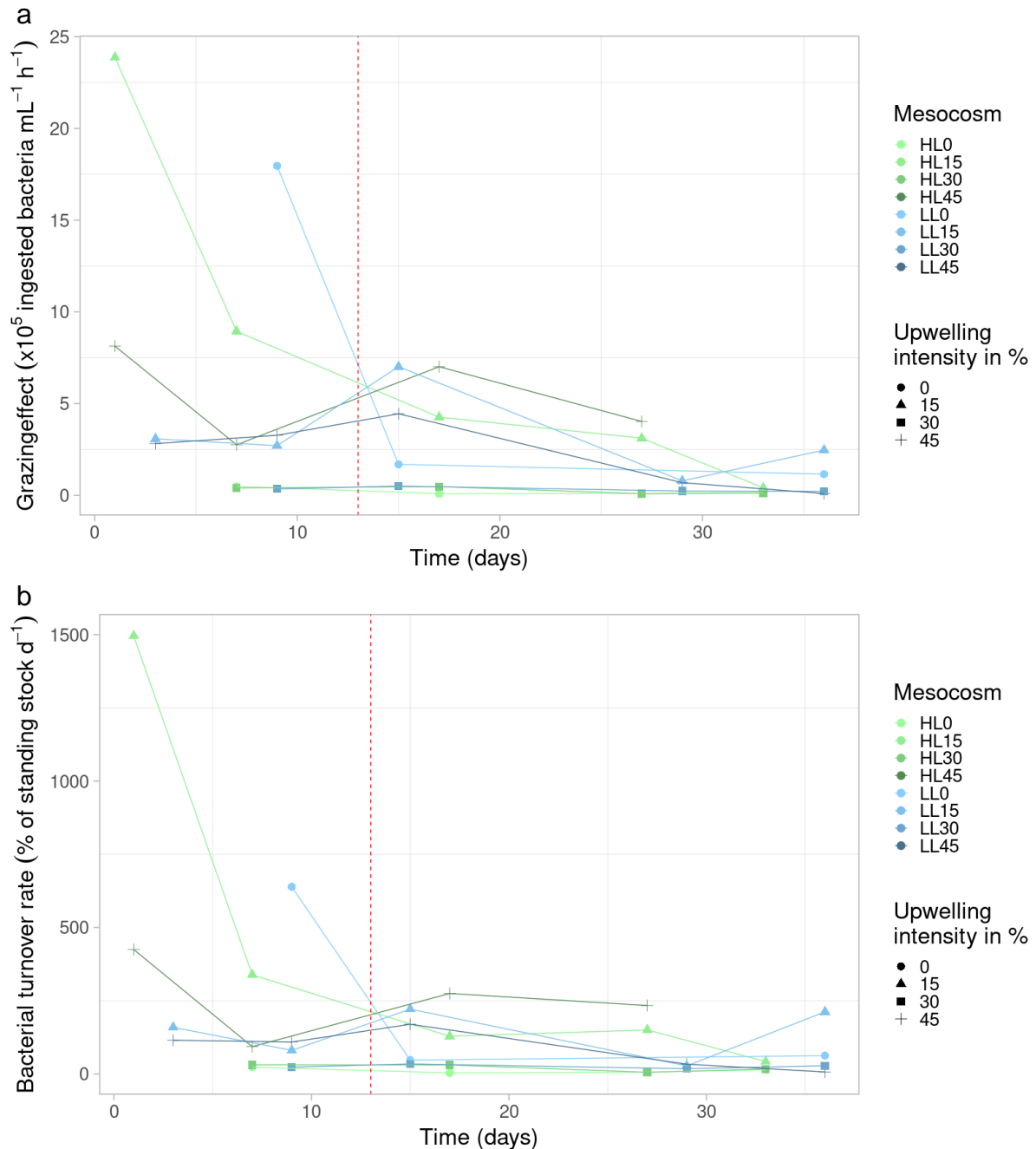


Figure 43. Development of grazing effect (a) and prokaryotic turnover rate (b) in the mesocosms. Deep-water addition is highlighted by the red dashed line. Light treatment is colored in green for high light (HL) and blue for low light (LL).

7.2.3 Correlation Analysis

To determine significant relationships between the physicochemical parameters and the abundance of prokaryotes and protists, as well as the phagotrophy estimators, correlation analysis was performed using the Spearman rank test (Figure 44).

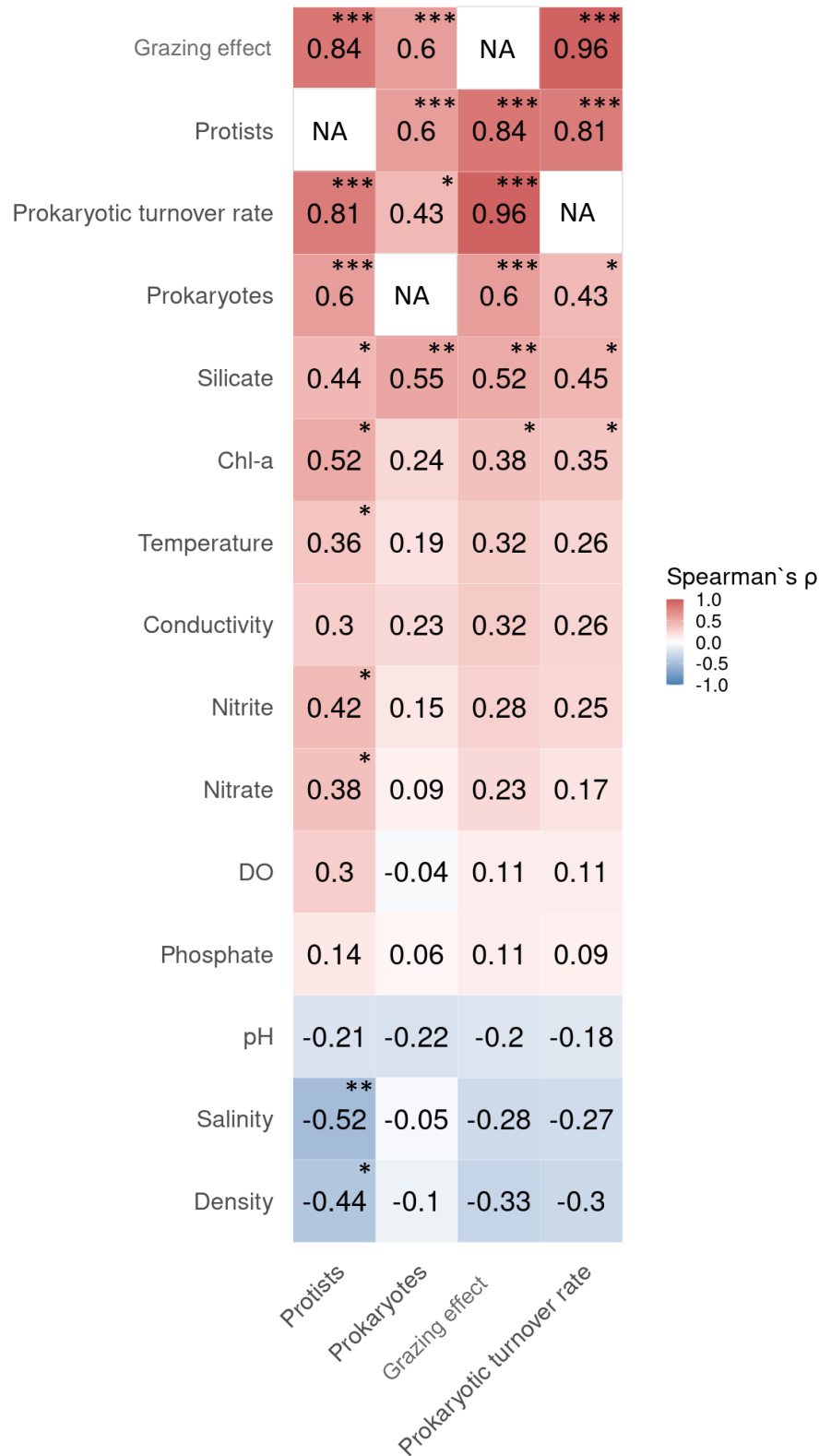


Figure 44. Correlation of physicochemical parameters, grazing effect, prokaryotic and protistan abundances and prokaryotic turnover rate. Color scale represents Spearman's ρ ; and not applicable (NA). Significant correlations are highlighted by asterisks (*: $p < 0.05$; **: $p < 0.01$; ***: $p < 0.001$). DO: dissolved oxygen; Chl: Chlorophyll.

The microbial abundances and the phagotrophy estimators were highly associated with each other. Especially the interconnection between grazing effect, bacterial turnover rate and protistan abundance had highly significant positive correlations (Spearman $\rho > 0.81$; $p < 0.001$). The prokaryotic abundance was moderately and positively (Spearman $\rho = 0.43$; $p < 0.05$) correlated to the bacterial turnover rate and had a strong positive correlation with the protistan abundance and the grazing effect (Spearman $\rho > 0.6$; $p < 0.001$). The silicate concentration was the only physicochemical parameter with significant results connected to all four microbial measurements ($p < 0.05$). They were moderately associated with Spearman ρ values between 0.44 and 0.55. Chlorophyll-a had weak to moderate significant relations with the grazing effect, bacterial turnover rate and the protistan abundance (Spearman $\rho = 0.38, 0.35, 0.52$, respectively; $p < 0.05$). Temperature, nitrite, and nitrate were positively correlated with the prokaryotic cell number (Spearman $\rho = 0.36, 0.42, 0.38$, respectively; $p < 0.05$). The only significant negative correlation results were determined for salinity and density. Both had negative associations with the protistan abundance (Spearman $\rho = -0.52, -0.44$, respectively; $p < 0.05$).

8 Discussion

8.1 Protistan Plankton Dynamics in the Humboldt Current System

8.1.1 *Effect of Light & Upwelling Scenarios on Regional Protistan Plankton Diversity*

Future consequences of the anthropogenic climate change are alterations in the coastal light regimes and upwelling dynamics, which are proposed to have a major impact on the EBUS in Peru (Bakun et al., 2015; Messié and Chavez, 2015). Therefore, it is of utmost relevance to improve our understanding of protistan plankton communities to these alternating factors. The distinct light intensities coupled with multiple upwelling scenarios revealed significant effects on the diversity and the community composition of protistan plankton with pronounced effects on their trophic interactions. The findings provided in this study may foreshadow future scenarios of how unicellular eukaryote dynamics in EBUS will evolve in the context of climate change.

Immigrant Plankton Types Enhance Protistan Plankton Diversity by Simulated Upwelling

The upwelling simulations induced a significant increase in alpha diversity, which contradicts the paradox of enrichment due to competitive interactions where the promotion of fast-growing species (*r*-strategists, ‘opportunists’) to the detriment of others (*k*-strategists, ‘gleaners’) consequently results in a loss of diversity (Grover, 1990; Papanikolopoulou et al., 2018; Tubay et al., 2013). A reduction in diversity by inducing a pronounced artificial plankton bloom could most likely not be recorded due to the applied upwelling mode. A single upwelling pulse, as conducted in this experiment, has diminished effects which may not force less adapted species to extinction as opposed to the mode of continuous upwelling seen in natural systems (Ortiz et al., 2022a; Papanikolopoulou et al., 2018). The results are more congruent to microcosm experiments analyzing the diversity changes with varying levels of nutrient supply (Anderson et al., 2022; Dittrich et al., 2023). Dittrich and colleagues (2023) reported a positive correlation between species richness and nutrient concentrations and assumed that these treatments not obligatorily eliminate less adapted species. In the experimental design by Anderson et al. (2022) the incubations with limited nutrient concentrations exhibited the lowest evenness, which corroborates well with the findings in this thesis. Contrary to the mechanism underlying the paradox of enrichment, the inevitable nutrient depletion in the mesocosms (faster in low upwelling treatments) might favor the dominance of *k*-strategists acclimated to nutrient deficiency leading to a reduced alpha diversity (Grover, 1990; Margalef, 1978;

Papanikolopoulou et al., 2018). The logical premise that no immigrant plankton types (a_i) within the DW were supplied to the local plankton community (a_{lo}) in the 0% mesocosms explains this result by the ‘dispersal driven diversity theory’ (Cadotte, 2006; Clayton et al., 2013). Hence, no increase in diversity by merging ($a_i + a_{lo}$) occurred in the non-treated mesocosm as opposed to the 15-45% upwelling simulations. Furthermore, the findings are consistent with the concept of the ‘intermediate disturbance hypothesis’, as well as a recent field study in the California Current System which emphasized that ‘moderate intermittent upwelling’ conditions yield the highest diversity (Connell, 1978; Harvey et al., 2021). Admittedly, defining an intermediate disturbance in regards to upwelling intensity has to be investigated in further research, as the classification of intensities is not easily applicable without measuring the implication of the whole spectrum (Huston, 1979).

Seasonal Fluctuations of Phytoplankton Diversity Induced by Distinct Light Intensities

The assumed seasonal variations induced by the light treatment likewise revealed significant alterations in alpha diversity (Shannon Index H' and evenness), which can dramatically affect ecosystem functions (Brose and Hillebrand, 2016). The natural austral summer, reflected by HL conditions, had a generally higher alpha diversity as recorded in the austral winter simulation, instigated by LL treatment, which is in agreement with previous aquatic studies throughout prokaryotes, phytoplankton and zooplankton (Gong et al., 2023; Suleiman et al., 2022; Wang et al., 2023). However, contrary findings were also reported, showing a negative relationship between phytoplankton diversity and light intensity (Flöder et al., 2002; Rodrigues et al., 2015). This predicament could result from physiological characteristics related to distinct light dependencies of individual plankton species for optimal photosynthetic activity (Huisman et al., 1999; Yang et al., 2020). Since the mid-1970s, light intensity was already theorized as a crucial factor responsible for niche separation, thus structuring coexistence and exclusion in communities (Flöder et al., 2002; Litchman, 1998; van Gemerden, 1974). Through monoculture experiments, Huisman and colleagues (1999) validated theorized model predictions for species specific ‘critical light intensities’. The critical light intensity is the minimum light availability at which a species still exhibits a steady state of abundance. Thus, the species that requires the lowest critical light intensity will dominate the community at the expense of other species when light is deprived, leading to a lower alpha diversity. Consequently, the effects of light on diversity should be highly dependent on the local plankton community. This competition for light as a limiting factor resembles the exclusion

principle for nutrient dynamics and corresponds well to the findings in this study (Flöder et al., 2002; Hardin, 1960; Huisman et al., 1999). The results in this thesis indicate that most of the resident plankton communities on the Peruvian coast are adapted to natural light conditions and subject to immediate light limitation. However, individual plankton species seem well suited to thrive in austral winter with reduced light intensities compared to austral summer.

Effect of Distinct Upwelling Intensities on Protistan Plankton Structure in a Mimicked Austral Winter Situation

In the initial phase of the austral winter simulation, a reduction in the relative abundance of diatoms was determined, which links well to the high silicic acid concentrations, as diatoms process this inorganic compound for building frustules consisting of silica (Lopez et al., 2005). It is well known that the silica accumulation by diatoms is light-dependent (Blank and Sullivan, 1979). The incorporation of silicic acid is reduced under low light intensities, which explains the elevated concentrations compared to the values measured in the austral summer mesocosms (Azam and Chisholm, 1976; Taylor, 1985). The relative decrease of diatoms was likewise mirrored in a reduction of dissolved oxygen, which clearly showed a severe collapse of their photosynthetic activity which was assumably caused by the rapid light reduction to mimic austral winter conditions (Alderkamp et al., 2019; Sekerci and Petrovskii, 2018).

The DW addition yielded nutrient concentrations that mirrored concentrations in natural upwelling system, albeit for a short time frame (Hauschildt et al., 2021; Igarza et al., 2019; Messié et al., 2009). This new input of macro- and micronutrients into the system created a permanent change in the community composition, validating hypotheses H_C1.1 and H_C1.2. The initial decline in the proportion of diatoms reversed, leading to the dominance of ASVs assigned to diatoms after DW addition and thereby indicating that nutrients are a strong selection factor for these algae. This further signifies that diatoms in the Peruvian coast have an accelerated response to nutrient availability at the expense of other species. The fast nutrient uptake, as well as rapid growth rates of diatoms, were previously reported for the subtropical North Pacific and the eastern equatorial Pacific, which validates their role as *r*-strategists or opportunists (Brown et al., 2008; Landry et al., 2000; Van Dam, 1982). A steep decline in the silicic acid concentration, reasonably caused by the biomineralization of diatoms, clearly supports this finding. The most important contributor to this phylum was the family Polar-centric-Mediophyceae (*Thalassiosira* spp., *Minidiscus* spp. and *Skeletonema* spp.), which are ubiquitous in the world's oceans and play a pivotal role as primary producers in the HCS

(González et al., 2007; Montero et al., 2007). Thriving under low light conditions allows the assumption of pronounced photoadaptation of these plankton species, which is widely observed in marine waters and responsible for the global scale chlorophyll patterns (Geider et al., 1996; Masuda et al., 2021; Talmy et al., 2013). Furthermore, diatoms are known as major contributors to the biological carbon pump in the HCS, especially during austral winter (González et al., 2009; Messié and Chavez, 2015).

Under nutrient deficiency, Chlorophyta were prevalent and primarily contributed to the osmotrophic foraging strategy in the trait approach. This corresponds well to the results in this thesis as osmotrophs are generally smaller and thrive under low nutrient concentrations compared to non-limiting conditions where larger cells are generally present (Våge et al., 2013). This divergent size class distribution induced by distinct upwelling scenarios can have major impacts on the food web structure and could alter ecosystem services (Stibor et al., 2019). Chlorophyta are in general less abundant in these waters but can bloom under low nutrient conditions induced by El Niño events in the HCS (Arntz et al., 2006; DiTullio et al., 2005; Mogollón and Calil, 2017). Bach et al. (2020) likewise reported chlorophytes in the mesocosms in the earlier Peru study. This could furthermore indicate a suppression of chlorophytes in turbulent waters due to niche segregation, despite the fact that mesocosms are designed to transmit turbulence from the ocean, a reduction is still to be expected (Bach et al., 2020; Margalef, 1978; Sharma et al., 2021). These green algae are likewise known for their photoacclimation mechanisms and yield an efficient photosynthetic activity under low light conditions (Fisher et al., 1989; Masojídek et al., 1999; Parsons et al., 2013). The optimal light intensity for chlorophytes is lower compared to diatoms, yet they were outcompeted in the mesocosms treated with DW (Figure 45; Parsons et al., 2013). This supports the classification of the local chlorophytes in the HCS as *k*-strategists (Dutkiewicz et al., 2009).

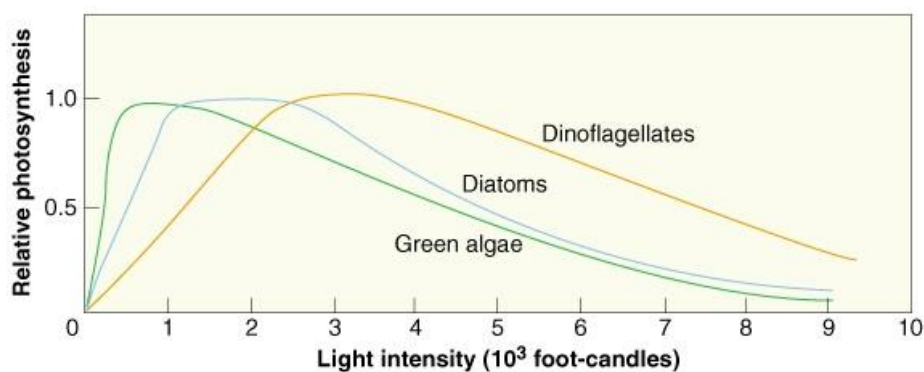


Figure 45. Relative photosynthetic activity in relation to light intensity for three plankton groups. Curve progression for Dinoflagellates, diatoms, and green algae are colored. Adapted from Parson et al. (2013).

Abeoformidae-Group-MAIP-2 accounted for most of the annotated Mesomycetozoa and was one of the predominant parasitic taxon groups in the austral winter simulation. Knowledge about their ecology and parasite-host dynamics are scarce, but hosts of Ichthyosporea described to date include diatoms and fish (Käse et al., 2021; Marshall and Berbee, 2011; Rowley et al., 2013). This corroborates well with the results in this thesis as the proportion of diatoms as well as the introduction of fish in the mesocosms coincided with the relative abundance and occurrence of Ichthyosporea, respectively. Furthermore, Abeoformidae (Group MAIP) are associated to enhanced carbon flux across the global oceans and thus could play an important role in the biological carbon pump (Guidi et al., 2016).

Effect of Distinct Upwelling Intensities on Protistan Plankton Structure During Austral Summer

Dinoflagellates dominated the relative sequence reads during austral summer, which is consistent with previous studies in the HCS where dinoflagellates prevailed the protistan plankton community (Min et al., 2023). Furthermore, it was shown that dinoflagellates substantially accounted for the carbon flux into deep layers during austral summer (González et al., 2009). Exhibiting an elevated photosynthetic activity under high light conditions compared to diatoms and green algae explains a reduced proportion of ~50% in chlorophytes and diatoms compared to the austral winter simulation (Figure 45; Parsons et al., 2013). Thus, dinoflagellates acquire a competitive advantage under high light intensities (Huisman et al., 1999; Parsons et al., 2013). Diatoms, however, were previously reported to contribute majorly to the community composition in the Peruvian HCS during austral summer (Min et al., 2023). Combined with the premise that in mesocosms an intensified stratification and reduced turbulences deviate from the optimal environment promoting diatom growth, dinoflagellates could maintain a competitive advantage even under nutrient-rich conditions (Margalef, 1978). They could further gain a benefit in competing for nutrients due to their ability to acquire potentially more resources by vertical migration (Heaney and Eppley, 1981; Peacock and Kudela, 2014). The prevalent occurrence of dinoflagellates under all upwelling treatments indicates nutrients as a subsidiary selection factor for this taxon. As dinoflagellates exhibit a variety of life styles (parasites, symbionts, heterotrophs, mixotrophs and phototrophs), these dynamic features could mitigate limitations by nutrient deficiency (Hansen, 2011; Santi et al., 2019; Stoecker, 1999). However, a structural change within this phylum could be assumed, as many dinoflagellate species are still dependent on dissolved nutrient availability (Wu et al., 2020). Indeed, with an increase in ASVs assigned to Syndiniales (Dino Group-I-Clade-4), a

shift within dinoflagellates exhibiting a heterotrophic or mixotrophic (external and internal) mode to a parasitic lifestyle under nutrient deficiency, which demonstrated the functional diversity of dinoflagellates (Santi et al., 2019). This trophic shift was likewise mirrored by the fitted traits on the NMDS analysis and could impede the trophic transfer efficiency (Ward and Follows, 2016).

Syndiniales, as an exclusively parasitic taxon, were previously documented in these waters, but their parasite-host dynamics are diverse as they infect other dinoflagellates, acanthareans, diatoms, radiolarians, Cercozoa, but also metazoans (Guillou et al., 2008; Käse et al., 2021; Min et al., 2023; Nagarkar and Palenik, 2023; Siano et al., 2011). Thus, Syndiniales could play a major role in the top-down control of protistan plankton as well as zooplankton communities and contribute to the particulate carbon flux to deeper waters (Anderson et al., 2023). Evidence of competition within the Dinoflagellata was also provided by the divergent relative abundances of specific Dinophyceae (e.g., Suessiaceae and Prorocentraceae). Suessiaceae exhibit, however, a variety of potential ES that include free-living, symbiotic, and parasitic forms (Hehenberger et al., 2018; Montresor et al., 1999; Siano et al., 2010). Since their relative abundance followed the pattern of the Syndiniales assigned sequence reads, it is reasonable to assume that most Suessiaceae likewise occupied a parasitic lifestyle or are potential hosts for the Syndiniales lineage. Despite the acceptance of Dinophyceae as hosts of Syndiniales, there is no evidence of parasite-host relationships with Syndiniales and Suessiaceae in the literature (Guillou et al., 2008; Nagarkar and Palenik, 2023).

Haptophyta, with Phaeocystaceae as the prevalent family, represented a further dominant protistan plankton group in the mesocosms (austral summer as well as austral winter simulation). They play a pivotal role in ocean carbon cycling and harbor the potential for climate regulation due to the ability of *Phaeocystis* species in producing dimethyl sulfide as cloud forming nuclei (Charlson et al., 1987; Schoemann et al., 2005; Smith Jr et al., 1991; Stefels et al., 1995). This high ecological relevance emphasizes the importance of these algae in view of the impending climate change. These unicellular eukaryotes were distributed relatively uniformly across the contrasting treatments, which suggests a sufficient ability for photoadaptation of the Phaeocystaceae in the HCS. Indeed, many reports confirm the flexibility of *Phaeocystis* spp. to a wide variety of light intensities (Peperzak et al., 2000; Schoemann et al., 2005; van Hilst and Smith Jr, 2002). *Phaeocystis* species evolve in nutrient, especially nitrogen rich waters but no significant association to the higher upwelling intensities could be determined (Schoemann et al., 2005; Smith Jr et al., 1991). The highest contribution to the relative sequence reads was found under nutrient depleted conditions, which suggests a

competitive disadvantage of these algae compared to the local diatom and dinoflagellate community under intensified upwelling.

The observed changes in community composition coupled with the shifts in size class distribution led to altered trophic interactions and carbon cycling dynamics. These changes have far-reaching implications for the ecosystem and its services. A decrease of trophic transfer efficiency by favoring small cells coupled with the loss of mixotrophic organisms under reduced upwelling could lengthen the food web and impede fisheries (Mehner et al., 2018; Stibor et al., 2019; Ward and Follows, 2016). Low nutrient concentrations were likewise linked to intensified parasitism, corresponding to an increased top-down control of phytoplankton which could result in reduced rates of carbon fixation (Frenken et al., 2016; Klawonn et al., 2023; Worden et al., 2015). On the other hand, parasitic interactions were reported to reinforce particulate carbon fluxes to deeper layers (Anderson et al., 2023). The impact on the ocean carbon cycle of these opposing mechanisms needs to be evaluated and quantified in future research. Considering the effects of climate change with the potential displacement of EBUS leading to equatorward (poleward) reductions (increases) in upwelling, and the intensification of El Niño–Southern Oscillation events, the results of this study provide circumstantial evidence of how protistan plankton communities may evolve and influence the HCS in the future (Rykaczewski et al., 2015; Wang et al., 2017).

8.2 Microzooplankton Bacterivory in the Humboldt Current System

8.2.1 Impact of Light & Upwelling Scenarios on Microbial Abundances & Carbon Flow

The HCS off the coast of Peru is one of the most productive fishing grounds in the world (Cushing, 1971; Messié et al., 2009). The exceptionally high fish population in this region, despite the small area, is presumably attributed to a very efficient and short food chain (Guénette et al., 2008; Massing et al., 2022). However, the microbial loop is mostly unattenuated in field studies and not considered in trophic models due to the lack of data or dismissed as unimportant (Ayón et al., 2008; Guénette et al., 2008; Moloney et al., 1991; Taylor et al., 2008). This is one of the first studies examining the trophic link between prokaryotes and unicellular eukaryotes in the HCS off Peru. The results provide circumstantial evidence that previous studies underrate the importance of the microbial loop and phagotrophic protistan plankton in the carbon cycle as well as sustaining the high productivity in the HCS. Furthermore, the data suggest a switch from pronounced top-down control by bacterivory under immediate nutrient limitation to other mechanisms regulating the bacterial standing stock.

The microbial abundances were in general relatively high for marine waters (Isao et al., 1990; Veldhuis and Kraay, 2000). Bacterial cell numbers of $\sim 5.0 \times 10^6 \pm 1.9 \times 10^6 \text{ mL}^{-1}$ are not uncommon in surface waters of the HCS off Peru with a previous study reporting concentrations up to $\sim 8.0 \times 10^6 \text{ mL}^{-1}$ (Engel and Galgani, 2016; Spinrad et al., 1989). Protistan abundances are also in agreement with data from natural surface waters along the coast off Peru. The measured abundances, with an average count of $\sim 3.1 \times 10^4 \pm 2.2 \times 10^4 \text{ mL}^{-1}$, fall accurately within the range of published data, which vary from $\sim 0.5 \times 10^4 \text{ mL}^{-1}$ to $\sim 5.0 \times 10^4 \text{ mL}^{-1}$ (Engel and Galgani, 2016). The high microbial abundances determined during this study suggest a pronounced primary production and carbon assimilation at the sampling site, which could play an important role in the biological carbon pump and the trophic pathways to pelagic fish (Vargas et al., 2007). Surveys in the southern part of the HCS off the Chilean coast documented lower bacterial as well as protistan plankton abundances (Cuevas et al., 2004; Cuevas and Morales, 2006; Troncoso et al., 2003). These variations within the Peru-Chile Current System (or HCS) could result from divergent wind strength coupled with upwelling intensities influencing turbulence, nutrient availability, and light exposure, which are well known to alter microbial dynamics (Engel and Galgani, 2016; Falkowski, 1984; Harrison et al., 1990; Hormazabal et al., 2001; Illig et al., 2014; Margalef, 1978; Vazquez-Cuervo et al., 2017). In this study, however, no significant effect caused by the light treatment and the DW addition could be determined. Albeit, trends for elevated bacterial and reduced protistan abundances in LL samples could be determined, which are in agreement with previous studies comparing the influence of different light intensities on microbial dynamics (Calbet et al., 2012; Ptacnik et al., 2016). This result could be attributed to increased top-down control by mixotrophic eukaryotes under high light conditions paired with light limitation impeding their photosynthetic activity and thus growth in the darkened mesocosms (Hansen and Hjorth, 2002; Ptacnik et al., 2016). Although no significant association with the upwelling treatment could be calculated, a significant positive correlation between nitrite and nitrate were determined for the protistan abundances, which demonstrates the bottom-up regulation of protistan plankton. This result furthermore supports the proposed nitrogen limitation in the HCS for primary production (Messié and Chavez, 2015; Thiel et al., 2007).

The overall patterns observed by linking the changes of the microbial dynamics during the experiment are remarkable and integrate oligotrophic and eutrophic conditions of the extended 'plankton ecology group model' (Figure 46; Sommer et al., 2012). In the initial stage prior to the upwelling treatment, an inverse relationship between unicellular eukaryotes and bacterial abundances was determined, which is reminiscent of the classical 'Lotka-Volterra

population model'. Albeit, the time delay could not be detected presumably due to the long sampling intervals (Bacaër, 2011; Varon and Zeigler, 1978). The dynamics of the microorganisms, thus, indicate a pronounced top-down control of bacterial abundances. These predator-prey interactions were, however, not observed in the subsequent stage after DW addition, suggesting that other mechanisms controlled the bacterial abundance. Here, the prokaryotic and the protistan cell counts decreased steadily after a short initial increase. Although, nutrient availability clearly explained the protistan plankton concentrations, this was not observed for the bacterial trend. Other control mechanisms, like virus mediated mortality, could have prevailed (Proctor and Fuhrman, 1990). A strong dependency of prokaryotes on the produced organic carbon by protistan plankton (secretion or decease) should not be disregarded. The limiting factor of organic matter for bacterial production in upwelling regions was previously reported, which indicates a bottom-up control initiated by the lack of primary production of protistan plankton under prolonged nutrient deficiency (Montecino and Lange, 2009; Vargas et al., 2007).

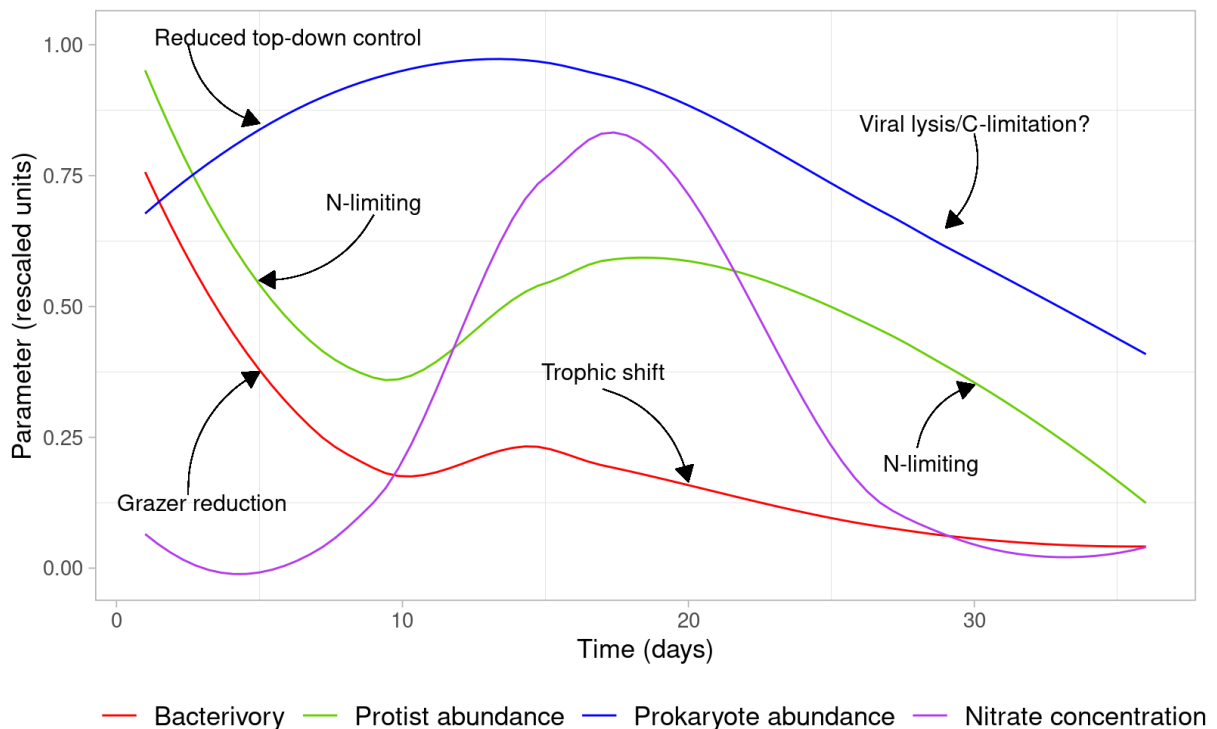


Figure 46. Conceptual summary of the microbial dynamics with the mechanisms controlling the standing stock of prokaryotes and protistan plankton as well as the measured bacterivory. Nitrate concentration is included to underpin nutrient development. Data were averaged for each sampling day and rescaled between 0-1 for better comparison. N: nitrogen; C: carbon.

The measured bacterivory was exceptionally high in the initial stage of the experiment but diminished analogous to the protistan abundances, which supports the established concept (Figure 46). This seems logical since a reduction of grazers is accompanied by a decline of the constituted grazing pressure on bacteria. Values reaching prokaryotic turnover rates of up to 15 times the standing stock per day were the highest rates reported in the HCS. Previous studies reached maximal turnover rates of up to 180% of the standing stock per day (Cuevas and Morales, 2006; Vargas et al., 2007). However, the microbial abundances were likewise a magnitude higher in this study, which could explain the elevated carbon transfer by higher encounter rates (Sanders et al., 1990). Whether these high grazing rates are also recorded under natural conditions or only in mesocosms remains to be discovered in future research. However, these data support the findings of previous studies, which showed high variability in microbial dynamics in the HCS off the Peruvian coast (Echevin et al., 2014; Engel and Galgani, 2016).

The DW addition did induce a slight increase of the grazing effect, albeit a less pronounced elevation was determined compared to the rise in unicellular eukaryotes. This supports the results of the DNA-metabarcoding coupled with the trait-based approach, revealing a trophic shift from phagotrophic (external and internal) to osmotrophic, saprotrophic foraging modes and parasitic lifestyles. If this change in energy acquisition was triggered by nutrient deficiency, copepod or fish mediated grazing pressure, or maybe all at once, requires further investigation by compiling all the data of the CUSCO-consortium. Deciphering these interactions could further advance the extended ‘plankton ecology group model’ (Sommer et al., 2012). In addition, the incubation effect should not be neglected. Even if the mesocosms employed are intended to mimic natural conditions as accurately as possible, an alteration of the protistan plankton structure and function induced by containment could be possible (Countway et al., 2005; Riebesell et al., 2013; Sharma et al., 2021). The grazing effect, however, was not marginal in the post-upwelling phase. Prokaryotic turnover rates in the range of ~63 to ~120% of the standing stock per day were determined, which is congruent to the spectrum reported in the HCS off Chile (Cuevas and Morales, 2006; Vargas et al., 2007). This suggests protistan mediated mortality as one of the main factors controlling bacterial production. Furthermore, the results indicate the significance of the microbial food web, as a major fraction of the bacterial production passes through the microbial food web and is subsequently accessible for higher trophic levels.

The upwelling treatment revealed no significant alteration of the grazing effect. However, in most upwelling-treated mesocosms a rise in bacterivory was determined. The evaluation advocates an influence of the DW addition, which partly approves the hypothesis

H_C2.1. This is consistent with the literature, reporting that coastal regions subjected to upwelling have higher grazing rates compared to the open ocean (Schmoker et al., 2013; Wickham et al., 2022). These enhanced grazing rates were not a consequence of higher encounter rates due to high abundances, as LL0 peaked in bacterial cell counts and did not exhibit the lowest number of unicellular eukaryotes. Thus, the assumption that the trophic shift accelerated more rapidly in the untreated mesocosms is reasonable. The fact that no clear relation of the bacterivory to distinct upwelling intensities was observed may be due to potential methodological and experimental limitations. Methodological disadvantages in the application of bacterial analogs are related to chemosensory detection of prey which would result in non-preferential uptake of microspheres by protistan plankton and reduced grazing rates (Pace and Bailiff, 1987; Sherr et al., 1987; Wootton et al., 2007). A single upwelling stimulus, as performed in this experiment, has attenuated effects. By applying continuous or recurrent injections of DW into the system, which seems much more natural, more pronounced differences could be triggered (Ortiz et al., 2022a, 2022b).

Significant associations between the light treatments could likewise not be determined for the measured bacterivory. Analog trends to the protistan abundances were identified with an elevated grazing effect of ~30% in the austral summer compared to the mimicked austral winter situation which supports hypothesis H_C2.2. This result is consistent with previous studies reporting higher carbon fluxes with up to ~50% through microzooplankton in illuminated compared to darkened conditions (Calbet et al., 2012; Ptacnik et al., 2016). This light-induced promotion of the microbial food web could be attributed to the stimulation of mixotrophic activity as well as the higher encounter rate due to raised microbial abundances (Ptacnik et al., 2016; Sanders et al., 1990). In addition, by examining the protistan plankton community composition, it is noticeable that the relative ciliate abundance - these organisms can contribute massively to the grazing effect - peaked in the austral summer mesocosms (Boras et al., 2010; Kisand and Zingel, 2000; Sherr and Sherr, 2002, 1994; Wickham et al., 2022). Applied to the ecosystem under study, the result allows the conclusion that the microbial loop plays a more prominent role in the food web structure of austral summer in the HCS. In combination with the findings deduced in the DNA-metabarcoding survey, the food web structure during austral winter is, therefore, more dependent on diatom utilization. This hypothesis was likewise proposed in a previous study that evaluated isotopic signatures to investigate carbon fluxes in the northern HCS off Chile (Castro et al., 2020).

9 Subject II: Summary & Conclusion

The HCS, which hosts one of the largest marine fisheries in the world, is expected to be severely impacted by anthropogenic climate change, leading to potentially severe socio-economic repercussions. Therefore, understanding the consequence of predicted alterations (light impediment; shift of upwelling) on protistan plankton structure and function is of major importance. The findings in this study could identify specific plankton taxa associated with distinct light and nutrient regimes. In addition, the data suggest that the microbial food web plays a substantial role in the biological carbon pump but may exhibit significant seasonal variation.

DW injection not only served as a nutrient input promoting phytoplankton growth, but also introduced immigrant plankton types, which generated diversity hotspots in the ‘highly’ upwelled mesocosms. The impediment of light resulted in a reduced alpha diversity, potentially due to the loss of organisms that demand a high critical light intensity. The loss of diversity under low upwelling scenarios, especially in combination with the darkened conditions, could lead to alterations of biochemical cycles, trophic interactions, and ecosystem services.

Specific protistan plankton taxa dominated the individual mesocosms due to niche differentiation induced by altered environmental conditions. Diatoms thrived under mimicked austral winter conditions with high nutrient availability demonstrating the characteristic properties of opportunists and *r*-strategists. The antagonist during the austral winter simulation were small-celled chlorophytes, which prevailed under nutrient deficiency and thus, exhibited gleaner and *k*-strategic traits. In austral summer, Dinoflagellata dominated due to their elevated photosynthetic activity under high light conditions compared to diatoms and green algae. They contributed the most to the relative read abundance under nutrient availability and deficiency assumably because of their substantial trophic diversity and versatile lifestyles. The dynamic occurrence of dinoflagellate species was revealed by the trophic shift from phagotrophic to parasitic energy acquisition when nutrients were limited. This could result in reduced rates of carbon fixation by elevated top-down control of phytoplankton by parasitism.

These transitions had direct effects on the carbon flux from bacteria to phagotrophic protistan plankton and could be detected by the grazing experiments. The initially tremendous grazing effect decreased due to the change in energy acquisition of the plankton community. In addition, C-limitation or potential viral lysis resulted in low prokaryotic abundances and thus, lower encounter rates. Nevertheless, a high carbon flux, even under nutrient limitation, suggests

that protistan-mediated mortality is one of the main factors controlling bacterial production in the HCS. This indicates the importance of the microbial food web, as a large fraction of bacterial production passes through it, which is subsequently accessible to higher trophic levels. Trends could also be inferred that the microbial loop plays a more prominent factor in the structure of the food web in austral summer and is more concentrated on diatom uptake during austral winter in the HCS off Peru.

Combining the decrease of trophic transfer efficiency by favoring small cells or parasitic organisms and obstructing phagotrophic species under reduced upwelling and light impediment could lead to severe consequences. These would entail reduced primary production as well as lengthening the food web structure and ultimately impeding fisheries. Particularly, in light of the implications posed by climate change, with the potential relocation of EBUS and intensification of El Niño-Southern Oscillation events, this study contributes circumstantial evidence for how protist plankton structure and function may develop in the HCS.

IV. Synthesis

The physical analogies of the eddy characteristics (enclosed water masses and cyclonic eddy stirring) and the experimental design of the mesocosm approach (enclosed water masses and upwelling simulation) enable a comparison of the results from both subjects, which illustrates several elements with similarities and discrepancies (Figure 47 and Figure 48). All three mesoscale eddies as well as the individual mesocosms harbored distinct protistan plankton communities with varying structure and function due to diverse physicochemical drivers.

The results could substantiate that cyclonic eddies serve as transport mechanisms that enhance diversity in the open ocean. In the mesocosm experiment, on the other hand, diversity was enhanced by introducing new plankton assemblages into the enclosed system by DW addition. Therefore, the injection of DW into the mesocosms could be equivalent to the disintegration of an eddy where local and immigrant plankton types mingle and thus, enhance the regional protistan plankton community of the open ocean.

The comparison of the protistan plankton communities demonstrates that even the youngest eddy under study resembled mesocosms under nutrient-poor conditions. The highest correspondence was observed between the youngest eddy and the mesocosms under nutrient deficiency in the austral summer situation with its high proportion of parasitic dinoflagellates. Parallels between the eddy communities and the simulated austral winter situation in the mesocosms with the prevalent abundances of diatoms could not be observed, even though, it is likely that diatoms contribute substantially to the primary production in the CanCS (Romero and Fischer, 2017; Romero and Ramondenc, 2022). However, this was most likely not observed in the eddies due to their level of maturity. It is assumed that the trapped plankton communities within an eddy consume most of the upwelled nutrients within a short timeframe (days) after formation (Peterson et al., 2011). New nutrient input into offshore eddy systems occurs through cyclonic eddy stirring or aerosol deposition, therefore, the mesocosm approach seems to represent the initial stage after eddy formation (Baker et al., 2003; McGillicuddy et al., 1998). Although a higher relative abundance of green algae could be detected in the youngest eddy, they did not dominate the community as it was seen in the nutrient-poor mesocosms in the austral winter simulation, which could be attributed to succession patterns or prolonged nutrient deficiency in the mesoscale ocean feature.

The trophic role of the phagotrophic protists revealed similar findings in the HCS and CanCS. Seasonal fluctuations in microbial dynamics were observed in both systems, which, however, could be attributed to different mechanisms. In the HCS enhanced Saharan dust

deposition could be the cause of higher microbial abundances and higher microbial loop activity between the two ‘eddy hunts’. In the CanCS, the variations were attributed to the severe shift in plankton community composition due to light impediment in the mimicked austral winter. The microbial abundances and protistan-mediated mortality, which were reduced in more mature eddies and with progressive nutrient depletion in the mesocosm approach, are likewise in agreement. Reasonable assumptions, as a consequence of nutrient deficiency, are the possible shift from bacterivory to virus-mediated control of bacterial production and the limitation of carbon content due to reduced primary production in both study areas. The latter, in combination with the reduced abundance of organisms, would reasonably lead to reduced deposition of marine snow into the deep sea.

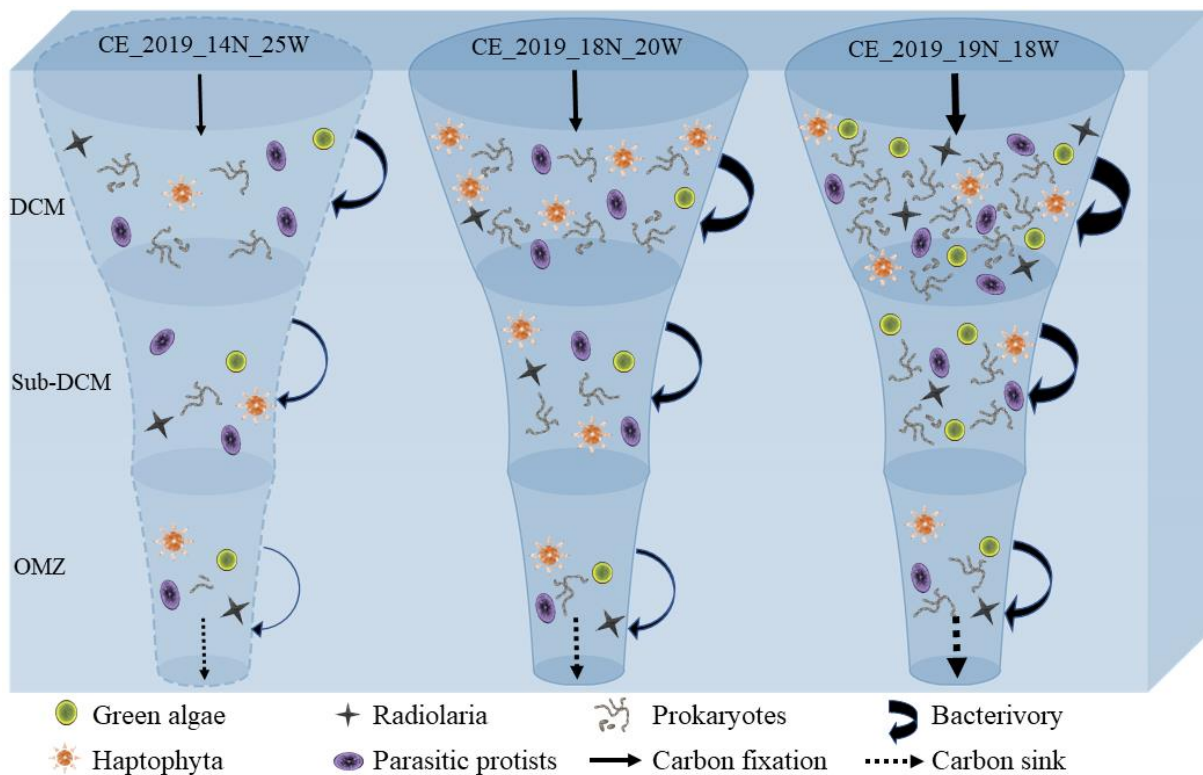


Figure 47. Conceptual overview of the findings in the different aged cyclonic mesoscale eddies in the Canary Current System. Distinct protistan plankton communities are represented by the proportion of selected taxa (green algae, haptophytes, radiolarians, and parasitic protists). The most pronounced differences in protistan plankton communities were detected in the deep-chlorophyll maximum (DCM) and relatively similar communities in the oxygen-minimum zone (OMZ). The abundances of protists and prokaryotes are represented by the frequency of occurrence (low: old eddy CE_2019_14N_25W; intermediate: stable eddy CE_2019_18N_20W; high: young eddy CE_2019_19N_18W;). The quantity of measured and derived carbon flow is highlighted by straight arrows (carbon fixation by phototrophs/mixotrophs), curved arrows (measured bacterivory by phagotrophic protists) and dashed arrows (carbon sink of particulate organic matter). Dashed sheath line of the eddy CE_2019_14N_25W represents the potential disintegrating state.

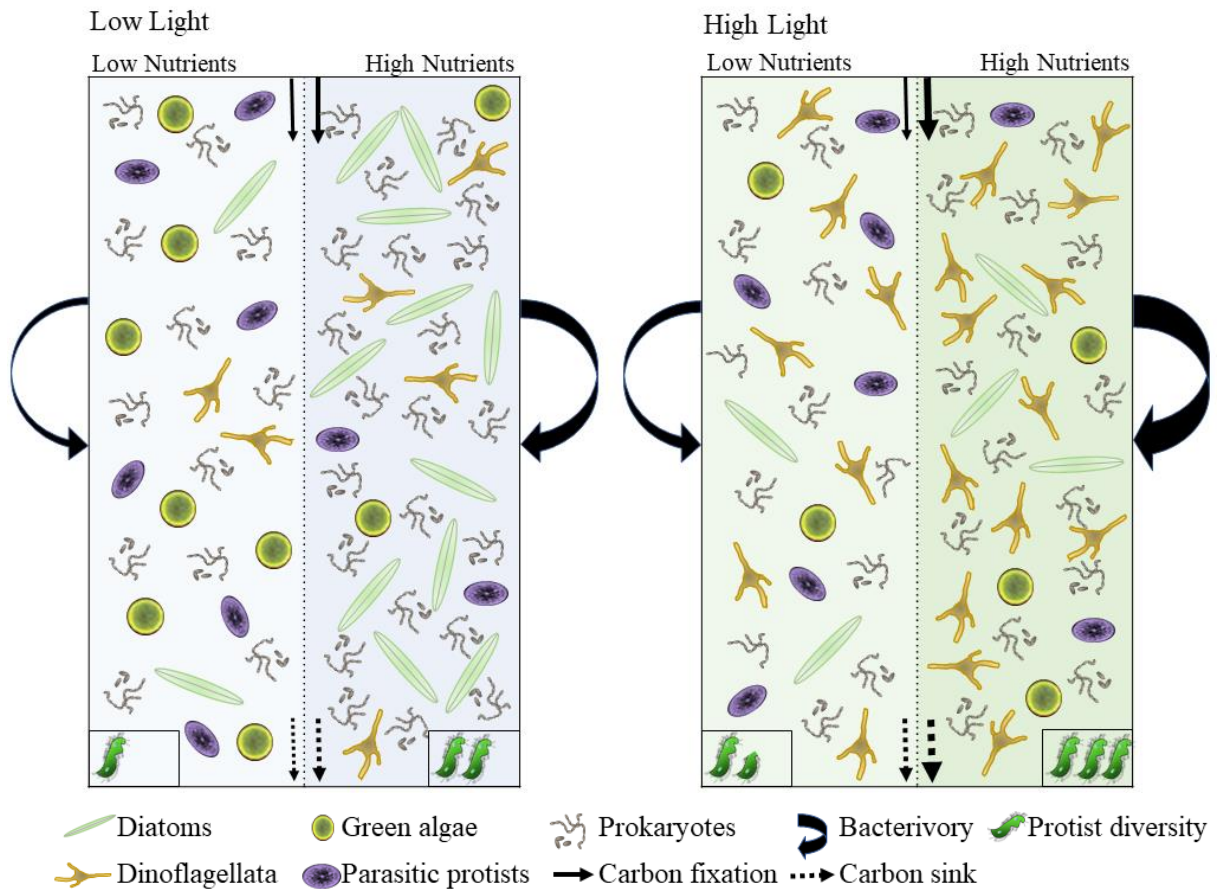


Figure 48. Conceptual overview of the findings for the main treatments in the mesocosms in the Humboldt Current System. Distinct protistan plankton communities are represented by the proportion of selected taxa (diatoms, dinoflagellates, green algae, and parasitic protists in low light conditions with low nutrient concentrations; diatoms in low light conditions with high nutrient concentrations; dinoflagellates and parasitic protists in high light conditions with low nutrient concentrations; dinoflagellates in high light conditions with high nutrient concentrations). The abundances of protists and prokaryotes are represented by the frequency of occurrence. The quantity of measured and derived carbon flow is highlighted by straight arrows (carbon fixation by phototrophs/mixotrophs), curved arrows (measured bacterivory by phagotrophic protists) and dashed arrows (carbon sink of particulate organic matter). Quantity of protistan alpha diversity is represented by frequency of the symbol. Dashed line separates low and high nutrient concentrations.

It stands to reason that further research is imperative to comprehend the entire scope of how eddies influence protistan plankton structures and functions, not to mention how future communities will evolve in the face of climate change. Eddies function like mesocosms by entrapping coastal waters which vary greatly from the surroundings in terms of physicochemical properties and thus, protistan plankton community composition. *Vice versa*, mesocosms represent enclosed water masses which appear very suitable to investigate eddy perturbations. Especially factors influencing eddy dynamics, in particular time and place of eddy origin as well as age of the mesoscale feature, could be simulated in mesocosm experimental set-ups. Thereby, the effect of distinct seed communities, the succession patterns

of protistan plankton communities and ultradian rhythms could be further unraveled without shipboard restrictions. Eddy characteristics like intrusion, merge and split events could likewise be mirrored by introducing open ocean and eddy waters into the experimental enclosure. However, accurate predictions on how microbial communities evolve, even without abiotic variability and only through biotic interactions ('paradox of chaos'), is by no means an effortless endeavor (Benincà et al., 2008; Telesh et al., 2019). Unraveling the 'paradox of chaos' paired with environmental changes still requires a considerable dedication from future researchers.

In light of climate change, increased eddy activity in EBUS, based on the findings in this thesis, would enhance the biological carbon pump and potentially counteract climate change. In contrast, eddies diminish the nutrient concentrations at the nearshore, and consequently, the primary production, which could impede small-scaled fisheries through cascading effects. The displacement of EBUS with the poleward intensification or equatorward reduction of upwelling intensity would relocate key primary production areas which could have dramatic consequences. Especially the enhanced stratification, reduced nutrient input and increasing temperatures could lead to the absence of primary production hotspots and would interfere with the whole food chain and biological carbon pump.

V. Abstract / Zusammenfassung

Abstract

Climate change will have severe consequences on Eastern Boundary Upwelling Systems (EBUS). They host the largest fisheries in the world supporting the life of millions of people due to their tremendous primary production. Therefore, it is of utmost importance to better understand predicted impacts like alternating upwelling intensities and light impediment on the structure and the trophic role of protistan plankton communities as they form the basis of the food web. Numerical models estimate the intensification of the frequency in eddy formation. These ocean features are of particular importance due to their influence on the distribution and diversity of plankton communities and the access to resources, which are still not well understood even to the present day. My PhD thesis entails two subjects conducted during large-scaled cooperation projects REEBUS (Role of Eddies in Eastern Boundary Upwelling Systems) and CUSCO (Coastal Upwelling System in a Changing Ocean).

Subject I of my study was conducted within the multidisciplinary framework REEBUS to investigate the influence of eddies on the biological carbon pump in the Canary Current System (CanCS). More specifically, the aim was to find out how mesoscale cyclonic eddies affect the regional diversity, structure, and trophic role of protistan plankton communities in a subtropical oligotrophic oceanic offshore region.

Samples were taken during the M156 and M160 cruises in the Atlantic Ocean around Cape Verde during July and December 2019, respectively. Three eddies with varying ages of emergence and three water layers (deep chlorophyll maximum DCM, right beneath the DCM and oxygen minimum zone OMZ) were sampled. Additional stations without eddy perturbation were analyzed as references. The effect of oceanic mesoscale cyclonic eddies on protistan plankton communities was analyzed by implementing three approaches. (i) V9 18S rRNA gene amplicons were examined to analyze the diversity and structure of the plankton communities and to infer their role in the biological carbon pump. (ii) By assigning functional traits to taxonomically assigned eDNA sequences, functional richness and ecological strategies (ES) were determined. (iii) Grazing experiments were conducted to assess abundance and carbon transfer from prokaryotes to phagotrophic protists.

All three eddies examined in this study differed in their ASV abundance, diversity, and taxonomic composition with the most pronounced differences in the DCM. Dinoflagellates were the most abundant taxa in all three depth layers. Other dominating taxa were radiolarians, Discoba and haptophytes. The trait-approach could only assign ~15% of all ASVs and revealed in general a relatively high functional richness. But no unique ES was determined within a

specific eddy. This indicates pronounced functional redundancy, which is recognized to be correlated with ecosystem resilience and robustness by providing a degree of buffering capacity in the face of biodiversity loss. Elevated microbial abundances as well as bacterivory were clearly associated to mesoscale eddy features, albeit with remarkable seasonal fluctuations. Since eddy activity is expected to increase on a global scale in future climate change scenarios, cyclonic eddies could counteract climate change by enhancing carbon sequestration to abyssal depths. The findings demonstrate that cyclonic eddies are unique, heterogeneous, and abundant ecosystems with trapped water masses in which characteristic protistan plankton develop as the eddies age and migrate westward into subtropical oligotrophic offshore waters. Therefore, eddies influence regional protistan plankton diversity qualitatively and quantitatively.

Subject II of my PhD project contributed to the CUSCO field campaign to identify the influence of varying upwelling intensities in combination with distinct light treatments on the whole food web structure and carbon pump in the Humboldt Current System (HCS) off Peru. To accomplish such a task, eight offshore-mesocosms were deployed and two light scenarios (low light, LL; high light, HL) were created by darkening half of the mesocosms. Upwelling was simulated by injecting distinct proportions (0%, 15%, 30% and 45%) of collected deep-water (DW) into each of the moored mesocosms. My aim was to examine the changes in diversity, structure, and trophic role of protistan plankton communities for the induced manipulations by analyzing the V9 18S rRNA gene amplicons and performing short-term grazing experiments.

The upwelling simulations induced a significant increase in alpha diversity under both light conditions. In austral summer, reflected by HL conditions, a generally higher alpha diversity was recorded compared to the austral winter simulation, instigated by LL treatment. Significant alterations of the protistan plankton community structure could likewise be observed. Diatoms were associated to increased levels of DW addition in the mimicked austral winter situation. Under nutrient depletion, chlorophytes exhibited high relative abundances in the simulated austral winter scenario. Dinoflagellates dominated the austral summer condition in all upwelling simulations. Tendencies of reduced unicellular eukaryotes and increased prokaryotic abundances were determined under light impediment. Protistan-mediated mortality of prokaryotes also decreased by ~30% in the mimicked austral winter scenario.

The findings indicate that the microbial loop is a more relevant factor in the structure of the food web in austral summer and is more focused on the utilization of diatoms in austral winter in the HCS off Peru. It was evident that distinct light intensities coupled with multiple

upwelling scenarios could lead to alterations in biochemical cycles, trophic interactions, and ecosystem services. Considering the threat of climate change, the predicted relocation of EBUS could limit primary production and lengthen the food web structure with severe socio-economic consequences.

Zusammenfassung

Der Klimawandel wird schwerwiegende Folgen für die östlichen Auftriebssysteme (Eastern Boundary Upwelling Systems – EBUS) haben. Sie beherbergen die größten Fischereigründe der Welt, die aufgrund ihrer enormen Primärproduktion das Leben von Millionen von Menschen sichern. Daher ist es äußerst wichtig, die vorhergesagten Auswirkungen von Änderungen in Auftriebsintensitäten sowie Lichtverhältnissen auf die Struktur und trophische Rolle von Protisten-Planktongemeinschaften besser zu verstehen, da sie die Grundlage des Nahrungsnetzes bilden. Numerische Modelle sagen die Intensivierung der Häufigkeit von Wirbelbildung in EBUS voraus. Diese sogenannten Eddies sind aufgrund ihres Einflusses auf die Verteilung und Vielfalt von Planktongemeinschaften und den Zugang zu Ressourcen von besonderer Bedeutung, die auch heute noch nicht gut verstanden sind. Meine Doktorarbeit umfasst zwei Themen, die im Rahmen der groß angelegten Kooperationsprojekte REEBUS (Role of Eddies in Eastern Boundary Upwelling Systems) und CUSCO (Coastal Upwelling System in a Changing Ocean) durchgeführt wurden.

Thema I meiner Studie wurde im Rahmen des multidisziplinären Vorhabens REEBUS durchgeführt, um den Einfluss von Meereswirbeln auf die biologische Kohlenstoffpumpe im Kanarenstromsystem (CanCS) zu untersuchen. Genauer gesagt, wie mesoskalige zyklonale Eddies die regionale Vielfalt, Struktur und trophische Rolle von Protisten-Planktongemeinschaften in einer subtropischen oligotrophen ozeanischen Offshore-Region beeinflussen.

Die Proben wurden während der Ausfahrten M156 und M160 im Atlantik um Kap Verde im Juli bzw. Dezember 2019 genommen. Es wurden drei Eddies mit unterschiedlichem Entstehungsalter und drei Wasserschichten (tiefes Chlorophyllmaximum DCM, direkt unter dem DCM und Sauerstoffminimumzone OMZ) beprobt. Zusätzliche Stationen ohne Wirbelstörung wurden als Referenz analysiert. Zur Analyse der Auswirkungen ozeanischer mesoskaliger zyklonaler Wirbel auf Protisten-Planktongemeinschaften wurden drei Ansätze verfolgt: (i) V9 18S rRNA-Genamplikons wurden untersucht, um die Vielfalt und Struktur der Planktongemeinschaften zu analysieren und Rückschlüsse auf ihre Rolle in der biologischen Kohlenstoffpumpe zu ziehen. (ii) Durch den Abgleich von funktionellen Merkmalen zu taxonomisch zugeordneten eDNA-Sequenzen wurden funktioneller Reichtum und ökologische Strategien (ES) bestimmt. (iii) Fraßexperimente wurden durchgeführt, um die Abundanz und den Kohlenstofftransfer von Prokaryoten zu phagotrophen Protisten zu bewerten.

Alle drei in dieser Studie untersuchten Eddies unterschieden sich in ihrer ASV-Häufigkeit, Diversität und taxonomischen Zusammensetzung, wobei die Unterschiede zwischen den Stationen am deutlichsten in der DCM waren. Dinoflagellaten waren in allen drei Tiefen die häufigsten Taxa. Andere dominierende Taxa waren Radiolarien, Discoba und Haptophyten. Der Abgleich mit den funktionellen Merkmalen konnte nur ca. 15 % aller ASVs zuordnen und ergab im Allgemeinen einen relativ hohen funktionalen Reichtum, aber es wurde keine einzigartige ES innerhalb eines bestimmten Eddies ermittelt. Dies deutet auf eine ausgeprägte funktionelle Redundanz hin, die anerkanntermaßen mit der Widerstandsfähigkeit und Robustheit von Ökosystemen korreliert, da sie eine gewisse Pufferkapazität angesichts des Verlusts der biologischen Vielfalt bietet. Erhöhte mikrobielle Abundanzen sowie Bakterivorie wurden eindeutig mit mesoskaligen Wirbelmerkmalen in Verbindung gebracht, wenn auch mit bemerkenswerten saisonalen Schwankungen.

Da erwartet wird, dass die Wirbelaktivität in zukünftigen Klimawandelszenarien auf globaler Ebene zunehmen wird, könnten zyklonale Eddies dem Klimawandel entgegenwirken, indem sie die Kohlenstoffspeicherung in tiefe Meeresschichten verstärken. Die Ergebnisse zeigen, dass zyklonale Wirbel einzigartige, heterogene und diverse Ökosysteme mit eingeschlossenen Wassermassen sind, in denen sich charakteristisches Protistenplankton entwickelt, während die Wirbel altern und nach Westen in subtropische oligotrophe küstennahe Gewässer abwandern und den Ozean qualitativ und quantitativ beeinflussen.

Thema II meines Promotionsprojekts trug zur CUSCO-Feldkampagne bei, um den Einfluss unterschiedlicher Auftriebsintensitäten in Kombination mit verschiedenen Lichtbehandlungen auf die gesamte Nahrungsnetzstruktur und die Kohlenstoffpumpe im Humboldt-Stromsystem (HCS) vor Peru zu ermitteln. Um diese Aufgabe zu bewältigen, wurden acht Offshore-Mesokosmen aufgestellt und zwei Lichtszenarien (niedriges Licht, LL; starkes Licht, HL) durch Abdunkeln der Hälfte der Mesokosmen geschaffen. Auftriebsvariationen wurden simuliert, indem unterschiedliche Anteile (0 %, 15 %, 30 % und 45 %) des gesammelten Tiefenwassers in die verankerten Mesokosmen eingeleitet wurden. Mein Ziel war es, die Veränderungen in der Diversität, der Struktur und der trophischen Rolle von Protisten-Plankton-Gemeinschaften für die induzierten Manipulationen zu untersuchen, indem V9 18S rRNA-Gen-Amplikons analysiert und Kurzzeit-Weideexperimente durchgeführt wurden.

Die Auftriebssimulationen führten unter beiden Lichtverhältnissen zu einem signifikanten Anstieg der Alpha-Diversität. Im Sommer, der sich in den HL-Bedingungen widerspiegelt, wurde eine allgemein höhere Alpha-Diversität festgestellt als in der Wintersimulation, die

durch die LL-Behandlung simuliert wurde. Signifikante Veränderungen in der Struktur der Protisten-Plankton-Gemeinschaft konnten ebenfalls beobachtet werden. Kieselalgen wurden mit einer hohen Zugabe von Tiefenwasser während der Wintersimulation in Verbindung gebracht. Unter Nährstoffverarmung dominierten Chlorophyten die relative Häufigkeit im nachgeahmten Winterszenario. Dinoflagellaten dominierten im Sommer in allen Auftriebssimulationen. Bei Lichtreduzierung wurden tendenziell weniger einzellige Eukaryoten und mehr Prokaryoten festgestellt. Die durch Protisten vermittelte Sterblichkeit von Prokaryoten ging im simulierten Winterszenario ebenfalls um ca. 30 % zurück.

Die Ergebnisse deuten darauf hin, dass der mikrobielle Kreislauf im Sommer ein relevanter Faktor für die Struktur des Nahrungsnetzes ist und sich im Winter im HCS vor Peru mehr auf die Nutzung von Kieselalgen konzentriert. Es wurde deutlich, dass unterschiedliche Lichtintensitäten in Verbindung mit verschiedenen Auftriebsszenarien zu Veränderungen der biochemischen Zyklen, der trophischen Interaktionen und der Ökosystemleistungen führen können. In Anbetracht der Bedrohung durch den Klimawandel könnte die vorhergesagte Verlagerung der EBUS die Primärproduktion einschränken und die Struktur des Nahrungsnetzes verlängern, was schwerwiegende sozioökonomische Folgen hätte.

VI. References

- Aalto, N.J., Schweitzer, H., Grann-Meyer, E., Krsmanovic, S., Svenning, J.B., Dalheim, L., Petters, S., Ingebrigtsen, R.A., Hulatt, C.J., Bernstein, H.C., 2023. Microbial community dynamics during a harmful *Chrysochromulina leadbeateri* bloom in northern Norway. *Appl. Environ. Microbiol.* 89, e01895-22. <https://doi.org/10.1128/aem.01895-22>
- Abad, D., Albaina, A., Aguirre, M., Laza-Martínez, A., Uriarte, I., Iriarte, A., Villate, F., Estonba, A., 2016. Is metabarcoding suitable for estuarine plankton monitoring? A comparative study with microscopy. *Mar. Biol.* 163, 149. <https://doi.org/10.1007/s00227-016-2920-0>
- Abdala, Z.M., Clayton, S., Einarsson, S.V., Powell, K., Till, C.P., Coale, T.H., Chappell, P.D., 2022. Examining ecological succession of diatoms in California Current System cyclonic mesoscale eddies. *Limnol. Oceanogr.* 67, 2586–2602. <https://doi.org/10.1002/lno.12224>
- Abrahams, A., Schlegel, R.W., Smit, A.J., 2021. Variation and change of upwelling dynamics detected in the world's eastern boundary upwelling systems. *Front. Mar. Sci.* 8.
- Adl, S.M., Bass, D., Lane, C.E., Lukeš, J., Schoch, C.L., Smirnov, A., Agatha, S., Berney, C., Brown, M.W., Burki, F., Cárdenas, P., Čepička, I., Chistyakova, L., del Campo, J., Dunthorn, M., Edvardsen, B., Eglit, Y., Guillou, L., Hampl, V., Heiss, A.A., Hoppenrath, M., James, T.Y., Karnkowska, A., Karpov, S., Kim, E., Kolisko, M., Kudryavtsev, A., Lahr, D.J.G., Lara, E., Le Gall, L., Lynn, D.H., Mann, D.G., Massana, R., Mitchell, E.A.D., Morrow, C., Park, J.S., Pawlowski, J.W., Powell, M.J., Richter, D.J., Rueckert, S., Shadwick, L., Shimano, S., Spiegel, F.W., Torruella, G., Youssef, N., Zlatogursky, V., Zhang, Q., 2019. Revisions to the Classification, Nomenclature, and Diversity of Eukaryotes. *J. Eukaryot. Microbiol.* 66, 4–119. <https://doi.org/10.1111/jeu.12691>
- Agis, M., Granda, A., Dolan, J.R., 2007. A cautionary note: examples of possible microbial community dynamics in dilution grazing experiments. *J. Exp. Mar. Biol. Ecol.* 341, 176–183. <https://doi.org/10.1016/j.jembe.2006.09.002>
- Alderkamp, A.-C., Dijken, G.L. van, Lowry, K.E., Lewis, K.M., Joy-Warren, H.L., Poll, W. van de, Laan, P., Gerringa, L., Delmont, T.O., Jenkins, B.D., Arrigo, K.R., 2019. Effects of iron and light availability on phytoplankton photosynthetic properties in the Ross Sea. *Mar. Ecol. Prog. Ser.* 621, 33–50. <https://doi.org/10.3354/meps13000>
- Allison, E. H., Badjeck, M. C., Meinhold, K. 2011. The implications of global climate change for molluscan aquaculture. 461-490. *Shellfish aquaculture and the environment* (ed. S. E. S Humway), pp. 461–490. John Wiley & Sons Inc., Hoboken.
- Alvarez-Fernandez, S., Bach, L.T., Taucher, J., Riebesell, U., Sommer, U., Aberle, N., Brussaard, C.P.D., Boersma, M., 2018. Plankton responses to ocean acidification: The role of nutrient limitation. *Prog. Oceanogr.* 165, 11–18. <https://doi.org/10.1016/j.pocan.2018.04.006>
- Amir, A., McDonald, D., Navas-Molina, J.A., Kopylova, E., Morton, J.T., Zech Xu, Z., Kightley, E.P., Thompson, L.R., Hyde, E.R., Gonzalez, A., Knight, R., 2017. Deblur Rapidly Resolves Single-Nucleotide Community Sequence Patterns. *mSystems* 2, 10-1128. <https://doi.org/10.1128/msystems.00191-16>
- Anderson, S., Blanco-Bercial, L., Carlson, C., Harvey, E., 2023. Syndiniales parasites drive species networks and are a biomarker for carbon export in the oligotrophic ocean. *bioRxiv* 2023-06. <https://doi.org/10.1101/2023.06.29.547083>

- Anderson, S.I., Franzè, G., Kling, J.D., Wilburn, P., Kremer, C.T., Menden-Deuer, S., Litchman, E., Hutchins, D.A., Rynearson, T.A., 2022. The interactive effects of temperature and nutrients on a spring phytoplankton community. *Limnol. Oceanogr.* 67, 634–645. <https://doi.org/10.1002/lno.12023>
- Anderson, S.I., Franzè, G., Kling, J.D., Wilburn, P., Kremer, C.T., Menden-Deuer, S., Litchman, E., Hutchins, D.A., Rynearson, T.A., 2022. The interactive effects of temperature and nutrients on a spring phytoplankton community. *Limnol. Oceanogr.* 67, 634–645. <https://doi.org/10.1002/lno.12023>
- Anderson, T.R., Rice, T., 2006. Deserts on the sea floor: Edward Forbes and his azoic hypothesis for a lifeless deep ocean. *Endeavour* 30, 131–137. <https://doi.org/10.1016/j.endeavour.2006.10.003>
- Andersson, A., Tamminen, T., Lehtinen, S., Jürgens, K., Labrenz, M., Viitasalo, M., 2017. The pelagic food web, in: *Biological oceanography of the Baltic Sea*. Springer, Berlin, pp. 281–332. https://doi.org/10.1007/978-94-007-0668-2_8
- Angel, M.V., Fasham, M.J.R., 1983. Eddies and biological processes, in: Robinson, A.R. (Ed.), *Eddies in marine science, topics in atmospheric and oceanographic sciences*. Springer, Berlin, pp. 492–524. https://doi.org/10.1007/978-3-642-69003-7_22
- Arístegui, J., Álvarez-Salgado, X.A., Barton, E.D., Figueiras, F.G., Hernández León, S., Roy, C., Santos, A.M.P., 2004. *Oceanography and fisheries of the Canary Current Iberian region of the eastern North Atlantic*. Harvard University Press, Cambridge, pp 877–931.
- Arndt, H., Nomdedeu, M.M., 2016. Protozoans and global climate change in aquatic systems. *Clim. Change Microb. Ecol. Curr. Res. Future Trends* 41–52. <https://doi.org/10.21775/9781910190319.03>
- Arnold, T.W., 2010. Uninformative parameters and model selection using akaike’s information criterion. *J. Wildl. Manag.* 74, 1175–1178. <https://doi.org/10.1111/j.1937-2817.2010.tb01236.x>
- Arntz, W.E., Gallardo, V.A., Gutiérrez, D., Isla, E., Levin, L.A., Mendo, J., Neira, C., Rowe, G.T., Tarazona, J., Wolff, M., 2006. El Niño and similar perturbation effects on the benthos of the Humboldt, California, and Benguela Current upwelling ecosystems. *Adv. Geosci.* 6, 243–265. <https://doi.org/10.5194/adgeo-6-243-2006>
- Arrigo, K.R., DiTullio, G.R., Dunbar, R.B., Robinson, D.H., VanWoert, M., Worthen, D.L., Lizotte, M.P., 2000. Phytoplankton taxonomic variability in nutrient utilization and primary production in the Ross Sea. *J. Geophys. Res. Oceans* 105, 8827–8846. <https://doi.org/10.1029/1998JC000289>
- Atkinson, A., Lilley, M.K.S., Hirst, A.G., McEvoy, A.J., Tarran, G.A., Widdicombe, C., Fileman, E.S., Woodward, E.M.S., Schmidt, K., Smyth, T.J., Somerfield, P.J., 2021. Increasing nutrient stress reduces the efficiency of energy transfer through planktonic size spectra. *Limnol. Oceanogr.* 66, 422–437. <https://doi.org/10.1002/lno.11613>
- Atkinson, D., Ciotti, B.J., Montagnes, D.J.S., 2003. Protists decrease in size linearly with temperature: ca. 2.5% °C⁻¹. *Proc. R. Soc. Lond. B Biol. Sci.* 270, 2605–2611. <https://doi.org/10.1098/rspb.2003.2538>
- Ayón, P., Criales-Hernandez, M.I., Schwamborn, R., Hirche, H.-J., 2008. Zooplankton research off Peru: a review. *Prog. Oceanogr.* 79, 238–255. <https://doi.org/10.1016/j.pocean.2008.10.020>

- Azam, F., Chisholm, S.W., 1976. Silicic acid uptake and incorporation by natural marine phytoplankton populations. *Limnol. Oceanogr.* 21, 427–435. <https://doi.org/10.4319/lo.1976.21.3.0427>
- Azam, F., Fenchel, T., Field, J., Gray, J., Meyerreil, L., Thingstad, F., 1983. The ecological role of water-column microbes in the sea. *Mar. Ecol. Prog. Ser.* 10, 257–263. <https://doi.org/10.3354/meps010257>
- Bacaër, N., 2011. Lotka, Volterra and the predator–prey system (1920–1926), in: Bacaër, N. (Ed.), *A Short History of Mathematical Population Dynamics*. Springer, London, pp. 71–76. https://doi.org/10.1007/978-0-85729-115-8_13
- Bach, L.T., Paul, A.J., Boxhammer, T., von der Esch, E., Graco, M., Schulz, K.G., Achterberg, E., Aguayo, P., Arístegui, J., Ayón, P., Baños, I., Bernales, A., Boegeholz, A.S., Chavez, F., Chavez, G., Chen, S.-M., Doering, K., Filella, A., Fischer, M., Grasse, P., Haunost, M., Hennke, J., Hernández-Hernández, N., Hopwood, M., Igarza, M., Kalter, V., Kittu, L., Kohnert, P., Ledesma, J., Lieberum, C., Lischka, S., Löscher, C., Ludwig, A., Mendoza, U., Meyer, Jana, Meyer, Judith, Minutolo, F., Ortiz Cortes, J., Piiparinen, J., Sforna, C., Spilling, K., Sanchez, S., Spisla, C., Sswat, M., Zavala Moreira, M., Riebesell, U., 2020. Factors controlling plankton community production, export flux, and particulate matter stoichiometry in the coastal upwelling system off Peru. *Biogeosciences* 17, 4831–4852. <https://doi.org/10.5194/bg-17-4831-2020>
- Bach, L.T., Taucher, J., Boxhammer, T., Ludwig, A., Consortium, T.K.K., Achterberg, E.P., Algueró-Muñiz, M., Anderson, L.G., Bellworthy, J., Büdenbender, J., Czerny, J., Ericson, Y., Esposito, M., Fischer, M., Haunost, M., Hellemann, D., Horn, H.G., Hornick, T., Meyer, J., Sswat, M., Zark, M., Riebesell, U., 2016. Influence of ocean acidification on a natural winter-to-summer plankton succession: first insights from a long-term mesocosm study draw attention to periods of low nutrient concentrations. *PLoS One* 11, e0159068. <https://doi.org/10.1371/journal.pone.0159068>
- Baker, A.R., Kelly, S.D., Biswas, K.F., Witt, M., Jickells, T.D., 2003. Atmospheric deposition of nutrients to the Atlantic Ocean. *Geophys. Res. Lett.* 30. <https://doi.org/10.1029/2003GL018518>
- Bakun, A., 2017. Climate change and ocean deoxygenation within intensified surface-driven upwelling circulations. *Philos. Trans. R. Soc. Math. Phys. Eng. Sci.* 375, 20160327. <https://doi.org/10.1098/rsta.2016.0327>
- Bakun, A., 1990. Global climate change and intensification of coastal ocean upwelling. *Science* 247, 198–201. <https://doi.org/10.1126/science.247.4939.198>
- Bakun, A., Black, B.A., Bograd, S.J., García-Reyes, M., Miller, A.J., Rykaczewski, R.R., Sydeman, W.J., 2015. Anticipated effects of climate change on coastal upwelling ecosystems. *Curr. Clim. Change Rep.* 1, 85–93. <https://doi.org/10.1007/s40641-015-0008-4>
- Bakun, A., Field, D.B., Redondo-Rodríguez, A., Weeks, S.J., 2010. Greenhouse gas, upwelling-favorable winds, and the future of coastal ocean upwelling ecosystems. *Glob. Change Biol.* 16, 1213–1228. <https://doi.org/10.1111/j.1365-2486.2009.02094.x>
- Bakun, A., Nelson, C.S., 1991. The seasonal cycle of wind-stress curl in subtropical eastern boundary current regions. *J. Phys. Oceanogr.* 21, 1815–1834. [https://doi.org/10.1175/1520-0485\(1991\)021<1815:TSCOWS>2.0.CO;2](https://doi.org/10.1175/1520-0485(1991)021<1815:TSCOWS>2.0.CO;2)

- Bakun, A., Weeks, S.J., 2004. Greenhouse gas buildup, sardines, submarine eruptions and the possibility of abrupt degradation of intense marine upwelling ecosystems. *Ecol. Lett.* 7, 1015–1023. <https://doi.org/10.1111/j.1461-0248.2004.00665.x>
- Barber, R.T., 2007. Oceans: picoplankton do some heavy lifting. *Science* 315, 777–778. <https://doi.org/10.1126/science.1137438>
- Barlow, R., Lamont, T., Gibberd, M.-J., Airs, R., Jacobs, L., Britz, K., 2017. Phytoplankton communities and acclimation in a cyclonic eddy in the southwest Indian Ocean. *Deep Sea Res. Part Oceanogr. Res. Pap.* 124, 18–30. <https://doi.org/10.1016/j.dsr.2017.03.013>
- Bar-On, Y.M., Phillips, R., Milo, R., 2018. The biomass distribution on Earth. *Proc. Natl. Acad. Sci.* 115, 6506–6511. <https://doi.org/10.1073/pnas.1711842115>
- Barth, J.A., Menge, B.A., Lubchenco, J., Chan, F., Bane, J.M., Kirincich, A.R., McManus, M.A., Nielsen, K.J., Pierce, S.D., Washburn, L., 2007. Delayed upwelling alters nearshore coastal ocean ecosystems in the northern California current. *Proc. Natl. Acad. Sci.* 104, 3719–3724. <https://doi.org/10.1073/pnas.0700462104>
- Barton, A.D., Dutkiewicz, S., Flierl, G., Bragg, J., Follows, M.J., 2010. Patterns of diversity in marine phytoplankton. *Science* 327, 1509–1511. <https://doi.org/10.1126/science.1184961>
- Barton, A.D., Irwin, A.J., Finkel, Z.V., Stock, C.A., 2016. Anthropogenic climate change drives shift and shuffle in North Atlantic phytoplankton communities. *Proc. Natl. Acad. Sci.* 113, 2964–2969. <https://doi.org/10.1073/pnas.1519080113>
- Batten, P., Goldberg, U., Chakravarthy, S., 2004. Interfacing statistical turbulence closures with large-eddy simulation. *AIAA J.* 42, 485–492. <https://doi.org/10.2514/1.3496>
- Beardall, J., Raven, J.A., 2004. The potential effects of global climate change on microalgal photosynthesis, growth and ecology. *Phycologia* 43, 26–40. <https://doi.org/10.2216/i0031-8884-43-1-26.1>
- Beers, J.R., Stewart, G.L., 1971. Micro-zooplankters in the plankton communities of the upper waters of the eastern tropical Pacific. *Deep Sea Res. Oceanogr. Abstr.* 18, 861–883. [https://doi.org/10.1016/0011-7471\(71\)90061-1](https://doi.org/10.1016/0011-7471(71)90061-1)
- Behrenfeld, M.J., Bisson, K.M., Boss, E., Gaube, P., Karp-Boss, L., 2022. Phytoplankton community structuring in the absence of resource-based competitive exclusion. *PLoS One* 17, e0274183. <https://doi.org/10.1371/journal.pone.0274183>
- Behrenfeld, M.J., O'Malley, R., Boss, E., Karp-Boss, L., Mundt, C., 2021. Phytoplankton biodiversity and the inverted paradox. *ISME Commun.* 1, 1–9. <https://doi.org/10.1038/s43705-021-00056-6>
- Behrenfeld, M.J., O'Malley, R.T., Siegel, D.A., McClain, C.R., Sarmiento, J.L., Feldman, G.C., Milligan, A.J., Falkowski, P.G., Letelier, R.M., Boss, E.S., 2006. Climate-driven trends in contemporary ocean productivity. *Nature* 444, 752–755. <https://doi.org/10.1038/nature05317>
- Belcher, A., Manno, C., Thorpe, S., Tarling, G., 2018. Acantharian cysts: high flux occurrence in the bathypelagic zone of the Scotia Sea, Southern Ocean. *Mar. Biol.* 165, 117. <https://doi.org/10.1007/s00227-018-3376-1>
- Belkin, N., Guy-Haim, T., Rubín-Blum, M., Lazar, A., Sisma-Ventura, G., Kiko, R., Morov, A.R., Ozer, T., Gertman, I., Herut, B., Rahav, E., 2022. Influence of cyclonic and

- anticyclonic eddies on plankton in the southeastern Mediterranean Sea during late summertime. *Ocean Sci.* 18, 693–715. <https://doi.org/10.5194/os-18-693-2022>
- Bell, T., Newman, J.A., Silverman, B.W., Turner, S.L., Lilley, A.K., 2005. The contribution of species richness and composition to bacterial services. *Nature* 436, 1157–1160. <https://doi.org/10.1038/nature03891>
- Belveze, H., Erzini, K., 1983. The influence of hydroclimatic factors on the availability of the sardine (*Sardina pilchardus*, Walbaum) in the Moroccan Atlantic fishery, in: proceedings of the expert consultation to examine changes in abundance and species of neritic fish resources. San José, Costa, Rica, 18–29 April 1983, FAO Fisheries report. FAO Fisheries and aquaculture department publications, pp. 285–328.
- Benincà, E., Huisman, J., Heerkloss, R., Jöhnk, K.D., Branco, P., Van Nes, E.H., Scheffer, M., Ellner, S.P., 2008. Chaos in a long-term experiment with a plankton community. *Nature* 451, 822–825. <https://doi.org/10.1038/nature06512>
- Berk, S.G., Brownlee, D.C., Heinle, D.R., Kling, H.J., Colwell, R.R., 1977. Ciliates as a food source for marine planktonic copepods. *Microb. Ecol.* 4, 27–40. <https://doi.org/10.1007/BF02010427>
- Biard, T., 2022. Diversity and ecology of Radiolaria in modern oceans. *Environ. Microbiol.* 24, 2179–2200. <https://doi.org/10.1111/1462-2920.16004>
- Bibby, T.S., Gorbunov, M.Y., Wyman, K.W., Falkowski, P.G., 2008. Photosynthetic community responses to upwelling in mesoscale eddies in the subtropical North Atlantic and Pacific Oceans. *Deep Sea Res. Part II Top. Stud. Oceanogr.* 55, 1310–1320. <https://doi.org/10.1016/j.dsr2.2008.01.014>
- Biggs, C.R., Yeager, L.A., Bolser, D.G., Bonsell, C., Dichiera, A.M., Hou, Z., Keyser, S.R., Khursigara, A.J., Lu, K., Muth, A.F., Negrete Jr., B., Erisman, B.E., 2020. Does functional redundancy affect ecological stability and resilience? A review and meta-analysis. *Ecosphere* 11, e03184. <https://doi.org/10.1002/ecs2.3184>
- Bittner, L., Gobet, A., Audic, S., Romac, S., Egge, E.S., Santini, S., Ogata, H., Probert, I., Edvardsen, B., de Vargas, C., 2013. Diversity patterns of uncultured haptophytes unravelled by pyrosequencing in Naples Bay. *Mol. Ecol.* 22, 87–101. <https://doi.org/10.1111/mec.12108>
- Blank, G.S., Sullivan, C.W., 1979. Diatom mineralization of silicic acid. *Arch. Microbiol.* 123, 157–164. <https://doi.org/10.1007/BF00446815>
- Boenigk, J., 2002. Variability of ingestion rates with stage in cell cycle of a heterotrophic nanoflagellate (*Spumella* sp.) measured by an individual-based approach. *Eur. J. Protistol.* 38, 299–306. <https://doi.org/10.1078/0932-4739-00881>
- Bonino, G., Di Lorenzo, E., Masina, S., Iovino, D., 2019. Interannual to decadal variability within and across the major eastern boundary upwelling systems. *Sci. Rep.* 9, 19949. <https://doi.org/10.1038/s41598-019-56514-8>
- Boras, J.A., Montserrat Sala, M., Baltar, F., Arístegui, J., Duarte, C.M., Vaqué, D., 2010. Effect of viruses and protists on bacteria in eddies of the Canary Current region (subtropical northeast Atlantic). *Limnol. Oceanogr.* 55, 885–898. <https://doi.org/10.4319/lo.2010.55.2.0885>
- Brady, R.X., Lovenduski, N.S., Alexander, M.A., Jacox, M., Gruber, N., 2019. On the role of climate modes in modulating the air–sea CO₂ fluxes in eastern boundary upwelling systems. *Biogeosciences* 16, 329–346. <https://doi.org/10.5194/bg-16-329-2019>

- Brand, L.E., Sunda, W.G., Guillard, R.R.L., 1983. Limitation of marine phytoplankton reproductive rates by zinc, manganese, and iron. *Limnol. Oceanogr.* 28, 1182–1198. <https://doi.org/10.4319/lo.1983.28.6.1182>
- Brett, M.T., Goldman, C.R., 1997. Consumer versus resource control in freshwater pelagic food webs. *Science* 275, 384–386. <https://doi.org/10.1126/science.275.5298.384>
- Brose, U., Hillebrand, H., 2016. Biodiversity and ecosystem functioning in dynamic landscapes. *Philos. Trans. R. Soc. B Biol. Sci.* 371, 20150267. <https://doi.org/10.1098/rstb.2015.0267>
- Brown, S.L., Landry, M.R., Selph, K.E., Jin Yang, E., Rii, Y.M., Bidigare, R.R., 2008. Diatoms in the desert: plankton community response to a mesoscale eddy in the subtropical North Pacific. *Deep Sea Res. Part II Top. Stud. Oceanogr.* 55, 1321–1333. <https://doi.org/10.1016/j.dsr2.2008.02.012>
- Browning, T.J., Al-Hashem, A.A., Hopwood, M.J., Engel, A., Belkin, I.M., Wakefield, E.D., Fischer, T., Achterberg, E.P., 2021. Iron regulation of North Atlantic eddy phytoplankton productivity. *Geophys. Res. Lett.* 48, e2020GL091403. <https://doi.org/10.1029/2020GL091403>
- Brussard, P.F., 1992. Biotic Prognostications: Global warming and biological diversity. Robert L. Peters and Thomas E. Lovejoy, Eds. Yale University Press, New Haven, CT, 1992. xxii, 386 pp., illus. \$45. From a conference. Washington, DC, Oct. 1988. *Science* 258, 1505–1506. <https://doi.org/10.1126/science.258.5087.1505>
- Buesseler, K.O., Boyd, P.W., Black, E.E., Siegel, D.A., 2020. Metrics that matter for assessing the ocean biological carbon pump. *Proc. Natl. Acad. Sci.* 117, 9679–9687. <https://doi.org/10.1073/pnas.1918114117>
- Burki, F., Sandin, M.M., Jamy, M., 2021. Diversity and ecology of protists revealed by metabarcoding. *Curr. Biol.* CB 31, R1267–R1280. <https://doi.org/10.1016/j.cub.2021.07.066>
- Cadotte, M.W., 2006. Dispersal and species diversity: a meta-analysis. *Am. Nat.* 167, 913–924. <https://doi.org/10.1086/504850>
- Calbet, A., Landry, M.R., 1999. Mesozooplankton influences on the microbial food web: direct and indirect trophic interactions in the oligotrophic open ocean. *Limnol. Oceanogr.* 44, 1370–1380. <https://doi.org/10.4319/lo.1999.44.6.1370>
- Calbet, A., Martínez, R.A., Isari, S., Zervoudaki, S., Nejstgaard, J.C., Pitta, P., Sazhin, A.F., Sousoni, D., Gomes, A., Berger, S.A., Tsagaraki, T.M., Ptacnik, R., 2012. Effects of light availability on mixotrophy and microzooplankton grazing in an oligotrophic plankton food web: evidences from a mesocosm study in Eastern Mediterranean waters. *J. Exp. Mar. Biol. Ecol.* 424–425, 66–77. <https://doi.org/10.1016/j.jembe.2012.05.005>
- Callahan, B.J., McMurdie, P.J., Holmes, S.P., 2017. Exact sequence variants should replace operational taxonomic units in marker-gene data analysis. *ISME J.* 11, 2639–2643. <https://doi.org/10.1038/ismej.2017.119>
- Callahan, B.J., McMurdie, P.J., Rosen, M.J., Han, A.W., Johnson, A.J.A., Holmes, S.P., 2016. DADA2: high-resolution sample inference from Illumina amplicon data. *Nat. Methods* 13, 581–583. <https://doi.org/10.1038/nmeth.3869>
- Caron, D.A., 1994. Inorganic nutrients, bacteria, and the microbial loop. *Microb. Ecol.* 28, 295–298. <https://doi.org/10.1007/BF00166820>

- Caron, D.A., Countway, P.D., 2009. Hypotheses on the role of the protistan rare biosphere in a changing world. *Aquat. Microb. Ecol.* 57, 227–238. <https://doi.org/10.3354/ame01352>
- Caron, D.A., Goldman, J.C., Dennett, M.R., 1988. Experimental demonstration of the roles of bacteria and bacterivorous protozoa in plankton nutrient cycles. *Hydrobiologia* 159, 27–40. <https://doi.org/10.1007/BF00007365>
- Carvalho, A. da C. de O., Mendes, C.R.B., Kerr, R., Azevedo, J.L.L. de, Galdino, F., Tavano, V.M., 2019. The impact of mesoscale eddies on the phytoplankton community in the South Atlantic Ocean: HPLC-CHEMTAX approach. *Mar. Environ. Res.* 144, 154–165. <https://doi.org/10.1016/j.marenvres.2018.12.003>
- Castro, L.R., González, V., Claramunt, G., Barrientos, P., Soto, S., 2020. Stable isotopes ($\delta^{13}\text{C}$, $\delta^{15}\text{N}$) seasonal changes in particulate organic matter and in different life stages of anchoveta (*Engraulis ringens*) in response to local and large scale oceanographic variations in north and central Chile. *Prog. Oceanogr.* 186, 102342. <https://doi.org/10.1016/j.pocean.2020.102342>
- Cesar-Ribeiro, C., Piedras, F.R., da Cunha, L.C., de Lima, D.T., Pinho, L.Q., Moser, G.A.O., 2020. Is oligotrophy an equalizing factor driving microplankton species functional diversity within agulhas rings? *Front. Mar. Sci.* 7, 599185. <https://doi.org/10.3389/fmars.2020.599185>
- Chambouvet, A., Morin, P., Marie, D., Guillou, L., 2008. Control of toxic marine dinoflagellate blooms by serial parasitic killers. *Science* 322, 1254–1257. <https://doi.org/10.1126/science.1164387>
- Chan, F., Barth, J.A., Lubchenco, J., Kirincich, A., Weeks, H., Peterson, W.T., Menge, B.A., 2008. Emergence of anoxia in the California Current large marine ecosystem. *Science* 319, 920–920. <https://doi.org/10.1126/science.1149016>
- Chan, Y. H., 2003. Biostatistics 104: correlational analysis. *Singap. Med. J.* 44(12), 614–619.
- Chapman, A.R.O., Craigie, J.S., 1978. Seasonal growth in *Laminaria longicuris*: relations with reserve carbohydrate storage and production. *Mar. Biol.* 46, 209–213. <https://doi.org/10.1007/BF00390682>
- Charlson, R.J., Lovelock, J.E., Andreae, M.O., Warren, S.G., 1987. Oceanic phytoplankton, atmospheric sulphur, cloud albedo and climate. *Nature* 326, 655–661. <https://doi.org/10.1038/326655a0>
- Chavez, F.P., Messié, M., 2009. A comparison of eastern boundary upwelling ecosystems. *Prog. Oceanogr.*, 83, 80–96. <https://doi.org/10.1016/j.pocean.2009.07.032>
- Chavez, F.P., Ryan, J., Lluch-Cota, S.E., Ñiquen C., M., 2003. From anchovies to sardines and back: multidecadal change in the Pacific Ocean. *Science* 299, 217–221. <https://doi.org/10.1126/science.1075880>
- Chelton, D.B., Schlax, M.G., Samelson, R.M., de Szoeke, R.A., 2007. Global observations of large oceanic eddies. *Geophys. Res. Lett.* 34. <https://doi.org/10.1029/2007GL030812>
- Chen, G., Han, G., 2019. Contrasting short-lived with long-lived mesoscale eddies in the global ocean. *J. Geophys. Res. Oceans* 124, 3149–3167. <https://doi.org/10.1029/2019JC014983>
- Chesson, P., 2000. Mechanisms of maintenance of species diversity. *Annu. Rev. Ecol. Syst.* 31, 343–366. <https://doi.org/10.1146/annurev.ecolsys.31.1.343>

- Chow, C.-E.T., Kim, D.Y., Sachdeva, R., Caron, D.A., Fuhrman, J.A., 2014. Top-down controls on bacterial community structure: microbial network analysis of bacteria, T4-like viruses and protists. *ISME J.* 8, 816–829. <https://doi.org/10.1038/ismej.2013.199>
- Chust, G., Irigoien, X., Chave, J., Harris, R.P., 2013. Latitudinal phytoplankton distribution and the neutral theory of biodiversity. *Glob. Ecol. Biogeogr.* 22, 531–543. <https://doi.org/10.1111/geb.12016>
- Clayton, S., Dutkiewicz, S., Jahn, O., Follows, M.J., 2013. Dispersal, eddies, and the diversity of marine phytoplankton. *Limnol. Oceanogr. Fluids Environ.* 3, 182–197. <https://doi.org/10.1215/21573689-2373515>
- Cleven, E.-J., Weisse, T., 2001. Seasonal succession and taxon-specific bacterial grazing rates of heterotrophic nanoflagellates in Lake Constance. *Aquat. Microb. Ecol.* 23, 147–161. <https://doi.org/10.3354/ame023147>
- Condie, S., Condie, R., 2016. Retention of plankton within ocean eddies. *Glob. Ecol. Biogeogr.* 25, 1264–1277. <https://doi.org/10.1111/geb.12485>
- Connell, J.H., 1978. Diversity in tropical rain forests and coral reefs. *Science* 199, 1302–1310. <https://doi.org/10.1126/science.199.4335.1302>
- Connell, J.H., Orias, E., 1964. The ecological regulation of species diversity. *Am. Nat.* 98, 399–414. <https://doi.org/10.1086/282335>
- Cotner, J.B., Biddanda, B.A., 2002. Small players, large role: microbial influence on biogeochemical processes in pelagic aquatic ecosystems. *Ecosyst.* 5, 105–121. <https://doi.org/10.1007/s10021-001-0059-3>
- Countway, P.D., Gast, R.J., Savai, P., Caron, D.A., 2005. Protistan diversity estimates based on 18S rDNA from seawater incubations in the western North Atlantic. *J. Eukaryot. Microbiol.* 52, 95–106. <https://doi.org/10.1111/j.1550-7408.2005.05202006.x>
- Cuevas, L.A., Daneri, G., Jacob, B., Montero, P., 2004. Microbial abundance and activity in the seasonal upwelling area off Concepción (~36°S), central Chile: a comparison of upwelling and non-upwelling conditions. *Deep Sea Res. Part II Top. Stud. Oceanogr., Oceanography in the eastern South Pacific: Part I* 51, 2427–2440. <https://doi.org/10.1016/j.dsr2.2004.07.026>
- Cuevas, L.A., Morales, C.E., 2006. Nanoheterotroph grazing on bacteria and cyanobacteria in oxic and suboxic waters in coastal upwelling areas off northern Chile. *J. Plankton Res.* 28, 385–397. <https://doi.org/10.1093/plankt/fbi124>
- Cullen, J.J., 2015. Subsurface chlorophyll maximum layers: enduring enigma or mystery solved? *Annu. Rev. Mar. Sci.* 7, 207–239. <https://doi.org/10.1146/annurev-marine-010213-135111>
- Cury, P., Bakun, A., Crawford, R.J.M., Jarre, A., Quiñones, R.A., Shannon, L.J., Verheye, H.M., 2000. Small pelagics in upwelling systems: patterns of interaction and structural changes in “wasp-waist” ecosystems. *ICES J. Mar. Sci.* 57, 603–618. <https://doi.org/10.1006/jmsc.2000.0712>
- Cury, P., Roy, C., 1989. Optimal environmental window and pelagic fish recruitment success in upwelling areas. *Can. J. Fish. Aquat. Sci.* 46, 670–680. <https://doi.org/10.1139/f89-086>
- Cushing, D.H., 1990. Plankton production and year-class strength in fish populations: an update of the match/mismatch hypothesis, in: Blaxter, J.H.S., Southward, A.J. (Eds.), *Advances*

- in Marine Biology. Academic Press, pp. 249–293. [https://doi.org/10.1016/S0065-2881\(08\)60202-3](https://doi.org/10.1016/S0065-2881(08)60202-3)
- Cushing, D.H., 1971. Upwelling and the production of fish, in: Russell, F.S., Yonge, M. (Eds.), *Advances in Marine Biology*. Academic Press, pp. 255–334. [https://doi.org/10.1016/S0065-2881\(08\)60344-2](https://doi.org/10.1016/S0065-2881(08)60344-2)
- Cushman-Roisin, B., Beckers, J.-M., 2011. *Introduction to geophysical fluid dynamics: physical and numerical aspects*. 2nd edition, Academic Press.
- Czerny, J., Schulz, K.G., Krug, S.A., Ludwig, A., Riebesell, U., 2013. Technical note: the determination of enclosed water volume in large flexible-wall mesocosms “KOSMOS.” *Biogeosciences* 10, 1937–1941. <https://doi.org/10.5194/bg-10-1937-2013>
- Daam, M.A., Teixeira, H., Lillebø, A.I., Nogueira, A.J.A., 2019. Establishing causal links between aquatic biodiversity and ecosystem functioning: Status and research needs. *Sci. Total Environ.* 656, 1145–1156. <https://doi.org/10.1016/j.scitotenv.2018.11.413>
- Dahl, E., Bagøien, E., Edvardsen, B., Stenseth, N.Chr., 2005. The dynamics of *Chrysochromulina* species in the Skagerrak in relation to environmental conditions. *J. Sea Res.* 54, 15–24. <https://doi.org/10.1016/j.seares.2005.02.004>
- D’Asaro, E.A., 1988. Generation of submesoscale vortices: a new mechanism. *J. Geophys. Res. Oceans* 93, 6685–6693. <https://doi.org/10.1029/JC093iC06p06685>
- de Vargas, C., Audic, S., Henry, N., Decelle, J., Mahé, F., Logares, R., Lara, E., Berney, C., Le Bescot, N., Probert, I., Carmichael, M., Poulain, J., Romac, S., Colin, S., Aury, J.-M., Bittner, L., Chaffron, S., Dunthorn, M., Engelen, S., Flegontova, O., Guidi, L., Horák, A., Jaillon, O., Lima-Mendez, G., Lukeš, J., Malviya, S., Morard, R., Mulot, M., Scalco, E., Siano, R., Vincent, F., Zingone, A., Dimier, C., Picheral, M., Searson, S., Kandels-Lewis, S., Tara Oceans Coordinators, Acinas, S.G., Bork, P., Bowler, C., Gorsky, G., Grimsley, N., Hingamp, P., Iudicone, D., Not, F., Ogata, H., Pesant, S., Raes, J., Sieracki, M.E., Speich, S., Stemmann, L., Sunagawa, S., Weissenbach, J., Wincker, P., Karsenti, E., 2015. Ocean plankton. Eukaryotic plankton diversity in the sunlit ocean. *Science* 348, 1261605. <https://doi.org/10.1126/science.1261605>
- Decelle, J., Martin, P., Paborstava, K., Pond, D.W., Tarling, G., Mahé, F., Vargas, C. de, Lampitt, R., Not, F., 2013. Diversity, ecology and biogeochemistry of cyst-forming acantharia (Radiolaria) in the oceans. *PLoS One* 8, e53598. <https://doi.org/10.1371/journal.pone.0053598>
- Decelle, J., Stryhanyuk, H., Gallet, B., Veronesi, G., Schmidt, M., Balzano, S., Marro, S., Uwizeye, C., Jouneau, P.-H., Lupette, J., Jouhet, J., Maréchal, E., Schwab, Y., Schieber, N.L., Tucoulou, R., Richnow, H., Finazzi, G., Musat, N., 2019. Algal remodeling in a ubiquitous planktonic photosymbiosis. *Curr. Biol. CB* 29, 968-978.e4. <https://doi.org/10.1016/j.cub.2019.01.073>
- Degerman, R., Lefébure, R., Byström, P., Båmstedt, U., Larsson, S., Andersson, A., 2018. Food web interactions determine energy transfer efficiency and top consumer responses to inputs of dissolved organic carbon. *Hydrobiologia* 805, 131–146. <https://doi.org/10.1007/s10750-017-3298-9>
- Deutsch, C., Emerson, S., Thompson, L., 2005. Fingerprints of climate change in North Pacific oxygen. *Geophys. Res. Lett.* 32. <https://doi.org/10.1029/2005GL023190>
- Devresse, Q., Becker, K.W., Dilmahamod, A.F., Ortega-Retuerta, E., Engel, A., 2023. Dissolved organic matter fluorescence as a tracer of upwelling and microbial activities

- in two cyclonic eddies in the eastern tropical North Atlantic. *J. Geophys. Res. Oceans* 128(8), e2023JC019821. <https://doi.org/10.1029/2023JC019821>
- Dilmahamod, A.F., Karstensen, J., Dietze, H., Löptien, U., Fennel, K., 2021. Generation mechanisms of mesoscale eddies in the Mauritanian upwelling region. *J. Phys. Oceanogr.* 52, 161-182. <https://doi.org/10.1175/JPO-D-21-0092.1>
- Dittrich, J., Dias, J.D., de Paula, A.C.M., Padial, A.A., 2023. Experimental nutrient enrichment increases plankton taxonomic and functional richness and promotes species dominance overtime. *Hydrobiologia* 850, 4029-4048. <https://doi.org/10.1007/s10750-023-05285-5>
- DiTullio, G.R., Geesey, M.E., Maucher, J.M., Alm, M.B., Riseman, S.F., Bruland, K.W., 2005. Influence of iron on algal community composition and physiological status in the Peru upwelling system. *Limnol. Oceanogr.* 50, 1887–1907. <https://doi.org/10.4319/lo.2005.50.6.1887>
- Díez, B., Pedrós-Alió, C., Massana, R., 2001. Study of genetic diversity of eukaryotic picoplankton in different oceanic regions by small-subunit rRNA gene cloning and sequencing. *Appl. Environ. Microbiol.* 67, 2932–2941. <https://doi.org/10.1128/AEM.67.7.2932-2941.2001>
- Dlugosch, L., Poehlein, A., Wemheuer, B., Pfeiffer, B., Badewien, T.H., Daniel, R., Simon, M., 2022. Significance of gene variants for the functional biogeography of the near-surface Atlantic Ocean microbiome. *Nat. Commun.* 13, 456. <https://doi.org/10.1038/s41467-022-28128-8>
- Dolan, J.R., Claustre, H., Carlotti, F., Plounevez, S., Moutin, T., 2002. Microzooplankton diversity: relationships of tintinnid ciliates with resources, competitors and predators from the Atlantic Coast of Morocco to the Eastern Mediterranean. *Deep Sea Res. Part Oceanogr. Res. Pap.* 49, 1217–1232. [https://doi.org/10.1016/S0967-0637\(02\)00021-3](https://doi.org/10.1016/S0967-0637(02)00021-3)
- Dolan, J.R., Šimek, K., 1998. Ingestion and digestion of an autotrophic picoplankton, *Synechococcus*, by a heterotrophic nanoflagellate, *Bodo saltans*. *Limnol. Oceanogr.* 43, 1740–1746. <https://doi.org/10.4319/lo.1998.43.7.1740>
- Domingues, R.B., Guerra, C.C., Barbosa, A.B., Galvão, H.M., 2017. Will nutrient and light limitation prevent eutrophication in an anthropogenically-impacted coastal lagoon? *Cont. Shelf Res.* 141, 11–25. <https://doi.org/10.1016/j.csr.2017.05.003>
- Doney, S.C., Busch, D.S., Cooley, S.R., Kroeker, K.J., 2020. The impacts of ocean acidification on marine ecosystems and reliant human communities. *Annu. Rev. Environ. Resour.* 45, 83–112. <https://doi.org/10.1146/annurev-environ-012320-083019>
- Doney, S.C., Ruckelshaus, M., Emmett Duffy, J., Barry, J.P., Chan, F., English, C.A., Galindo, H.M., Grebmeier, J.M., Hollowed, A.B., Knowlton, N., Polovina, J., Rabalais, N.N., Sydeman, W.J., Talley, L.D., 2012. Climate change impacts on marine ecosystems. *Annu. Rev. Mar. Sci.* 4, 11–37. <https://doi.org/10.1146/annurev-marine-041911-111611>
- Duce, R.A., LaRoche, J., Altieri, K., Arrigo, K.R., Baker, A.R., Capone, D.G., Cornell, S., Dentener, F., Galloway, J., Ganeshram, R.S., Geider, R.J., Jickells, T., Kuypers, M.M., Langlois, R., Liss, P.S., Liu, S.M., Middelburg, J.J., Moore, C.M., Nickovic, S., Oschlies, A., Pedersen, T., Prospero, J., Schlitzer, R., Seitzinger, S., Sorensen, L.L., Uematsu, M., Ulloa, O., Voss, M., Ward, B., Zamora, L., 2008. Impacts of atmospheric anthropogenic nitrogen on the open ocean. *Science* 320, 893–897. <https://doi.org/10.1126/science.1150369>

- Dunthorn, M., Stoeck, T., Clamp, J., Warren, A., Mahé, F., 2014. Ciliates and the rare biosphere: a review. *J. Eukaryot. Microbiol.* 61, 404–409. <https://doi.org/10.1111/jeu.12121>
- Dutkiewicz, S., Boyd, P.W., Riebesell, U., 2021. Exploring biogeochemical and ecological redundancy in phytoplankton communities in the global ocean. *Glob. Change Biol.* 27, 1196–1213. <https://doi.org/10.1111/gcb.15493>
- Dutkiewicz, S., Follows, M.J., Bragg, J.G., 2009. Modeling the coupling of ocean ecology and biogeochemistry. *Glob. Biogeochem. Cycles* 23. <https://doi.org/10.1029/2008GB003405>
- Echevin, V., Albert, A., Lévy, M., Graco, M., Aumont, O., Piétri, A., Garric, G., 2014. Intraseasonal variability of nearshore productivity in the northern Humboldt Current System: the role of coastal trapped waves. *Cont. Shelf Res.* 73, 14–30. <https://doi.org/10.1016/j.csr.2013.11.015>
- Edgar, R.C., 2016. UNOISE2: improved error-correction for Illumina 16S and ITS amplicon sequencing. *BioRxiv*. <https://doi.org/10.1101/081257>
- Edgar, R.C., Haas, B.J., Clemente, J.C., Quince, C., Knight, R., 2011. UCHIME improves sensitivity and speed of chimera detection. *Bioinforma. Oxf. Engl.* 27, 2194–2200. <https://doi.org/10.1093/bioinformatics/btr381>
- EGGE, E.S., EIKREM, W., EDVARDSEN, B., 2015. Deep-branching novel lineages and high diversity of haptophytes in the Skagerrak (Norway) uncovered by 454 pyrosequencing. *J. Eukaryot. Microbiol.* 62, 121–140. <https://doi.org/10.1111/jeu.12157>
- Eiler, A., Drakare, S., Bertilsson, S., Pernthaler, J., Peura, S., Rofner, C., Simek, K., Yang, Y., Znachor, P., Lindström, E.S., 2013. Unveiling distribution patterns of freshwater phytoplankton by a next generation sequencing based approach. *PLoS One* 8, e53516. <https://doi.org/10.1371/journal.pone.0053516>
- Ekman, V., 1905. On the influence of earth's rotation on ocean currents. *Ark Mat Astron Fys.* 2, 1-53.
- Engel, A., Galgani, L., 2016. The organic sea-surface microlayer in the upwelling region off the coast of Peru and potential implications for air–sea exchange processes. *Biogeosciences* 13, 989–1007. <https://doi.org/10.5194/bg-13-989-2016>
- Engelstaedter, S., Tegen, I., Washington, R., 2006. North African dust emissions and transport. *Earth-Sci. Rev.* 79, 73–100. <https://doi.org/10.1016/j.earscirev.2006.06.004>
- Eppley, R.W., Peterson, B.J., 1979. Particulate organic matter flux and planktonic new production in the deep ocean. *Nature* 282, 677–680. <https://doi.org/10.1038/282677a0>
- Eren, A.M., Maignien, L., Sul, W.J., Murphy, L.G., Grim, S.L., Morrison, H.G., Sogin, M.L., 2013. Oligotyping: differentiating between closely related microbial taxa using 16S rRNA gene data. *Methods Ecol. Evol.* 4, 1111–1119. <https://doi.org/10.1111/2041-210X.12114>
- Eren, A.M., Morrison, H.G., Lescault, P.J., Reveillaud, J., Vineis, J.H., Sogin, M.L., 2015. Minimum entropy decomposition: unsupervised oligotyping for sensitive partitioning of high-throughput marker gene sequences. *ISME J.* 9, 968–979. <https://doi.org/10.1038/ismej.2014.195>
- Escaravage, V., Prins, T.C., Nijdam, C., Smaal, A.C., Peeters, J.C.H., 1999. Response of phytoplankton communities to nitrogen input reduction in mesocosm experiments. *Mar. Ecol. Prog. Ser.* 179, 187–199. <https://doi.org/10.3354/meps179187>

- Estep, K.W., MacIntyre, F., 1989. Taxonomy, life cycle, distribution and osmotrophy of *Chrysochromulina*: a theory accounting for scales, haptonema, muciferous bodies and toxicity. *Mar. Ecol. Prog. Ser.* 57, 11–21.
- Ewing B., Green P., 1998. Base-calling of automated sequencer traces using phred. II. Error probabilities. *Genome Res* 8, 186–194. <https://doi.org/10.1101/gr.8.3.186>.
- Falkowski, P.G., 1994. The role of phytoplankton photosynthesis in global biogeochemical cycles. *Photosynth. Res.* 39, 235–258. <https://doi.org/10.1007/BF00014586>
- Falkowski, P.G., 1984. Physiological responses of phytoplankton to natural light regimes. *J. Plankton Res.* 6, 295–307. <https://doi.org/10.1093/plankt/6.2.295>
- Falkowski, P.G., Barber, R.T., Smetacek, V., 1998. Biogeochemical controls and feedbacks on ocean primary production. *Science* 281, 200–206. <https://doi.org/10.1126/science.281.5374.200>
- Falkowski, P.G., Owens, T.G., 1980. Light—Shade Adaptation: two strategies in marine phytoplankton. *Plant Physiol.* 66, 592–595. <https://doi.org/10.1104/pp.66.4.592>
- Feely, R.A., Sabine, C.L., Hernandez-Ayon, J.M., Ianson, D., Hales, B., 2008. Evidence for upwelling of corrosive “acidified” water onto the continental shelf. *Science* 320, 1490–1492. <https://doi.org/10.1126/science.1155676>
- Fenchel, T., 2008. The microbial loop – 25 years later. *J. Exp. Mar. Biol. Ecol.* 366, 99–103. <https://doi.org/10.1016/j.jembe.2008.07.013>
- Field, C.B., Behrenfeld, M.J., Randerson, J.T., Falkowski, P., 1998. Primary production of the biosphere: integrating terrestrial and oceanic components. *Science* 281, 237–240. <https://doi.org/10.1126/science.281.5374.237>
- Fisher, T., Shurtz-Swirski, R., Gepstein, S., Dubinsky, Z., 1989. Changes in the levels of ribulose-1,5-bisphosphate carboxylase/oxygenase (Rubisco) in *Tetraedron minimum* (Chlorophyta) during light and shade adaptation. *Plant Cell Physiol.* 30, 221–228. <https://doi.org/10.1093/oxfordjournals.pcp.a077733>
- Flegontova, O., Flegontov, P., Malviya, S., Audic, S., Wincker, P., de Vargas, C., Bowler, C., Lukeš, J., Horák, A., 2016. Extreme diversity of diplomonid eukaryotes in the ocean. *Curr. Biol.* 26, 3060–3065. <https://doi.org/10.1016/j.cub.2016.09.031>
- Flöder, S., Urabe, J., Kawabata, Z., 2002. The influence of fluctuating light intensities on species composition and diversity of natural phytoplankton communities. *Oecologia* 133, 395–401. <https://doi.org/10.1007/s00442-002-1048-8>
- Forster, D., Lentendu, G., Filker, S., Dubois, E., Wilding, T.A., Stoeck, T., 2019. Improving eDNA-based protist diversity assessments using networks of amplicon sequence variants. *Environ. Microbiol.* 21, 4109–4124. <https://doi.org/10.1111/1462-2920.14764>
- Fox, J., Weisberg, S., 2019. *An R companion to applied regression*, Third edition. Sage, Thousand Oaks, California.
- Frenken, T., Velthuis, M., de Senerpont Domis, L.N., Stephan, S., Aben, R., Kosten, S., van Donk, E., Van de Waal, D.B., 2016. Warming accelerates termination of a phytoplankton spring bloom by fungal parasites. *Glob. Change Biol.* 22, 299–309. <https://doi.org/10.1111/gcb.13095>
- Frias-Lopez, J., Thompson, A., Waldbauer, J., Chisholm, S.W., 2009. Use of stable isotope-labelled cells to identify active grazers of picocyanobacteria in ocean surface waters. *Environ. Microbiol.* 11, 512–525. <https://doi.org/10.1111/j.1462-2920.2008.01793.x>

- Gamfeldt, L., Hillebrand, H., Jonsson, P.R., 2008. Multiple functions increase the importance of biodiversity for overall ecosystem functioning. *Ecology* 89, 1223–1231. <https://doi.org/10.1890/06-2091.1>
- García-Comas, C., Sastri, A.R., Ye, L., Chang, C.-Y., Lin, F.-S., Su, M.-S., Gong, G.-C., Hsieh, C., 2016. Prey size diversity hinders biomass trophic transfer and predator size diversity promotes it in planktonic communities. *Proc. R. Soc. B Biol. Sci.* 283, 20152129. <https://doi.org/10.1098/rspb.2015.2129>
- García-Gómez, C., Yebra, L., Cortés, D., Sánchez, A., Alonso, A., Valcárcel-Pérez, N., Gómez-Jakobsen, F., Herrera, I., Johnstone, C., Mercado, J.M., 2020. Shifts in the protist community associated with an anticyclonic gyre in the Alboran Sea (Mediterranean Sea). *FEMS Microbiol. Ecol.* 96, fiae197. <https://doi.org/10.1093/femsec/fiae197>
- García-Reyes, M., Sydeman, W.J., Schoeman, D.S., Rykaczewski, R.R., Black, B.A., Smit, A.J., Bograd, S.J., 2015. Under pressure: climate change, upwelling, and eastern boundary upwelling ecosystems. *Front. Mar. Sci.* 2, 109. <https://doi.org/10.3389/fmars.2015.00109>
- Gasol, J.M., Alonso-Sáez, L., Vaqué, D., Baltar, F., Calleja, M.Ll., Duarte, C.M., Arístegui, J., 2009. Mesopelagic prokaryotic bulk and single-cell heterotrophic activity and community composition in the NW Africa–Canary Islands coastal-transition zone. *Prog. Oceanogr., Eastern Boundary Upwelling Ecosystems: Integrative and Comparative Approaches* 83, 189–196. <https://doi.org/10.1016/j.pocean.2009.07.014>
- Gasol, J.M., Kirchman, D.L., 2018. *Microbial Ecology of the Oceans*. John Wiley & Sons, Hoboken, USA.
- Gast, R.J., Fay, S.A., Sanders, R.W., 2018. Mixotrophic activity and diversity of antarctic marine protists in austral summer. *Front. Mar. Sci.* 5, 13. <https://doi.org/10.3389/fmars.2018.00013>
- Geider, R.J., La Roche, J., 1994. The role of iron in phytoplankton photosynthesis, and the potential for iron-limitation of primary productivity in the sea. *Photosynth. Res.* 39, 275–301. <https://doi.org/10.1007/BF00014588>
- Geider, R.J., MacIntyre, H.L., Kana, T.M., 1996. A dynamic model of photoadaptation in phytoplankton. *Limnol. Oceanogr.* 41, 1–15. <https://doi.org/10.4319/lo.1996.41.1.0001>
- Genitsaris, S., Monchy, S., Viscogliosi, E., Sime-Ngando, T., Ferreira, S., Christaki, U., 2015. Seasonal variations of marine protist community structure based on taxon-specific traits using the eastern English Channel as a model coastal system. *FEMS Microbiol. Ecol.* 91, fiv034. <https://doi.org/10.1093/femsec/fiv034>
- Georgieva, M.N., Little, C.T.S., Maslennikov, V.V., Glover, A.G., Ayupova, N.R., Herrington, R.J., 2021. The history of life at hydrothermal vents. *Earth-Sci. Rev.* 217, 103602. <https://doi.org/10.1016/j.earscirev.2021.103602>
- Gibert, P., Debat, V., Ghalambor, C.K., 2019. Phenotypic plasticity, global change, and the speed of adaptive evolution. *Curr. Opin. Insect Sci.* 35, 34–40. <https://doi.org/10.1016/j.cois.2019.06.007>
- Gingerich, P.D., 2019. Temporal scaling of carbon emission and accumulation rates: modern anthropogenic emissions compared to estimates of PETM onset accumulation. *Paleoceanogr. Paleoclimatology* 34, 329–335. <https://doi.org/10.1029/2018PA003379>
- Gong, F., Zhang, Y., Xie, W., Wu, X., Zhang, H., Huang, S., Gong, J., Yin, K., 2023. Response of microbial community of surface and deep chlorophyll maximum to nutrients and light

- in South China Sea. *Front. Mar. Sci.* 10, 1122765. <https://doi.org/10.3389/fmars.2023.1122765>
- González, H.E., Daneri, G., Iriarte, J.L., Yannicelli, B., Menschel, E., Barría, C., Pantoja, S., Lizárraga, L., 2009. Carbon fluxes within the epipelagic zone of the Humboldt Current System off Chile: the significance of euphausiids and diatoms as key functional groups for the biological pump. *Prog. Oceanogr.* 83, 217–227. <https://doi.org/10.1016/j.pocean.2009.07.036>
- González, H.E., Menschel, E., Aparicio, C., Barría, C., 2007. Spatial and temporal variability of microplankton and detritus, and their export to the shelf sediments in the upwelling area off Concepción, Chile (~36°S), during 2002–2005. *Prog. Oceanogr.* 75, 435–451. <https://doi.org/10.1016/j.pocean.2007.08.025>
- González, J., Sherr, B., Sherr, E., 1993. Digestive enzyme activity as a quantitative measure of protistan grazing: the acid lysozyme assay for bacterivory. *Mar. Ecol. Prog. Ser.* 100, 197–206. <https://doi.org/10.3354/meps100197>
- Graco, M.I., Purca, S., Dewitte, B., Castro, C.G., Morón, O., Ledesma, J., Flores, G., Gutiérrez, D., 2017. The OMZ and nutrient features as a signature of interannual and low-frequency variability in the Peruvian upwelling system. *Biogeosciences* 14, 4601–4617. <https://doi.org/10.5194/bg-14-4601-2017>
- Grainger, T.N., Gilbert, B., 2016. Dispersal and diversity in experimental metacommunities: linking theory and practice. *Oikos* 125, 1213–1223. <https://doi.org/10.1111/oik.03018>
- Gran-Stadniczeňko, S., Šupraha, L., Egge, E.D., Edvardsen, B., 2017. Haptophyte diversity and vertical distribution explored by 18S and 28S ribosomal RNA gene metabarcoding and scanning electron microscopy. *J. Eukaryot. Microbiol.* 64, 514–532. <https://doi.org/10.1111/jeu.12388>
- Grantham, B.A., Chan, F., Nielsen, K.J., Fox, D.S., Barth, J.A., Huyer, A., Lubchenco, J., Menge, B.A., 2004. Upwelling-driven nearshore hypoxia signals ecosystem and oceanographic changes in the northeast Pacific. *Nature* 429, 749–754. <https://doi.org/10.1038/nature02605>
- Grasshoff, K., Kremling, K., Ehrhardt, M., 1999. *Methods of Seawater Analysis*. John Wiley & Sons, Homboken, USA.
- Grise, K.M., Davis, S.M., 2020. Hadley cell expansion in CMIP6 models. *Atmospheric Chem. Phys.* 20, 5249–5268. <https://doi.org/10.5194/acp-20-5249-2020>
- Groß, J., 2003. Variance Inflation Factors. *R news* 3, 13–15.
- Grömping, U., 2006. Relative importance for linear regression in R: the package relaimpo. *J. Stat. Softw.* 17(1), 1–27. <https://doi.org/10.18637/jss.v017.i01>
- Grover, J.P., 1990. Resource competition in a variable environment: phytoplankton growing according to Monod's model. *Am. Nat.* 136, 771–789. <https://doi.org/10.1086/285131>
- Gruber, N., Galloway, J.N., 2008. An Earth-system perspective of the global nitrogen cycle. *Nature* 451, 293–296. <https://doi.org/10.1038/nature06592>
- Gruber, N., Lachkar, Z., Frenzel, H., Marchesiello, P., Münnich, M., McWilliams, J.C., Nagai, T., Plattner, G.-K., 2011. Eddy-induced reduction of biological production in eastern boundary upwelling systems. *Nat. Geosci.* 4, 787–792. <https://doi.org/10.1038/ngeo1273>

- Guénette, S., Christensen, V., Pauly, D., 2008. Trophic modelling of the Peruvian upwelling ecosystem: towards reconciliation of multiple datasets. *Prog. Oceanogr.* 79, 326–335. <https://doi.org/10.1016/j.pocean.2008.10.005>
- Guidi, L., Chaffron, S., Bittner, L., Eveillard, D., Larhlimi, A., Roux, S., Darzi, Y., Audic, S., Berline, L., Brum, J.R., Coelho, L.P., Espinoza, J.C.I., Malviya, S., Sunagawa, S., Dimier, C., Kandels-Lewis, S., Picheral, M., Poulain, J., Searson, S., Stemmann, L., Not, F., Hingamp, P., Speich, S., Follows, M., Karp-Boss, L., Boss, E., Ogata, H., Pesant, S., Weissenbach, J., Wincker, P., Acinas, S.G., Bork, P., de Vargas, C., Iudicone, D., Sullivan, M.B., Raes, J., Karsenti, E., Bowler, C., Gorsky, G., 2016. Plankton networks driving carbon export in the oligotrophic ocean. *Nature* 532, 465–470. <https://doi.org/10.1038/nature16942>
- Guillou, L., Bachar, D., Audic, S., Bass, D., Berney, C., Bittner, L., Boutte, C., Burgaud, G., de Vargas, C., Decelle, J., Del Campo, J., Dolan, J.R., Dunthorn, M., Edvardsen, B., Holzmann, M., Kooistra, W.H.C.F., Lara, E., Le Bescot, N., Logares, R., Mahé, F., Massana, R., Montresor, M., Morard, R., Not, F., Pawlowski, J., Probert, I., Sauvadet, A.-L., Siano, R., Stoeck, T., Vaultot, D., Zimmermann, P., Christen, R., 2013. The Protist Ribosomal Reference database (PR²): a catalog of unicellular eukaryote small sub-unit rRNA sequences with curated taxonomy. *Nucleic Acids Res.* 41, D597-604. <https://doi.org/10.1093/nar/gks1160>
- Guillou, L., Viprey, M., Chambouvet, A., Welsh, R.M., Kirkham, A.R., Massana, R., Scanlan, D.J., Worden, A.Z., 2008. Widespread occurrence and genetic diversity of marine parasitoids belonging to Syndiniales (Alveolata). *Environ. Microbiol.* 10, 3349–3365. <https://doi.org/10.1111/j.1462-2920.2008.01731.x>
- Gutierrez-Rodriguez, A., Stukel, M.R., Lopes dos Santos, A., Biard, T., Scharek, R., Vaultot, D., Landry, M.R., Not, F., 2019. High contribution of Rhizaria (Radiolaria) to vertical export in the California Current Ecosystem revealed by DNA metabarcoding. *ISME J.* 13, 964–976. <https://doi.org/10.1038/s41396-018-0322-7>
- Haegeman, B., Loreau, M., 2011. A mathematical synthesis of niche and neutral theories in community ecology. *J. Theor. Biol.* 269, 150–165. <https://doi.org/10.1016/j.jtbi.2010.10.006>
- Hall, C., Lutjeharms, J.R.E., 2011. Cyclonic eddies identified in the Cape Basin of the South Atlantic Ocean. *J. Mar. Syst.* 85, 1–10. <https://doi.org/10.1016/j.jmarsys.2010.10.003>
- Hallegraeff, G.M., 2010. Ocean climate change, phytoplankton community responses, and harmful algal blooms: a formidable predictive challenge. *J. Phycol.* 46, 220–235. <https://doi.org/10.1111/j.1529-8817.2010.00815.x>
- Hallegraeff, G.M., Anderson, D.M., Belin, C., Bottein, M.-Y.D., Bresnan, E., Chinain, M., Enevoldsen, H., Iwataki, M., Karlson, B., McKenzie, C.H., Sunesen, I., Pitcher, G.C., Provoost, P., Richardson, A., Schweibold, L., Tester, P.A., Trainer, V.L., Yñiguez, A.T., Zingone, A., 2021. Perceived global increase in algal blooms is attributable to intensified monitoring and emerging bloom impacts. *Commun. Earth Environ.* 2, 1–10. <https://doi.org/10.1038/s43247-021-00178-8>
- Halsey, K.H., Jones, B.M., 2015. Phytoplankton strategies for photosynthetic energy allocation. *Annu. Rev. Mar. Sci.* 7, 265–297. <https://doi.org/10.1146/annurev-marine-010814-015813>

- Hammer, A., Grüttner, C., Schumann, R., 2001. New biocompatible tracer particles: use for estimation of microzooplankton grazing, digestion, and growth rates. *Aquat. Microb. Ecol.* 24, 153–161. <https://doi.org/10.3354/ame024153>
- Hansen, P.J., 2011. The role of photosynthesis and food uptake for the growth of marine mixotrophic dinoflagellates. *J. Eukaryot. Microbiol.* 58, 203–214. <https://doi.org/10.1111/j.1550-7408.2011.00537.x>
- Hansen, P.J., Hjorth, M., 2002. Growth and grazing responses of *Chrysochromulina ericina* (Prymnesiophyceae): the role of irradiance, prey concentration and pH. *Mar. Biol.* 141, 975–983. <https://doi.org/10.1007/s00227-002-0879-5>
- Hardin, G., 1960. The competitive exclusion principle. *Science* 131, 1292–1297.
- Harley, C.D.G., Randall Hughes, A., Hultgren, K.M., Miner, B.G., Sorte, C.J.B., Thornber, C.S., Rodriguez, L.F., Tomanek, L., Williams, S.L., 2006. The impacts of climate change in coastal marine systems. *Ecol. Lett.* 9, 228–241. <https://doi.org/10.1111/j.1461-0248.2005.00871.x>
- Harrison, P.J., Thompson, P.A., Calderwood, G.S., 1990. Effects of nutrient and light limitation on the biochemical composition of phytoplankton. *J. Appl. Phycol.* 2, 45–56. <https://doi.org/10.1007/BF02179768>
- Harvey, J.B.J., Ryan, J.P., Zhang, Y., 2021. Influences of extreme upwelling on a coastal retention zone. *Front. Mar. Sci.* 8, 648944. <https://doi.org/10.3389/fmars.2021.648944>
- Hauschildt, J., Thomsen, S., Echevin, V., Oeschies, A., José, Y.S., Krahnemann, G., Bristow, L.A., Lavik, G., 2021. The fate of upwelled nitrate off Peru shaped by submesoscale filaments and fronts. *Biogeosciences* 18, 3605–3629. <https://doi.org/10.5194/bg-18-3605-2021>
- Heaney, S.I., Eppley, R.W., 1981. Light, temperature and nitrogen as interacting factors affecting diel vertical migrations of dinoflagellates in culture. *J. Plankton Res.* 3, 331–344. <https://doi.org/10.1093/plankt/3.2.331>
- Hebbali, A., 2020. *olsrr*: Tools for building ols regression models. R package version 0.5.3. <https://CRAN.R-project.org/package=olsrr>
- Hecky, R.E., Kilham, P., 1988. Nutrient limitation of phytoplankton in freshwater and marine environments: a review of recent evidence on the effects of enrichment. *Limnol. Oceanogr.* 33, 796–822. <https://doi.org/10.4319/lo.1988.33.4part2.0796>
- Hehenberger, E., James, E.R., del Campo, J., Buckland-Nicks, J.A., Reimchen, T.E., Keeling, P.J., 2018. Fish parasite dinoflagellates *Haidadinium ichthyophilum* and *Piscinoodinium* share a recent common ancestor. *J. Eukaryot. Microbiol.* 65, 127–131. <https://doi.org/10.1111/jeu.12430>
- Heinze, C., Blenckner, T., Martins, H., Rusiecka, D., Döscher, R., Gehlen, M., Gruber, N., Holland, E., Hov, Ø., Joos, F., Matthews, J.B.R., Rødven, R., Wilson, S., 2021. The quiet crossing of ocean tipping points. *Proc. Natl. Acad. Sci.* 118, e2008478118. <https://doi.org/10.1073/pnas.2008478118>
- Heinze, C., Meyer, S., Goris, N., Anderson, L., Steinfeldt, R., Chang, N., Le Quéré, C., Bakker, D.C.E., 2015. The ocean carbon sink – impacts, vulnerabilities and challenges. *Earth Syst. Dyn.* 6, 327–358. <https://doi.org/10.5194/esd-6-327-2015>
- Hernández-Hernández, N., Arístegui, J., Montero, M.F., Velasco-Senovilla, E., Baltar, F., Marrero-Díaz, Á., Martínez-Marrero, A., Rodríguez-Santana, Á., 2020. Drivers of

- plankton distribution across mesoscale eddies at submesoscale range. *Front. Mar. Sci.* 7, 667. <https://doi.org/10.3389/fmars.2020.00667>
- Hernández-Hernández, N., Bach, L.T., Montero, M.F., Taucher, J., Baños, I., Guan, W., Espósito, M., Ludwig, A., Achterberg, E.P., Riebesell, U., Arístegui, J., 2018. High CO₂ under nutrient fertilization increases primary production and biomass in subtropical phytoplankton communities: a mesocosm approach. *Front. Mar. Sci.* 5, 213. <https://doi.org/10.3389/fmars.2018.00213>
- Hewitt, H.T., Bell, M.J., Chassignet, E.P., Czaja, A., Ferreira, D., Griffies, S.M., Hyder, P., McClean, J.L., New, A.L., Roberts, M.J., 2017. Will high-resolution global ocean models benefit coupled predictions on short-range to climate timescales? *Ocean Model.* 120, 120–136. <https://doi.org/10.1016/j.ocemod.2017.11.002>
- Hewitt, H.T., Roberts, M., Mathiot, P., Biastoch, A., Blockley, E., Chassignet, E.P., Fox-Kemper, B., Hyder, P., Marshall, D.P., Popova, E., Treguier, A.-M., Zanna, L., Yool, A., Yu, Y., Beadling, R., Bell, M., Kuhlbrodt, T., Arsouze, T., Bellucci, A., Castruccio, F., Gan, B., Putrasahan, D., Roberts, C.D., Van Roekel, L., Zhang, Q., 2020. Resolving and parameterising the ocean mesoscale in earth system models. *Curr. Clim. Change Rep.* 6, 137–152. <https://doi.org/10.1007/s40641-020-00164-w>
- Higgins, H.W., Wright, S., Schluter, L., 2011. Quantitative interpretation of chemotaxonomic pigment data. in: *Phytoplankton pigments: characterization, chemotaxonomy and applications in oceanography*. Cambridge University Press, New York 257–313. doi: 10.1017/cbo9780511732263.010
- Hofer, U., 2018. Climate change boosts cyanobacteria. *Nat. Rev. Microbiol.* 16, 122–123. <https://doi.org/10.1038/nrmicro.2018.15>
- Hollibaugh, J.T., Azam, F., 1983. Microbial degradation of dissolved proteins in seawater. *Limnol. Oceanogr.* 28, 1104–1116. <https://doi.org/10.4319/lo.1983.28.6.1104>
- Hopkinson, C.S., 1985. Nitrogen in the marine environment. *Estuaries* 8, 76–77. <https://doi.org/10.2307/1352124>
- Hormazabal, S., Shaffer, G., Letelier, J., Ulloa, O., 2001. Local and remote forcing of sea surface temperature in the coastal upwelling system off Chile. *J. Geophys. Res. Oceans* 106, 16657–16671. <https://doi.org/10.1029/2001JC900008>
- Horton, B.P., Rahmstorf, S., Engelhart, S.E., Kemp, A.C., 2014. Expert assessment of sea-level rise by AD 2100 and AD 2300. *Quat. Sci. Rev.* 84, 1–6. <https://doi.org/10.1016/j.quascirev.2013.11.002>
- Hu, S.K., Connell, P.E., Mesrop, L.Y., Caron, D.A., 2018. A hard day’s night: diel shifts in microbial eukaryotic activity in the North Pacific subtropical gyre. *Front. Mar. Sci.* 5, 351. <https://doi.org/10.3389/fmars.2018.00351>
- Huang, C., Zeng, L., Wang, D., Wang, Q., Wang, P., Zu, T., 2023. Submesoscale eddies in eastern Guangdong identified using high-frequency radar observations. *Deep Sea Res. Part II Top. Stud. Oceanogr.* 207, 105220. <https://doi.org/10.1016/j.dsr2.2022.105220>
- Huisman, J., 2010. Comment on “patterns of diversity in marine phytoplankton.” *Science* 329, 512–512. <https://doi.org/10.1126/science.1189880>
- Huisman, J., Jonker, R.R., Zonneveld, C., Weissing, F.J., 1999. Competition for light between phytoplankton species: experimental tests of mechanistic theory. *Ecology* 80, 211–222. [https://doi.org/10.1890/0012-9658\(1999\)080\[0211:CFLBPS\]2.0.CO;2](https://doi.org/10.1890/0012-9658(1999)080[0211:CFLBPS]2.0.CO;2)

- Huston, M., 1979. A general hypothesis of species diversity. *Am. Nat.* 113, 81–101. <https://doi.org/10.1086/283366>
- Hutchinson, G.E., 1961. The paradox of the plankton. *Am. Nat.* 95, 137–145.
- Ibarbalz, F.M., Henry, N., Brandão, M.C., Martini, S., Busseni, G., Byrne, H., Coelho, L.P., Endo, H., Gasol, J.M., Gregory, A.C., Mahé, F., Rigonato, J., Royo-Llonch, M., Salazar, G., Sanz-Sáez, I., Scalco, E., Soviadan, D., Zayed, A.A., Zingone, A., Labadie, K., Ferland, J., Marec, C., Kandels, S., Picheral, M., Dimier, C., Poulain, J., Pisarev, S., Carmichael, M., Pesant, S., Babin, M., Boss, E., Iudicone, D., Jaillon, O., Acinas, S.G., Ogata, H., Pelletier, E., Stemann, L., Sullivan, M.B., Sunagawa, S., Bopp, L., de Vargas, C., Karp-Boss, L., Wincker, P., Lombard, F., Bowler, C., Zinger, L., 2019. Global trends in marine plankton diversity across kingdoms of life. *Cell* 179, 1084–1097. <https://doi.org/10.1016/j.cell.2019.10.008>
- Igarza, M., Dittmar, T., Graco, M., Niggemann, J., 2019. Dissolved organic matter cycling in the coastal upwelling system off central Peru during an “El Niño” year. *Front. Mar. Sci.* 6, 198. <https://doi.org/10.3389/fmars.2019.00198>
- Illig, S., Dewitte, B., Goubanova, K., Cambon, G., Boucharel, J., Monetti, F., Romero, C., Purca, S., Flores, R., 2014. Forcing mechanisms of intraseasonal SST variability off central Peru in 2000–2008. *J. Geophys. Res. Oceans* 119, 3548–3573. <https://doi.org/10.1002/2013JC009779>
- Irwin, A.J., Finkel, Z.V., 2008. Mining a sea of data: deducing the environmental controls of ocean chlorophyll. *PLoS One* 3, e3836. <https://doi.org/10.1371/journal.pone.0003836>
- Isao, K., Hara, S., Terauchi, K., Kogure, K., 1990. Role of sub-micrometre particles in the ocean. *Nature* 345, 242–244. <https://doi.org/10.1038/345242a0>
- Iversen, M.H., 2023. Carbon export in the ocean: a biologist’s perspective. *Annu. Rev. Mar. Sci.* 15, 357–381. <https://doi.org/10.1146/annurev-marine-032122-035153>
- Jagadeesan, L., Kumar, G.S., Rao, D.N., babu, N.S., Srinivas, T.N.R., 2019. Role of eddies in structuring the mesozooplankton composition in coastal waters of the western Bay of Bengal. *Ecol. Indic.* 105, 137–155. <https://doi.org/10.1016/j.ecolind.2019.05.068>
- James, C.C., Barton, A.D., Allen, L.Z., Lampe, R.H., Rabines, A., Schulberg, A., Zheng, H., Goericke, R., Goodwin, K.D., Allen, A.E., 2022. Influence of nutrient supply on plankton microbiome biodiversity and distribution in a coastal upwelling region. *Nat. Commun.* 13, 2448. <https://doi.org/10.1038/s41467-022-30139-4>
- Jezbera, J., Hornák, K., Šimek, K., 2005. Food selection by bacterivorous protists: insight from the analysis of the food vacuole content by means of fluorescence in situ hybridization. *FEMS Microbiol. Ecol.* 52, 351–363. <https://doi.org/10.1016/j.femsec.2004.12.001>
- Ji, R., Edwards, M., Mackas, D.L., Runge, J.A., Thomas, A.C., 2010. Marine plankton phenology and life history in a changing climate: current research and future directions. *J. Plankton Res.* 32, 1355–1368. <https://doi.org/10.1093/plankt/fbq062>
- Jin, X., Gruber, N., Dunne, J.P., Sarmiento, J.L., Armstrong, R.A., 2006. Diagnosing the contribution of phytoplankton functional groups to the production and export of particulate organic carbon, CaCO₃, and opal from global nutrient and alkalinity distributions. *Glob. Biogeochem. Cycles* 20. <https://doi.org/10.1029/2005GB002532>
- John, U., Šupraha, L., Gran-Stadniczeňko, S., Bunse, C., Cembella, A., Eikrem, W., Janouškovec, J., Klemm, K., Kühne, N., Naustvoll, L., Voss, D., Wohlrab, S., Edvardsen, B., 2022. Spatial and biological oceanographic insights into the massive

- fish-killing bloom of the haptophyte *Chrysochromulina leadbeateri* in northern Norway. *Harmful Algae* 118, 102287. <https://doi.org/10.1016/j.hal.2022.102287>
- Kaladharan, P., Veena, S., Vivekanandan, E., 2009. Carbon sequestration by a few marine algae: observation and projection. *J. Mar. Biol. Assoc. India* 51, 107–110.
- Kapuscinski, J., 1995. DAPI: a DNA-specific fluorescent probe. *Biotech. Histochem. Off. Publ. Biol. Stain Comm.* 70, 220–233. <https://doi.org/10.3109/10520299509108199>
- Karner, M.B., DeLong, E.F., Karl, D.M., 2001. Archaeal dominance in the mesopelagic zone of the Pacific Ocean. *Nature* 409, 507–510. <https://doi.org/10.1038/35054051>
- Karstensen, J., Schütte, F., Pietri, A., Krahnemann, G., Fiedler, B., Grundle, D., Hauss, H., Körtzinger, A., Löscher, C.R., Testor, P., Vieira, N., Visbeck, M., 2017. Upwelling and isolation in oxygen-depleted anticyclonic modewater eddies and implications for nitrate cycling. *Biogeosciences* 14, 2167–2181. <https://doi.org/10.5194/bg-14-2167-2017>
- Käse, L., Metfies, K., Neuhaus, S., Boersma, M., Wiltshire, K.H., Kraberg, A.C., 2021. Host-parasitoid associations in marine planktonic time series: can metabarcoding help reveal them? *PLoS One* 16, e0244817. <https://doi.org/10.1371/journal.pone.0244817>
- Kassambara, A., 2020. ggpubr: 'ggplot2' based publication ready plots. R package version 0.4.0. <https://CRAN.R-project.org/package=ggpubr>
- Kassambara, A., 2021. rstatix: pipe-friendly framework for basic statistical tests. R package version 0.7.0. <https://CRAN.R-project.org/package=rstatix>
- Keeling, R.F., Körtzinger, A., Gruber, N., 2010. Ocean deoxygenation in a warming world. *Annu. Rev. Mar. Sci.* 2, 199–229. <https://doi.org/10.1146/annurev.marine.010908.163855>
- Kemp, P.F., Cole, J.J., Sherr, B.F., Sherr, E.B., 1993. *Handbook of methods in aquatic microbial ecology*. CRC Press, Boca Raton, USA.
- Kettle, H., Merchant, C.J., Jeffery, C.D., Filipiak, M.J., Gentemann, C.L., 2009. The impact of diurnal variability in sea surface temperature on the central Atlantic air-sea CO₂ flux. *Atmospheric Chem. Phys.* 9, 529–541. <https://doi.org/10.5194/acp-9-529-2009>
- Kisand, V., Zingel, P., 2000. Dominance of ciliate grazing on bacteria during spring in a shallow eutrophic lake. *Aquat. Microb. Ecol.* 22, 135–142. <https://doi.org/10.3354/ame022135>
- Klawonn, I., Van den Wyngaert, S., Iversen, M.H., Walles, T.J.W., Flintrop, C.M., Cisternas-Novoa, C., Nejtgaard, J.C., Kagami, M., Grossart, H.-P., 2023. Fungal parasitism on diatoms alters formation and bio-physical properties of sinking aggregates. *Commun. Biol.* 6, 1–14. <https://doi.org/10.1038/s42003-023-04453-6>
- Kléparski, L., Beaugrand, G., Kirby, R.R., 2022. How do plankton species coexist in an apparently unstructured environment? *Biol. Lett.* 18, 20220207. <https://doi.org/10.1098/rsbl.2022.0207>
- Klopfer, P.H., 1959. Environmental determinants of faunal diversity. *Am. Nat.* 93, 337–342. <https://doi.org/10.1086/282092>
- Kostianoy, A.G., Belkin, I.M., 1989. A survey of observations on intrathermocline eddies in the world ocean, in: Nihoul, J.C.J., Jamart, B.M. (Eds.), *Elsevier Oceanography Series, Mesoscale/synoptic coherent structures in geophysical turbulence*. Elsevier, pp. 821–841. [https://doi.org/10.1016/S0422-9894\(08\)70223-X](https://doi.org/10.1016/S0422-9894(08)70223-X)
- Krause, J.W., Schulz, I.K., Rowe, K.A., Dobbins, W., Winding, M.H.S., Sejr, M.K., Duarte, C.M., Agustí, S., 2019. Silicic acid limitation drives bloom termination and potential

- carbon sequestration in an Arctic bloom. *Sci. Rep.* 9, 8149. <https://doi.org/10.1038/s41598-019-44587-4>
- Kritzberg, E.S., Cole, J.J., Pace, M.L., Granéli, W., Bade, D.L., 2004. Autochthonous versus allochthonous carbon sources of bacteria: results from whole-lake ^{13}C addition experiments. *Limnol. Oceanogr.* 49, 588–596. <https://doi.org/10.4319/lo.2004.49.2.0588>
- Kurian, J., Colas, F., Capet, X., McWilliams, J.C., Chelton, D.B., 2011. Eddy properties in the California Current System. *J. Geophys. Res. Oceans* 116. <https://doi.org/10.1029/2010JC006895>
- Lamont, T., Barlow, R., 2017. Contrasting hydrography and phytoplankton distribution in the upper layers of cyclonic eddies in the Mozambique Basin and Mozambique Channel. *Afr. J. Mar. Sci.* 39, 293–306. <https://doi.org/10.2989/1814232X.2017.1367722>
- Landry, M.R., Brown, S.L., Rii, Y.M., Selph, K.E., Bidigare, R.R., Yang, E.J., Simmons, M.P., 2008. Depth-stratified phytoplankton dynamics in Cyclone Opal, a subtropical mesoscale eddy. *Deep Sea Res. Part II Top. Stud. Oceanogr.* 55, 1348–1359. <https://doi.org/10.1016/j.dsr2.2008.02.001>
- Landry, M.R., Constantinou, J., Latasa, M., Brown, S.L., Bidigare, R.R., Ondrusek, M.E., 2000. Biological response to iron fertilization in the eastern equatorial Pacific (IronEx II). III. Dynamics of phytoplankton growth and microzooplankton grazing. *Mar. Ecol. Prog. Ser.* 201, 57–72. <https://doi.org/10.3354/meps201057>
- Landry, M.R., Hassett, R.P., 1982. Estimating the grazing impact of marine micro-zooplankton. *Mar. Biol.* 67, 283–288. <https://doi.org/10.1007/BF00397668>
- Le Quéré, C., Buitenhuis, E.T., Moriarty, R., Alvain, S., Aumont, O., Bopp, L., Chollet, S., Enright, C., Franklin, D.J., Geider, R.J., Harrison, S.P., Hirst, A.G., Larsen, S., Legendre, L., Platt, T., Prentice, I.C., Rivkin, R.B., Salliey, S., Sathyendranath, S., Stephens, N., Vogt, M., Vallina, S.M., 2016. Role of zooplankton dynamics for Southern Ocean phytoplankton biomass and global biogeochemical cycles. *Biogeosciences* 13, 4111–4133. <https://doi.org/10.5194/bg-13-4111-2016>
- Le Vu, B., Stegner, A., Arsouze, T., 2018. Angular Momentum Eddy Detection and Tracking Algorithm (AMEDA) and its application to coastal eddy formation. *J. Atmospheric Ocean. Technol.* 35, 739–762. <https://doi.org/10.1175/JTECH-D-17-0010.1>
- Leach, H., Strass, V., 2019. Cyclonic eddies and upper thermocline fine-scale structures in the Antarctic Circumpolar Current. *Ocean Dyn.* 69, 157–173. <https://doi.org/10.1007/s10236-018-1241-x>
- Lee, H., Calvin, K., Dasgupta, D., Krinner, G., Mukherji, A., Thorne, P., 2023. Synthesis report of the IPCC sixth assessment report (AR6). Intergovernmental Panel on Climate Change, Geneva, Switzerland.
- Lee, S., Fuhrman, J. A., 1987. Relationships between biovolume and biomass of naturally derived marine bacterioplankton. *Appl. Environ. Microbiol.* 53(6), 1298–1303. <https://doi.org/10.1128/aem.53.6.1298-1303.1987>
- Legendre, L., Michaud, J., 1998. Flux of biogenic carbon in oceans: size-dependent regulation by pelagic food webs. *Mar. Ecol. Prog. Ser.* 164, 1–11. <https://doi.org/10.3354/meps164001>
- Legendre, P., Gallagher, E.D., 2001. Ecologically meaningful transformations for ordination of species data. *Oecologia* 129, 271–280. <https://doi.org/10.1007/s004420100716>

- Lévy, M., Jahn, O., Dutkiewicz, S., Follows, M.J., 2014. Phytoplankton diversity and community structure affected by oceanic dispersal and mesoscale turbulence. *Limnol. Oceanogr. Fluids Environ.* 4, 67–84. <https://doi.org/10.1215/21573689-2768549>
- Lin, L.I.-K., 1989. A concordance correlation coefficient to evaluate reproducibility. *biometrics* 45, 255–268. <https://doi.org/10.2307/2532051>
- Linlin., Y., 2021. ggvenn: draw venn diagram by 'ggplot2'. R package version 0.1.9. <https://CRAN.R-project.org/package=ggvenn>
- Litchman, E., 1998. Population and community responses of phytoplankton to fluctuating light. *Oecologia* 117, 247–257. <https://doi.org/10.1007/s004420050655>
- Little, A.G., Loughland, I., Seebacher, F., 2020. What do warming waters mean for fish physiology and fisheries? *J. Fish Biol.* 97, 328–340. <https://doi.org/10.1111/jfb.14402>
- Liu, F., Yin, K., He, L., Tang, S., Yao, J., 2018. Influence on phytoplankton of different developmental stages of mesoscale eddies off eastern Australia. *J. Sea Res.* 137, 1–8. <https://doi.org/10.1016/j.seares.2018.03.004>
- Liu, S.-S., Sun, L., Wu, Q., Yang, Y.-J., 2017. The responses of cyclonic and anticyclonic eddies to typhoon forcing: the vertical temperature-salinity structure changes associated with the horizontal convergence/divergence. *J. Geophys. Res. Oceans* 122, 4974–4989. <https://doi.org/10.1002/2017JC012814>
- Liu, T., Abernathy, R., Sinha, A., Chen, D., 2019. Quantifying Eulerian Eddy Leakiness in an Idealized Model. *J. Geophys. Res. Oceans* 124, 8869–8886. <https://doi.org/10.1029/2019JC015576>
- Long, A.M., Jurgensen, S.K., Petchel, A.R., Savoie, E.R., Brum, J.R., 2021. Microbial ecology of oxygen minimum zones amidst ocean deoxygenation. *Front. Microbiol.* 12. <https://doi.org/10.3389/fmicb.2021.748961>
- Lopez, P.J., Desclés, J., Allen, A.E., Bowler, C., 2005. Prospects in diatom research. *Curr. Opin. Biotechnol.* 16, 180–186. <https://doi.org/10.1016/j.copbio.2005.02.002>
- López-García, P., Rodríguez-Valera, F., Pedrós-Alió, C., Moreira, D., 2001. Unexpected diversity of small eukaryotes in deep-sea Antarctic plankton. *Nature* 409, 603–607. <https://doi.org/10.1038/35054537>
- Lukeš, J., Flegontova, O., Horák, A., 2015. Diplonemids. *Curr. Biol.* 25, R702–R704. <https://doi.org/10.1016/j.cub.2015.04.052>
- Lynam, C.P., Llope, M., Möllmann, C., Helaouët, P., Bayliss-Brown, G.A., Stenseth, N.C., 2017. Interaction between top-down and bottom-up control in marine food webs. *Proc. Natl. Acad. Sci.* 114, 1952–1957. <https://doi.org/10.1073/pnas.1621037114>
- Lynas, M., Houlton, B.Z., Perry, S., 2021. Greater than 99% consensus on human caused climate change in the peer-reviewed scientific literature. *Environ. Res. Lett.* 16, 114005. <https://doi.org/10.1088/1748-9326/ac2966>
- Mackas, D.L., Peterson, W.T., Ohman, M.D., Lavaniegos, B.E., 2006. Zooplankton anomalies in the California Current system before and during the warm ocean conditions of 2005. *Geophys. Res. Lett.* 33. <https://doi.org/10.1029/2006GL027930>
- Madoni, P., Bassanini, N., 1999. Longitudinal changes in the ciliated protozoa communities along a fluvial system polluted by organic matter. *Eur. J. Protistol.* 35, 391–402. [https://doi.org/10.1016/S0932-4739\(99\)80048-0](https://doi.org/10.1016/S0932-4739(99)80048-0)
- Mahadevan, A., 2014. Eddy effects on biogeochemistry. *Nature* 506, 168–169. <https://doi.org/10.1038/nature13048>

- Maire, E., Grenouillet, G., Brosse, S., Villéger, S., 2015. How many dimensions are needed to accurately assess functional diversity? A pragmatic approach for assessing the quality of functional spaces. *Glob. Ecol. Biogeogr.* 24(6), 728-740. <https://doi.org/10.1111/geb.12299>
- Margalef, R., 1978. Life-forms of phytoplankton as survival alternatives in an unstable environment. *Oceanol. Acta* 1, 493-509.
- Marrasé, C., Lim, E., Caron, D., 1992. Seasonal and daily changes in bacterivory in a coastal plankton community. *Mar. Ecol. Prog. Ser.* 82, 281–289. <https://doi.org/10.3354/meps082281>
- Mars Brisbin, M., Brunner, O.D., Grossmann, M.M., Mitarai, S., 2020. Paired high-throughput, in situ imaging and high-throughput sequencing illuminate acantharian abundance and vertical distribution. *Limnol. Oceanogr.* 65, 2953–2965. <https://doi.org/10.1002/lno.11567>
- Marshall, W.L., Berbee, M.L., 2011. Facing unknowns: living cultures (*Pirum gemmata* gen. nov., sp. nov., and *Abeoforma whisleri*, gen. nov., sp. nov.) from invertebrate digestive tracts represent an undescribed clade within the unicellular opisthokont lineage Ichthyosporia (Mesomycetozoa). *Protist* 162, 33–57. <https://doi.org/10.1016/j.protis.2010.06.002>
- Martin, C.L., Tortell, P.D., 2008. Bicarbonate transport and extracellular carbonic anhydrase in marine diatoms. *Physiol. Plant.* 133, 106–116. <https://doi.org/10.1111/j.1399-3054.2008.01054.x>
- Martin, M., 2011. Cutadapt removes adapter sequences from high-throughput sequencing reads. *EMBnet J* 17, 10–12. <https://doi.org/10.14806/ej.17.1.200>
- Martinez-Varela, A., Cerro-Gálvez, E., Auladell, A., Sharma, S., Moran, M.A., Kiene, R.P., Piña, B., Dachs, J., Vila-Costa, M., 2021. Bacterial responses to background organic pollutants in the northeast subarctic Pacific Ocean. *Environ. Microbiol.* 23, 4532–4546. <https://doi.org/10.1111/1462-2920.15646>
- Masojídek, J., Torzillo, G., Koblížek, M., Kopecký, J., Bernardini, P., Sacchi, A., Komenda, J., 1999. Photoadaptation of two members of the Chlorophyta (*Scenedesmus* and *Chlorella*) in laboratory and outdoor cultures: changes in chlorophyll fluorescence quenching and the xanthophyll cycle. *Planta* 209, 126–135. <https://doi.org/10.1007/s004250050614>
- Mason, N.W.H., de Bello, F., 2013. Functional diversity: a tool for answering challenging ecological questions. *J. Veg. Sci.* 24, 777–780. <https://doi.org/10.1111/jvs.12097>
- Mason, N.W.H., Mouillot, D., Lee, W.G., Wilson, J.B., 2005. Functional richness, functional evenness and functional divergence: the primary components of functional diversity. *Oikos* 111, 112–118. <https://doi.org/10.1111/j.0030-1299.2005.13886.x>
- Massing, J.C., Schukat, A., Auel, H., Auch, D., Kittu, L., Pinedo Arteaga, E.L., Correa Acosta, J., Hagen, W., 2022. Toward a solution of the “peruvian puzzle”: pelagic food-web structure and trophic interactions in the northern Humboldt Current upwelling system off Peru. *Front. Mar. Sci.* 8, 759603. <https://doi.org/10.3389/fmars.2021.759603>
- Masuda, Y., Yamanaka, Y., Smith, S.L., Hirata, T., Nakano, H., Oka, A., Sumata, H., 2021. Photoacclimation by phytoplankton determines the distribution of global subsurface chlorophyll maxima in the ocean. *Commun. Earth Environ.* 2, 1–8. <https://doi.org/10.1038/s43247-021-00201-y>

- McBride, G. B., 2005. A proposal for strength-of-agreement criteria for Lin's concordance correlation coefficient. NIWA client report: HAM2005-062, 45, 307-310.
- McGillicuddy, D.J., 2016. Mechanisms of physical-biological-biogeochemical interaction at the oceanic mesoscale. *Annu. Rev. Mar. Sci.* 8, 125–159. <https://doi.org/10.1146/annurev-marine-010814-015606>
- McGillicuddy, D.J., Robinson, A.R., 1997. Eddy-induced nutrient supply and new production in the Sargasso Sea. *Deep Sea Res. Part Oceanogr. Res. Pap.* 44, 1427–1450. [https://doi.org/10.1016/S0967-0637\(97\)00024-1](https://doi.org/10.1016/S0967-0637(97)00024-1)
- McGillicuddy, D.J., Robinson, A.R., Siegel, D.A., Jannasch, H.W., Johnson, R., Dickey, T.D., McNeil, J., Michaels, A.F., Knap, A.H., 1998. Influence of mesoscale eddies on new production in the Sargasso Sea. *Nature* 394, 263–266. <https://doi.org/10.1038/28367>
- McWilliams, J.C., 1985. Submesoscale, coherent vortices in the ocean. *Rev. Geophys.* 23, 165–182. <https://doi.org/10.1029/RG023i002p00165>
- Mehner, T., Lischke, B., Scharnweber, K., Attermeyer, K., Brothers, S., Gaedke, U., Hilt, S., Brucet, S., 2018. Empirical correspondence between trophic transfer efficiency in freshwater food webs and the slope of their size spectra. *Ecology* 99, 1463–1472. <https://doi.org/10.1002/ecy.2347>
- Menden-Deuer, S., Rowlett, J., 2014. Many ways to stay in the game: individual variability maintains high biodiversity in planktonic microorganisms. *J. R. Soc. Interface* 11, 20140031. <https://doi.org/10.1098/rsif.2014.0031>
- Messié, M., Chavez, F.P., 2015. Seasonal regulation of primary production in eastern boundary upwelling systems. *Prog. Oceanogr.* 134, 1–18. <https://doi.org/10.1016/j.pocean.2014.10.011>
- Messié, M., Ledesma, J., Kolber, D.D., Michisaki, R.P., Foley, D.G., Chavez, F.P., 2009. Potential new production estimates in four eastern boundary upwelling ecosystems. *Prog. Oceanogr., Eastern Boundary Upwelling Ecosystems: Integrative and Comparative Approaches* 83, 151–158. <https://doi.org/10.1016/j.pocean.2009.07.018>
- Michaels, A.F., Silver, M.W., 1988. Primary production, sinking fluxes and the microbial food web. *Deep Sea Res. Part Oceanogr. Res. Pap.* 35, 473–490. [https://doi.org/10.1016/0198-0149\(88\)90126-4](https://doi.org/10.1016/0198-0149(88)90126-4)
- Mills, K.E., Pershing, A.J., Brown, C.J., Chen, Y., Chiang, F.-S., Holland, D.S., Lehuta, S., Nye, J.A., Sun, J.C., Thomas, A.C., Wahle, R.A., 2013. Fisheries management in a changing climate: lessons from the 2012 ocean heat wave in the Northwest Atlantic. *Oceanography* 26, 191–195.
- Min, M.A., Needham, D.M., Sudek, S., Truelove, N.K., Pitz, K.J., Chavez, G.M., Poirier, C., Gardeler, B., von der Esch, E., Ludwig, A., Riebesell, U., Worden, A.Z., Chavez, F.P., 2023. Ecological divergence of a mesocosm in an eastern boundary upwelling system assessed with multi-marker environmental DNA metabarcoding. *Biogeosciences* 20, 1277–1298. <https://doi.org/10.5194/bg-20-1277-2023>
- Mittelstaedt, E., 1991. The ocean boundary along the northwest African coast: circulation and oceanographic properties at the sea surface. *Prog. Oceanogr.* 26, 307–355. [https://doi.org/10.1016/0079-6611\(91\)90011-A](https://doi.org/10.1016/0079-6611(91)90011-A)
- Moal, J., Martin-Jezequel, V., Harris, R.P., Samain, J.F., Poulet, S.A., 1987. Interspecific and intraspecific variability of the chemical-composition of marine-phytoplankton. *Oceanol. Acta* 10, 339–346.

- Mogollón, R., Calil, P.H.R., 2017. On the effects of ENSO on ocean biogeochemistry in the Northern Humboldt Current System (NHCS): a modeling study. *J. Mar. Syst.* 172, 137–159. <https://doi.org/10.1016/j.jmarsys.2017.03.011>
- Moisan, T.A., Rufty, K.M., Moisan, J.R., Linkswiler, M.A., 2017. Satellite observations of phytoplankton functional type spatial distributions, phenology, diversity, and ecotones. *Front. Mar. Sci.* 4, 189. <https://doi.org/10.3389/fmars.2017.00189>
- Mojica, K.D.A., Brussaard, C.P.D., 2020. Significance of viral activity for regulating heterotrophic prokaryote community dynamics along a meridional gradient of stratification in the northeast Atlantic Ocean. *Viruses* 12, 1293. <https://doi.org/10.3390/v12111293>
- Moloney, C.L., Field, J.G., Lucas, M.I., 1991. The size-based dynamics of plankton food webs. II. Simulations of three contrasting southern Benguela food webs. *J. Plankton Res.* 13, 1039–1092. <https://doi.org/10.1093/plankt/13.5.1039>
- Montecino, V., Lange, C.B., 2009. The Humboldt Current System: ecosystem components and processes, fisheries, and sediment studies. *Prog. Oceanogr.*, 83, 65–79. <https://doi.org/10.1016/j.pocean.2009.07.041>
- Montero, P., Daneri, G., Cuevas, L.A., González, H.E., Jacob, B., Lizárraga, L., Menschel, E., 2007. Productivity cycles in the coastal upwelling area off Concepción: the importance of diatoms and bacterioplankton in the organic carbon flux. *Prog. Oceanogr.*, 75, 518–530. <https://doi.org/10.1016/j.pocean.2007.08.013>
- Montesor, M., Procaccini, G., Stoecker, D.K., 1999. *Polarella Glacialis*, gen. nov., sp. nov. (Dinophyceae): Suessiaceae are still alive! *J. Phycol.* 35, 186–197. <https://doi.org/10.1046/j.1529-8817.1999.3510186.x>
- Moon-van der Staay, S.Y., De Wachter, R., Vaultot, D., 2001. Oceanic 18S rDNA sequences from picoplankton reveal unsuspected eukaryotic diversity. *Nature* 409, 607–610. <https://doi.org/10.1038/35054541>
- Moore, C.M., Mills, M.M., Arrigo, K.R., Berman-Frank, I., Bopp, L., Boyd, P.W., Galbraith, E.D., Geider, R.J., Guieu, C., Jaccard, S.L., Jickells, T.D., La Roche, J., Lenton, T.M., Mahowald, N.M., Marañón, E., Marinov, I., Moore, J.K., Nakatsuka, T., Oschlies, A., Saito, M.A., Thingstad, T.F., Tsuda, A., Ulloa, O., 2013. Processes and patterns of oceanic nutrient limitation. *Nat. Geosci.* 6, 701–710. <https://doi.org/10.1038/ngeo1765>
- More, K.D., Orsi, W.D., Galy, V., Giosan, L., He, L., Grice, K., Coolen, M.J.L., 2018. A 43 kyr record of protist communities and their response to oxygen minimum zone variability in the Northeastern Arabian Sea. *Earth Planet. Sci. Lett.* 496, 248–256. <https://doi.org/10.1016/j.epsl.2018.05.045>
- Morel, F.M.M., Rueter, J.G., Price, N.M., 1991. Iron nutrition of phytoplankton and its possible importance in the ecology of ocean regions with high nutrient and low biomass. *Oceanography* 4, 56–61.
- Morris, A.W., Riley, J.P., 1963. The determination of nitrate in sea water. *Anal. Chim. Acta* 29, 272–279. [https://doi.org/10.1016/S0003-2670\(00\)88614-6](https://doi.org/10.1016/S0003-2670(00)88614-6)
- Mouquet, N., Loreau, M., 2003. Community patterns in source-sink metacommunities. *Am. Nat.* 162, 544–557. <https://doi.org/10.1086/378857>
- Moutzouris-Sidiris, I., Topouzelis, K., 2021. Assessment of chlorophyll-a concentration from Sentinel-3 satellite images at the Mediterranean Sea using CMEMS open source in situ data. *Open Geosci.* 13, 85–97. <https://doi.org/10.1515/geo-2020-0204>

- Mullin, J.B., Riley, J.P., 1955. The colorimetric determination of silicate with special reference to sea and natural waters. *Anal. Chim. Acta* 12, 162–176. [https://doi.org/10.1016/S0003-2670\(00\)87825-3](https://doi.org/10.1016/S0003-2670(00)87825-3)
- Murphy, J., Riley, J.P., 1962. A modified single solution method for the determination of phosphate in natural waters. *Anal. Chim. Acta* 27, 31–36. [https://doi.org/10.1016/S0003-2670\(00\)88444-5](https://doi.org/10.1016/S0003-2670(00)88444-5)
- Naeem, S., 1998. Species redundancy and ecosystem reliability. *Conserv. Biol.* 12, 39–45. <https://doi.org/10.1111/j.1523-1739.1998.96379.x>
- Nagarkar, M., Palenik, B., 2023. Diversity and putative interactions of parasitic alveolates belonging to Syndiniales at a coastal Pacific site. *Environ. Microbiol. Rep.* 15, 157–169. <https://doi.org/10.1111/1758-2229.13138>
- Needham, D.M., Sachdeva, R., Fuhrman, J.A., 2017. Ecological dynamics and co-occurrence among marine phytoplankton, bacteria and myoviruses shows microdiversity matters. *ISME J.* 11, 1614–1629. <https://doi.org/10.1038/ismej.2017.29>
- Nejstgaard, J.C., Tang, K.W., Steinke, M., Dutz, J., Koski, M., Antajan, E., Long, J.D., 2007. Zooplankton grazing on Phaeocystis: a quantitative review and future challenges. *Biogeochemistry* 83, 147–172. <https://doi.org/10.1007/s10533-007-9098-y>
- Not, F., Latasa, M., Scharek, R., Viprey, M., Karleskind, P., Balagué, V., Ontoria-Oviedo, I., Cumino, A., Goetze, E., Vaultot, D., Massana, R., 2008. Protistan assemblages across the Indian Ocean, with a specific emphasis on the picoeukaryotes. *Deep Sea Res. Part Oceanogr. Res. Pap.* 55, 1456–1473. <https://doi.org/10.1016/j.dsr.2008.06.007>
- Nwankwegu, A.S., Li, Y., Huang, Y., Wei, J., Norgbey, E., Sarpong, L., Lai, Q., Wang, K., 2019. Harmful algal blooms under changing climate and constantly increasing anthropogenic actions: the review of management implications. *3 Biotech* 9, 449. <https://doi.org/10.1007/s13205-019-1976-1>
- Oikonomou, A., Filker, S., Breiner, H.-W., Stoeck, T., 2015. Protistan diversity in a permanently stratified meromictic lake (Lake Alutsee, SW Germany). *Environ. Microbiol.* 17, 2144–2157. <https://doi.org/10.1111/1462-2920.12666>
- Oksanen, J., Simpson, G.L., Blanchet, F.G., Kindt, R., Legendre, P., Minchin, P.R., O'Hara, R.B., Solymos, P., Stevens, M.H.H., Szoecs, E., Wagner, H., Barbour, M., Bedward, M., Bolker, B., Borcard, D., Carvalho, G., Chirico, M., Caceres, M.D., Durand, S., Evangelista, H.B.A., FitzJohn, R., Friendly, M., Furneaux, B., Hannigan, G., Hill, M.O., Lahti, L., McGlenn, D., Ouellette, M.-H., Cunha, E.R., Smith, T., Stier, A., Braak, C.J.F.T., Weedon, J., 2022. *vegan: community ecology package*.
- Orsi, W., Song, Y.C., Hallam, S., Edgcomb, V., 2012. Effect of oxygen minimum zone formation on communities of marine protists. *ISME J.* 6, 1586–1601. <https://doi.org/10.1038/ismej.2012.7>
- Ortiz, J., Arístegui, J., Hernández-Hernández, N., Fernández-Méndez, M., Riebesell, U., 2022a. Oligotrophic phytoplankton community effectively adjusts to artificial upwelling regardless of intensity, but differently among upwelling modes. *Front. Mar. Sci.* 9, 880550. <https://doi.org/10.3389/fmars.2022.880550>
- Ortiz, J., Arístegui, J., Taucher, J., Riebesell, U., 2022b. Artificial upwelling in singular and recurring mode: consequences for net community production and metabolic balance. *Front. Mar. Sci.* 8, 743105. <https://doi.org/10.3389/fmars.2021.743105>

- Owen, R.W., 1980. Eddies of the California current system: physical and ecological characteristics. In: The California Islands: proceedings of a multidisciplinary symposium, Power DM (ed.). Santa Barbara Museum of Natural History: Santa Barbara, CA; 237–263.
- Oyarzún, D., Brierley, C.M., 2019. The future of coastal upwelling in the Humboldt current from model projections. *Clim. Dyn.* 52, 599–615. <https://doi.org/10.1007/s00382-018-4158-7>
- Pace, M., Bailiff, M., 1987. Evaluation of a fluorescent microsphere technique for measuring grazing rates of phagotrophic microorganisms. *Mar. Ecol. Prog. Ser.* 40, 185–193. <https://doi.org/10.3354/meps040185>
- Paerl, H.W., Gardner, W.S., Havens, K.E., Joyner, A.R., McCarthy, M.J., Newell, S.E., Qin, B., Scott, J.T., 2016. Mitigating cyanobacterial harmful algal blooms in aquatic ecosystems impacted by climate change and anthropogenic nutrients. *Harmful Algae* 54, 213–222. <https://doi.org/10.1016/j.hal.2015.09.009>
- Papanikolopoulou, L.A., Smeti, E., Roelke, D.L., Dimitrakopoulos, P.G., Kokkoris, G.D., Danielidis, D.B., Spatharis, S., 2018. Interplay between r- and k-strategists leads to phytoplankton underyielding under pulsed resource supply. *Oecologia* 186, 755–764. <https://doi.org/10.1007/s00442-017-4050-x>
- Parsons, T.R., Takahashi, M., Hargrave, B., 2013. *Biological Oceanographic Processes*. Elsevier, Amsterdam.
- Paterson, E., Gebbing, T., Abel, C., Sim, A., Telfer, G., 2007. Rhizodeposition shapes rhizosphere microbial community structure in organic soil. *New Phytol.* 173, 600–610. <https://doi.org/10.1111/j.1469-8137.2006.01931.x>
- Pauly, D., Christensen, V., 1995. Primary production required to sustain global fisheries. *Nature* 374, 255–257. <https://doi.org/10.1038/374255a0>
- Peacock, M.B., Kudela, R.M., 2014. Evidence for active vertical migration by two dinoflagellates experiencing iron, nitrogen, and phosphorus limitation. *Limnol. Oceanogr.* 59, 660–673. <https://doi.org/10.4319/lo.2014.59.3.0660>
- Peck, M.A., Alheit, J., Bertrand, A., Catalán, I.A., Garrido, S., Moyano, M., Rykaczewski, R.R., Takasuka, A., van der Lingen, C.D., 2021. Small pelagic fish in the new millennium: a bottom-up view of global research effort. *Prog. Oceanogr.* 191, 102494. <https://doi.org/10.1016/j.pocean.2020.102494>
- Pegliasco, C., Chaigneau, A., Morrow, R., 2015. Main eddy vertical structures observed in the four major eastern boundary upwelling systems. *J. Geophys. Res. Oceans* 120, 6008–6033. <https://doi.org/10.1002/2015JC010950>
- Peperzak, L., Duin, R.N.M., Colijn, F., Gieskes, W.W.C., 2000. Growth and mortality of flagellates and non-flagellate cells of *Phaeocystis globosa* (Prymnesiophyceae). *J. Plankton Res.* 22, 107–120. <https://doi.org/10.1093/plankt/22.1.107>
- Pernice, M.C., Forn, I., Gomes, A., Lara, E., Alonso-Sáez, L., Arrieta, J.M., del Carmen Garcia, F., Hernando-Morales, V., MacKenzie, R., Mestre, M., Sintés, E., Teira, E., Valencia, J., Varela, M.M., Vaqué, D., Duarte, C.M., Gasol, J.M., Massana, R., 2015. Global abundance of planktonic heterotrophic protists in the deep ocean. *ISME J.* 9, 782–792. <https://doi.org/10.1038/ismej.2014.168>
- Pernice, M.C., Giner, C.R., Logares, R., Perera-Bel, J., Acinas, S.G., Duarte, C.M., Gasol, J.M., Massana, R., 2016. Large variability of bathypelagic microbial eukaryotic communities

- across the world's oceans. *ISME J.* 10, 945–958. <https://doi.org/10.1038/ismej.2015.170>
- Petchey, O.L., McPhearson, P.T., Casey, T.M., Morin, P.J., 1999. Environmental warming alters food-web structure and ecosystem function. *Nature* 402, 69–72. <https://doi.org/10.1038/47023>
- Peterson, T.D., Crawford, D.W., Harrison, P.J., 2011. Mixing and biological production at eddy margins in the eastern Gulf of Alaska. *Deep Sea Res. Part Oceanogr. Res. Pap.* 58, 377–389. <https://doi.org/10.1016/j.dsr.2011.01.010>
- Pianka, E.R., 1966. Latitudinal gradients in species diversity: a review of concepts. *Am. Nat.* 100, 33–46. <https://doi.org/10.1086/282398>
- Pinardi, N., Zavatarelli, M., Adani, M., Coppini, G., Fratianni, C., Oddo, P., Simoncelli, S., Tonani, M., Lyubartsev, V., Dobricic, S., Bonaduce, A., 2015. Mediterranean Sea large-scale low-frequency ocean variability and water mass formation rates from 1987 to 2007: a retrospective analysis. *Prog. Oceanogr., Oceanography of the Arctic and North Atlantic Basins* 132, 318–332. <https://doi.org/10.1016/j.pocean.2013.11.003>
- Pitcher, G.C., Figueiras, F.G., Kudela, R.M., Moita, T., Reguera, B., Ruiz-Villareal, M., 2018. Key questions and recent research advances on harmful algal blooms in eastern boundary upwelling systems, in: Glibert, P.M., Berdalet, E., Burford, M.A., Pitcher, G.C., Zhou, M. (Eds.), *Global ecology and oceanography of harmful algal blooms, Ecological Studies*. Springer International Publishing, Cham, pp. 205–227. https://doi.org/10.1007/978-3-319-70069-4_11
- Pitcher, G.C., Jiménez, A.B., Kudela, R.M., Reguera, B., 2017. Harmful algal blooms in eastern boundary upwelling systems: a geohab core research project. *Oceanography* 30, 22–35.
- Poloczanska, E.S., Brown, C.J., Sydeman, W.J., Kiessling, W., Schoeman, D.S., Moore, P.J., Brander, K., Bruno, J.F., Buckley, L.B., Burrows, M.T., Duarte, C.M., Halpern, B.S., Holding, J., Kappel, C.V., O'Connor, M.I., Pandolfi, J.M., Parmesan, C., Schwing, F., Thompson, S.A., Richardson, A.J., 2013. Global imprint of climate change on marine life. *Nat. Clim. Change* 3, 919–925. <https://doi.org/10.1038/nclimate1958>
- Pomeroy, L.R., 1974. The ocean's food web, a changing paradigm. *BioScience* 24, 499–504. <https://doi.org/10.2307/1296885>
- Pomeroy, L.R., Williams, P.J., Azam, F., Hobbie, J.E., 2007. The Microbial Loop. *Oceanography* 20, 28–33.
- Porter, K.G., Feig, Y.S., 1980. The use of DAPI for identifying and counting aquatic microflora. *Limnol. Oceanogr.* 25, 943–948. <https://doi.org/10.4319/lo.1980.25.5.0943>
- Preston, C.M., Durkin, C.A., Yamahara, K.M., 2020. DNA metabarcoding reveals organisms contributing to particulate matter flux to abyssal depths in the North East Pacific ocean. *Deep Sea Res. Part II Top. Stud. Oceanogr.* 173, 104708. <https://doi.org/10.1016/j.dsr2.2019.104708>
- Price, J.F., Weller, R.A., Schudlich, R.R., 1987. Wind-driven ocean currents and Ekman transport. *Science* 238, 1534–1538. <https://doi.org/10.1126/science.238.4833.1534>
- Proctor, L.M., Fuhrman, J.A., 1990. Viral mortality of marine bacteria and cyanobacteria. *Nature* 343, 60–62. <https://doi.org/10.1038/343060a0>
- Ptacnik, R., Gomes, A., Royer, S.-J., Berger, S.A., Calbet, A., Nejstgaard, J.C., Gasol, J.M., Isari, S., Moorthi, S.D., Ptacnikova, R., Striebel, M., Sazhin, A.F., Tsagaraki, T.M., Zervoudaki, S., Altoja, K., Dimitriou, P.D., Laas, P., Gazihan, A., Martínez, R.A.,

- Schabhüttl, S., Santi, I., Sousoni, D., Pitta, P., 2016. A light-induced shortcut in the planktonic microbial loop. *Sci. Rep.* 6, 29286. <https://doi.org/10.1038/srep29286>
- Rahmstorf, S., Cazenave, A., Church, J.A., Hansen, J.E., Keeling, R.F., Parker, D.E., Somerville, R.C.J., 2007. Recent Climate Observations Compared to Projections. *Science* 316, 709–709. <https://doi.org/10.1126/science.1136843>
- Ramond, P., Siano, R., Sourisseau, M., 2018. Functional traits of marine protists. *SEANOE*. <https://doi.org/10.17882/51662>
- Ramond, P., Siano, R., Schmitt, S., de Vargas, C., Marié, L., Memery, L., Sourisseau, M., 2021. Phytoplankton taxonomic and functional diversity patterns across a coastal tidal front. *Sci. Rep.* 11, 2682. <https://doi.org/10.1038/s41598-021-82071-0>
- Ramond, P., Siano, R., Sourisseau, M., Logares, R., 2023. Assembly processes and functional diversity of marine protists and their rare biosphere. *Environ. Microbiome* 18, 59. <https://doi.org/10.1186/s40793-023-00513-w>
- Ramond, P., Sourisseau, M., Simon, N., Romac, S., Schmitt, S., Rigaut-Jalabert, F., Henry, N., de Vargas, C., Siano, R., 2019. Coupling between taxonomic and functional diversity in protistan coastal communities. *Environ. Microbiol.* 21, 730–749. <https://doi.org/10.1111/1462-2920.14537>
- Rao, C.R., 1995. A review of canonical coordinates and an alternative to correspondence analysis using Hellinger distance. *Questiio Quad. Estad. Sist. Inform. Investig. Oper.* 19, 23–63.
- Redfield, A.C., 1958. The Biological Control of Chemical Factors in the Environment. *Am. Sci.* 46, 230A–221.
- Richardson, A.J., Schoeman, D.S., 2004. Climate impact on plankton ecosystems in the Northeast Atlantic. *Science* 305, 1609–1612. <https://doi.org/10.1126/science.1100958>
- Riebesell, J.F., 1974. Paradox of enrichment in competitive systems. *Ecology* 55, 183–187. <https://doi.org/10.2307/1934634>
- Riebesell, U., Czerny, J., von Bröckel, K., Boxhammer, T., Büdenbender, J., Deckelnick, M., Fischer, M., Hoffmann, D., Krug, S.A., Lentz, U., Ludwig, A., Mucbe, R., Schulz, K.G., 2013. Technical note: a mobile sea-going mesocosm system – new opportunities for ocean change research. *Biogeosciences* 10, 1835–1847. <https://doi.org/10.5194/bg-10-1835-2013>
- Rocke, E., Pachiadaki, M.G., Cobban, A., Kujawinski, E.B., Edgcomb, V.P., 2015. Protist community grazing on prokaryotic prey in deep ocean water masses. *PLoS One* 10, e0124505. <https://doi.org/10.1371/journal.pone.0124505>
- Rodrigues, L.C., Simões, N.R., Bovo-Scamparin, V.M., Jati, S., Santana, N.F., Roberto, M.C., Train, S., 2015. Phytoplankton alpha diversity as an indicator of environmental changes in a neotropical floodplain. *Ecol. Indic.* 48, 334–341. <https://doi.org/10.1016/j.ecolind.2014.08.009>
- Roemmich, D., McGowan, J., 1995. Climatic warming and the decline of zooplankton in the California Current. *Science* 267, 1324–1326. <https://doi.org/10.1126/science.267.5202.1324>
- Romero, O.E., Fischer, G., 2017. Shift in the species composition of the diatom community in the eutrophic Mauritanian coastal upwelling: results from a multi-year sediment trap experiment (2003–2010). *Prog. Oceanogr.* 159, 31–44. <https://doi.org/10.1016/j.pocean.2017.09.010>

- Romero, O.E., Ramondenc, S., 2022. A 17-year time-series of diatom populations' flux and composition in the Mauritanian coastal upwelling. *Front. Mar. Sci.* 9, 1006345. <https://doi.org/10.3389/fmars.2022.1006345>
- Rose, J.M., Caron, D.A., 2007. Does low temperature constrain the growth rates of heterotrophic protists? Evidence and implications for algal blooms in cold waters. *Limnol. Oceanogr.* 52, 886–895. <https://doi.org/10.4319/lo.2007.52.2.0886>
- Rowley, J.J.L., Gleason, F.H., Andreou, D., Marshall, W.L., Lilje, O., Gozlan, R., 2013. Impacts of mesomycetozoean parasites on amphibian and freshwater fish populations. *Fungal Biol. Rev.* 27, 100–111. <https://doi.org/10.1016/j.fbr.2013.09.002>
- Roy, S., Chattopadhyay, J., 2007. Towards a resolution of 'the paradox of the plankton': a brief overview of the proposed mechanisms. *Ecol. Complex.* 4, 26–33. <https://doi.org/10.1016/j.ecocom.2007.02.016>
- Rykaczewski, R.R., Dunne, J.P., 2010. Enhanced nutrient supply to the California Current Ecosystem with global warming and increased stratification in an earth system model. *Geophys. Res. Lett.* 37. <https://doi.org/10.1029/2010GL045019>
- Rykaczewski, R.R., Dunne, J.P., Sydeman, W.J., García-Reyes, M., Black, B.A., Bograd, S.J., 2015. Poleward displacement of coastal upwelling-favorable winds in the ocean's eastern boundary currents through the 21st century. *Geophys. Res. Lett.* 42, 6424–6431. <https://doi.org/10.1002/2015GL064694>
- Ryther, J.H., 1969. Photosynthesis and fish production in the sea. *Science* 166, 72–76. <https://doi.org/10.1126/science.166.3901.72>
- Sakaguchi, M., Murakami, H., Suzuki, T., 2001. Involvement of a 40-kDa glycoprotein in food recognition, prey capture, and induction of phagocytosis in the protozoan *Actinophrys sol*. *Protist* 152, 33–41. <https://doi.org/10.1078/1434-4610-00041>
- Salvatteci, R., Field, D., Gutiérrez, D., Baumgartner, T., Ferreira, V., Ortlieb, L., Sifeddine, A., Grados, D., Bertrand, A., 2018. Multifarious anchovy and sardine regimes in the Humboldt Current System during the last 150 years. *Glob. Change Biol.* 24, 1055–1068. <https://doi.org/10.1111/gcb.13991>
- Sampaio, E., Santos, C., Rosa, I.C., Ferreira, V., Pörtner, H.-O., Duarte, C.M., Levin, L.A., Rosa, R., 2021. Impacts of hypoxic events surpass those of future ocean warming and acidification. *Nat. Ecol. Evol.* 5, 311–321. <https://doi.org/10.1038/s41559-020-01370-3>
- San Martin, E., Irigoien, X., Roger P, H., Urrutia, Â.L.-, Zubkov, M.V., Heywood, J.L., 2006. Variation in the transfer of energy in marine plankton along a productivity gradient in the Atlantic Ocean. *Limnol. Oceanogr.* 51, 2084–2091. <https://doi.org/10.4319/lo.2006.51.5.2084>
- Sanders, R.W., Porter, K.G., Bennett, S.J., 1990. Heterotrophic, autotrophic, and mixotrophic nanoflagellates: seasonal abundances and bacterivory in a eutrophic lake. *Limnol. Oceanogr.* 35, 1821–1832. <https://doi.org/10.4319/lo.1990.35.8.1821>
- Sanford, E., 1999. Regulation of keystone predation by small changes in ocean temperature. *Science* 283, 2095–2097. <https://doi.org/10.1126/science.283.5410.2095>
- Santi, I., Tsiola, A., Dimitriou, P.D., Fodelianakis, S., Kasapidis, P., Papageorgiou, N., Daffonchio, D., Pitta, P., Karakassis, I., 2019. Prokaryotic and eukaryotic microbial community responses to N and P nutrient addition in oligotrophic Mediterranean coastal waters: novel insights from DNA metabarcoding and network analysis. *Mar. Environ. Res.* 150, 104752. <https://doi.org/10.1016/j.marenvres.2019.104752>

- Sarma, V.V.S.S., Jagadeesan, L., Dalabehera, H.B., Rao, D.N., Kumar, G.S., Durgadevi, D.S., Yadav, K., Behera, S., Priya, M.M.R., 2018. Role of eddies on intensity of oxygen minimum zone in the Bay of Bengal. *Cont. Shelf Res.* 168, 48–53. <https://doi.org/10.1016/j.csr.2018.09.008>
- Sarmiento, J.L., Gruber, N., Brzezinski, M.A., Dunne, J.P., 2004. High-latitude controls of thermocline nutrients and low latitude biological productivity. *Nature* 427, 56–60. <https://doi.org/10.1038/nature02127>
- Schmitz, T., Ritter, J., Mueller, S., Felderhoff-Mueser, U., Chew, L.-J., Gallo, V., 2011. Cellular changes underlying hyperoxia-induced delay of white matter development. *J. Neurosci.* 31, 4327–4344. <https://doi.org/10.1523/JNEUROSCI.3942-10.2011>
- Schmoker, C., Hernández-León, S., Calbet, A., 2013. Microzooplankton grazing in the oceans: impacts, data variability, knowledge gaps and future directions. *J. Plankton Res.* 35, 691–706. <https://doi.org/10.1093/plankt/fbt023>
- Schoemann, V., Becquevort, S., Stefels, J., Rousseau, V., Lancelot, C., 2005. *Phaeocystis* blooms in the global ocean and their controlling mechanisms: a review. *J. Sea Res.* 53, 43–66. <https://doi.org/10.1016/j.seares.2004.01.008>
- Schütte, F., Brandt, P., Karstensen, J., 2016. Occurrence and characteristics of mesoscale eddies in the tropical northeastern Atlantic Ocean. *Ocean Sci.* 12, 663–685. <https://doi.org/10.5194/os-12-663-2016>
- Segura, A.M., Calliari, D., Kruk, C., Conde, D., Bonilla, S., Fort, H., 2011. Emergent neutrality drives phytoplankton species coexistence. *Proc. R. Soc. B Biol. Sci.* 278, 2355–2361. <https://doi.org/10.1098/rspb.2010.2464>
- Seitzinger, S.P., Mayorga, E., Bouwman, A.F., Kroeze, C., Beusen, A.H.W., Billen, G., Van Drecht, G., Dumont, E., Fekete, B.M., Garnier, J., Harrison, J.A., 2010. Global river nutrient export: a scenario analysis of past and future trends. *Glob. Biogeochem. Cycles* 24. <https://doi.org/10.1029/2009GB003587>
- Sekerci, Y., Petrovskii, S., 2018. Global warming can lead to depletion of oxygen by disrupting phytoplankton photosynthesis: a mathematical modelling approach. *Geosciences* 8, 201. <https://doi.org/10.3390/geosciences8060201>
- Shannon, C. E., Weaver, W., 1949. *The Mathematical Theory of Communication*, University of Illinois Press, Urbana.
- Sharma, K.V., Sarvalingam, B.K., Marigoudar, S.R., 2021. A review of mesocosm experiments on heavy metals in marine environment and related issues of emerging concerns. *Environ. Sci. Pollut. Res.* 28, 1304–1316. <https://doi.org/10.1007/s11356-020-11121-3>
- Sharoni, S., Halevy, I., 2020. Nutrient ratios in marine particulate organic matter are predicted by the population structure of well-adapted phytoplankton. *Sci. Adv.* 6, eaaw9371. <https://doi.org/10.1126/sciadv.aaw9371>
- Sherr, B.F., Sherr, E.B., Fallon, R.D., 1987. Use of monodispersed, fluorescently labeled bacteria to estimate in situ protozoan bacterivory. *Appl. Environ. Microbiol.* 53, 958–965. <https://doi.org/10.1128/aem.53.5.958-965.1987>
- Sherr, E.B., Sherr, B.F., 2002. Significance of predation by protists in aquatic microbial food webs. *Antonie Van Leeuwenhoek* 81, 293–308.
- Sherr, E.B., Sherr, B.F., 1999. β -Glucosaminidase activity in marine microbes. *FEMS Microbiol. Ecol.* 28, 111–119. <https://doi.org/10.1111/j.1574-6941.1999.tb00566.x>

- Sherr, E.B., Sherr, B.F., 1994. Bacterivory and herbivory: Key roles of phagotrophic protists in pelagic food webs. *Microb. Ecol.* 28, 223–235. <https://doi.org/10.1007/BF00166812>
- Shih, Y., Hung, C., Tuo, S., Shao, H., Chow, C.H., Muller, F.L.L., Cai, Y., 2020. The impact of eddies on nutrient supply, diatom biomass and carbon export in the northern South China Sea. *Front. Earth Sci.* 8, 537332. <https://doi.org/10.3389/feart.2020.537332>
- Siano, R., Alves-de-Souza, C., Foulon, E., Bendif, E.M., Simon, N., Guillou, L., Not, F., 2011. Distribution and host diversity of Amoebozoa parasites across oligotrophic waters of the Mediterranean Sea. *Biogeosciences* 8, 267–278. <https://doi.org/10.5194/bg-8-267-2011>
- Siano, R., Montresor, M., Probert, I., Not, F., de Vargas, C., 2010. *Pelagodinium* gen. nov. and *P. béii* comb. nov., a dinoflagellate symbiont of planktonic Foraminifera. *Protist* 161, 385–399. <https://doi.org/10.1016/j.protis.2010.01.002>
- Sigman, D.M., Hain, M.P., 2012. The biological productivity of the ocean. *Nat. Educ. Knowl.* 3, 1–16.
- Šimek, K., Kojecká, P., Nedoma, J., Hartman, P., Vrba, J., Dolan, J.R., 1999. Shifts in bacterial community composition associated with different microzooplankton size fractions in a eutrophic reservoir. *Limnol. Oceanogr.* 44, 1634–1644. <https://doi.org/10.4319/lo.1999.44.7.1634>
- Singer, D., Seppey, C.V.W., Lentendu, G., Dunthorn, M., Bass, D., Belbahri, L., Blandenier, Q., Debroyas, D., de Groot, G.A., de Vargas, C., Domaizon, I., Duckert, C., Izaguirre, I., Koenig, I., Mataloni, G., Schiaffino, M.R., Mitchell, E.A.D., Geisen, S., Lara, E., 2021. Protist taxonomic and functional diversity in soil, freshwater and marine ecosystems. *Environ. Int.* 146, 106262. <https://doi.org/10.1016/j.envint.2020.106262>
- Smalley, G., Coats, D., Adam, E., 1999. A new method using fluorescent microspheres to determine grazing on ciliates by the mixotrophic dinoflagellate *Ceratium furca*. *Aquat. Microb. Ecol.* 17, 167–179. <https://doi.org/10.3354/ame017167>
- Smayda, T.J., 2000. Ecological features of harmful algal blooms in coastal upwelling ecosystems. *Afr. J. Mar. Sci.* 22.
- Smith Jr, W.O., Carlson, C.A., Ducklow, H.W., Hansell, D.A., 1998. Growth dynamics of *Phaeocystis antarctica*-dominated plankton assemblages from the Ross Sea. *Mar. Ecol. Prog. Ser.* 168, 229–244. <https://doi.org/10.3354/meps168229>
- Smith Jr, W.O., Codispoti, L.A., Nelson, D.M., Manley, T., Buskey, E.J., Niebauer, H.J., Cota, G.F., 1991. Importance of *Phaeocystis* blooms in the high-latitude ocean carbon cycle. *Nature* 352, 514–516. <https://doi.org/10.1038/352514a0>
- Sommer, U., Adrian, R., De Senerpont Domis, L., Elser, J.J., Gaedke, U., Ibelings, B., Jeppesen, E., Lüring, M., Molinero, J.C., Mooij, W.M., van Donk, E., Winder, M., 2012. Beyond the Plankton Ecology Group (PEG) Model: mechanisms driving plankton succession. *Annu. Rev. Ecol. Evol. Syst.* 43, 429–448. <https://doi.org/10.1146/annurev-ecolsys-110411-160251>
- Sooria, P.M., Hatha, A.A.M., Menon, N.N., Saramma, A.V., 2022. Constraints in using relative biomass as a measure of competitive success in phytoplankton – a review. *J. Exp. Mar. Biol. Ecol.* 557, 151819. <https://doi.org/10.1016/j.jembe.2022.151819>
- Spellerberg, I.F., Fedor, P.J., 2003. A tribute to Claude Shannon (1916–2001) and a plea for more rigorous use of species richness, species diversity and the ‘Shannon–Wiener’

- Index. *Glob. Ecol. Biogeogr.* 12, 177–179. <https://doi.org/10.1046/j.1466-822X.2003.00015.x>
- Spinrad, R.W., Glover, H., Ward, B.B., Codispoti, L.A., Kullenberg, G., 1989. Suspended particle and bacterial maxima in Peruvian coastal waters during a cold water anomaly. *Deep Sea Res. Part Oceanogr. Res. Pap.* 36, 715–733. [https://doi.org/10.1016/0198-0149\(89\)90147-7](https://doi.org/10.1016/0198-0149(89)90147-7)
- Spisla, C., Taucher, J., Bach, L.T., Haunost, M., Boxhammer, T., King, A.L., Jenkins, B.D., Wallace, J.R., Ludwig, A., Meyer, J., Stange, P., Minutolo, F., Lohbeck, K.T., Nauendorf, A., Kalter, V., Lischka, S., Sswat, M., Dörner, I., Ismar-Rebitz, S.M.H., Aberle, N., Yong, J.C., Bouquet, J.-M., Lechtenböcker, A.K., Kohnert, P., Krudewig, M., Riebesell, U., 2021. Extreme levels of ocean acidification restructure the plankton community and biogeochemistry of a temperate coastal ecosystem: a mesocosm study. *Front. Mar. Sci.* 7, 611157. <https://doi.org/10.3389/fmars.2020.611157>
- Sswat, M., Bach, L.T., Boxhammer, T., Riebesell, U., 2019. Overview of activities during the KOSMOS mesocosm study 2017 in the coastal upwelling system off Peru. https://doi.org/10.3289/KOSMOS_Peru_2017
- Stefels, J., Dijkhuizen, L., Gieskes, W.W.C., 1995. DMSP-lyase activity in a spring phytoplankton bloom off the Dutch coast, related to *Phaeocystis* sp. abundance. *Mar. Ecol. Prog. Ser.* 123, 235–243.
- Stein, A., Gerstner, K., Kreft, H., 2014. Environmental heterogeneity as a universal driver of species richness across taxa, biomes and spatial scales. *Ecol. Lett.* 17, 866–880. <https://doi.org/10.1111/ele.12277>
- Stibor, H., Stockenreiter, M., Nejstgaard, J.C., Ptacnik, R., Sommer, U., 2019. Trophic switches in pelagic systems. *Curr. Opin. Syst. Biol.*, • Systems biology of model organisms • Systems ecology and evolution 13, 108–114. <https://doi.org/10.1016/j.coisb.2018.11.006>
- Stoeck, T., Bass, D., Nebel, M., Christen, R., Jones, M.D.M., Breiner, H.-W., Richards, T.A., 2010. Multiple marker parallel tag environmental DNA sequencing reveals a highly complex eukaryotic community in marine anoxic water. *Mol. Ecol.* 19 Suppl 1, 21–31. <https://doi.org/10.1111/j.1365-294X.2009.04480.x>
- Stoecker, D.K., 1999. Mixotrophy among dinoflagellates. *J. Eukaryot. Microbiol.* 46, 397–401. <https://doi.org/10.1111/j.1550-7408.1999.tb04619.x>
- Stramma, L., Bange, H.W., Czeschel, R., Lorenzo, A., Frank, M., 2013. On the role of mesoscale eddies for the biological productivity and biogeochemistry in the eastern tropical Pacific Ocean off Peru. *Biogeosciences* 10, 7293–7306. <https://doi.org/10.5194/bg-10-7293-2013>
- Stramma, L., Prince, E.D., Schmidtko, S., Luo, J., Hoolihan, J.P., Visbeck, M., Wallace, D.W.R., Brandt, P., Körtzinger, A., 2012. Expansion of oxygen minimum zones may reduce available habitat for tropical pelagic fishes. *Nat. Clim. Change* 2, 33–37. <https://doi.org/10.1038/nclimate1304>
- Stramma, L., Schmidtko, S., Levin, L.A., Johnson, G.C., 2010. Ocean oxygen minima expansions and their biological impacts. *Deep Sea Res. Part Oceanogr. Res. Pap.* 57, 587–595. <https://doi.org/10.1016/j.dsr.2010.01.005>
- Strickland, J.D.H., Parsons, T.R., 1968. A practical handbook of seawater analysis. *Fish. Res. Bd. Canada Bull.*, 167, 185–194.

- Strom, S., 2000. Bacterivory : interactions between bacteria and their grazers. *Microb. Ecol. Oceans*.
- Studholme, J., Gulev, S., 2018. Concurrent changes to Hadley Circulation and the meridional distribution of tropical cyclones. *J. Clim.* 31, 4367–4389. <https://doi.org/10.1175/JCLI-D-17-0852.1>
- Suleiman, M., Pennekamp, F., Choffat, Y., Petchey, O.L., 2022. Contrasting resistance and resilience to light variation of the coupled oxic and anoxic components of an experimental microbial ecosystem. *Ecol. Evol.* 12, e8793. <https://doi.org/10.1002/ece3.8793>
- Sun, M., Tian, F., Liu, Y., Chen, G., 2017. An improved automatic algorithm for global eddy tracking using satellite altimeter data. *Remote Sens.* 9, 206. <https://doi.org/10.3390/rs9030206>
- Suter, E.A., Pachiadaki, M., Taylor, G.T., Edgcomb, V.P., 2022. Eukaryotic parasites are integral to a productive microbial food web in oxygen-depleted waters. *Front. Microbiol.* 12, 764605. <https://doi.org/10.3389/fmicb.2021.764605>
- Sydeman, W.J., Santora, J.A., Thompson, S.A., Marinovic, B., Lorenzo, E.D., 2013. Increasing variance in North Pacific climate relates to unprecedented ecosystem variability off California. *Glob. Change Biol.* 19, 1662–1675. <https://doi.org/10.1111/gcb.12165>
- Taberlet, P., Bonin, A., Zinger, L., Coissac, E., 2018. *Environmental DNA: for biodiversity research and monitoring*. Oxford University Press, Oxford, London.
- Talmy, D., Blackford, J., Hardman-Mountford, N.J., Dumbrell, A.J., Geider, R.J., 2013. An optimality model of photoadaptation in contrasting aquatic light regimes. *Limnol. Oceanogr.* 58, 1802–1818. <https://doi.org/10.4319/lo.2013.58.5.1802>
- Taucher, J., Bach, L.T., Boxhammer, T., Nauendorf, A., The Gran Canaria KOSMOS Consortium, Achterberg, E.P., Algueró-Muñiz, M., Arístegui, J., Czerny, J., Esposito, M., Guan, W., Haunost, M., Horn, H.G., Ludwig, A., Meyer, J., Spisla, C., Sswat, M., Stange, P., Riebesell, U., 2017. Influence of ocean acidification and deep water upwelling on oligotrophic plankton communities in the subtropical North Atlantic: insights from an in situ mesocosm study. *Front. Mar. Sci.* 4, 85. <https://doi.org/10.3389/fmars.2017.00085>
- Taylor, G.T., Pace, M.L., 1987. Validity of eucaryote inhibitors for assessing production and grazing mortality of marine bacterioplankton. *Appl. Environ. Microbiol.* 53, 119–128. <https://doi.org/10.1128/aem.53.1.119-128.1987>
- Taylor, M.H., Wolff, M., Mendo, J., Yamashiro, C., 2008. Changes in trophic flow structure of Independence Bay (Peru) over an ENSO cycle. *Prog. Oceanogr.* 79, 336–351. <https://doi.org/10.1016/j.pocean.2008.10.006>
- Taylor, N.J., 1985. Silica incorporation in the diatom *Cosinodiscus granii* as affected by light intensity. *Br. Phycol. J.* 20, 365–374. <https://doi.org/10.1080/00071618500650371>
- Team, R.D.C., 2010. R: a Language and environment for statistical computing. <http://www.r-project.org/index.html>
- Telesh, I.V., Schubert, H., Joehnk, K.D., Heerkloss, R., Schumann, R., Feike, M., Schoor, A., Skarlato, S.O., 2019. Chaos theory discloses triggers and drivers of plankton dynamics in stable environment. *Sci. Rep.* 9, 20351. <https://doi.org/10.1038/s41598-019-56851-8>
- Thiel, M., Macaya, E.C., Acuña, E., Bastias, H., Brokordt, K., Cortés, M., Dumont, C.P., Gajardo, J.A., Gaymer, C.F., González, A.E., Haye, P.A., Illanes J.-E., Lancellotti,

- D.A., Luna-Jorquera G., Luxoro, C., Muñoz, P., Perez, E., Sellanes, J., Stotz, W., Tala, F., Vasquez, J.A., Vega J.m.a., Arntz, W.E., Camus, P.A., Castilla, J.C., Fernandez, M., Navarrete, S.A., Castro, L.R., Escribano, R., Gomez, I., González, H.E., Manriquez, P.H., Iriarte, J.L., Marín, V., Poulin, E., Sepúlveda, H.H., Thomas, A., Vargas, C.A., 2007. The Humboldt Current System of northern and central Chile - oceanographic processes, ecological interactions and socioeconomic feedback. *Oceanogr. Mar. Biol.* 45, 195–344.
- Thomas, A.C., Brickley, P., 2006. Satellite measurements of chlorophyll distribution during spring 2005 in the California Current. *Geophys. Res. Lett.* 33. <https://doi.org/10.1029/2006GL026588>
- Thomas, C.D., Gillingham, P.K., 2015. The performance of protected areas for biodiversity under climate change. *Biol. J. Linn. Soc.* 115, 718–730. <https://doi.org/10.1111/bij.12510>
- Thomas, C.D., Gillingham, P.K., Bradbury, R.B., Roy, D.B., Anderson, B.J., Baxter, J.M., Bourn, N.A.D., Crick, H.Q.P., Findon, R.A., Fox, R., Hodgson, J.A., Holt, A.R., Morecroft, M.D., O’Hanlon, N.J., Oliver, T.H., Pearce-Higgins, J.W., Procter, D.A., Thomas, J.A., Walker, K.J., Walmsley, C.A., Wilson, R.J., Hill, J.K., 2012. Protected areas facilitate species’ range expansions. *Proc. Natl. Acad. Sci.* 109, 14063–14068. <https://doi.org/10.1073/pnas.1210251109>
- Thomas, L.N., 2008. Formation of intrathermocline eddies at ocean fronts by wind-driven destruction of potential vorticity. *Dyn. Atmospheres Oceans* 45, 252–273. <https://doi.org/10.1016/j.dynatmoce.2008.02.002>
- Thompson, R.M., Brose, U., Dunne, J.A., Hall, R.O., Hladysz, S., Kitching, R.L., Martinez, N.D., Rantala, H., Romanuk, T.N., Stouffer, D.B., Tylianakis, J.M., 2012. Food webs: reconciling the structure and function of biodiversity. *Trends Ecol. Evol.* 27, 689–697. <https://doi.org/10.1016/j.tree.2012.08.005>
- Thoral, F., Pinkerton, M.H., Tait, L.W., Schiel, D.R., 2023. Spectral light quality on the seabed matters for macroalgal community composition at the extremities of light limitation. *Limnol. Oceanogr.* 68, 902–916. <https://doi.org/10.1002/lno.12318>
- Tilman, D., Kilham, S.S., Kilham, P., 1982. Phytoplankton community ecology: the role of limiting nutrients. *Annu. Rev. Ecol. Syst.* 13, 349–372. <https://doi.org/10.1146/annurev.es.13.110182.002025>
- Tragin, M., Vaultot, D., 2018. Green microalgae in marine coastal waters: the Ocean Sampling Day (OSD) dataset. *Sci. Rep.* 8, 14020. <https://doi.org/10.1038/s41598-018-32338-w>
- Tréguer, P., Bowler, C., Moriceau, B., Dutkiewicz, S., Gehlen, M., Aumont, O., Bittner, L., Dugdale, R., Finkel, Z., Iudicone, D., Jahn, O., Guidi, L., Lasbleiz, M., Leblanc, K., Levy, M., Pondaven, P., 2018. Influence of diatom diversity on the ocean biological carbon pump. *Nat. Geosci.* 11, 27–37. <https://doi.org/10.1038/s41561-017-0028-x>
- Tremaine, S.C., Mills, A.L., 1987. Inadequacy of the eucaryote inhibitor cycloheximide in studies of protozoan grazing on bacteria at the freshwater-sediment interface. *Appl. Environ. Microbiol.* 53, 1969–1972. <https://doi.org/10.1128/aem.53.8.1969-1972.1987>
- Troncoso, V.A., Daneri, G., Cuevas, L.A., Jacob, B., Montero, P., 2003. Bacterial carbon flow in the Humboldt Current System off Chile. *Mar. Ecol. Prog. Ser.* 250, 1–12. <https://doi.org/10.3354/meps250001>

- Tsiola, A., Tsagaraki, T.M., Giannakourou, A., Nikolioudakis, N., Yücel, N., Herut, B., Pitta, P., 2017. Bacterial growth and mortality after deposition of Saharan dust and mixed aerosols in the eastern Mediterranean Sea: a mesocosm experiment. *Front. Mar. Sci.* 3, 281. <https://doi.org/10.3389/fmars.2016.00281>
- Tubay, J.M., Ito, H., Uehara, T., Kakishima, S., Morita, S., Togashi, T., Tainaka, K., Niraula, M.P., Casareto, B.E., Suzuki, Y., Yoshimura, J., 2013. The paradox of enrichment in phytoplankton by induced competitive interactions. *Sci. Rep.* 3, 2835. <https://doi.org/10.1038/srep02835>
- Ullah, H., Nagelkerken, I., Goldenberg, S.U., Fordham, D.A., 2018. Climate change could drive marine food web collapse through altered trophic flows and cyanobacterial proliferation. *PLoS Biol.* 16, e2003446. <https://doi.org/10.1371/journal.pbio.2003446>
- Unrein, F., Gasol, J.M., Not, F., Forn, I., Massana, R., 2014. Mixotrophic haptophytes are key bacterial grazers in oligotrophic coastal waters. *ISME J.* 8, 164–176. <https://doi.org/10.1038/ismej.2013.132>
- Unrein, F., Massana, R., Alonso-Sáez, L., Gasol, J.M., 2007. Significant year-round effect of small mixotrophic flagellates on bacterioplankton in an oligotrophic coastal system. *Limnol. Oceanogr.* 52, 456–469. <https://doi.org/10.4319/lo.2007.52.1.0456>
- Våge, S., Castellani, M., Giske, J., Thingstad, T.F., 2013. Successful strategies in size structured mixotrophic food webs. *Aquat. Ecol.* 47, 329–347. <https://doi.org/10.1007/s10452-013-9447-y>
- Valach, M., Moreira, S., Petitjean, C., Benz, C., Butenko, A., Flegontova, O., Nenarokova, A., Prokopchuk, G., Batstone, T., Lapébie, P., Lemogo, L., Sarrasin, M., Stretenowich, P., Tripathi, P., Yazaki, E., Nara, T., Henrissat, B., Lang, B.F., Gray, M.W., Williams, T.A., Lukeš, J., Burger, G., 2023. Recent expansion of metabolic versatility in *Diplonema papillatum*, the model species of a highly speciose group of marine eukaryotes. *BMC Biol.* 21, 99. <https://doi.org/10.1186/s12915-023-01563-9>
- Vallina, S.M., Follows, M.J., Dutkiewicz, S., Montoya, J.M., Cermeno, P., Loreau, M., 2014. Global relationship between phytoplankton diversity and productivity in the ocean. *Nat. Commun.* 5, 4299. <https://doi.org/10.1038/ncomms5299>
- Van Dam, H., 1982. On the use of measures of structure and diversity in applied diatom ecology. *Hydrobiol. Bull.* 16, 288–288. <https://doi.org/10.1007/BF02255385>
- van der Does, M., Brummer, G.-J.A., van Crimpen, F.C.J., Korte, L.F., Mahowald, N.M., Merkel, U., Yu, H., Zuidema, P., Stuut, J.-B.W., 2020. Tropical rains controlling deposition of Saharan dust across the North Atlantic Ocean. *Geophys. Res. Lett.* 47, e2019GL086867. <https://doi.org/10.1029/2019GL086867>
- van der Jagt, H., Friese, C., Stuut, J.-B.W., Fischer, G., Iversen, M.H., 2018. The ballasting effect of Saharan dust deposition on aggregate dynamics and carbon export: aggregation, settling, and scavenging potential of marine snow. *Limnol. Oceanogr.* 63, 1386–1394. <https://doi.org/10.1002/lno.10779>
- van Gemberden, H., 1974. Coexistence of organisms competing for the same substrate: An example among the purple sulfur bacteria. *Microb. Ecol.* 1, 104–119. <https://doi.org/10.1007/BF02512382>
- van Hilst, C.M., Smith Jr, W.O., 2002. Photosynthesis/irradiance relationships in the Ross Sea, Antarctica, and their control by phytoplankton assemblage composition and

- environmental factors. *Mar. Ecol. Prog. Ser.* 226, 1–12. <https://doi.org/10.3354/meps226001>
- Vanni, M.J., Findlay, D.L., 1990. Trophic cascades and phytoplankton community structure. *Ecology* 71, 921–937. <https://doi.org/10.2307/1937363>
- Varela, R., Rodríguez-Díaz, L., de Castro, M., Gómez-Gesteira, M., 2021. Influence of eastern upwelling systems on marine heatwaves occurrence. *Glob. Planet. Change* 196, 103379. <https://doi.org/10.1016/j.gloplacha.2020.103379>
- Vargas, C.A., González, H.E., 2004. Plankton community structure and carbon cycling in a coastal upwelling system. I. Bacteria, microprotozoans and phytoplankton in the diet of copepods and appendicularians. *Aquat. Microb. Ecol.* 34, 151–164. <https://doi.org/10.3354/ame034151>
- Vargas, C.A., Martínez, R.A., Cuevas, L.A., Pavez, M.A., Cartes, C., González, H.E., Escribano, R., Daneri, G., 2007. The relative importance of microbial and classical food webs in a highly productive coastal upwelling area. *Limnol. Oceanogr.* 52, 1495–1510. <https://doi.org/10.4319/lo.2007.52.4.1495>
- Varon, M., Zeigler, B.P., 1978. Bacterial predator-prey interaction at low prey density. *Appl. Environ. Microbiol.* 36, 11–17. <https://doi.org/10.1128/aem.36.1.11-17.1978>
- Vazquez-Cuervo, J., Torres, H.S., Menemenlis, D., Chin, T., Armstrong, E.M., 2017. Relationship between SST gradients and upwelling off Peru and Chile: model/satellite data analysis. *Int. J. Remote Sens.* 38, 6599–6622. <https://doi.org/10.1080/01431161.2017.1362130>
- Veldhuis, M.J.W., Kraay, G.W., 2000. Application of flow cytometry in marine phytoplankton research: current applications and future perspectives. *Sci. Mar.* 64, 121–134.
- Ventura, A., Simões, E.F.C., Almeida, A.S., Martins, R., Duarte, A.C., Loureiro, S., Duarte, R.M.B.O., 2021. Deposition of aerosols onto upper ocean and their impacts on marine biota. *Atmosphere* 12, 684. <https://doi.org/10.3390/atmos12060684>
- Vergnon, R., van Nes, E.H., Scheffer, M., 2012. Emergent neutrality leads to multimodal species abundance distributions. *Nat. Commun.* 3, 663. <https://doi.org/10.1038/ncomms1663>
- Vihtakari, M., 2022. Plot Data on Oceanographic Maps using ‘ggplot2’. R Package ggOceanMaps Version 1.2.6.
- Visco, J.A., Apothéloz-Perret-Gentil, L., Cordonier, A., Esling, P., Pillet, L., Pawlowski, J., 2015. Environmental monitoring: inferring the diatom index from next-generation sequencing data. *Environ. Sci. Technol.* 49, 7597–7605. <https://doi.org/10.1021/es506158m>
- Vitova, M., Bisova, K., Kawano, S., Zachleder, V., 2015. Accumulation of energy reserves in algae: from cell cycles to biotechnological applications. *Biotechnol. Adv.* 33, 1204–1218. <https://doi.org/10.1016/j.biotechadv.2015.04.012>
- Vrba, J., Šimek, K., Nedoma, J., Hartman, P., 1993. 4-methylumbelliferyl- β -N-acetylglucosaminide hydrolysis by a high-affinity enzyme, a putative marker of protozoan bacterivory. *Appl. Environ. Microbiol.* 59, 3091–3101. <https://doi.org/10.1128/aem.59.9.3091-3101.1993>
- Walker, B.H., 1992. Biodiversity and ecological redundancy. *Conserv. Biol.* 6, 18–23. <https://doi.org/10.1046/j.1523-1739.1992.610018.x>

- Walters, K., Moriarty, D.J.W., 1993. The effects of complex trophic interactions on a marine microbenthic community. *Ecology* 74, 1475–1489. <https://doi.org/10.2307/1940076>
- Wang, G., Cai, W., Gan, B., Wu, L., Santoso, A., Lin, X., Chen, Z., McPhaden, M.J., 2017. Continued increase of extreme El Niño frequency long after 1.5 °C warming stabilization. *Nat. Clim. Change* 7, 568–572. <https://doi.org/10.1038/nclimate3351>
- Wang, L., Ma, X., Chen, J., 2023. Do submerged macrophyte species influence crustacean zooplankton functional group richness and their resource use efficiency in the low-light environment? *Front. Plant Sci.* 14.
- Ward, B.A., Follows, M.J., 2016. Marine mixotrophy increases trophic transfer efficiency, mean organism size, and vertical carbon flux. *Proc. Natl. Acad. Sci.* 113, 2958–2963. <https://doi.org/10.1073/pnas.1517118113>
- Wickham, H., 2016. Programming with ggplot2, in: Wickham, H. (Ed.), *Ggplot2: elegant graphics for data analysis, use R!* Springer International Publishing, Cham, pp. 241–253. https://doi.org/10.1007/978-3-319-24277-4_12
- Wickham, H., Seidel, D., 2020. scales: Scale Functions for Visualization. R package version 1.1.1. <https://CRAN.R-project.org/package=scales>
- Wickham, S.A., Wentz, P., Sinner, A., Weiss, R., 2022. Microzooplankton grazing and community composition in a high-productivity marine ecosystem. *J. Plankton Res.* 44, 414–426. <https://doi.org/10.1093/plankt/fbac015>
- Winter, C., Moeseneder, M.M., Herndl, G.J., Weinbauer, M.G., 2008. Relationship of geographic distance, depth, temperature, and viruses with prokaryotic communities in the eastern tropical Atlantic Ocean. *Microb. Ecol.* 56, 383–389. <https://doi.org/10.1007/s00248-007-9343-x>
- Winton, M., Griffies, S.M., Samuels, B.L., Sarmiento, J.L., Frölicher, T.L., 2013. Connecting changing ocean circulation with changing climate. *J. Clim.* 26, 2268–2278. <https://doi.org/10.1175/JCLI-D-12-00296.1>
- Wootton, E.C., Zubkov, M.V., Jones, D.H., Jones, R.H., Martel, C.M., Thornton, C.A., Roberts, E.C., 2007. Biochemical prey recognition by planktonic protozoa. *Environ. Microbiol.* 9, 216–222. <https://doi.org/10.1111/j.1462-2920.2006.01130.x>
- Worden, A.Z., Follows, M.J., Giovannoni, S.J., Wilken, S., Zimmerman, A.E., Keeling, P.J., 2015. Rethinking the marine carbon cycle: factoring in the multifarious lifestyles of microbes. *Science* 347, 1257594. <https://doi.org/10.1126/science.1257594>
- Wright, R.T., Coffin, R.B., 1984. Measuring microzooplankton grazing on planktonic marine bacteria by its impact on bacterial production. *Microb. Ecol.* 10, 137–149. <https://doi.org/10.1007/BF02011421>
- Wu, C.-R., Chiang, T.-L., 2007. Mesoscale eddies in the northern South China Sea. *Deep Sea Res. Part II Top. Stud. Oceanogr.* 54, 1575–1588. <https://doi.org/10.1016/j.dsr2.2007.05.008>
- Wu, J., Sunda, W., Boyle, E.A., Karl, D.M., 2000. Phosphate depletion in the western North Atlantic Ocean. *Science* 289, 759–762. <https://doi.org/10.1126/science.289.5480.759>
- Wu, P.-F., Li, D.-X., Kong, L.-F., Li, Y.-Y., Zhang, H., Xie, Z.-X., Lin, L., Wang, D.-Z., 2020. The diversity and biogeography of microeukaryotes in the euphotic zone of the northwestern Pacific Ocean. *Sci. Total Environ.* 698, 134289. <https://doi.org/10.1016/j.scitotenv.2019.134289>

- Wyatt, T., 2014. Margalef's mandala and phytoplankton bloom strategies. *Deep Sea Res. Part II Top. Stud. Oceanogr.* 101, 32–49. <https://doi.org/10.1016/j.dsr2.2012.12.006>
- Xiu, P., Chai, F., Curchitser, E.N., Castruccio, F.S., 2018. Future changes in coastal upwelling ecosystems with global warming: the case of the California Current System. *Sci. Rep.* 8, 2866. <https://doi.org/10.1038/s41598-018-21247-7>
- Yamaguchi, R., 2022. Intermediate dispersal hypothesis of species diversity: new insights. *Ecol. Res.* 37, 301–315. <https://doi.org/10.1111/1440-1703.12313>
- Yang, X., Liu, L., Yin, Z., Wang, X., Wang, S., Ye, Z., 2020. Quantifying photosynthetic performance of phytoplankton based on photosynthesis–irradiance response models. *Environ. Sci. Eur.* 32, 24. <https://doi.org/10.1186/s12302-020-00306-9>
- Yu, L., Jin, X., Weller, R.A., 2006. Role of net surface heat flux in seasonal variations of sea surface temperature in the tropical Atlantic Ocean. *J. Clim.* 19, 6153–6169. <https://doi.org/10.1175/JCLI3970.1>

VII. Appendix

List of Figures

- Figure 1. Location of the four EBUS (white boxes). Mean chlorophyll concentrations in mg/m^3 by Sea-Wide Field-of-view Sensor (SeaWiFS) data are colored. Modified from Messié and Chavez 2015. 2
- Figure 2. Upwelling dynamics. a) Ekman spiral. Schematic movements of water layers due to wind stress and the water drag, resulting in a drifting net water movement at an angle of 90° to the upwelling-favorable winds. Adapted from Cushman-Roisin et al. (2011). b) Schematic view of the nutrient upwelled waters and the mesoscale eddy-induced reduction of nutrients at the nearshore. Adapted from Gruber et al. (2011). 3
- Figure 3. Depression and elevation of the three eddy types associated with the isopycnal displacements. In cyclones and mode-water eddies, isopycnal elevation causes upwelling and in anticyclones downwelling due to isopycnal depression. Adapted from McGillicuddy et al. (2016). 5
- Figure 4. The simplified pelagic food web. Trophic interactions (energy flux) are separated into two parts: The microbial loop components (base) and the classical food web (black triangle). Energy fluxes are marked by arrows. Figure modified after Andersson et al. (2017). 6
- Figure 5. Anthropogenic climate change impacts on the global ocean. Fossil fuel combustion, as the main driver of enhanced greenhouse gas concentrations, is responsible for several abiotic changes in the global ocean. Figure adapted from Allison et al. (2011; original version from Harley et al., 2006)... 9
- Figure 6. Predicted changes of EBUS due to climate change. a) Contemporary schema of coastal upwelling. b) Future schema of coastal upwelling. H is oceanic high; L is continental thermal low. Intensification of wind and currents are represented by the arrow's thickness. Figure adapted from Bakun et al. (2015). 10
- Figure 7. Map of the study area in the Canary Current System. Bathymetry data from the r package ggOceanMaps v1.2.6 (Vitakari, 2022) are grayscale colored. The sampling locations are marked by symbols and the blank circles represent the eddy circumference. 22
- Figure 8. Exemplary CTD-profile. Exemplary CTD-profile during the M160 cruise for the station Reference_CVOO. Chlorophyll concentration in $\mu\text{g}/\text{L}$ (green) and oxygen concentration in $\mu\text{mol}/\text{kg}$ (blue) were decisive parameters for determining the sample layers (DCM, sub-DCM, OMZ). Additionally, temperature in $^\circ\text{C}$ (red) is shown and the complete graphics of all CTD-profiles are presented in Supplementary File 1. DCM: deep-chlorophyll-maximum; OMZ: oxygen minimum zone. 25
- Figure 9. Principle component analysis based on the physicochemical parameters. Eddy samples are connected forming segments for the specific depth layers (colored) and sampling sites are indicated by symbols. DCM: deep-chlorophyll-maximum; OMZ: oxygen minimum zone; OA: orthosilicic acid; DO: dissolved oxygen. 35
- Figure 10. Boxplots visualizing alpha diversity measures. a) Rarefied ASV richness for concatenated eddy and reference samples over the depth layers. Pairwise Wilcoxon test revealed significant differences with $p < 0.01$ for two group comparisons highlighted by asterisks. b) Shannon Index H' for concatenated eddy and reference samples over the depth layers. Pairwise Wilcoxon test revealed significant differences with $p < 0.01$ for one group comparison highlighted by asterisks. The boxplot horizontal line represents the median value, whiskers represent the minimum and maximum values. Outliers are indicated as filled circles. KW: Kruskal Wallis; n: number of samples. 37
- Figure 11. Bar plot showing changes in alpha diversity measures. a) Relative changes in Rarefied ASV richness after merging eddy and reference samples for the concatenated depth strata and for DCM, sub-DCM, and OMZ. b) Relative changes in Shannon Index H' after merging eddy and reference samples separately for the concatenated depth strata and for DCM, sub-DCM, and OMZ. 100% corresponds to no change and is indicated by the dotted line. DCM: deep-chlorophyll-maximum; OMZ: oxygen minimum zone. 38

- Figure 12. NMDS of protistan plankton community structures based on Bray-Curtis distances. The specific depth layers are colored and sampling sites are differentiated by symbols. DCM: deep-chlorophyll-maximum; OMZ: oxygen minimum zone. 40
- Figure 13. Beta-diversity dendrogram of protistan plankton community structures based on Bray-Curtis dissimilarities. a) DCM; b) sub-DCM; c) OMZ depth layers for all samples. Only the individual clusters of specific eddy samples or references are colored. DCM: deep-chlorophyll-maximum; OMZ: oxygen minimum zone. 41
- Figure 14. Taxonomic inventories of protistan plankton ASVs. The bars represent the relative abundance of ASVs assigned to each of the different taxon groups at the phylum-level. Only the top ten most abundant taxa are shown individually and the remaining taxa are grouped under other protists. DCM: deep-chlorophyll-maximum; OMZ: oxygen minimum zone..... 42
- Figure 15. Taxonomic inventories of haptophyte-assigned ASVs. The bars represent the relative abundance of ASVs assigned to Haptophyta at the family-level. Only the top ten most abundant taxa are shown individually and the remaining taxa are grouped under other Haptophyta. DCM: deep-chlorophyll-maximum; OMZ: oxygen minimum zone. 43
- Figure 16. Taxonomic inventories of radiolarian-assigned ASVs. The bars represent the relative abundance of ASVs assigned to Radiolaria at the family-level. Only the top ten most abundant taxa are shown individually and the remaining taxa are grouped under other Radiolaria. DCM: deep-chlorophyll-maximum; OMZ: oxygen minimum zone. 44
- Figure 17. Taxonomic inventories of Discoba-assigned ASVs. The bars represent the relative abundance of ASVs assigned to Discoba at the family-level. Only the top ten most abundant taxa are shown individually and the remaining taxa are grouped under other Discoba. DCM: deep-chlorophyll-maximum; OMZ: oxygen minimum zone. 45
- Figure 18. Taxonomic inventories of dinoflagellate-assigned ASVs. The bars represent the relative abundance of ASVs assigned to Dinoflagellata at the family-level. Only the top ten most abundant taxa are shown individually and the remaining taxa are grouped under other Dinoflagellata. DCM: deep-chlorophyll-maximum; OMZ: oxygen minimum zone. 46
- Figure 19. Venn diagrams for the distribution of the shared and unique ASVs. a) Unique and common ASV distribution in the three eddies and reference sites calculated for the original ASV-to-sample matrix. b) Unique and common ASV distribution in the three eddies and reference sites calculated for the reduced ASV-to-sample matrix after alignment to the trait-database. 47
- Figure 20. NMDS of downscaled protistan plankton community structures based on Bray-Curtis distances. The specific depth layers are colored and sampling sites are differentiated by symbols. DCM: deep-chlorophyll-maximum; OMZ: oxygen minimum zone. 49
- Figure 21. Boxplot visualizing functional richness derived from the functional traits. Functional richness calculated for eddy and reference samples merged over the depth layers. Pairwise Wilcoxon test revealed significant differences with $p < 0.05$ for one group comparison highlighted by an asterisk. The boxplot horizontal line represents the median value, whiskers represent the minimum and maximum values. Outliers are indicated as filled circles. KW: Kruskal Wallis; n: number of samples. 50
- Figure 22. Ecological strategies distribution for sampling sites and depth layers. The bars represent the relative abundance of ASVs assigned to individual ecological strategies. DCM: deep-chlorophyll-maximum; OMZ: oxygen minimum zone. 54
- Figure 23. Boxplots visualizing abundances of prokaryotes (a, c, e) and protists (b, d, f). The concentrations for the individual depth layers are represented in a, b for DCM; c, d for sub-DCM; e, f for OMZ. The boxplot horizontal line represents the median value, whiskers represent the minimum and maximum values. Outliers are indicated as filled circles. Significant variations were first identified using Kruskal-Wallis (KW) test with ad hoc pairwise Wilcoxon test and are highlighted by asterisks (*: $p < 0.05$; **: $p < 0.01$; ***: $p < 0.001$). abund.: abundance; DCM: deep-chlorophyll-maximum; OMZ: oxygen minimum zone; n: number of samples. 57

- Figure 24. Boxplot visualizing grazing effect and carbon flow. The results for the individual depth layers are represented in a for DCM; b for sub-DCM; c for OMZ. The boxplot horizontal line represents the median value, whiskers represent the minimum and maximum values. Outliers are indicated as filled circles. Significant variations were first identified using Kruskal-Wallis test (DCM: $p = 0.0003$; sub-DCM: $p = 0.0091$; OMZ: $p = 0.0741$) with ad hoc pairwise Wilcoxon test and are highlighted by asterisks (*: $p < 0.05$; **: $p < 0.01$; ***: $p < 0.001$). GE: grazing effect; ing.: ingested; C: carbon; DCM: deep-chlorophyll-maximum; OMZ: oxygen minimum zone; n: number of samples. 59
- Figure 25. Correlation of physicochemical parameters, grazing effect, prokaryotic and protistan abundances. Color scale represents Spearman's ρ ; and not applicable (NA). Significant correlations are highlighted by asterisks (*: $p < 0.05$; **: $p < 0.01$; ***: $p < 0.001$). DO: dissolved oxygen; NA: not applicable. 60
- Figure 26. Predicted versus measured prokaryote abundance (a) and protistan abundance (b) using the multiple linear regression models for the respective depth layers. CCC with 95% CI are added. The dotted line indicates a perfect prediction, the black line and the grey area the depth integrated regression line and 95% confidence intervals, respectively. CCC: concordance correlation coefficient; CI: confidence interval; DCM: deep-chlorophyll-maximum; OMZ: oxygen minimum zone. 65
- Figure 27. Predicted versus measured grazing effect with (a) and without outliers (b) using the multiple linear regression models for the respective depth layers. CCC with 95% CI are added. The dotted line indicates a perfect prediction, the black line and the grey area the depth integrated regression line and 95% confidence intervals, respectively. CCC: concordance correlation coefficient; CI: confidence interval; DCM: deep-chlorophyll-maximum; OMZ: oxygen minimum zone. 66
- Figure 28. Experimental design and study location. a) Dimensions of one mesocosm with an underwater bag. Please note the size ratio for the underwater bag is not to scale. b) Large-scale map of the study site in the Humboldt Current System. c) Detailed map of the study area and the mesocosm arrangement for the light and upwelling manipulation. The star marks the location where the collection of the deep-water (DW) occurred. The percentages indicate the volume of water exchanged with DW for each mesocosm. This corresponds to the darkening of the color. The high light (HL), as no manipulation, and low light (LL) to simulate austral winter are colored green and gray, respectively. Modified from Bach et al. (2020). 85
- Figure 29. pH (a), dissolved oxygen (b) and temperature (c) development in the mesocosms. Deep-water addition is highlighted by the red dashed line. Light treatment is colored in green for high light (HL) and blue for low light (LL). 94
- Figure 30. Nitrate (a), silicate (b) and phosphate (c) development in the mesocosms. Deep-water addition is highlighted by the red dashed line. Light treatment is colored in green for high light (HL) and blue for low light (LL). 95
- Figure 31. ASV richness (a) and evenness (b) dependent on upwelling intensity and light manipulation derived from integrating all time points. The evenness and ASV richness were calculated for the rarefied data set. The light treatments are colored. Linear trendlines and coefficient of determination (R^2) for each light treatment were calculated using linear regression analysis. 97
- Figure 32. Shannon Index (a) and Simpson Index (b) dependent on upwelling intensity and light manipulation derived from integrating all time points. The Shannon and Simpson index were calculated for the rarefied data set. The light treatments are colored. Linear trendlines and coefficient of determination (R^2) for each light treatment were calculated using linear regression analysis. 98
- Figure 33. NMDS of protistan plankton community structures based on Bray Curtis distances. The light treatments are colored and the upwelling intensities are highlighted by symbols. Black circles are the 95% confidence intervals of samples pre and post upwelling. The black dashed line separates the samples without and with fish larvae addition. The blue dashed line separates the samples before and after deep-water treatment. DO: dissolved oxygen. 102
- Figure 34. NMDS of protistan plankton community structures based on Bray-Curtis distances with significantly correlated biotic functions. The light treatments are colored and the upwelling

	intensities are highlighted by symbols. Intern: internal ingestion; Extern: external ingestion; Mutualist.: mutualistic.....	103
Figure 35.	Taxonomic inventories of protistan plankton ASVs reads for (a) HL mesocosm and (b) LL mesocosms. The bars represent the relative abundance of ASVs assigned to each of the different taxon groups at the phylum level.....	105
Figure 36.	Changes in relative read abundance of the five most abundant phyla in relation to upwelling intensities derived from integrating all time points. The light treatments are colored and a respective trend line is added.	107
Figure 37.	Changes in relative read abundance of the dominant families within the most abundant phyla in relation to upwelling intensities derived from integrating all time points. The light treatments are colored and a respective trend line is added.	111
Figure 38.	Prokaryotic abundance for upwelling intensities derived from integrating all time points. The light treatments are colored. Linear trendlines and coefficient of determination (R^2) for each light treatment were calculated using linear regression analysis.	113
Figure 39.	Protistan abundance for upwelling intensities derived from integrating all time points. The light treatments are colored. Linear trendlines and coefficient of determination (R^2) for each light treatment were calculated using linear regression analysis.	114
Figure 40.	Development of prokaryote (a) and protistan (b) abundance in the mesocosms. Deep-water addition is highlighted by the red dashed line. Light treatment is colored in green for high light (HL) and blue for low light (LL).	115
Figure 41.	Grazing effect for upwelling intensities derived from integrating all time points. The light treatments are colored. Linear trendlines and coefficient of determination (R^2) for each light treatment were calculated using linear regression analysis.	116
Figure 42.	Prokaryotic turnover rate for upwelling intensities derived from integrating all time points. The light treatments are colored. Linear trendlines and coefficient of determination (R^2) for each light treatment were calculated using linear regression analysis.	117
Figure 43.	Development of grazing effect (a) and prokaryotic turnover rate (b) in the mesocosms. Deep-water addition is highlighted by the red dashed line. Light treatment is colored in green for high light (HL) and blue for low light (LL).	118
Figure 44.	Correlation of physicochemical parameters, grazing effect, prokaryotic and protistan abundances and prokaryotic turnover rate. Color scale represents Spearman's ρ ; and not applicable (NA). Significant correlations are highlighted by asterisks (*: $p < 0.05$; **: $p < 0.01$; ***: $p < 0.001$). DO: dissolved oxygen; Chl: Chlorophyll.	119
Figure 45.	Relative photosynthetic activity in relation to light intensity for three plankton groups. Curve progression for Dinoflagellates, diatoms, and green algae are colored. Adapted from Parson et al. (2013).	124
Figure 46.	Conceptual summary of the microbial dynamics with the mechanisms controlling the standing stock of prokaryotes and protistan plankton as well as the measured bacterivory. Nitrate concentration is included to underpin nutrient development. Data were averaged for each sampling day and rescaled between 0-1 for better comparison. N: nitrogen; C: carbon.	129
Figure 47.	Conceptual overview of the findings in the different aged cyclonic mesoscale eddies in the Canary Current System. Distinct protistan plankton communities are represented by the proportion of selected taxa (green algae, haptophytes, radiolarians, and parasitic protists). The most pronounced differences in protistan plankton communities were detected in the deep-chlorophyll maximum (DCM) and relatively similar communities in the oxygen-minimum zone (OMZ). The abundances of protists and prokaryotes are represented by the frequency of occurrence (low: old eddy CE_2019_14N_25W; intermediate: stable eddy CE_2019_18N_20W; high: young eddy CE_2019N_18W;). The quantity of measured and derived carbon flow is highlighted by straight arrows (carbon fixation by phototrophs/mixotrophs), curved arrows (measured bacterivory by phagotrophic protists) and dashed arrows (carbon sink of particulate organic matter). Dashed sheath line of the eddy CE_2019_14N_25W represents the potential disintegrating state.....	136

Figure 48. Conceptual overview of the findings for the main treatments in the mesocosms in the Humboldt Current System. Distinct protistan plankton communities are represented by the proportion of selected taxa (diatoms, dinoflagellates, green algae, and parasitic protists in low light conditions with low nutrient concentrations; diatoms in low light conditions with high nutrient concentrations; dinoflagellates and parasitic protists in high light conditions with low nutrient concentrations; dinoflagellates in high light conditions with high nutrient concentrations). The abundances of protists and prokaryotes are represented by the frequency of occurrence. The quantity of measured and derived carbon flow is highlighted by straight arrows (carbon fixation by phototrophs/mixotrophs), curved arrows (measured bacterivory by phagotrophic protists) and dashed arrows (carbon sink of particulate organic matter). Quantity of protistan alpha diversity is represented by frequency of the symbol. Dashed line separates low and high nutrient concentrations. 137

List of Tables

Table 1. Sampling overview. Location and sampling date of stations in the zero-velocity boundary of the eddies and the reference stations sampled during the M156 and M160 cruise.....	24
Table 2. Primer sequences. Nucleotide sequences of the forward and reverse primers used to amplify the V9 18S rDNA.....	26
Table 3. Components for polymerase chain reaction. Reaction mixture for polymerase chain reaction to amplify the V9 18S rDNA.....	27
Table 4. Correlation of the environmental parameters to the NMDS ordination. <i>Envfit</i> results of the physicochemical parameters. R ² : coefficient of determination.	40
Table 5. Statistics for Spearman correlation between functional richness and the alpha diversity measurements. Grading of ρ was done following Chan et al. (2003). FR: functional richness; H': Shannon Index; ρ : Spearman correlation coefficient.....	51
Table 6. Dominant features of ecological strategies (ES). Main traits of the ten ES and examples derived from taxonomic composition at the family and phylum levels.	51
Table 7. Significant differences between ecological strategies (ES) of the sampling stations. Kruskal Wallis test (KW), followed by pairwise Wilcoxon test was used to calculate significant differences.	55
Table 8. Significant differences between Ecological strategies (ES) of the depth layers Kruskal Wallis test (KW), followed by pairwise Wilcoxon test was used to calculate significant differences. DCM: deep-chlorophyll-maximum; OMZ: oxygen minimum zone.....	55
Table 9. Multiple linear regression model statistics. The respective models were investigated for normal distribution of residuals with the Kolmogorov-Smirnov test (KS). R ² , coefficient of determination. NA: not applicable; DCM: deep-chlorophyll-maximum; OMZ: oxygen minimum zone.	61
Table 10. Physicochemical parameters and the interaction terms of the respective models based on parsimony generation. Variance inflation factors (VIF) were only inspected before adding interactions to the model. SE: standard error; R ² : coefficient of determination; NA: not applicable; DCM: deep-chlorophyll-maximum; OMZ: oxygen minimum zone.	62
Table 11. Regression analysis of measured and predicted values. Coefficient of determination (R ²) and significance of regression analysis for the predicted parameters in each depth layer if applicable. DCM: deep-chlorophyll-maximum; OMZ: oxygen minimum zone.	64
Table 12. Nutrient concentrations of the mesocosms. Nutrient concentrations of each KOSMOS after deep-water (DW) addition on day 15 and the 100% DW. It should be noted that the nutrient concentrations do not reflect the concentration directly after DW injection due to the time delay in the process and water sampling. HL: high light; LL: low light; M: mesocosm.....	87
Table 13. Sampling scheme of mesocosms. The sampling sequence has changed (day 21/23) during the field campaign due to the possibility of experiment termination due to COVID-19 regulations. HL: high light; LL: low light; M: mesocosm.....	88
Table 14. Shapiro Wilk and Levene's test results for each alpha diversity measurement. Verification of the normal distribution and variance homogeneity for ASV richness, evenness, Shannon and Simpson Index.....	99
Table 15. Analysis of covariance (ANCOVA) for each alpha diversity measurement. ANCOVA test results for the mesocosm manipulations, their interactions, and the residuals for each alpha diversity measurement. DF: degrees of freedom; SS: sum of squares.	99
Table 16. Dominant protistan plankton groups associated to the specific treatments. Chlorophyta, Dinoflagellata, Haptophyta and diatoms arranged in decreasing order of relative abundance for the specific treatment.	104
Table 17. Shapiro Wilk and Levene's test results for the relative abundance of the most dominant plankton groups. Verification of the normal distribution and variance homogeneity for Chlorophyta, Dinoflagellata, Haptophyta, Mesomycetozoa and Ochrophyta.	106

Table 18. Analysis of covariance (ANCOVA) for the most dominant plankton groups. ANCOVA test results for the mesocosm manipulations, their interactions, and the residuals for Chlorophyta, Dinoflagellata, Haptophyta, Mesomycetozoa and Ochrophyta. DF: degrees of freedom; SS: sum of squares..... 108

Table 19. Shapiro Wilk and Levene’s test results for the relative abundance of the dominant families within the most abundant phyla. Verification of the normal distribution and variance homogeneity for Abeoformidae Group MAIP 2, Dino-Group-I-Clade-4, Polar-centric-Mediophyceae, Suessiaceae, unassigned Chlorellales and unassigned Dinophyceae..... 109

Table 20. Analysis of covariance (ANCOVA) for the relative abundance of the dominant families within the most abundant phyla. ANCOVA test results for the mesocosm manipulations, their interactions, and the residuals Abeoformidae Group MAIP 2, Dino-Group-I-Clade-4, Polar-centric-Mediophyceae, Suessiaceae, unassigned Chlorellales and unassigned Dinophyceae. DF: degrees of freedom; SS: sum of squares..... 112

List of Equations

- Equation 1. Calculation of cell and microsphere abundance. Particle and organism abundances were calculated per milliliter. n is the mean value of counted cells in 10 grids. A represents the filter area and A_c the grid area in μm^2 . V is the volume of subsamples drawn on each filter in mL..... 32
- Equation 2. Calculation of grazing rate (I) and grazing effect (II). The ingestion rate (ir) of food particles in MS grazer $^{-1} \text{h}^{-1}$ is multiplied by the concentrations of bacteria ($c_{\text{prokaryotes}}$) and divided by the MS concentration (c_{MS}) in cells/mL. The grazing rate (gr) is the number of prokaryotes grazer $^{-1} \text{h}^{-1}$ and c_{grazer} is the concentration of phagotrophic protists in cells/mL. MS: microspheres..... 32

Supplementary Files / Contents of enclosed USB stick

Supplementary File 1. CTD-profiles of the sampling stations. Chlorophyll concentration in $\mu\text{g/L}$ (green) and oxygen concentration in $\mu\text{mol/kg}$ (blue) were decisive parameters for determining the sample layers (DCM, sub-DCM, OMZ). Additionally, temperature in $^{\circ}\text{C}$ (red) is shown and the complete graphics of all CTD-profiles are presented in supplementary S. DCM: deep-chlorophyll-maximum; OMZ: oxygen minimum zone.

On the USB stick under the file name “Supplementary_file_1.png”.

Supplementary File 2. Physicochemical and nutrient data for each sampling station with the respective depth layer. OA: orthosilicic acid; DO: dissolved oxygen; u.d. = under detection limit.

On the USB stick under the file name “Supplementary_file_2.docx”.

Supplementary File 3. Raw data of the microscopic counts to calculate protistan and prokaryotic abundances as well as the phagotrophic estimators for Subject I (a) and Subject II (b).

On the USB stick under the file name “Supplementary_file_3_a.zip” and “Supplementary_file_3_b.zip”.

Supplementary File 4. a) Sequence data overview from raw sequence files to high-quality sequences used in downstream analyses for all sampling stations of the three eddies (CE_2019_19N_18W, CE_2019_18N_20W CE_2019_14N_25W) under study and the two reference stations (CVOO, Cape Blanc). b) ASV-to-sample matrix with assigned taxonomy for all samples of the three eddies and the two reference stations.

On the USB stick under the file name “Supplementary_file_4_a.csv” and “Supplementary_file_4_b.csv”.

Supplementary File 5. Rarefaction profiles for all sampling stations of the three eddies (CE_2019_19_N_18W, CE_2019_18N_20W, CE 2019_14N_25W) under study and the two reference stations (CVOO, Cape Blanc) for DCM (a), sub-DCM (b) and OMZ (c). Profiles show (near-)sample saturation for all samples. Cut-off for the smallest sequence size is represented by the black vertical line.

On the USB stick under the file name “Supplementary_file_5.jpg”.

Supplementary File 6. ASV richness and Shannon Index H' for all sampling stations of the three eddies (CE_2019_19_N_18W, CE_2019_18N_20W, CE 2019_14N_25W) under study and the two reference stations (CVOO, Cape Blanc) for DCM, sub-DCM and OMZ.

On the USB stick under the file name “Supplementary_file_6.png”.

Supplementary File 7. Output of the Kruskal-Wallis test (KW; chi-square = 14.455, DF = 3) and the post-hoc pairwise Wilcoxon test (W) with Bonferroni corrected p-values of the comparison of the sampling sites for the Shannon Index and the ASV richness. DF: degrees of freedom.

Comparison		Shannon Index		ASV richness	
Station 1	Station 2	p (KW)	p (W)	p (KW)	p (W)
CE_2019_18N_20W	CE_2019_14N_25W	0.002	0.008	0.006	0.088
CE_2019_19N_18W	CE_2019_14N_25W		1		0.6
References	CE_2019_14N_25W		1		1
CE_2019_19N_18W	CE_2019_18N_20W		1		1
References	CE_2019_18N_20W		0.005		0.003
References	CE_2019_19N_18W		1		0.57

Supplementary File 8. PERMANOVA analysis on Bray-Curtis distances. PERMANOVA was performed to test significance for the depth strata and the sampling sites (Reference samples were merged). DF: degree of freedom; SS: sum of squares; F: F-statistic.

PERMANOVA	DF	SS	F	R ²	p-value
Layer	2	2.91	7.02	0.27	0.0001
Site	3	1.87	3.00	0.17	0.0001
Layer x Site	6	2.49	2.00	0.23	0.0002

Supplementary File 9. Proportions of all phyla (a), haptophyte (b), radiolarian (c), Discoba (d) and dinoflagellate (e) taxa estimated by relative sequence read proportions in the DCM, sub-DCM and OMZ of each individual sample of the three eddies under study (CE_2019_19N_18W, CE_2019_18N_20W, CE_2019_14N_25W) and the two background waters (CVOO and CB). Based on these data, the averaged taxonomic plots of figures 14-18 were generated.

On the USB stick under the file name "Supplementary_file_9_a-e.pdf".

Supplementary File 10. PERMANOVA statistics on BC distances of the reduced ASV-to-sample matrix. PERMANOVA was performed to test significance for the depth strata and the sampling sites (Reference samples were merged). DF: degree of freedom; SS: sum of squares; F: F-statistic.

PERMANOVA	DF	SS	F	R²	p-value
Layer	2	2.52	5.39	0.23	0.0001
Site	3	2.18	2.33	0.20	0.0001
Layer x Site	6	2.32	1.65	0.21	0.0002

Supplementary File 11. a) Output of the Kruskal-Wallis test (KW; chi-square = 9.6075, DF = 3) and the post-hoc pairwise Wilcoxon test (W) with Bonferroni corrected p-values of the comparison of the sampling sites for the functional richness. DF: degrees of freedom. b) Raw data of the calculated functional richness.

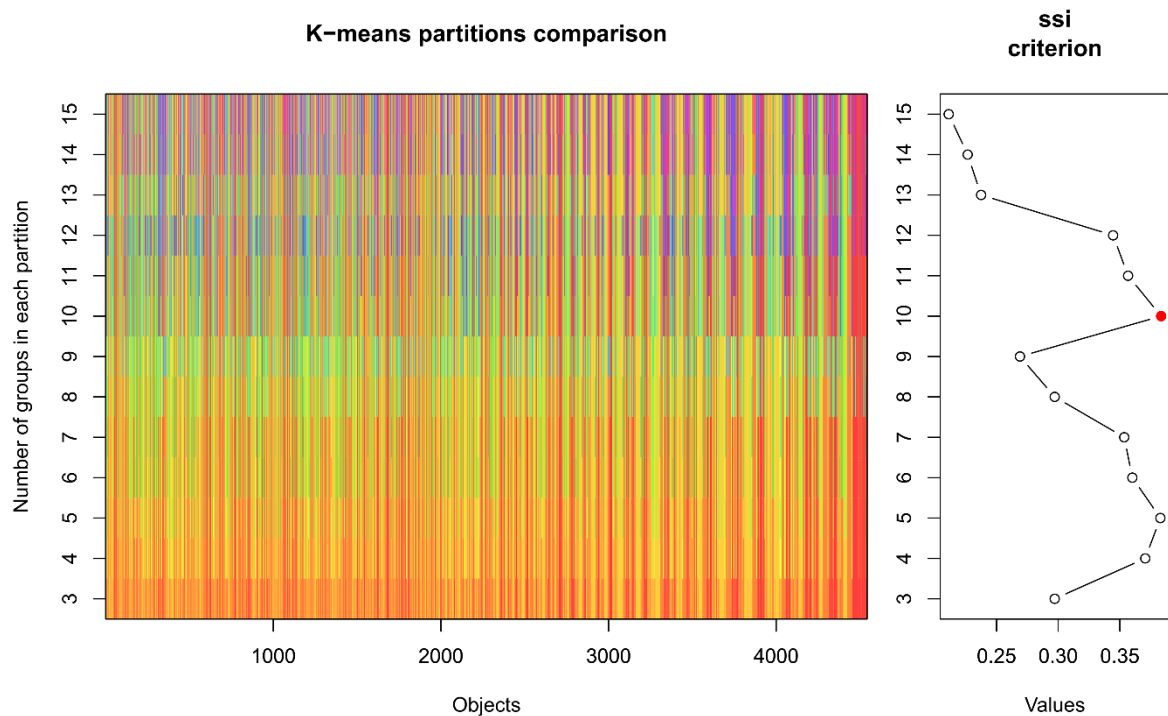
a

Comparison		Functional Richness	
Station 1	Station 2	p (KW)	p (W)
CE_2019_18N_20W	CE_2019_14N_25W	0.022	0.245
CE_2019_19N_18W	CE_2019_14N_25W		0.873
References	CE_2019_14N_25W		1
CE_2019_19N_18W	CE_2019_18N_20W		1
References	CE_2019_18N_20W		0.041
References	CE_2019_19N_18W		0.571

b

Sampling station	DCM	Sub-DCM	OMZ
CE_2019_19N_18W	0.69	0.68	0.72
CE_2019_18N_20W(1)	0.74	0.69	0.74
CE_2019_18N_20W(2)	0.67	0.64	0.75
CE_2019_18N_20W(3)	0.70	0.68	0.67
CE_2019_18N_20W(4)	0.69	0.66	0.65
CE_2019_14N_25W(1)	0.70	0.81	0.73
CE_2019_14N_25W(2)	0.73	0.73	0.71
CE_2019_14N_25W(3)	0.68	0.74	0.77
Reference_CB	0.75	0.69	0.74
Reference_CVOO	0.75	0.71	0.80

Supplementary File 12. Partition clustering with the K-means algorithm and the SSI-criterion on the trait-assigned ASV matrix to infer the number of ecological strategies.



Supplementary File 13. Relative distribution of the eleven functional traits and their respective characteristics for the ten ecological strategies.

On the USB stick under the file name "Supplementary_file_13.png".

Supplementary File 14. Calculated protistan and prokaryotic abundances as well as grazing effect and prokaryotic turnover rate for each sample and replicate.

On the USB stick under the file name "Supplementary_file_14.csv".

Supplementary File 15. Output of the Kruskal-Wallis test and the post-hoc pairwise Wilcoxon test (W) with Bonferroni corrected p-values of the comparison of the sampling sites for the bacterial and protistan abundances, as well as the grazing effect and the bacterial turnover rate.

On the USB stick under the file name "Supplementary_file_15.xlsx".

Supplementary File 16. Mesocosm volume determined through salt addition.

Mesocosm	Volume in L	Uncertainty in L
M1	36.440	2.064
M2	35.195	2.167
M3	35.984	2.242
M4	30.743	2.166
M5	32.786	454
M6	34.116	963
M7	33.242	1.507
M8	35.097	1.713

Supplementary File 17. a) Raw data for the V9 SSU rDNA sequence files. Sequencing was performed by SeqIT GmbH & Co. KG using the paired-end Illumina MiSeq technique. b) Overview of the multiplexed libraries to assign the samples correctly.

On the USB stick under the file name “Supplementary_file_17_a.tar” and “Supplementary_file_17_b.csv”.

Supplementary File 18. ASV-to-sample matrix with assigned taxonomy for the samples of the eight mesocosms.

On the USB stick under the file name “Supplementary_file_18.csv”.

Supplementary File 19. Physicochemical and nutrient data for each sample.

On the USB stick under the file name “Supplementary_file_19.csv”.

Supplementary File 20. Sequence data overview from raw sequence files to high-quality sequences used in downstream analyses for all samples of the eight mesocosms under study.

On the USB stick under the file name “Supplementary_file_20.csv”.

Supplementary File 21. Rarefaction profiles for all samples of the eight mesocosms under study for 0% (a), 15% (b), 30% (c) and 45% (d) upwelling intensity. Profiles show (near-)sample saturation for all samples.

On the USB stick under the file name “Supplementary_file_21_a.pdf”, “Supplementary_file_21_b.pdf”, “Supplementary_file_21_c.pdf” and “Supplementary_file_21_d.pdf”.

Supplementary File 22. ASV richness, evenness, Shannon Index and Simpson Index for each sample.

On the USB stick under the file name “Supplementary_file_22.csv”.

Supplementary File 23. PERMANOVA analysis on Bray-Curtis distances. PERMANOVA was performed to test significant effects for mesocosm manipulations. DF: degree of freedom; SS: sum of squares; F: F-statistic.

PERMANOVA	DF	SS	F	R²	p-value
DW addition	1	2.40	12.90	0.19	0.0001
Light treatment	1	0.91	4.91	0.07	0.0002
Fish introduction	1	0.83	4.48	0.07	0.0001
Upwelling intensity	3	0.31	1.64	0.02	0.0560

Supplementary File 24. Correlation of the environmental parameters to the NMDS ordination. *Envfit* results of the physicochemical parameters. R²: coefficient of determination; PAR: photosynthetically active radiation.

Parameter	NMDS1	NMDS2	R²	p-value
Temperature	-0.49	-0.13	0.26	0.001
Salinity	0.62	0.18	0.41	0.0001
Density	0.63	0.17	0.42	0.0001
pH	-0.17	0.62	0.42	0.0001
Dissolved oxygen	-0.45	0.44	0.40	0.0001
Chlorophyll a	-0.77	0.18	0.62	0.0001
PAR	-0.03	0.22	0.05	0.3265
Nitrate	0.07	-0.09	0.01	0.7704
Nitrite	0.02	-0.27	0.07	0.1862
Phosphate	0.22	-0.70	0.54	0.0001
Orthosilicic acid	-0.64	-0.33	0.52	0.0001

Supplementary File 25. Correlation of the relative abundance of the biotic traits to the NMDS ordination. *Envfit* results of the physicochemical parameters. R²: coefficient of determination.

Parameter	NMDS1	NMDS2	R²	p-value
Extern	-0.68	-0.13	0.48	0.0001
Intern	-0.83	0.15	0.72	0.0001
No Ingestion	0.23	-0.15	0.07	0.1726
Osmotrophic	0.33	-0.70	0.60	0.0001
Saprotrophic	0.32	0.23	0.16	0.0227
Unknown Ingestion	0.09	0.64	0.42	0.0001
Commensalist	0.44	-0.06	0.20	0.0055
Mutualist Photosynthetic	-0.12	0.49	0.25	0.0013
No Symbiosis	-0.50	0.08	0.25	0.0015
Parasite	0.09	-0.38	0.15	0.0252
Unknown Symbiosis	0.46	-0.44	0.41	0.0001

Supplementary File 26. Calculated protistan and prokaryotic abundances as well as grazing effect and prokaryotic turnover rate for each sample and replicate. Sample name consists of mesocosm, replicate and the date (day, month) the sample was taken.

On the USB stick under the file name "Supplementary_file_26.csv".

Supplementary File 27. Dissertation in digital version.

On the USB stick under the file name "Dissertation_Katzenmeier.pdf".

Acronyms

ACE	anticyclonic eddy
ACME	anticyclonic mode water eddy
ADCP	Acoustic Doppler Current Profiler
AIC	Akaike's information criterion
ANCOVA	analysis of covariance
ASV	amplicon sequence variants
AT	adenine - thymine
AVISO	Archiving, Validation and Interpretation of Satellite Oceanographic
BP	band pass
BC	Bray-Curtis
BS	beam splitter
BSA	bovine serum albumin
C	carbon
CanCS	Canary Current System
CB	Cap Blanc
CCC	concordance correlation coefficient
CE	cyclonic eddy
Chl	chlorophyll
CMEMS	Copernicus Marine Environment Monitoring Service
CO ₂	carbon dioxide
CTD	conductivity, temperature, density
CUSCO	Coastal Upwelling System in a Changing Ocean
CVOO	Cape Verde Ocean Observatory
D	Simpson Index
DCM	deep-chlorophyll maximum
DF	degrees of freedom
dNTP	deoxynucleoside triphosphate
DO	dissolved oxygen
DOM	dissolved organic matter
ddH ₂ O	double-distilled water

DSPD	deep-sea pelagic diplonemids
DW	deep water
EBUS	Eastern Boundary Upwelling Systems
eDNA	environmental desoxyribonucleic acid
ES	ecological strategies
EVA	ethylene-vinyl acetate
FLB	fluorescently labeled bacteria
FT	thin-film filter
GC	guanin-cytosin
H	oceanic high
H'	Shannon Index
HCS	Humboldt Current System
HL	high light
HQ	high quality
HTS	high throughput sequencing
KS	Kolmogorov-Smirnov
KW	Kruskal Wallis
L	continental thermal low
LCA	last common ancestor
LL	low light
LP	long pass
MAIP	Marine Ichthyosporea
MS	fluorescent polycarbonate microspheres
N	nitrogen
NA	not applicable
NaCl	sodium chloride
NMDS	non-metric multidimensional scaling
NO ₂ ⁻	nitrite
NO ₃ ⁻	nitrate
O ₂	oxygen
OMZ	oxygen minimum zone

PAR	photosynthetically active radiation
PCA	principal component analysis
PCR	polymerase chain reaction
PERMONVA	Permutational multivariate analysis of variance
PO ₄	phosphate
POM	particulate organic matter
RCP	Representative Concentration Pathways
REEBUS	Role of Eddies in the Carbon Pump of Eastern Boundary Upwelling Systems – Demonstration Case Canary Current System
RPTU	Rheinland-Pfälzischen Technischen Universität Kaiserslautern-Landau
rRNA	ribosomal ribonucleic acid
SeaWiFS	Sea-Wide Field-of-view Sensor
SI(OH) ₄	orthosilicic acid
SS	sum of squares
SSI	simple structure index
SSU	small subunit
UV	ultraviolet
VIF	variation inflation factor
ρ	Spearman correlation coefficient

Chemicals

- Calcium chloride dihydrate, Carl-Roth GmbH, Karlsruhe, Germany
- DAPI (4',6-diamidino-2-phenylindole), Sigma-Aldrich Chemie GmbH, Steinheim, Germany
- Dinatriumtetraborat-Decahydrat, Carl-Roth GmbH, Karlsruhe, Germany
- Dipotassium hydrogen phosphate trihydrate, Carl-Roth GmbH, Karlsruhe, Germany
- Ethanol absolute $\geq 99.9\%$, Sigma-Aldrich Chemie GmbH, Steinheim, Germany
- Fluoresbrite® YG Microspheres 0.5 μm , Polyscience, Hirschberg an der Bergstraße, Germany
- Formaldehyde (37%), Sigma-Aldrich Chemie GmbH, Steinheim, Germany
- Lugol solution, Carl-Roth GmbH, Karlsruhe, Germany
- Magnesium sulfate heptahydrate, Carl-Roth GmbH, Karlsruhe, Germany
- Potassium chloride, Carl-Roth GmbH, Karlsruhe, Germany
- Vectashield antifade mounting media, Biozol, Eching, Germany
- LifeGuard Soil Preservation Solution, MoBio, Laboratories Inc., QIAGEN Company, Düsseldorf, Germany

VIII. Acknowledgments

I would like to express my deepest thanks to the following people. I omitted academic titles except for the first three persons – they all have been incredibly helpful.

Prof. Dr. Thorsten Stoeck for giving me the opportunity to work on this project.

Prof. Dr. Matthias Hahn for acting as secondary supervisor to this thesis.

Prof. Dr. Stefan Kins for being the chair of the examination committee.

Hans-Werner Breiner for supporting in sampling during the M156 cruise and always being there to help organizing and finding laboratory equipment.

Maren Nothof for supporting in sampling during the M160 cruise.

Megan Gross for supporting in sampling during the CUSCO campaign.

Megan Gross, Maren Nothof, Mahshid Oladi, Verena Rubel and Julia Zimmer (Zhishuai Qu) for taking time to read the thesis (introduction) and give fruitful feedback and tips in regards to English and scientific writing.

Last but not least – thanks to all the people on the M156 and M160 cruise, the colleagues during the CUSCO campaign and my colleagues in the lab, my friends and to everyone I might have forgotten.

Ein besonderer Dank gilt meinen Eltern Birgit und Bernd Katzenmeier sowie meinen Großeltern Irmgard und Walter Reich, die mich trotz schweren Zeiten immer ermutigt und unterstützt haben. Ebenso meine Geschwister Melanie und Björn, ohne die ich nur halb so viel Spaß gehabt hätte. Außerdem hat mich mein Vater in Sachen Formatierungsarbeit und mein Bruder bei der Erstellung der Konzeptgrafiken unterstützt.

IX. Curriculum Vitae

PERSONAL INFORMATION

Name: Sven Nicolai
Family name: Katzenmeier
Place of birth: Ludwigshafen am Rhein, Germany

EDUCATION

Ph.D. student, since June 2019.
Department of Ecology, University of Kaiserslautern, Germany.

M.Sc. degree, 2019. Protozoan bacterivory estimation using fluorescently labeled microspheres as food analogues,
Department of Ecology, University of Kaiserslautern, Germany.

B.Sc. degree, 2017. Flow-cytometry of microorganism— Quantification of phototrophic, heterotrophic protists and bacteria using flow cytometry,
Original title of thesis in German: Durchfluss-Zytometrie von Mikroorganismen – Quantifizierung von Bakterien und heterotrophen, phototrophen Protisten mit einem Durchflusszytometer
Department of Ecology, University of Kaiserslautern, Germany.

State-certified biological-technical assistant,
2011. Berufsbildende Schule für Naturwissenschaften,
Ludwigshafen am Rhein, Germany

RESEARCH / WORKING EXPERIENCE

October 2022: Field research (four weeks), Berlin; “Microbiological monitoring of a groundwater ecosystem affected by an aquifer thermal energy storage (ATES)”.

Since April 2022: Teaching “Evolution”
Department of Ecology, University of Kaiserslautern, Germany.

2022: Teaching assistant “Molecular Ecology”
Department of Ecology, University of Kaiserslautern, Germany.

2020 - 2023: Teaching assistant “Limnologie und Mikrobielle Ökologie”
Department of Ecology, University of Kaiserslautern, Germany.

Feb.-April 2020: Field research (three months), Peru; “The trophic role of bacterivorous protistan plankton in a changing coastal upwelling system”.

December 2019: Field research, METEOR; research vessel Campaign M160 2019-11-23 (Mindelo) – 2019-12-20 (Mindelo);
Research locations: Canary Islands; North Atlantic Ocean.

- July 2019: Field research, METEOR; research vessel Campaign M156 2019-07-03 (Mindelo) – 2019-08-01 (Mindelo);
Research locations: Canary Islands; North Atlantic Ocean.
- 2017-2019: Research assistant (2 years), Department of Resource Efficient Wastewater Technology, University of Kaiserslautern, Germany.

PUBLICATIONS

Qu, Z., Weinisch, L., Fan, X., **Katzenmeier, S.**, Stoeck, T., & Filker, S. (2020). Morphological, Phylogenetic and ecophysiological characterization of a new ciliate, *Platynematum rossellomorai* n. sp. (Oligohymenophorea, Scuticociliatia), detected in a hypersaline pond on Mallorca, Spain. *Protist*, 171(4), 125751.

ORAL PRESENTATIONS

Rettenmaier, D., Zorn, R., Blum, P., Menberg, K., Herrmann, M., Viernickel, M., Eichelbaum, F., Fleuchhaus, P., Stoeck, T., **Katzenmeier, S.**, Breiner, H. W., Hahn, H.-J., Fuchs, A. (2023). DemoStorage - an ATEs demonstrator in an urban environment; European Geosciences Union, Vienna.

Katzenmeier S., Breiner H.W., Salvatore S., & Stoeck T. (2021). Community response of protistan plankton and their mediated carbon flow to eddies; 40th meeting of the German Society for Protozoology, Vienna.

Gross M., **Katzenmeier S.**, CUSCO consortium, & Stoeck T. (2021). Effects of different simulated upwelling intensities on protistan plankton structures in the Peruvian Humboldt current system; 40th meeting of the German Society for Protozoology, Vienna.

POSTERS

Katzenmeier S., Breiner H.W., Salvatore S., & Stoeck T. (2021). Community response of protistan plankton and their mediated carbon flow to eddies; the 4th Asian Congress of Protistology -internet 2021.

GRANTS / SCHOLARSHIP

Grant: AQUACOSM – KOSMOS-Peru 2020; “The trophic role of bacterivorous protistan plankton in a changing coastal upwelling system (BacPro)”.